

Diss. ETH No. 27323

**Metabolic Insights Related to Sleep and Circadian Clocks  
from Mass Spectrometry-Based Analysis of Blood and  
Breath**

A thesis submitted to attain the degree of  
**DOCTOR OF SCIENCES of ETH ZURICH**  
(Dr. sc. ETH Zurich)

presented by

**Nora Kristina Nowak**

MSc in Chemistry, Friedrich Schiller Universität Jena, Germany

born on 02.07.1991

German citizen

accepted on the recommendation of

Prof. Dr. Renato Zenobi, examiner  
Prof. Dr. Steven Brown, co-examiner  
Prof. Dr. Emma Wetter Slack, co-examiner

2021



# Acknowledgements

On the exciting journey of my PhD I received support from many people in various ways, for which I feel very grateful.

First of all, I would like to thank Renato Zenobi for giving me the opportunity to work on such interdisciplinary projects in such a pleasant and international environment. I am very grateful for all the freedom you gave me and for accompanying me on my journey from breath analysis in sleeping persons to studying metabolism in arctic reindeer. I also highly appreciate that you supported my attendance at various international conferences and that your door was always open.

A huge thank you goes to Steven Brown for infecting me with his enthusiasm about circadian biology. I am very grateful for all our inspiring discussions and for everything you taught me about biology and science. And thank you so much for the unforgettable experience of flying me through spectacular Northern lights!

In addition to the field of mass spectrometry and circadian clocks, Malcolm Kohler introduced me to the clinical world. I appreciate all the medical knowledge about sleep and OSA you shared with me and would like to thank you a lot for all your support in our sleep study.

My first steps in the field of breath analysis and SESI-MS would have been much harder without Pablo Sinues. Thank you very much for all your explanations, helpful discussions and support.

I would like to thank Emma Slack for being the co-examiner of this thesis as well as for involving me in her lecturing.

Along my way, I had the chance to collaborate with many people from various fields, making my journey so diverse. Thank you Thomas and Martin for realizing the sleep study together with me. It would have been impossible and much less fun, to spend all the nights in the lab without you! Thanks Djordje, Ricards and Stefan for contributing with your mathematical expertise to the project. Thank you, Wuschi and Christoph for fixing our sampling line immediately, every time we came with this super urgent request. Thank you Anna Engler, Anna Stöberl, Sira, Damaris and Lisa and the whole USZ breath analysis team for your commitment in the OSA study. I really appreciate how you organized the transfer of every participant from USZ to Hönggerberg. I'd also like to thank Marloes Maathuis for your statistical advice and Sanzio for your efforts to unravel the influence of different normalization methods.

I would like to thank the whole Brown lab for integrating me so warmly at the EBRS in Lyon and every time I came to your lab at Irchel. My special thanks goes to Sara, Hien and Audrey, with whom I experienced wonderful collaborations. It was my pleasure to write the

---

book chapter together with you, Audrey. I really liked our productive early morning coffee meetings. And thank you Seraina for spicing the chapter up with your artistic talent. Thank you Hien for all your effort and enthusiasm in our multi-omics project. I learned a lot about GWAS and clocks from you and enjoyed our discussions. And thank you so much Sara, for the great collaboration on the reindeer project, it was great fun to work with you. Keep your endless good mood and big smile! At this point, I'd also like to thank you, Gabi and Melanie, for your enthusiasm and engagement in this project and for giving me such a warm welcome and great time in Tromsø.

A big thank you goes to the Zenobi group. I enjoyed the international spirit in our group a lot and I will always remember adventures we experienced together in the Alps. Martin, thanks for sharing all your SESI and breath analysis knowledge with me. I would like to thank the whole breath analysis team for all the helpful discussions we had. Thank you, Adrien, for your pleasant company in our joint office. I enjoyed our chats about science and life. Thank you, Bettina, Luzia, Katharina, Jasmin and Wuschi for all the recreative coffee, tea and ice cream breaks. Thank you, Brigit, for helping me with any administrative work. A huge thank you goes to Bettina, not only for being a great colleague, for all the helpful discussions, your support and proofreading parts of this thesis, but also for being a lovely friend. And Luzia, where should I start...? When you asked me on my first day if I join for an ice cream, I would have never imagined that this results in such an amazing friendship! Thank you for everything you taught me during my PhD including Luzärn-Dütsch, for proofreading my thesis, for all your support and for always understanding my thoughts. I'm looking forward to many more spontaneous adventures with you. And thanks for introducing me to Lyndsey, Laura and Debi. I enjoyed all the lunches, coffee breaks, trips and zoom calls we had together and can't wait for our next escape room challenge.

A big thank you goes to JUCHZ and my dear Lindy hopping friends who made me feel home in Zurich very quickly. After singing and dancing with you, any hard work day or failed experiment was forgotten and I fell into bed with a big smile.

Last but not least, I would like to express my gratitude to my parents and my friends, who always supported me. Thank you Tobi, Theresa and Maria, for all your care and patience during the last few months, when I was always busy with accomplishing this thesis! Thank you Saskia for proof-reading parts of this thesis and exploring the iciest and most beautiful parts of the world together with me.



# Abstract

Most physiological processes in humans are synchronized with their environment by so-called circadian clocks. These molecular time-keeping machineries are present in almost every cell. While light is the most important external stimulus to reset the circadian clocks, they can also be entrained by other stimuli, such as feeding or rest/activity cycles. Sleep is both, one of the major outputs of circadian clocks and also an independently regulated recuperative neurobiological process. Both, circadian clocks and sleep are closely intertwined with metabolic regulation and their disruption is associated with adverse effects on metabolic health, such as type 2 diabetes, metabolic syndrome, obesity and cardiovascular diseases. Since sleep restriction and disruption of circadian clocks are common issues in a modern 24/7 society, their negative metabolic consequences constitute a major concern of public health. However, despite clear evidence for the association between sleep, circadian clocks and metabolism, many aspects of this relationship remain unclear.

In this thesis, novel insights into metabolic processes related to sleep and circadian clocks were gained using cutting-edge high-resolution mass spectrometry (HRMS) techniques. The combination of high resolution and high mass accuracy enables the analysis of complex mixtures and delivers molecular information. HRMS therefore provides a powerful tool for metabolic profiling. Here, two HRMS approaches were used. Metabolites in exhaled breath were measured in real time by secondary electrospray ionization high-resolution mass spectrometry (SESI-HRMS), offering a non-invasive technique with a virtually unlimited sampling frequency for studying systemic metabolic processes. Moreover, metabolic profiling from blood samples was performed using electrospray ionization mass spectrometry coupled to ultra-high performance liquid chromatography. Thereby, chromatography adds an additional dimension of separation, which improves unambiguous compound identification.

Within this thesis, a setup for the analysis of exhaled breath during sleep by SESI-HRMS was developed. This allowed an unprecedented monitoring of metabolome-wide regulation during sleep with a ten-second time resolution. Major metabolic pathways were found to undergo rapid and reversible changes upon sleep stage transitions. It seems likely that the relevance of this complex synchronization of metabolism and sleep architecture for human health and performance is higher than previously thought.

The non-invasive fashion of SESI-HRMS and its capability for real-time information qualify this technique also as a promising tool for clinical diagnostics. Here, breath biomarkers for obstructive sleep apnea (OSA) were validated in a larger and broader cohort of patients confirming the previously stated association between breath levels of these metabolites and the severity of the disease. These findings suggest that breath analysis by SESI-HRMS may

add a substantial objective value, especially for OSA screening, and bring SESI-HRMS a step closer to its clinical application.

By analyzing breath, it was possible to unravel metabolic processes related to sleep architecture and obstructive sleep apnea, while the metabolic profiling of blood provided insights into the connection between circadian clocks and metabolism. An elongating effect on the circadian period length was observed for a range of metabolic factors in serum from metabolically unhealthy obese patients. The combination of the molecular information provided by HRMS and results from genome-wide association revealed insulin resistance as central aspect of this association.

In contrast to humans, arctic species, such as Norwegian reindeer, have always been exposed to seasonally occurring conditions of constant light. Therefore, they might have developed strategies to cope with this reoccurring circadian disruption. In the scope of this thesis circadian regulation of metabolism in arctic reindeer was investigated in combination with their behavior across all seasons. In contrast their activity patterns, metabolism in reindeer was not synchronized with the experienced light schedule. While less rhythmic metabolites were found during constant light in summer, a surprisingly high number of metabolites displayed circadian rhythms in winter. These findings suggest that reindeer have developed mechanisms to decouple circadian regulation of metabolism from behavioral rhythmicity.

In conclusion, this thesis demonstrates the value of breath analysis and the versatility of high-resolution mass spectrometry for the field of metabolomics. By using this technique, metabolic processes related to sleep and circadian clocks were unraveled and the diagnostic value of metabolic profiling in exhaled breath by SESI-HRMS was further validated.

# Zusammenfassung

Die meisten physiologischen Prozesse im Menschen werden durch die sogenannte zirkadiane oder innere Uhr mit der Umgebung synchronisiert. Solche molekularen Schrittmacher sind in fast jeder Zelle des Körpers vorhanden. Licht ist zwar der wichtigste Zeitgeber für die innere Uhr, aber auch andere Stimuli, wie zum Beispiel Nahrungsaufnahme oder Ruhe-/Aktivitätszyklen können die Uhr beeinflussen. Schlaf ist nicht nur ein von der zirkadianen Uhr bestimmter Prozess, sondern gleichzeitig ein davon unabhängig regulierter, erholfördernder neurobiologischer Prozess. Sowohl die innere Uhr als auch Schlaf sind eng mit dem menschlichen Stoffwechsel verflochten, und eine Beeinträchtigung beider Prozesse geht mit negativen Auswirkungen auf die Gesundheit einher. Diese äussern sich beispielsweise durch das Auftreten von Typ-2-Diabetes, metabolischem Syndrom, Adipositas oder Herz-Kreislauf-Erkrankungen. Da Schlafmangel und Unterbrechungen des Tagesrhythmus in einer modernen, rund um die Uhr funktionierenden Gesellschaft weitverbreitet sind, stellen ihre negativen Folgen einige wichtige Herausforderungen für das aktuelle Gesundheitswesen dar. Trotz eindeutiger wissenschaftlicher Belege für einen bestehenden Zusammenhang zwischen Schlaf, zirkadianen Uhren und dem Stoffwechsel sind jedoch viele Aspekte dieser Interaktionen noch wenig erforscht.

In dieser Arbeit wurden mit modernster hochauflösender Massenspektrometrie (HRMS) neue Einblicke in Stoffwechselforgänge im Zusammenhang mit Schlaf und zirkadianen Uhren gewonnen. Die Kombination von hoher Auflösung und hoher Massengenauigkeit ermöglicht die Analyse komplexer Stoffgemische und liefert zudem Informationen über deren molekulare Zusammensetzung. HRMS ist daher ein leistungsstarkes Werkzeug für eine möglichst umfassende Analyse von Stoffwechselprodukten (Metabolomik). Hier wurden zwei verschiedene HRMS-Methoden verwendet: Metabolite in der Atemluft wurden in Echtzeit mittels hochauflösender Sekundärelektrospray-Ionisations-Massenspektrometrie (SESI-HRMS) gemessen, zur Analyse von Blutproben wurde Elektrospray-Ionisations-Massenspektrometrie mit Ultra-Hochleistungs-Flüssigkeitschromatographie gekoppelt. Während SESI-HRMS die Untersuchung systemischer Stoffwechselprozesse auf nicht-invasive Weise und mit nahezu unbegrenzter Probennahmefrequenz ermöglichte, konnten durch den zusätzlichen Trennungsschritt bei der Kopplung mit Chromatographie chemischen Verbindungen eindeutiger identifiziert werden. Im Rahmen der vorliegenden Arbeit wurde für die Analyse von Atemluft von Schlafenden ein Versuchsaufbau mittels SESI-HRMS entwickelt. Dieser ermöglichte eine bislang beispiellose simultane Überwachung vieler verschiedener Stoffwechselforgänge während des Schlafs mit einer zeitlichen Auflösung von zehn Sekunden. Es zeigte sich, dass bei Übergängen zwischen verschiedenen Schlafphasen

schnelle und reversible Veränderungen in Hauptstoffwechselwegen stattfinden. Diese komplexe Orchestrierung von Stoffwechsel und Schlafarchitektur könnte für die menschliche Gesundheit und Leistungsfähigkeit von höherer Relevanz sein als bislang angenommen.

Da SESI-HRMS nicht invasiv ist und Echtzeit-Informationen liefert, ist die Technologie auch für die klinische Diagnostik von grossem Interesse. In dieser Arbeit wurden Biomarker für obstruktive Schlafapnoe (OSA) validiert, indem die Atemluft einer größeren und breiteren Patientenkohorte analysiert wurde. Auf diese Weise konnte der zuvor bei einer kleinen Gruppe festgestellte Zusammenhang zwischen der Menge dieser Stoffwechselprodukte in der Atemluft und dem Schweregrad der Erkrankung bestätigt werden. Die Ergebnisse deuten darauf hin, dass die Atemanalyse mittels SESI-HRMS insbesondere zur Früherkennung von OSA eine bedeutende objektive Diagnosegrundlage beisteuern könnte. Durch diese erstmalige Validierungsstudie wurde SESI-HRMS ihrer klinischen Anwendung einen entscheidenden Schritt näher gebracht.

Während mittels Atemanalyse neue Erkenntnisse zu Stoffwechselprozessen im Zusammenhang mit Schlaf und Schlafapnoe gewonnen werden konnten, lieferte die Analyse von Metaboliten in Blutproben neue Einblicke in den Zusammenhang zwischen Stoffwechsel und zirkadianen Uhren. Für eine Reihe von Metaboliten in Blutproben adipöser Patienten wurde ein verlängernder Effekt auf die zirkadiane Periode festgestellt. Die Kombination der von der HRMS gelieferten molekularen Informationen mit den Ergebnissen einer genomweiten Assoziationsstudie ergab, dass Insulinresistenz hier eine zentrale Rolle spielt.

Während beim Menschen Verschiebungen des Tagesrhythmus mit gesundheitlichen Problemen einhergehen, waren arktische Spezies wie zum Beispiel das Norwegische Rentier schon immer saisonal auftretenden Bedingungen mit konstantem Licht ausgesetzt. Daher könnten solche Arten interessante Strategien entwickelt haben, um mit der immer wieder auftretenden Veränderung des Tagesrhythmus umzugehen. Im Rahmen dieser Arbeit wurde deshalb die zirkadiane Regulierung des Stoffwechsels bei arktischen Rentieren sowie deren Verhalten über alle Jahreszeiten hinweg untersucht. Während die Verhaltensmuster den Lichtverhältnissen folgten, zeigten Metaboliten in allen Jahreszeiten zirkadiane Rhythmen, und das in besonderem Masse bei konstanter Dunkelheit im Winter. Besonders viele wurden überraschenderweise bei konstanter Dunkelheit im Winter beobachtet. Diese Ergebnisse deuten darauf hin, dass die Rentiere Mechanismen entwickelt haben, um die zirkadiane Kontrolle des Stoffwechsels von ihren Verhaltensmustern zu entkoppeln.

Insgesamt demonstriert die vorliegende Arbeit die Bedeutung und die vielseitigen Einsatzmöglichkeiten der hochauflösenden Massenspektrometrie für das Gebiet der Metabolomik. Mit Hilfe dieser Technik konnten hier zum einen mit Schlaf und zirkadianen Rhythmen einhergehende Stoffwechselprozesse nachgewiesen werden und zum anderen wurde der Wert der Atemanalyse mittels SESI-HRMS für die klinische Diagnostik bestätigt.

# Contents

<b>Abstract</b>	<b>iii</b>
<b>Zusammenfassung</b>	<b>v</b>
<b>1. Circadian clocks, sleep and metabolism</b>	<b>1</b>
1.1. Introduction . . . . .	3
1.2. The circadian clock . . . . .	3
1.2.1. Clock molecules and circuits . . . . .	3
1.2.2. The circadian clock and metabolism . . . . .	5
1.2.3. Pathophysiology related to the circadian clock and metabolism . . . . .	8
1.3. Sleep . . . . .	10
1.3.1. Sleep architecture and regulation . . . . .	10
1.3.2. Sleep molecules and circuits . . . . .	11
1.3.3. Sleep and metabolism . . . . .	11
1.3.4. Pathophysiological consequences of Impaired sleep . . . . .	15
1.4. Clocks or sleep: perspectives . . . . .	17
<b>2. Aims and outline of this thesis</b>	<b>19</b>
<b>3. Experimental techniques for the investigation of sleep, circadian rhythms and metabolism</b>	<b>23</b>
3.1. Polysomnography . . . . .	24
3.2. Bioluminescence assay for clock gene expression in fibroblasts . . . . .	24
3.3. Metabolomics based on mass spectrometry . . . . .	25
3.3.1. High-resolution mass spectrometry . . . . .	25
3.3.2. Blood metabolomics using UPLC-MS . . . . .	29
3.3.3. Breath metabolomics using SESI-MS . . . . .	30
<b>4. Rapid and reversible control of human metabolism by individual sleep states</b>	<b>33</b>
4.1. Introduction . . . . .	35
4.2. Methods . . . . .	36
4.2.1. Study participants . . . . .	36
4.2.2. SESI-HRMS measurements during sleep . . . . .	38
4.2.3. Polysomnography . . . . .	38

---

4.2.4.	Data preprocessing . . . . .	39
4.2.5.	Statistics . . . . .	39
4.2.6.	Pathway enrichment analysis and compound identification . . . . .	40
4.2.7.	Blood breath comparison experiments . . . . .	41
4.3.	Results . . . . .	44
4.3.1.	Breath analysis during sleep . . . . .	44
4.3.2.	Sleep stage-specific metabolic patterns . . . . .	44
4.3.3.	Immediate metabolic regulation . . . . .	44
4.3.4.	Pathway mapping of MS features . . . . .	49
4.3.5.	Sleep stages control axes of metabolism . . . . .	49
4.4.	Discussion . . . . .	52
4.5.	Conclusion . . . . .	57
<b>5.</b>	<b>Validation of breath biomarkers for obstructive sleep apnea</b>	<b>59</b>
5.1.	Introduction . . . . .	61
5.2.	Methods . . . . .	62
5.2.1.	Study participants . . . . .	62
5.2.2.	SESI-HRMS measurements . . . . .	64
5.2.3.	Data preprocessing . . . . .	64
5.2.4.	Statistical analysis . . . . .	64
5.2.5.	Classification procedure . . . . .	65
5.2.6.	Attempts of improvement of classification performance . . . . .	65
5.3.	Results . . . . .	65
5.3.1.	Study design and patient characteristics . . . . .	65
5.3.2.	Metabolic patterns in exhaled breath associated with OSA . . . . .	67
5.3.3.	Significant differences in metabolic breath patterns between OSA patients and individuals without OSA . . . . .	67
5.3.4.	Association between disease severity and breath signal intensity . . . . .	67
5.3.5.	Association between sleepiness and breath signal intensity . . . . .	71
5.3.6.	Classification . . . . .	71
5.4.	Discussion . . . . .	71
5.5.	Conclusion . . . . .	78
<b>6.</b>	<b>Multi-omics correlates of insulin signaling and circadian function</b>	<b>79</b>
6.1.	Introduction . . . . .	81
6.2.	Methods . . . . .	82
6.2.1.	Participant characteristics and study design . . . . .	82
6.2.2.	Harvesting of sera . . . . .	83
6.2.3.	Primary dermal fibroblast culture, in vitro synchronization and DNA extraction . . . . .	83
6.2.4.	Lentivector production . . . . .	83
6.2.5.	U2OS cell culture, in vitro synchronization and real-time bioluminescence recording . . . . .	83
6.2.6.	Metabolomics by UPLC-MS . . . . .	84

---

6.2.7.	Statistical analysis . . . . .	87
6.2.8.	Metabolic pathway analysis and compound annotation . . . . .	87
6.2.9.	Genotyping . . . . .	88
6.2.10.	Genome wide association analysis . . . . .	88
6.3.	Results . . . . .	90
6.3.1.	Study design . . . . .	90
6.3.2.	Circadian period length increases with severity of obesity . . . . .	92
6.3.3.	Branched-chain amino acid pathway activity associated with circadian period elongation . . . . .	92
6.3.4.	March1 as genetic origin of the link between serum composition and period length in obese subjects . . . . .	94
6.4.	Discussion . . . . .	96
6.5.	Conclusion . . . . .	97
<b>7.</b>	<b>Understanding metabolic effects of seasonal light schedules in arctic reindeer</b>	<b>101</b>
7.1.	Introduction . . . . .	103
7.2.	Methods . . . . .	104
7.2.1.	Animals . . . . .	104
7.2.2.	Actigraphy . . . . .	105
7.2.3.	Catheterization and skin biopsy under anesthesia . . . . .	106
7.2.4.	Primary fibroblast culture from skin biopsy . . . . .	106
7.2.5.	Bioluminometry of Bmal1 expression in reindeer skin fibroblasts . . . . .	107
7.2.6.	Blood metabolomics . . . . .	108
7.2.7.	Data analysis . . . . .	110
7.2.8.	Metabolic pathway enrichment analysis and compound annotation . . . . .	111
7.3.	Results . . . . .	111
7.3.1.	Study design . . . . .	111
7.3.2.	Circadian behavior in spring, autumn and winter . . . . .	112
7.3.3.	Metabolism under circadian control in spring, autumn and winter with high inter-individual variability . . . . .	112
7.3.4.	Phase and amplitude distribution of circadian metabolic features . . . . .	115
7.3.5.	Metabolic pathway enrichment analysis reveals consistent circadian regulation of certain pathways across the whole year . . . . .	121
7.4.	Discussion . . . . .	121
7.5.	Conclusion . . . . .	124
<b>8.</b>	<b>Conclusions and outlook</b>	<b>125</b>
	<b>References</b>	<b>131</b>
	<b>Appendices</b>	<b>157</b>
<b>A.</b>	<b>Abbreviations</b>	<b>159</b>

<b>B. Supplementary information</b>	<b>163</b>
B.1. Rapid and reversible control of human metabolism by individual sleep states	164
B.1.1. Inferring nonlinear Granger causality with neural networks . . . . .	164
B.1.2. Supplementary figures . . . . .	169
B.1.3. Supplementary tables . . . . .	174
B.2. Validation of breath biomarkers for obstructive sleep apnea . . . . .	176
B.2.1. Supplementary results . . . . .	176
B.2.2. Supplementary discussion . . . . .	176
B.2.3. Supplementary figures . . . . .	177
B.2.4. Supplementary tables . . . . .	188
B.3. Multi-omics correlates of insulin signaling and circadian function . . . . .	193
B.3.1. Supplementary figures . . . . .	193
B.3.2. Supplementary tables . . . . .	195
B.4. Understanding metabolic effects of seasonal light schedules in arctic reindeer	199
B.4.1. Supplementary tables . . . . .	199
 <b>C. Scientific contributions</b>	 <b>201</b>
 <b>D. Curriculum vitae</b>	 <b>205</b>



# 1

Circadian clocks, sleep and metabolism

This chapter is adapted from:

Nora Nowak\*, Audrey Rawleigh\*, Steven A. Brown, CIRCADIAN CLOCKS, SLEEP AND METABOLISM. In: Circadian clock in brain health and illness. Advances in Experimental Medicine and Biolog. Springer, Cham. *Manuscript submitted for publication.*

\* These authors contributed equally to this work

## 1.1. Introduction

Modern society has allowed humans easy access to light, food, transportation, and entertainment, twenty-four hours per day. Perhaps, increased productivity and hedonistic pleasure has resulted, but also increased shift work, social jetlag, sleep loss, and an epidemic of obesity, type 2 diabetes (T2D), and associated metabolic syndrome.<sup>1-3</sup> At the same time, there has also been an increase in other aspects of pathology such as psychological disorders, cancers, immune system dysregulation, and gastrointestinal diseases.<sup>4-7</sup> In this chapter, we focus on the relationship between circadian clocks, sleep, and metabolism, and the consequences of these connections for modern health. The circadian clockwork, the sleep homeostat, and their regulatory networks have been studied considerably throughout the past decades, and there has also been extensive work tying each of these processes to metabolism. Despite this, very few studies exist that focus on the interplay between circadian and sleep processes in terms of metabolic regulation, function, and pathology. We propose that by looking through the lenses of both chronobiology and sleep science together, fresh insights may be found which will further the understanding and development of novel strategies for metabolic health.

## 1.2. The circadian clock

### 1.2.1. Clock molecules and circuits

#### 1.2.1.1. The molecular pacemaker

A circadian clock temporally controls virtually every aspect of the cellular function, including energy balance, macromolecular synthesis, and signaling. Circadian mechanisms and outputs have been reviewed elsewhere previously,<sup>8,9</sup> and we outline briefly only the main transcriptional mechanism for this review. At the core of the molecular clock in mammals are two transcriptional-translational feedback loops in which the protein products inhibit their own transcription (figure 1.1). Conventionally, this mechanism is separated into two “limbs”. In the positive limb, circadian locomotor output cycles kaput protein (CLOCK) and aryl hydrocarbon receptor nuclear translocator-like protein 1 (BMAL1), form heterodimers that bind to cis-acting DNA elements (E-boxes) to activate transcription of *Period* (*Per1-3*) and *Cryptochrome* (*Cry1-2*) genes, which are translated into proteins in the cytoplasm. These proteins form the negative limb, in which PER and CRY proteins then are transported from the cytoplasm to the nucleus and inhibit their own transcription. These positive and negative limbs are further interwoven by a connected molecular circuit in which the gene encoding the nuclear orphan receptor REV-ERB $\alpha$  is induced by CLOCK/BMAL1, and REVERB $\alpha$  itself is a transcriptional repressor of *Bmal1* while other nuclear receptors binding the same site (RORs) activate it.

#### 1.2.1.2. The master pacemaker

It is thought that virtually every mammalian cell possesses a clock of its own.<sup>10</sup> In mammals, a master pacemaker is necessary to keep all of these clocks synchronously tracking geophysical time; this is the job of the suprachiasmatic nucleus (SCN). The SCN are bilateral nuclei

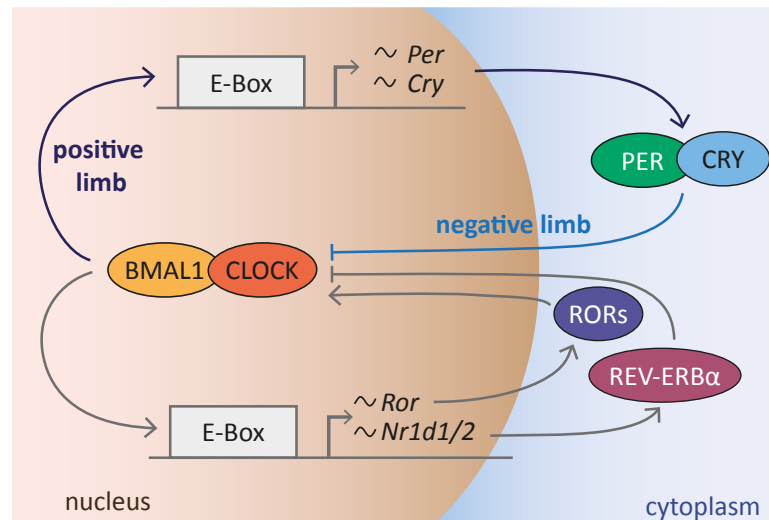


**Figure 1.1.:** Circadian rhythms in clock proteins are driven by the molecular feedback loop, which allows for a 24-hour period length in protein expression. In the positive arm CLOCK and BMAL1 bind to the E-box which drives expression of PER and CRY. In the negative arm, PER and CRY inhibit CLOCK and BMAL1 from binding DNA, which leads eventually to a reduction of PER and CRY levels. The positive arm restarts once levels of PER and CRY are low enough to allow binding of CLOCK and BMAL1 to DNA again. Additional loops such as REV-ERB $\alpha$  regulating Bmal1 expression or modifications via Casein Kinase 1 (CK1d,e) fine-tune and strengthen oscillations. Expression of additional clock controlled genes (CCGs) which function in numerous cell processes, are also driven by circadian clock genes.

of about 20,000 neurons located in the hypothalamus of the brain. They integrate time of day and environmental lighting cues via input received from the eyes via the retinohypothalamic tract,<sup>11</sup> and via a web of direct and indirect cues then coordinates all cellular clocks in the body.<sup>12</sup> Each cell of the SCN has an autonomous clock, and these clocks are coupled together via synaptic connections, gap junctions, and neuropeptidergic signaling to create a precisely oscillating entity.<sup>8</sup> In turn, the SCN synchronizes body clocks through electrical and endocrine mechanisms, food timing and body temperature, and various other signaling pathways to peripheral cells.<sup>13</sup> Studies have shown that the sleep-wake cycle, activity, and feeding behavior are under the control of the SCN, as well as hormone secretions and many other aspects of physiology.<sup>14</sup>

### 1.2.1.3. Peripheral clocks

Peripheral clocks refer to any cellular or organ clock outside of the SCN, including elsewhere in the brain. Peripheral clocks are capable of integrating phase information with respect to a stimulus (either at a cellular or organ level), and integrating this information to time output – generally at a clock phase slightly later than in SCN, as demonstrated nicely in young male baboons.<sup>15</sup> One example of this is glucocorticoid signaling. Via the hypothalamic-pituitary-adrenal axis, the SCN triggers the release of glucocorticoids from the adrenal glands in a time-of-day-dependent manner.<sup>16</sup> Once released into the blood stream, glucocorticoids act as a Zeitgeber (German for “time giver”) to peripheral clocks by inducing clock gene expression, which in turn alters oscillations in these cells. Importantly, the SCN is not the only Zeitgeber

for peripheral clocks. For example, transcription in the liver is not only driven by the clock, but also by the timing of food intake.<sup>17</sup> When food is consistently given at an abnormal time, the peripheral clocks become uncoupled from the central ones.<sup>18</sup> It is likely that a diversity of similar cues exist, providing avenues by which different signals such as metabolic and immune state might influence circadian timing. Thus, although the circadian clock circuitry itself is cell-autonomous and robustly self-sustained, nevertheless it is systemically coordinated across cells and tissues. Even in the absence of SCN, experimental models show that clocks in different organs retain coherence via signals that are currently unknown.<sup>19</sup>

## 1.2.2. The circadian clock and metabolism

One of the primary functional outputs of the circadian clock is metabolic regulation: virtually all aspects of metabolism exhibit daily oscillations, which persist even in constant environmental conditions.<sup>8</sup> Recently, there has been a growing interest about the interplay between metabolism and the circadian clock, and for compelling reasons. The circadian clock exercises its metabolic control at every level of physiology from individual cells to the organism as a whole, but at the same time metabolic state can influence circadian timing. This regulation may be thought of as the clock anticipating and preparing the body so that it can respond in a timely manner to predictable stimuli, such as feeding. In turn, the timing of such stimuli can feed back to affect clock time and refine such prediction. In this section, the ways in which the circadian clock impacts metabolic processes and regulation will be broken up into four main categories: cellular control, system-wide or organ-specific control, neuronal or central control, and behavioral control.

### 1.2.2.1. Cellular control

There is an overwhelming amount of evidence that supports the coordination of cellular energy metabolism by the circadian clock. Some examples of how the clock exercises its metabolic control include, but are not limited to: regulation of transcription and metabolite levels<sup>20–22</sup> integration of nutrient sensors and nuclear receptors with the circadian clock,<sup>23–25</sup> and mitochondrial respiration.<sup>26</sup> A diversity of mechanisms have been elucidated to explain this extensive control.

At the level of transcription, it has been reported that around 10% of transcripts in any given tissue are regulated in a circadian manner. A significant portion of these in all tissues relate to metabolic function.<sup>15</sup> In individual cellular compartments, this proportion can be even higher. For example, 67% of synaptic mRNA display biphasic circadian oscillations, and the peak preceding dawn is entirely related to metabolism and mitochondrial function.<sup>27</sup>

An example of a post-translational modification under clock control is seen in mitochondrial bioenergetics and morphology. Daily rhythms in mitochondrial fission is dependent on the circadian phosphorylation of DRP1 and this in turn controls cellular oxygen consumption and ATP levels, as they correlate with the morphological state of mitochondria.<sup>26</sup> Phosphorylation control of circadian metabolism is by no means limited to mitochondrial function. A study of liver circadian phosphoproteomics revealed control of most major cellular signaling pathways,<sup>28</sup> thereby regulating both cellular energetics and xenobiotic metabolism in

rhythmic fashion. Lipid levels also show dynamic circadian regulation. One study looked at temporal dynamics in membrane lipids of the nucleus and mitochondria of the mouse liver, and found that lipid species regulation is driven by feeding time and the circadian clock.<sup>29</sup> Another study demonstrated that circadian variations in lipid metabolites are independent of feeding, because they also occur in cultured myotubes. This suggests cell-autonomous regulation in diurnal lipid profiles, and this control was dependent upon the local circadian clock in these cells.<sup>30</sup>

Broadly speaking, multiple cellular circuits have been characterized that at least partially explain widespread circadian control of metabolism. Glucocorticoid hormone-dependent gene expression certainly explains a portion of this control. It was also found that CRY1 and 2 repress glucocorticoid receptor activation, adding an additional layer of complexity in this regulation.<sup>31</sup>

Another major axis is the level of redox cofactors such as NAD<sup>+</sup> and NADH. This control occurs through circadian clock regulation of the rate-limiting enzyme nicotinamide phosphoribosyltransferase, a key enzyme within the NAD<sup>+</sup> salvage pathway.<sup>21</sup> An additional important pathway in the circadian regulation of metabolism centers around AMP-Dependent Protein Kinase (AMPK), which regulates ATP production.<sup>32</sup> Additionally, the circadian clock protein BMAL1 not only plays a crucial role in circadian transcription, but also in translation and coupling the mTOR signaling pathway to the circadian clock.<sup>33</sup> Finally, clock proteins can also act together with factors that modify chromatin, thereby globally orchestrating transcriptional activation and repression across families of related genes. These chromatin modifying factors include histone acetylases and deacetylases, methyltransferases and demethylases, and nucleosome remodeling complexes, among others.<sup>8,34</sup> For example, the sirtuin class of histone deacetylases is regulated in circadian fashion via its NAD cofactor,<sup>20,24</sup> and circadian transcriptional regulation of the deacetylase HDAC3 and the REV-ERB and ROR transcription factors controls a large swath of fatty acid metabolism.<sup>35</sup> Another clock protein, PER2, coregulates nuclear receptor-mediated transcription through its interaction with PPAR $\alpha$  and other nuclear hormone receptors.<sup>23</sup> Importantly, for each of these mechanisms feedback control from metabolic state to circadian clock function has also been characterized. Levels of NAD<sup>+</sup> also control the deacetylation of the clock protein PER2,<sup>24</sup> and AMPK is able to phosphorylate the cryptochrome circadian proteins.<sup>32</sup> Thus, redox and cellular energetics can directly influence the core transcription-translation feedback loop that drives the circadian clock.

A second, more speculative class of control occurs via possible “non-canonical” circadian timing mechanisms based entirely on post-translational idioms. Although a post-translational circadian clock mechanism is well-established in bacteria,<sup>36</sup> so far it has been documented in mammalian cells for only a limited family of redox enzymes (peroxiredoxins), and operates via an unknown mechanism.<sup>37,38</sup> Nevertheless, given recently reported widespread circadian control of metabolism in mammalian cells and tissues genetically modified to destroy the “canonical” mechanism, it is possible that post-translational clock mechanisms provide important additional layers of control.

### 1.2.2.2. Organ-specific control

The circadian clock coordinates peripheral tissues so that they are able to carry out appropriate metabolic responses. One way this is carried out is through clock-controlled genes (CCGs), which regulate various tissue-specific functions in different tissues or organs.<sup>39</sup> For example, gluconeogenesis and glycogenolysis are promoted in the liver during sleep (fasting time) and glycogen/cholesterol synthesis are promoted during wake (feeding time). Examining the liver metabolome, amino acids, carbohydrates, nucleotides, lipids, cofactors, vitamins, and xenobiotics all display rhythmicity under the control of the circadian clock transcriptional machinery.<sup>20</sup> Similarly, the circadian clock is of imperative importance in regulating glucose sensing and insulin secretion in the pancreas, and loss of these clocks (even specifically in  $\beta$ -cells) leads to glucose intolerance.<sup>40,41</sup> Another important peripheral clock for mammalian metabolism is adipose tissue. Adipocytes store energy as triglycerides when the body has an excess. They also act as a regulator of triglycerides in the blood stream, and this regulation is compromised when adipocytes lack a functional clock and results in obesity and a defect in the adipocyte-hypothalamic axis.<sup>42</sup> Finally, circadian rhythms in human skeletal myotubes have been reported to have self-sustained rhythms *in vitro*, and skeletal muscle in general plays a massive role in whole body glucose homeostasis as it is the principal organ responsive to insulin. The circadian clock might also be implicated in muscle myokine secretion, which is also important in glucose homeostasis.<sup>43</sup>

As mentioned earlier, for circadian rhythms in all of these peripheral tissues, the SCN is not the only Zeitgeber. Timing of food intake can also entrain peripheral clocks, and in mammals is even dominant to light after about a week of timed feeding. Indeed, the majority of oscillating mouse liver gene expression was recently found to be controlled by rhythmic food intake.<sup>44</sup> When the timing of food intake was arrhythmic more than 70% of cycling genes lost rhythmicity.<sup>44</sup> The pancreas also shifts its clock time along with the liver, heart, kidney, and muscle in response to feeding in the inactive period.<sup>18</sup> The mechanisms by which food or feeding entrains peripheral circadian clocks have not yet been fully elucidated, but likely includes a variety of cues including temperature<sup>45</sup> and redox state.<sup>46</sup> Post-transcriptional mechanisms likely play an important role: for example, the circadian-implicated RNA-binding protein non-POU domain-containing octamer-binding protein (NONO), which regulates the pre-mRNA processing of liver circadian genes in response to glucose,<sup>47</sup> or poly-ADP ribosyl-transferase, which modifies clock factors in NAD<sup>+</sup>-dependent manner.<sup>48</sup>

### 1.2.2.3. Central control by activity and behavioral

At the level of the whole organism, glucocorticoid hormones, insulin, and appetite hormones play key roles in the regulation of rhythms in activity and behavior.<sup>8</sup> It has been proposed that the molecular circadian clock acts as a metabolic rheostat, and circadian regulation of glucose metabolism has been extensively reviewed.<sup>49</sup> More broadly, however, the control of feeding behavior and metabolism by hypothalamic circuits themselves play an essential part in the circadian control of metabolism.<sup>50</sup> Glucocorticoid hormones, whose secretion is commanded by the hypothalamic-pituitary-adrenal axis, have been discussed earlier in this chapter. Glucocorticoids show daily oscillations, ultradian rhythms, and are also secreted in response to acute stress,<sup>51</sup> playing a major circadian role in anticipating metabolic requirements im-

posed by food intake.<sup>52</sup> An additional facet is provided by appetite itself, which is also clock-controlled and in human peaks in the evening before sleep and fasting, as opposed to in the morning following an extended fasting period.<sup>53</sup> Some of the main hormones at play here include leptin, ghrelin, cholecystokinin, and insulin. Leptin is released mainly from adipocytes and binds to its receptor in the hypothalamus; this signaling is essential for this hormone's suppressive effects on feeding.<sup>54</sup> It has been proposed that obesity and leptin resistance can disrupt circadian regulation, as well as the reverse.<sup>54</sup> It was recently established in mice that the clock of energy-sensing AgRP neurons mediates transcriptional responses to leptin to help align appetite behaviors to the sleep-wake cycle.<sup>55</sup> Ghrelin, an orexigenic peptide hormone essential for appetite stimulation, has recently been found to oscillate in humans.<sup>56</sup> This hints at a neuroendocrine mediated circadian variation in hunger, perhaps involving the entrainment of the stomach cells which secrete ghrelin.<sup>56</sup> Further information regarding the circadian regulation of appetite behavior with respects to nutrient state and sleep-wake behavior has recently been reviewed.<sup>57</sup>

### 1.2.3. Pathophysiology related to the circadian clock and metabolism

Disruption to the circadian clock – for example via sleep deprivation, jetlag, or diet – can have numerous negative effects on the circadian coordination of metabolic systems.<sup>58</sup> Some examples relevant to human disease include, but are certainly not limited to cancer and tumor development, obesity and related comorbidities, death rate from cardiovascular disease and stroke, disrupted menstrual cycles, night time asthma, abnormal cortisol rhythm in Cushing's syndrome, and some psychiatric disorders.<sup>59–62</sup> Metabolic syndrome describes an increased risk of diabetes, stroke, and heart disease due to a collection of risk factors such as obesity, high blood sugar, cholesterol, and high blood pressure.<sup>8</sup> The link between metabolic syndrome and associated metabolic diseases with circadian dysfunction has been evident since it was found that mice with a deficient clock gene have obesity and metabolic syndrome including hyperleptinemia, hyperlipidemia, hepatic steatosis, hyperglycemia, and hypoinsulinemia.<sup>63</sup> The interplay and cross-talk between the circadian clock and metabolism has been reviewed recently and often, and it is important to note that is it a reciprocal relationship.<sup>46</sup>

A simple example to illustrate the importance of the clock to metabolism was demonstrated in a study where high-fat food was fed to mice at either a normal or an inappropriate circadian time. The mice who received food at an inappropriate time (the inactive phase) gained significantly more fat than mice fed at a normal time.<sup>64</sup> Conversely, when feeding is restricted to a normal time (the active phase), it promotes synchrony with circadian rhythms and actually prevents obesity.<sup>65</sup> In normal or homeostatic conditions, metabolic physiology is driven by the clock.<sup>58</sup> However, when shift work or high-fat feeding for example disrupts either system, this disruption in metabolic pathways leads to dampening and lengthening of circadian oscillations.<sup>66</sup> There is also evidence that the correct timing of eating applies also to humans, and has recently been reviewed.<sup>67</sup> Such approaches might help in the prevention or treatment of obesity, diabetes, metabolic syndrome, and many other metabolic dysregulations, although more long-term and large-scale clinical trials are necessary to clarify and optimize this treatment potential.

Research over the past decade has placed circadian dysfunction as a strong possible con-



tributor to diabetic pathology. Normally, pancreatic  $\beta$ -cell located in the islets of Langerhans operate to secrete insulin in response to food intake, and abnormalities such as a reduction in  $\beta$ -cell mass is considered to be the main cause of T2D.<sup>68</sup> However, defects in islet function are also linked to circadian clock perturbations, since the  $\beta$ -cell clock coordinates transcription and eventual insulin release.<sup>40</sup> The intrinsic clock regulates many cellular processes that are crucial to normal  $\beta$ -cell function including glucose-sensing, substrate metabolism, mitochondrial function, stress response, and insulin secretion via exocytosis and proliferation.<sup>69</sup> In reverse, circadian period length in cells from human diabetic subjects is inversely correlated with HbA1c values, a measure of chronic blood sugar levels and hence diabetic severity.<sup>70</sup>

Long-term epidemiological studies have shown that prolonged desynchrony between circadian clock and environment is demonstrably deleterious not only to metabolic syndrome and diabetes,<sup>71</sup> but also to many other aspects of health. Chronic jet lag is associated with increased risk of cancer.<sup>61,72</sup> Shift work in nursing is one of the most prevalent examples of circadian misalignment and internal desynchrony. It is known that shift work is associated with metabolic syndrome and cancer.<sup>73,74</sup> Mechanistically, night shift work affected gene expression in peripheral blood mononucleated cells and circadian alignment in core body temperature, peak cortisol, and melatonin onset compared to day shift work,<sup>75</sup> suggesting that shiftwork might lead to circadian desynchrony among internal organs. Metabolomics studies of simulated shiftwork have provided further evidence for this idea.<sup>76,77</sup> It has also been shown that the gut microbiota play a key role in this equilibrium. When gut microbiota were eradicated via antibiotics, these mice did not develop obesity or glucose intolerance,<sup>78</sup> suggesting that they were spared at least some aspects of metabolic syndrome. Thus, the ill effects of circadian desynchrony might also be a problem of dysbiosis.

Recent studies have suggested that even simple chronotype – an individual's timing in their sleep-wake schedules and circadian physiology – may affect metabolic health in fundamental ways. Morning-types have earlier timing and evening-types have a later timing in their circadian and sleep-wake physiology, and most people fall somewhere in between these two groups. Surprisingly, one study found that evening types are more prone to diabetes, metabolic syndrome, and sarcopenia (the loss of skeletal muscle mass and strength with aging).<sup>79</sup> A second study found that an evening chronotype is associated with diabetes and also a greater all-cause mortality and cardiovascular disease mortality.<sup>80</sup> Even for “normal” chronotypes, weekend schedules often differ significantly from weekday ones due to social activities and obligations, a phenomenon called “social jetlag”. This creates a shift every week, which disrupts both the circadian and sleep systems. In rats it was found that social jet lag altered cholesterol, elevating the risk of metabolic syndrome and increasing appetite for fat-rich and carbohydrate heavy food.<sup>81</sup> It has also been suggested that people with evening chronotypes who work regular hours during the week are at an increased risk of social jet lag and T2D since their endogenous schedule is later.<sup>82,83</sup> Thus, awareness of one's chronotype could be one strategy to preventively combat metabolic disorders, for example by adjusting daily schedules.

Overall, much has been discovered in the past few decades about how the circadian clock might contribute to health and disease. Above, we have discussed extensively how circadian rhythms might themselves be important for health. Equally important, however, and beyond the scope of this review are circadian effects upon drug delivery, due either to circadian

pharmacokinetic effects (daily changes in drug metabolism and excretion) or circadian pharmacodynamics (daily changes in target susceptibility). The same drug may be more effective when taken at one time of day, regardless if this was considered during the development of the drug, and many examples are included in another review.<sup>84</sup>

## 1.3. Sleep

Sleep is both one of the major outputs of the circadian clock and an important recuperative neurobiological process independently regulated and essential for health and well-being. However, distinct functions of sleep are still poorly understood and the question “Why do we need to sleep?” is difficult to answer. Nevertheless, there are several hypotheses about the functions of sleep. Apart from sleep acting as an important mechanism for brain plasticity and cognitive functions,<sup>85–87</sup> there are clear indications that sleep has a fundamental impact on metabolism.

### 1.3.1. Sleep architecture and regulation

In brief, mammalian sleep is categorized into different sleep stages based on types of cortical neural oscillations, and consists of cycles of alternating rapid-eye movement (REM) sleep and non-rapid eye movement (NREM) sleep. REM sleep is characterized not only by rapid eye movements, but also by a very low muscle tonus throughout the body. In contrast, brain activity during REM sleep is comparable with wakefulness, showing high frequency and low voltage waves. REM sleep occurs primarily during the second half of the night and it is associated with dreaming. NREM sleep, in contrast, occurs predominantly during the first half of the night and is characterized mainly by brain waves of lower frequency.<sup>88</sup> It is therefore also called slow wave sleep (SWS). Dreaming may also occur during NREM sleep. In humans, NREM sleep is further divided into N1, N2 and N3 sleep. N3 sleep is specified by high-amplitude brain waves of 0-3 Hz and is commonly referred to as deep sleep; N1 and N2 sleep are gradual transitions from wakefulness to deep sleep.

How does the brain control sleep and wakefulness? In broad theoretical terms, sleep-wake cycles are known to be driven by two main “processes”: a homeostatic process and a circadian one. Sleep propensity grows with increasing time awake. When it reaches an upper threshold, sleep onset occurs and at a lower threshold, awakening is induced. This hourglass-like mechanism defines the homeostatic process. However, the propensity levels sufficient to trigger wake and sleep vary with time of day: these thresholds are under circadian control. In this way, both circadian and homeostatic influences can contribute additively to sleep duration and intensity. SWS is well predicted by duration of wakefulness at all circadian phases, leading some to suggest that SWS is determined mostly by homeostatic factors.<sup>89,90</sup> Nevertheless, both REM and SWS is altered in mice lacking core clock genes, adding confusion to this picture.<sup>91,92</sup>

### 1.3.2. Sleep molecules and circuits

At a molecular level, in contrast to the circadian clock relatively little is known about the workings of the sleep homeostat. Early studies hypothesized that specific molecules (“somnogens”) might accumulate with time awake and thereby drive sleep.<sup>93</sup> Interestingly, one of these molecules, adenosine, is also a metabolic byproduct – a topic that we discuss below as a connection between sleep and metabolism. Although adenosine is well established to promote sleep and may accumulate in the brain during sleep deprivation,<sup>94</sup> nevertheless its possible role as the principal molecular “currency” of sleep need remains ambiguous. Beyond adenosine, various sleep-promoting as well as wake-promoting neurotransmitters have been identified. Examples of sleep-promoting molecules are gamma-aminobutyric acid (GABA), galanin, growth hormone releasing hormone (GHRH), and also cytokines. Wakefulness is promoted for example by acetylcholine, norepinephrine,<sup>95</sup> glutamate, histamine, serotonin, and orexins.<sup>95,96</sup> Recent studies have suggested that a general increase in phosphorylation of specific synaptic proteins might serve the same somnogenic function,<sup>97,98</sup> though this simple idea is complicated by the fact that other phosphorylations in the same proteins are also driven oppositely and in circadian fashion.<sup>99</sup> Other recent studies have focused upon the molecular determinants of sleep oscillations such as slow waves, and concluded that cortical potassium channels play key roles.<sup>100,101</sup> Transcriptional regulation, perhaps controlled via MAP kinase signaling, is likely also implicated.<sup>102</sup> Other yet unelucidated pathways likely exist. At a circuit level, a considerable amount is known about the control of sleep and wake. Origins of major sleep oscillations have been proposed. For example, although not the only mechanism to generate slow waves, a thalamocortical circuit certainly plays a major role.<sup>103</sup> More broadly, several brain nuclei mostly in the hypothalamus are involved in the regulation of sleep and wakefulness.<sup>104</sup> In the lateral hypothalamus, so-called arousal centers such as the tuberomammillary nucleus (TMN) and raphe nuclei send neurotransmitters to the cerebral cortex, promoting wakefulness. Closely connected to the arousal centers is the ventrolateral preoptic nucleus (VLPO), which counteracts them and thus promotes sleep. Switching between inactivation and activation of wake- and sleep-promoting nuclei regulates sleep and wakefulness<sup>105,106</sup> (figure 1.2). A similar “flip-flop” mechanism has been proposed for the switch between REM and NREM sleep involving the sublaterodorsal nucleus (SLD) and the ventrolateral part of the periaqueductal grey matter (vIPAG) in the brainstem.<sup>106</sup> A recent study suggests that two groups of neurons in the dorsomedial nucleus of the hypothalamus (DMH) project to the preoptic area and to the raphe pallidus area are involved in the REM sleep switch as well.<sup>107</sup>

### 1.3.3. Sleep and metabolism

Many of the molecules mentioned above as somnogens are also involved in the regulation of metabolic functions such as energy homeostasis, hormone regulation, and immune response. Brain regions controlling metabolic functions are also located close to sleep and arousal centers. This spatial arrangement makes it appear likely that neuronal circuits connecting both are an important link between sleep and its metabolic functions, a subject to which we turn next.

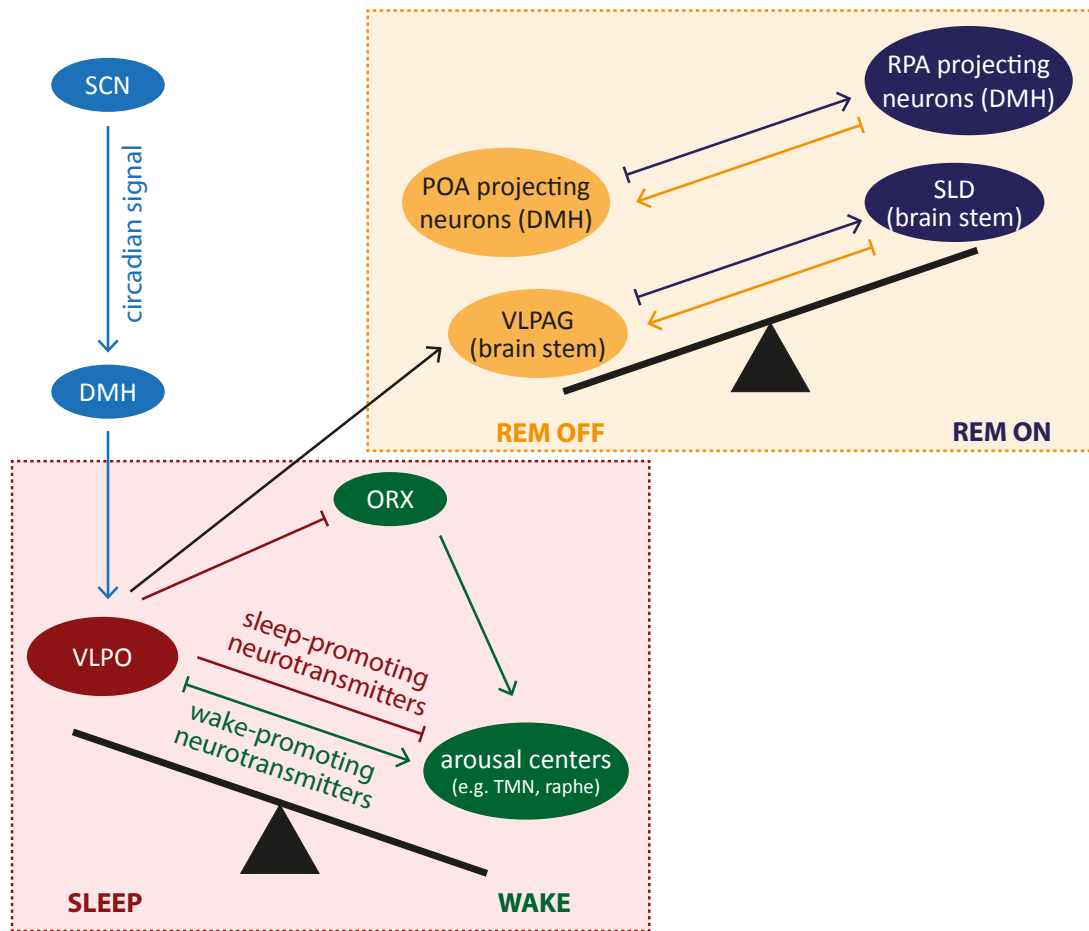


**Figure 1.2.:** Neuronal circuits in the brain involved in sleep regulation. Switching between sleep and wakefulness happens mostly in the hypothalamus. While activation of GABAergic neurons in the VLPO promotes sleep, the activation of arousal centers, such as TMN or raphe nuclei, promotes wakefulness. Orexinergic neurons are able to activate these arousal centers. A similar flip-flop switch is a hypothesis for REM sleep regulation involving neurons in the DMH and in the brain stem. The DMH also mediates the projection of circadian signals from the SCN towards the VLPO.

### 1.3.3.1. Cellular control: restoration of brain energy

It has been suggested that sleep plays an important role in the restoration of brain energy. In particular, cerebral energy metabolism and its relation to sleep has been reviewed recently. According to these arguments, during wakefulness glucose is the main cerebral fuel and brain metabolism is mainly glycolytic.<sup>108</sup> (N.B. Whether neurons are directly using this glucose, or rather burning lactate provided to them by astrocytes, is an interesting question that has also been a subject of recent discussion, though not yet in the context of sleep<sup>109</sup>). During sleep, brain levels of glucose increase and lactate levels decrease. Correspondingly, metabolic rates of glucose drop significantly during sleep. The metabolic cost of sleep for the brain is probably almost the same during sleep as quiet wakefulness – a mere 5% difference in whole-body respiratory quotient in humans.<sup>110</sup> These changes therefore indicate a transition from glycolysis to oxidative metabolism during sleep. Moreover, enhanced lactate efflux from the brain

during sleep has also been measured.<sup>108</sup> Interestingly, glucose and lactate are both involved in sleep regulation in the brain as well. Extracellular glucose levels, for example, have been shown to promote sleep by inhibiting orexinergic neurons in the lateral hypothalamus<sup>111</sup> and by activating sleep-promoting GABAergic neurons in VLPO.<sup>112</sup> They also act by inhibiting wake-promoting orexinergic neurons.<sup>113</sup> In contrast, an association between elevated extracellular levels of lactate and the activation of noradrenergic neurons in the locus coeruleus, promoting wakefulness, has been reported.<sup>114</sup>

In addition to these potentially direct connections between metabolism and sleep, various studies suggest that other neurotransmitters and signaling molecules might coordinate both processes in synchrony. For example, norepinephrine (NE) not only stimulates arousal centers, but also promotes aerobic glycolysis.<sup>115</sup> NE might thus represent a link between sleep regulation and cerebral energy metabolism. Furthermore, there is evidence for specific biosynthetic pathways to be upregulated in the brain during sleep. Several studies reported alterations in glycogen storage, and gene expression experiments in rat brain revealed enhanced biosynthesis of lipids and proteins during sleep.<sup>116,117</sup> AMPK might serve as a switch between anabolic (energy-consuming) and catabolic (energy-producing) processes in order to maintain sleep homeostasis.<sup>118</sup>

Although multiple studies including those above have suggested general links between metabolism and sleep, knowledge about sleep-stage specific cerebral metabolism remains limited. However, some studies report differences between REM and NREM sleep, such as higher glucose utilization during REM sleep compared to NREM sleep.<sup>119–121</sup>

### 1.3.3.2. Organ-specific control: energy homeostasis

At the level of the entire organism, one major function attributed to sleep is the maintenance of energy homeostasis.<sup>122</sup> Sleep is the most energy-efficient human behavior and metabolic rate during sleep is reduced compared to resting during wakefulness.<sup>123</sup> In mammals, sleep duration decreases with increasing size of the animal,<sup>124</sup> perhaps suggesting that a higher metabolic rate requires more sleep to keep the energy balance. In humans, inter-individual differences in sleep duration have been associated with genetic polymorphism of the SUR2 subunit of ATP sensitive potassium channels, which sense the state of cellular energy metabolism.<sup>125</sup> In addition to this, a genetic link between sleep duration and lipid levels in blood has been found with TRIB1.<sup>126</sup>

Despite overnight fasting, blood glucose levels remain stable during the night with a small increase towards the end of the night. Under constant glucose infusion, an increase in glucose levels is observed with sleep onset, independent of time of day.<sup>127</sup> This decreased glucose tolerance is caused by reduced glucose utilization by brain and muscles, but also due to decreased insulin sensitivity.<sup>128</sup> Thus, not only circadian influences but direct sleep-dependent mechanisms likely regulate circulating glucose levels.

Findings about differences in whole-body energy expenditure across different sleep stages are contradictory. Whereas some studies report lower energy expenditure during SWS compared to REM sleep,<sup>129,130</sup> others did not confirm this finding.<sup>131–134</sup> A recent study using whole-room calorimetry has found differences in respiration quotients across different stages of sleep. Carbohydrate oxidation was lowest during NREM sleep, which was explained with

decreased glucose consumption by the brain during NREM sleep.<sup>135</sup>

### 1.3.3.3. Central control: hormone regulation

Appetite regulating hormones Leptin and ghrelin are hormones that regulate hunger and appetite as a response to changes in energy balance. It has been shown that there is a link between these hormones and sleep.<sup>136</sup> Ghrelin is released in the stomach and acts rapidly in response to caloric shortage or fasting by promoting hunger and appetite.<sup>137</sup> It also acts as a sleep-promoting factor and can induce SWS.<sup>138</sup> Leptin, in contrast suppresses appetite and is produced in adipose tissue.<sup>139</sup> Both of these hormones increase during sleep and decrease in the morning. In the first part of the night, it is thought that leptin masks the effect of rising ghrelin levels in order to prevent arousals due to hunger.<sup>136</sup> Leptin is also under circadian control and food intake is a confounding factor. However, under continuous enteral nutrition and during daytime sleep, increased leptin levels are observed with sleep onset.<sup>140</sup> Moreover, animal studies have given evidence for leptin reducing REM sleep and modulating SWS. Leptin deficient mice have more arousals and mice with mutated leptin receptors show increased total sleep time, but more fragmented sleep as well as a decrease in compensatory response to acute sleep deprivation.<sup>141</sup> Hence, these appetite regulating hormones might be an important link between sleep, circadian rhythms, and metabolism.

Orexins Orexin A and B (hypocretins) could represent another major part of the link between hormonal control of metabolism and sleep. These excitatory neuropeptide hormones are expressed by neurons in the hypothalamus where energy homeostasis is regulated.<sup>142</sup> They are influenced by peripheral hormones like ghrelin and leptin and also by glucose.<sup>136</sup> Orexin administration has effects on sleep regulation as well as metabolism. It induces wakefulness, which comes along with increased energy expenditure and increased food intake.<sup>113</sup> However, orexin deficient mice also show reduced energy expenditure regardless of sleep duration.<sup>143</sup> This suggests that there is a direct link between orexins and metabolism, and metabolic changes are not just a secondary effect of orexins regulating sleep-wake time.

**Pituitary Hormones** The pituitary hormones growth hormone<sup>144</sup> and prolactin<sup>145</sup> are both secreted upon sleep onset and reach a maximum 2 hours later. The extent of this hormonal release is associated with delta activity during NREM sleep.<sup>146</sup> Also, levels of posterior pituitary hormones, such as plasma arginine vasopressin and oxytocin, are increased during sleep. These hormones profoundly regulate different aspects of metabolism, ranging from protein anabolism and triglyceride breakdown to milk production. Moreover, these hormones are also involved in sleep regulation and their administration is associated with alterations in sleep.<sup>147</sup> Therefore, also here, the connection between sleep and metabolism is bidirectional.

### 1.3.3.4. Immune function

Another function associated with sleep is the immune response. Similar to hormonal regulation, there is a bidirectional communication between the immune system and the central nervous system and therefore sleep. Cytokines are main messenger molecules involved in immune responses, which are produced and released by the central nervous system with highest levels during sleep. Examples are interleukins (ILs) and tumor necrosis factors (TNF).<sup>148</sup> Cytokines are also involved in sleep-wake regulation.<sup>149</sup> Immune function also broadly regulates

metabolism, especially adipocyte function,<sup>150</sup> making immune modulation a possible further route by which sleep influences metabolism.

#### 1.3.4. Pathophysiological consequences of Impaired sleep

When sleep is impaired, the negative consequences for health and metabolic as well as cognitive functions are well established. Typical experiments to investigate these negative effects in healthy individuals are sleep restriction, partial sleep deprivation, and total sleep deprivation studies. Metabolic alterations in patients with sleep related diseases, metabolic diseases, and their comorbidities can also be studied.

From these experiments, a relatively homogenous picture emerges. Insufficient sleep across several days results in a 5% increase of daily energy expenditure.<sup>151</sup> Acute sleep deprivation has also been shown to increase energy expenditure, supporting the hypothesis that energy conservation is a function of sleep.<sup>134</sup> Under controlled conditions of caloric intake and physical activity prolonged wake can artificially provoke a negative energy balance. However, this does not correspond to real-life situations in modern society, where food shortage is no longer an issue. It has been shown that short sleep promotes snacking behavior<sup>152</sup> and reduces physical activity.<sup>153</sup> With *ad libitum* feeding, an increased energy intake during wakefulness was observed, especially after dinner, resulting in a positive energy balance.<sup>151</sup> Overeating occurred despite proper signalling of leptin and ghrelin, indicating that it is not just due to a longer period of food availability, but also physiological adaptation: energy intake is increased to sustain prolonged wakefulness.<sup>154</sup> Non-homeostatic food intake is likely to be driven by brain mechanisms similar to those by which mood and comfort regulate feeding.<sup>155</sup> This imbalance between food intake and energy expenditure due to a lack of sleep might partly explain the association between short and fragmented sleep and an increased risk for metabolic diseases such as T2D and obesity, which has been found in various epidemiologic studies.<sup>156</sup> Importantly, recent studies suggest that even unlimited “recovery sleep” on weekends is insufficient to compensate for metabolic dysregulation incurred during weekday sleep restriction.<sup>157</sup>

##### 1.3.4.1. Obesity, T2D and sleep

Sleep restriction has been associated with reduced insulin sensitivity, indicating that impaired sleep alters glucose metabolism.<sup>158</sup> Similarly, large epidemiological studies have related insufficient sleep and disturbed sleep to obesity and T2D.<sup>159,160</sup> Mechanistically, appetite and metabolic hormones – the same that we describe above as capable of altering sleep per se – are believed to play a strong role in this pathology. Leptin, ghrelin, endocannabinoids, and other appetite peptides have all been shown to be dysregulated by sleep loss, restriction, or disturbance, and the direction of dysregulation is consistent with increased caloric intake and decreased glucose clearance. This topic has been reviewed recently.<sup>161</sup>

##### 1.3.4.2. Obesity, T2D, and obstructive sleep apnea

Obesity is considered as one of the most important risk factors for obstructive sleep apnea (OSA). In turn, OSA was also found to promote weight gain. Causal relationships are still

unclear and it is hypothesised as a vicious cycle.<sup>162</sup> Both physiopathologies are linked genetically, and worsen each other. Adipose tissue deposits in obese patients lead to reduced ventilatory stability and promotes the development of OSA. OSA often goes along with physical inactivity, dysregulated appetite hormones, and insulin resistance, thereby increasing the risk for obesity. Dysregulated appetite hormones are also likely contributors, since OSA patients have increased ghrelin levels.<sup>163</sup>

Apart from obesity, a link between OSA and T2D has been found,<sup>164,165</sup> and especially amongst obese T2D patients there is a high prevalence of OSA.<sup>166</sup> One suggested mechanism for the link between T2D and OSA is that OSA causes sympathetic activation, which inhibits leptin secretion and promotes HPA axis stimulation. This leads to increased cortisol secretion resulting in impaired glucose homeostasis.<sup>167</sup> Several studies have shown that treatment of OSA patients with continuous positive airway pressure (CPAP) also improved insulin sensitivity, corroborating the hypothesis that impaired sleep is promoting T2D.<sup>168</sup> However, other studies suggest the opposite: no effect of CPAP therapy on glucose metabolism or T2D.<sup>169,170</sup> The problem here is that obesity acts as a confounding factor, since obesity is considered as an important risk factor for OSA and occurs often together with T2D.<sup>171</sup> In order to elucidate causal relationships, non-obese OSA patients with and without T2D would need to be investigated.

OSA is not the only sleep disorder linked to metabolic dysfunction. Narcolepsy, a REM sleep disorder resulting from a deficiency in orexigenic neurons, is associated with excessive daytime sleepiness and poor sleep quality, abnormalities in REM sleep and orexin deficiency,<sup>172</sup> and has been linked to obesity.<sup>173</sup>

#### **1.3.4.3. Inflammatory response to impaired sleep**

Sleep deprivation is associated with altered immune responses due to an increase of pro-inflammatory markers.<sup>174</sup> This is supported by increased systemic levels of TNF- $\alpha$  in OSA, narcolepsy and insomnia patients.<sup>147</sup> Moreover, CPAP treatment can decrease TNF- $\alpha$  levels.<sup>175</sup> Furthermore, sleep deprivation results in impaired host defense against pathogens<sup>176</sup> and many autoimmune diseases are associated with sleep disruption, daytime sleepiness, and an increased risk for sleep disorders.<sup>147</sup>

#### **1.3.4.4. Alzheimer's disease and sleep**

There is evidence of a link between sleep, T2D, and Alzheimer's disease (AD). These interactions suggest that sleep impairment and metabolic dysregulation promote the progression of AD.<sup>177</sup> AD patients often show sleep impairments<sup>178</sup> and recently, reduced amounts of SWS have been associated recently with tau pathophysiology of AD.<sup>179</sup> Additionally, cerebrospinal fluid (CSF) levels of several AD biomarkers have been found to correlate with sleep-wake cycles.<sup>180</sup> Moreover, elevated CSF levels of orexin A are reported in AD patients.<sup>181</sup> Links between T2D, AD, and sleep further suggest that impaired glucose metabolism might be a key player in interactions between sleep impairment and cognitive dysfunction in AD.<sup>182</sup> An interesting alternative is that connections between AD and sleep impairment might relate to glymphatic flow – the “waste clearance” system of the brain – which increases during sleep and contributes to Alzheimer-associated peptide (A $\beta$ ) clearance from the brain.<sup>183</sup>



## 1.4. Clocks or sleep: perspectives

It is clear that modern society has increasingly intruded upon natural circadian rhythms in humans, possibly leading to profound metabolic consequences. Classically, the phase desynchrony between central and peripheral clocks is thought of as the main contributor. However, one direct test of this assumption has failed: it was shown that a 6 hour phase misalignment between central and peripheral clocks was not sufficient to cause obesity and glucose intolerance in mice.<sup>184</sup> Thus, we favor the hypothesis that metabolic consequences of circadian disruption arise via multiple mechanisms, rather than solely from internal desynchrony. In humans, it is unlikely that central and peripheral clocks would have such a large phase misalignment as those artificially tested in animals outside situations of shiftwork. Thus, if circadian disruptions such as social jet lag result in metabolic dysfunction, it is likely that other factors are at work, and sleep disturbance is a prime possibility.

Equally, sleep restriction is an omnipresent issue in contemporary society, with adverse effects on health and metabolism. However, these metabolic considerations are mostly based on measures of total energy expenditure rather than pathway-specific investigations. It is likely that advances in metabolomics techniques using high-resolution mass spectrometry that have been made in recent years have great potential for novel insights. The sensitivity of some methods is sufficient to identify thousands of compounds in a single human breath, making them powerful noninvasive techniques to overcome limitations in sampling rate.<sup>185,186</sup>

Strikingly, most aspects of metabolism regulated by sleep and circadian clocks are shared (figure 1.3). Molecular mechanisms are continually discovered about single aspects of the relationship between the circadian clock or sleep and the downstream physiology they control, but often these studies look at a single facet. More recent studies that compare effects of circadian disruption and sleep disruption demonstrate that each might play a role in cellular physiology. For example, considering brain, individual transcripts might be regulated by either circadian or sleep influences, or both.<sup>187</sup> Even more locally, it has been suggested that at synapses, RNA abundance is primarily clock-driven, whereas translation and phosphorylation of proteins is mostly controlled by sleep-wake cycles.<sup>27,99</sup>

These studies, as well as this review, have mostly addressed the idea that different aspects of physiology might be controlled by circadian clocks or sleep. However, in practice the two rather difficult to separate, creating a major confounding factor. Indeed, circadian rhythm sleep disorder is often misdiagnosed as insomnia.<sup>188,189</sup> Experimentally, circadian clock gene disruptions in mice also affect sleep consolidation.<sup>91,190</sup> Thus, the classical paradigm of a clock gene deletion as a way to ascertain that a process is directly clock controlled contains an unavoidable flaw. Similarly, most epidemiological studies – and many laboratory ones – examining effects of sleep disruption are in fact examining unknown degrees of circadian disruption as well. The only real solution to this conundrum is a detailed mechanistic understanding of the regulatory processes involved. Without a doubt, such an understanding will lead to improved therapies as well.

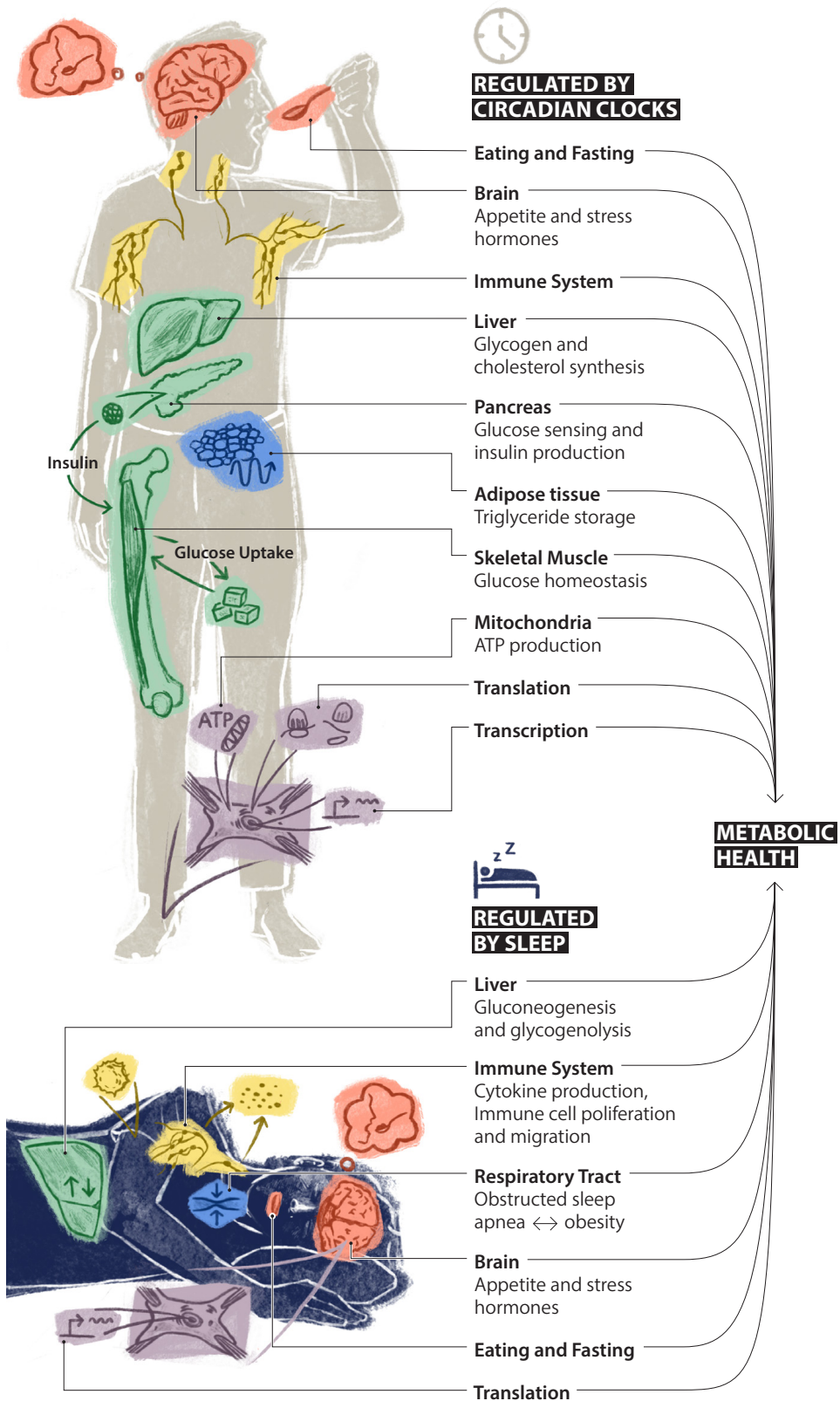


**Figure 1.3.:** Circadian clocks and sleep: two related factors in the multifaceted regulation of metabolism. Processes related to food intake (red), immune function (yellow), glucose metabolism (green), cellular functions (purple) and adiposity (blue) are regulated by circadian clocks, sleep or both. The efficient interplay of both, clocks and sleep, is crucial for metabolic health.

# 2

Aims and outline of this thesis

Metabolic profiles reflect fundamental aspects of physiology and metabolomics. The analysis of such metabolic profiles therefore represents a versatile tool that can provide answers to a variety of biological questions. In this thesis, latest mass spectrometry techniques were applied to unravel metabolic processes related to sleep and circadian clocks (figure 2.1). While it is evident that sleep and circadian clocks are closely intertwined with human metabolic regulation, many aspects of this relationship remain unclear.

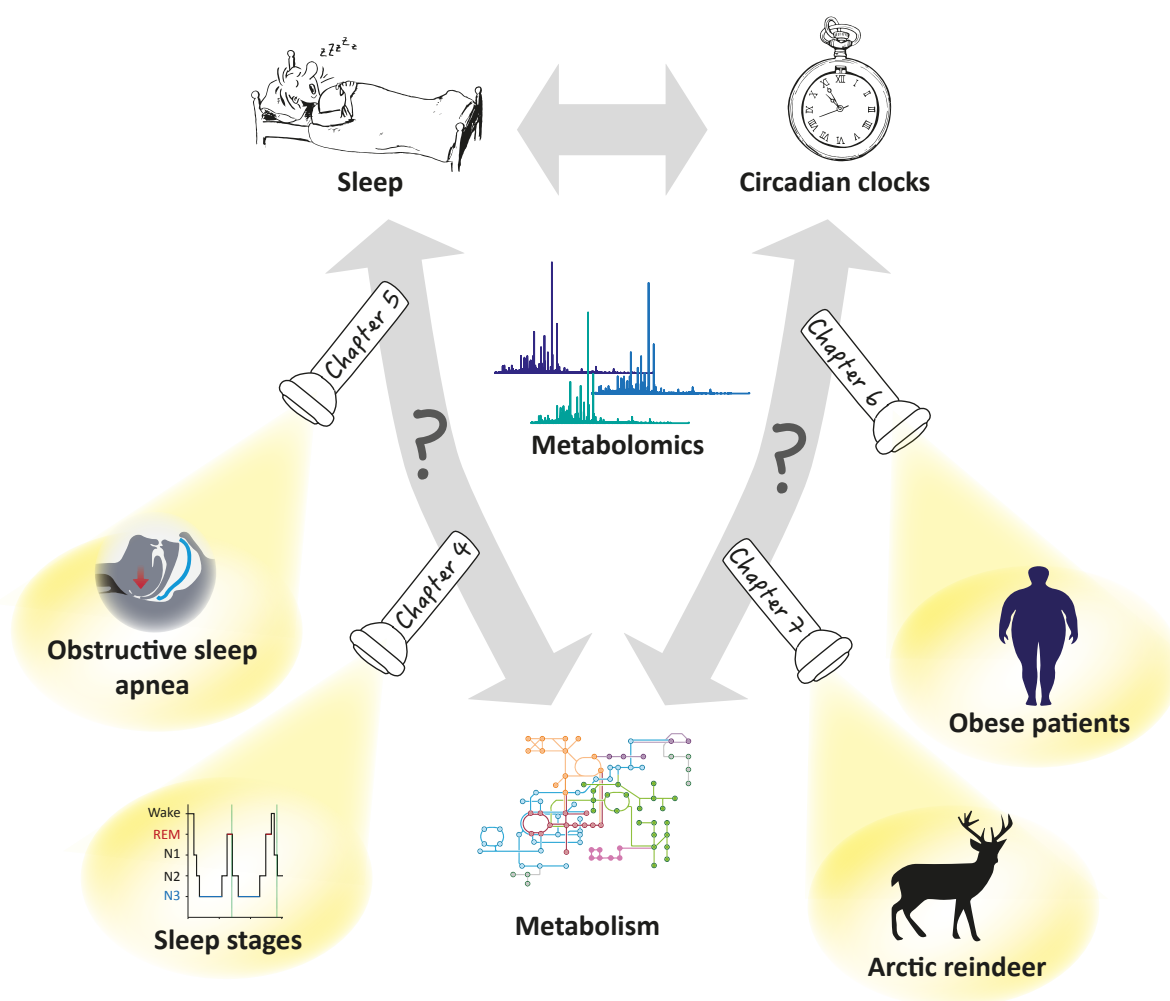


**Figure 2.1.:** In this thesis, metabolomics by high-resolution mass spectrometry was used to shed light on several aspects of the complex interplay between sleep, circadian clocks and metabolism. Breath analysis by secondary electrospray ionization high-resolution mass spectrometry (SESI-HRMS) was used to investigate metabolic processes during normal sleep and its applicability as a non-invasive diagnostic tool for obstructive sleep apnea was evaluated. The analysis of metabolites from blood samples by liquid chromatography coupled to mass spectrometry unraveled connections between metabolic alterations associated with obesity and circadian clocks. Moreover, this technique provided insights into metabolic adaptation to seasonally changing circadian light conditions in arctic reindeer.

The biology of sleep and circadian clocks is explained in **Chapter 1**. Known molecular mechanisms are reported, their impact on human health is described and the current state of

---

knowledge about the connection of sleep and circadian rhythms to metabolism is reviewed.

The experimental techniques and instruments used in this thesis are described and explained in **Chapter 3**. Amongst them are methods for the assessment of biological parameters, such as polysomnography for the characterization of sleep and a bioluminescence assay for measuring levels of circadian gene expression. Moreover, high-resolution mass spectrometry techniques and their implementation for the analysis of metabolites in blood and exhaled breath are introduced.

In **Chapter 4**, metabolic regulation is investigated across different sleep stages. While there is evidence from numerous studies for a negative effect of disturbed or restricted sleep on metabolic health, metabolism during sleep itself remains largely unexplored. In this study, we made use of the virtually unlimited sampling frequency provided by real-time breath analysis. We analyzed the exhaled breath of healthy individuals by secondary electrospray ionization high-resolution mass spectrometry (SESI-HRMS) while they were sleeping at night. In parallel, sleep stages were recorded by polysomnography.

Not only the high sampling frequency but also its non-invasiveness and the instantaneously available results are outstanding qualities of metabolic profiling in exhaled breath. These factors are the reasons breath analysis is considered to be a promising tool for clinical diagnostics. Previous work on SESI-HRMS indicated the existence of specific metabolic patterns in exhaled breath for several diseases, amongst them obstructive sleep apnea (OSA). In **Chapter 5**, the robustness of these breath biomarkers for OSA was evaluated in a validation cohort of 149 patients with suspected OSA. This brings the rapid and non-invasive diagnostic tool SESI-HRMS a step closer to its clinical application.

Similar to disturbed sleep, a disrupted circadian clock is also associated with adverse health effects. Metabolic diseases, such as obesity, metabolic syndrome or type 2 diabetes are highly prevalent in shift workers, for example. Even though there is clear evidence for this connection from epidemiologic as well as animal studies, there is only little mechanistic understanding about it on metabolic pathway level. To get further insights, we investigated the impact of metabolite levels in serum from obese patients on the circadian expression of the core clock gene *Bmal1* in U2OS cells as described in **Chapter 6**.

Due to the negative health consequences, there is a high demand for strategies to cope with circadian disruption. In **Chapter 7**, we tackled this issue with an evolutionary approach. We studied circadian metabolism in arctic reindeer, a species, which has always been exposed to constant light during summer and constant darkness during winter. We investigated how their metabolism adapted to these seasonally changing light conditions by analyzing blood plasma with liquid chromatography coupled to high-resolution mass spectrometry across all four seasons.

In **Chapter 8**, all conclusions from this thesis are briefly summarized and discussed together, before remaining questions and possible future research directions are considered.



# 3

Experimental techniques for the  
investigation of sleep, circadian rhythms  
and metabolism

### 3.1. Polysomnography

Polysomnography is the current gold standard for the assessment of sleep quality and quantity and an essential diagnostic tool for various sleep disorders.<sup>191</sup> In this diagnostic procedure, a range of physiological parameters are measured simultaneously and continuously by numerous electrodes and sensors attached to the body (figure 3.1). These recordings include electroencephalography (EEG), electrocardiography (ECG), electrooculography (EOG) and electromyography (EMG) as well as abdominal and thoracic breathing effort and body position. Oxygen saturation is captured by pulse-oximetry and snoring is recorded with a microphone. By default, breathing airflow is also measured and the patient is video monitored. From defined patterns of muscle and brain activity, sleep stages can be deduced. In addition, information about the functions of different organs is obtained and abnormalities can be detected.<sup>192–194</sup>

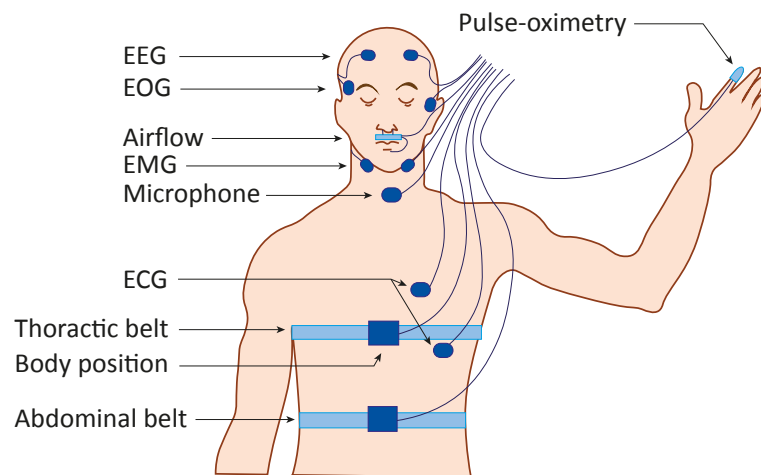


**Figure 3.1.:** Setup of electrodes and sensors for polysomnography. Electrodes for EEG, ECG, EOG and EMG are attached to the head and body, a pulse oximeter is attached to a finger, sensors for breathing effort and body position are mounted to the torso. The figure is reproduced with permission from Pandi-Perumal *et al.*<sup>192</sup> Copyright 2014, Springer Nature.

### 3.2. Bioluminescence assay for clock gene expression in fibroblasts

*In vivo* measurements of human circadian period are difficult and require a time-consuming observation of subjects under laboratory conditions. However, since most cell types are equipped with circadian clocks, which are synchronized with the SCN as major pacemaker, circadian parameters can also be assessed by a simple bioluminescence assay *in vitro* from single skin biopsies.<sup>195</sup> It has been shown that clock gene expression measured in fibroblasts from human skin biopsies reflect physiological circadian phenotypes well.<sup>196</sup>

These *in vitro* assays are based on bioluminescent circadian reporters. In such reporters, a luciferase gene is fused with the promoter of a clock gene, such as *Bmal1*. These reporter



constructs are incorporated into the genome of the cells, which can be achieved by lentiviral infection (figure 3.2a). As a consequence, the enzyme luciferase is expressed in dependence of the clock gene promoter activity. Luciferase catalyzes the reaction of its substrate luciferin with oxygen, which results in the emission of light (bioluminescence). (figure 3.2b) The intensity of the emitted light is proportional to the amount of luciferase and therefore also proportional to the clock gene expression.<sup>197</sup>

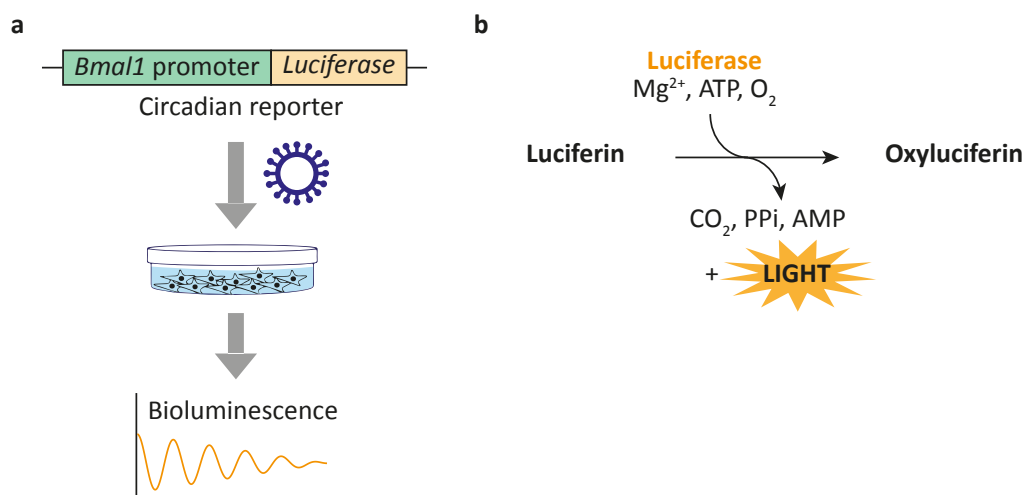


**Figure 3.2.:** **a** A circadian reporter is incorporated into the genome of fibroblasts by lentiviral infection. Subsequently, bioluminescence is measured. **b** Luciferase catalyzes the oxidation of Luciferin under emission of light.

### 3.3. Metabolomics based on mass spectrometry

#### 3.3.1. High-resolution mass spectrometry

Mass spectrometry (MS) is one of the most widely used techniques for metabolomics,<sup>198</sup> which is mostly due to advances in the development of high-resolution mass spectrometry (HRMS) in the last few decades.<sup>199</sup> Especially in untargeted metabolomics approaches where hundreds of compounds are measured simultaneously in complex matrices (such as blood, urine, cerebrospinal fluid, tissue samples or breath), high mass resolution is essential. It enables discrimination between isobaric compounds (molecules with the same nominal mass) and compound identification.<sup>200,201</sup> Two common mass analyzers with high-resolution capabilities used in this thesis are time-of-flight (TOF) and orbitrap mass analyzers. In the corresponding commercial instruments, they are combined with quadrupole units for precursor selection and the possibility of fragmentation. The basic principles of these mass analyzers and the instrumental setup of an AB Sciex TripleTOF 5600 and a Thermo Fisher Orbitrap QExactive Plus instrument, which were used in this thesis, are explained in the following sections.

### Time-of-flight mass analyzer

The principle of time-of-flight mass spectrometry (figure 3.3a) relies on the separation of accelerated ions based on their velocity in a field-free region.<sup>202</sup> The potential energy  $E_p$  of charged particles that were accelerated by an electric field is defined by their charge  $q$  and the electric field strength  $U$ . The charge of ions can be expressed by the product of their charge state  $z$  and the elementary charge  $e$ .

$$E_p = qU = ezU$$

When the ions enter the field-free flight tube, their potential energy is converted into kinetic energy, which is determined by their mass  $m$  and their velocity  $v$ .

$$E_k = \frac{mv^2}{2}$$

Thus, the velocity of ions in the field-free region depends on their mass-to-charge ratio ( $m/z$ ). Ions with lower  $m/z$  are faster and reach the detector first.

$$ezU = \frac{mv^2}{2}$$

$$v = \sqrt{\frac{2eU}{m/z}}$$

Since the length of the flight path is known, the  $m/z$  of the detected ions can be deduced from their time of flight. However, the differences in time of flight are very small and thus, a slight initial energy spread of ions with the same  $m/z$  does already cause a substantial loss of resolving power. To achieve high resolution, it is therefore crucial to correct for this spread. This is achieved with a reflectron, which is inserted in the flight path and serves as an ion mirror. Ions of the same  $m/z$  but with a higher initial energy travel deeper into the reflectron than ions with lower energies. Thus, their flight path gets elongated and ions with the same  $m/z$  but slightly different initial energies are refocused and reach the detector simultaneously. In addition, the use of a reflectron doubles the length of the flight path at the same instrument size, which results in a further gain of resolution.<sup>203</sup>

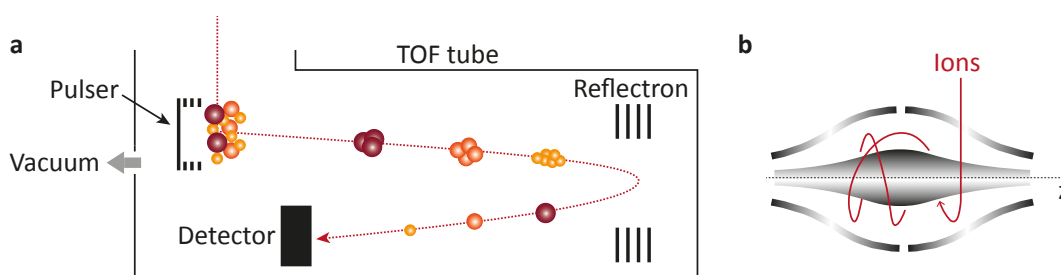


**Figure 3.3.:** Schematic representations of the principle of a reflectron time-of-flight mass analyzer (a) and an orbitrap mass analyzer (b).

### Orbitrap mass analyzer

The orbitrap mass analyzer (figure 3.3b) consists of a spindle-shaped inner electrode and two surrounding outer electrodes. With this geometry a very well defined electric field is achieved and ions entering the orbitrap tangentially are oscillating on stable trajectories around the spindle. The frequency of the axial oscillation along the z-axis is proportional to the square root of the mass-to-charge ratio. The two outer electrodes are detecting an image current, generated by the oscillating ions. This is subsequently converted by Fourier transformation into a frequency spectrum of the axial oscillation, from which the  $m/z$  is deduced according to the following equation ( $k$  represents the field curvature):

$$\omega_z = \sqrt{k \cdot \frac{q}{m}}$$

The resolving power of the orbitrap is proportional to the number of detected harmonic oscillations and can therefore be enhanced by increasing the time in the trap. Thus, a trade-off between acquisition speed and resolving power needs to be chosen.<sup>202,204</sup>

### Commercial instruments

All mass spectra in this thesis were measured either on an AB Sciex TripleTOF 5600 or a Thermo Fisher Orbitrap QExactive Plus instrument. Both instruments combine high resolution and high mass accuracy with an acquisition speed sufficient for their coupling to ultra-high performance liquid chromatography (UPLC) and for real-time breath analysis (table 3.1).<sup>205</sup>

**Table 3.1.:** Specifications of the two commercial mass spectrometers used in this work.

Instrument	Resolving power (FWHM)	Mass accuracy (ppm)	Acquisition speed (Hz)
TripleTOF 5600	35,000	< 5	100
Orbitrap QExactive Plus	140,000 (at $m/z$ 200)	< 5	12 (at 17,500 resolution)

The ion paths through the two mass spectrometers are depicted in figure 3.4 and 3.5. After entering the TripleTOF 5600 mass spectrometer (figure 3.4) through an orifice, the ions are guided through several quadrupoles in sections of decreasing pressure towards the TOF tube. The first two quadrupoles (QJet and Q0) serve only as ion guides. In full scan mode, the Q1 quadrupole operates also as ion guide, while it is used as mass filter for precursor selection in tandem-MS experiments. The collision cell Q2 is filled with a collision gas (in this work nitrogen). Collision between this gas and the parent ions lead to molecule-specific fragmentations.<sup>206</sup> By application of a collision energy (CE), the kinetic energy of the precursor ions is increased and the extend of fragmentation can be tuned with the use of different collision energies. The (fragmented) ions are further guided towards the high vacuum region. In the pulser, short high voltage pulses accelerate ion packages orthogonal to their original path into the TOF region, where they are separated by their  $m/z$  and detected by a microchannel plate (MCP) detector<sup>205,207</sup>

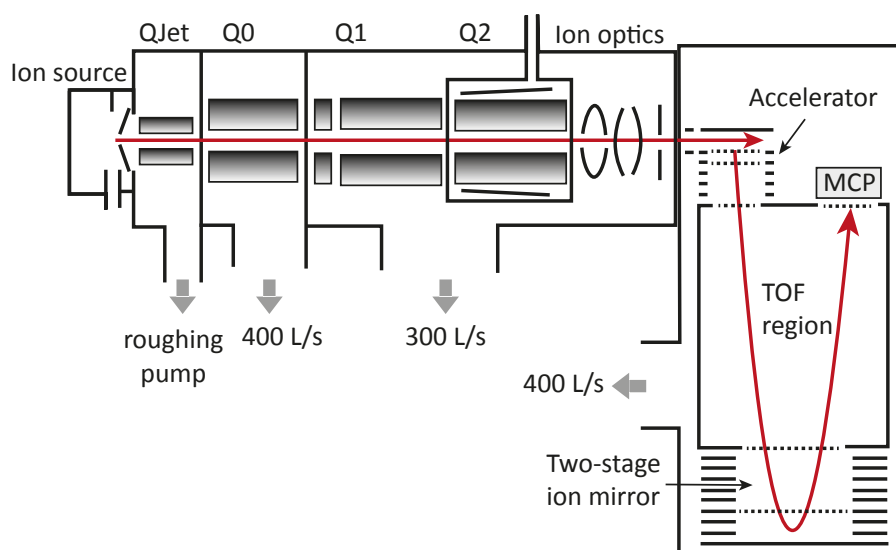


**Figure 3.4.:** Schematic drawing of the quadrupole time-of-flight hybrid instrument used in this thesis (AB Sciex, TripleTOF 5600). The ion path is highlighted in red. (MCP: microchannel plate, Q: quadrupole). Adapted with permissions from Andrews, G. L. *et al.*<sup>207</sup> Copyright 2011 American Chemical Society.

In the Orbitrap QExactive Plus (figure 3.5), the ions enter the mass spectrometer through a heated inlet capillary into the S-lens, a stacked-ring ion guide, where they are focused. After two subsequent ion guides, the ions arrive at a quadrupole, which acts as in the TripleTOF instrument as mass filter for precursor selection in multistage mass spectrometry (MS<sub>n</sub>) experiments. The ions are then guided into the C-trap, a bent RF quadrupole, where the ions are either accumulated and thermalized or they are first sent to a multipole collision cell filled with nitrogen for fragmentation. Finally, they are injected into the orbitrap mass analyzer, where they are separated by their  $m/z$  and detected.<sup>208</sup>

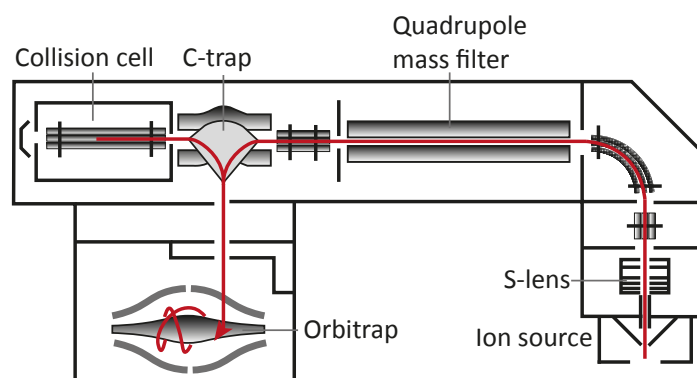


**Figure 3.5.:** Schematic drawing of the quadrupole orbitrap hybrid instrument used in this thesis (Thermo Fisher, Orbitrap QExactive Plus). The ion path is highlighted in red. Adapted from Michalski, A. *et al.*<sup>208</sup>

### 3.3.2. Blood metabolomics using UPLC-MS

Blood supplies every organ and tissue with gases and nutrients and it also transports metabolic waste. Its molecular composition is therefore dependent of metabolic function and activity and even though withdrawal of blood is slightly invasive, this body fluid is easily accessible. That is why blood is one of the most common biofluids used for metabolomics studies. Nuclear magnetic resonance (NMR) spectroscopy, and gas chromatography (GC) or liquid chromatography (LC) coupled to mass spectrometry are the techniques mostly used for the analysis of metabolites in blood.<sup>209</sup> This section focuses on LC-MS, since this technique was used in this thesis. The chromatographic separation prior to mass spectrometric analysis adds a dimension of separation, which is valuable especially for complex mixtures of analytes, such as biological samples.<sup>210</sup> A typical workflow for the analysis of metabolites in blood by LC-MS is presented in figure 3.6.<sup>211</sup>

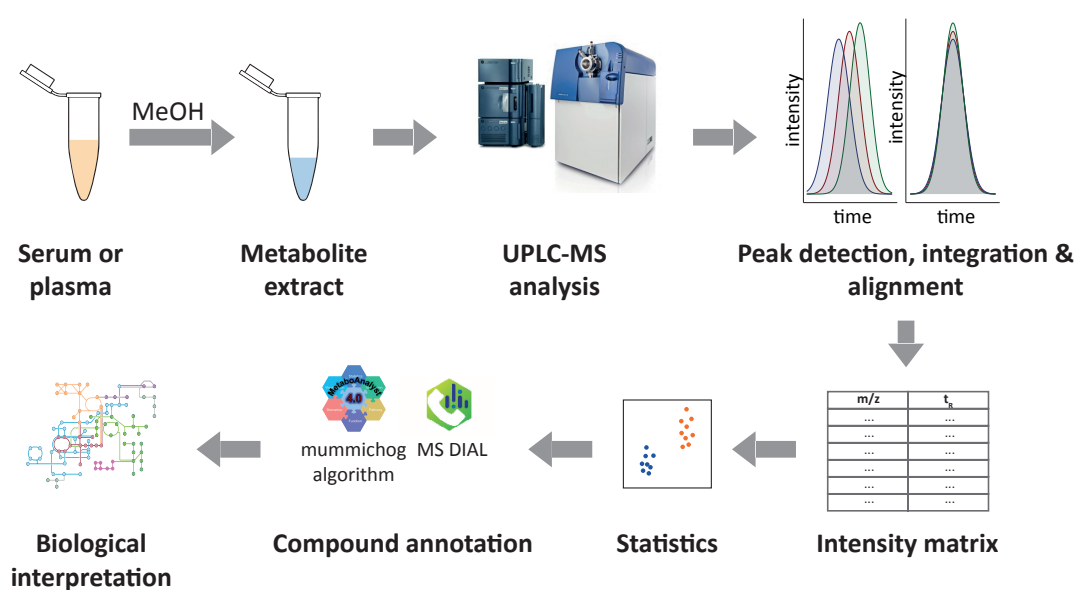


**Figure 3.6.:** Workflow for blood metabolomics studies using UPLC-MS. Proteins are precipitated from serum or plasma samples with methanol and the obtained metabolite extract is analyzed by UPLC-MS. For data pre-processing, peak detection and integration and retention time alignment is performed to obtain an intensity matrix. Then statistics are carried out and features of interest are annotated to enable biological interpretation of the results.

In metabolomics investigations, small molecules are of particular interest. Therefore, proteins are depleted from the extract in a first step by precipitation with methanol. The metabolite extract can then be analyzed directly, or it can be further up-concentrated and solvents might be exchanged prior to analysis. Then, the sample is injected into the mobile phase flowing through a chromatographic column, which contains the stationary phase. Depending on the properties (especially the polarity) of the analyte and the chosen combination of stationary and mobile phase, the analyte elutes from the column after a specific time (retention time). In this thesis, ultra-high performance liquid chromatography (UPLC) coupled to electrospray ionization (ESI) mass spectrometry was used. In comparison with high-performance

liquid chromatography (HPLC), UPLC operates with stationary phases consisting of smaller particles and therefore at higher pressures. This reduces the required analysis time as well as solvent consumption and increases resolving power.<sup>212</sup> It is therefore especially advantageous for large scale metabolomics studies with large sample numbers. In order to achieve a good separation for a broad range of compounds, two different stationary phases were used in this work. A reversed phase (RP) column was applied for the separation of unpolar metabolites and a hydrophilic interaction column with a trifunctionally-bonded amide phase was applied for more polar compounds.

Ions for mass spectrometry analysis were generated by ESI. In this ionization technique, a conducting liquid that contains the analyte is pushed through a thin capillary and high voltage is applied. By electrostatic repulsion, a spray of fine charged droplets is formed during this process. The solvent evaporates from these charged droplets and they undergo Coulomb fission until free ions are generated. This ionization technique can be coupled directly to liquid chromatography.<sup>213</sup>

Data preprocessing of LC-MS data comprises peak picking and integration. Further, chromatogram alignment is needed to correct for retention time shifts. Then, an intensity matrix is obtained and statistical analysis can be performed. When features of interest have been retrieved, they need to be identified. Compound identification remains the main challenge in the field of untargeted metabolomics.<sup>201</sup> However, advances have been made in the automated compound annotation by library matching of MS/MS spectra (e.g. MS DIAL software<sup>214</sup>) or pathway mapping (e.g. mummichog algorithm<sup>215</sup>). Ideally, standards are measured afterwards to confirm the annotations with retention time and MS/MS spectra matching. Finally, open biological research questions can be answered with the results obtained.

### 3.3.3. Breath metabolomics using SESI-MS

Approximately 1% of the molecular composition of human exhaled breath consists of volatile organic compounds (VOCs). Amongst them are various exogenous compounds, but also an endogenous fraction.<sup>216</sup> These endogenous compounds originate partly from lung tissue, however, volatile metabolites can also pass the blood-air barrier and diffuse from blood into the lungs (figure 3.7).<sup>217,218</sup> Therefore, exhaled breath contains valuable biochemical information about physiology and alterations in the metabolic breath print can point towards different pathologies. This makes the analysis of exhaled breath a promising diagnostic tool, which combines non-invasiveness with a virtually unlimited sampling frequency.

A variety of analytical methods is suitable for the analysis of exhaled breath, amongst them mass spectrometry approaches, as well as optical spectroscopy and sensor-based methodologies. A widely used technique is gas chromatography coupled to mass spectrometry (GC-MS). However, these measurements are performed offline and require sample preparation and storage, which can lead to analyte degradation and affect results. On the other hand, there are several online measurement methods based on mass spectrometry, such as selected ion flow tube mass spectrometry (SIFT-MS), proton transfer reaction mass spectrometry (PTR-MS) and secondary electrospray ionization mass spectrometry (SESI-MS).<sup>219</sup> Here, only SESI-MS, which has been used in this thesis, will be further explained.

The principle of SESI-MS (figure 3.8) is based on an aqueous electrospray, which contains

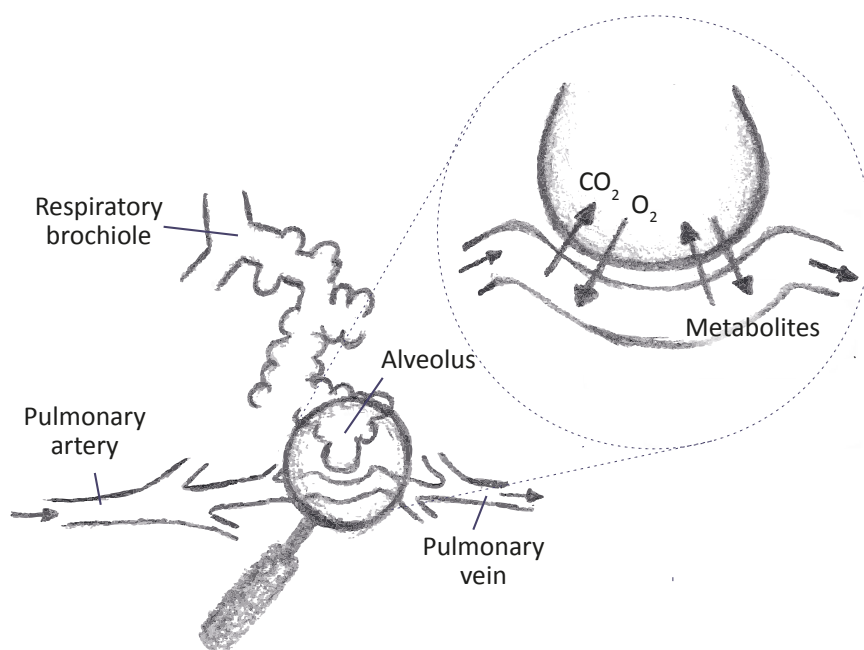


**Figure 3.7.:** Blood-gas exchange. Similar to carbon dioxide and oxygen, volatile metabolites can diffuse in the alveoli from blood into the lungs.

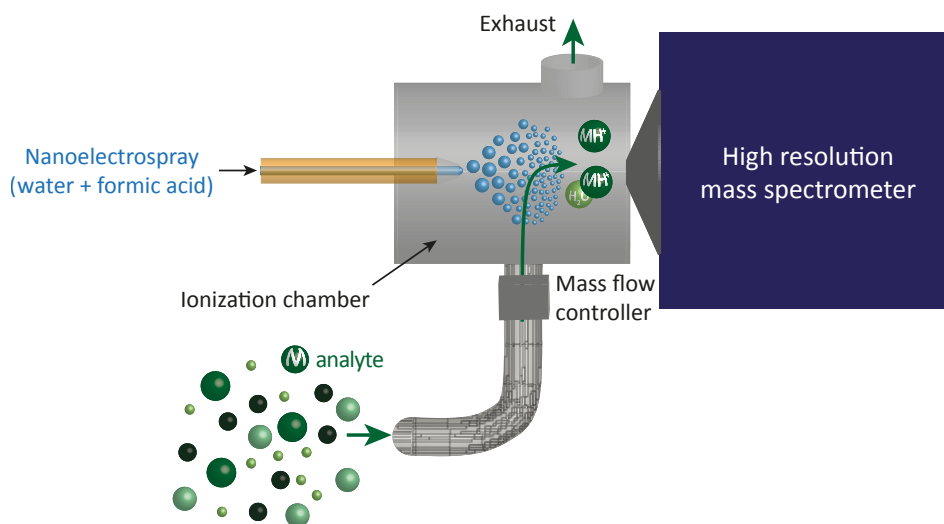


**Figure 3.8.:** The principle of SESI-MS. The analyte is introduced into a nanoelectrospray consisting of water and formic acid and thus gets ionized. The ions can then be detected with a mass spectrometer.

an additive such as formic acid to increase the conductivity of the liquid. In the ionization chamber, the analyte vapor is introduced into the electrospray plume where it gets ionized.<sup>220</sup> The ionization mechanism of SESI-MS is not yet fully understood. However, in a recent study Rioseras *et al.* suggest that ionization happens predominantly via gas-phase proton transfer reactions.<sup>221</sup> They proposed that protonated water clusters formed in the electrospray plume undergo proton exchange with solvent vapors from the carrier gas, i.e. water molecules in the case of exhaled breath. Subsequently, other neutral vapors are protonated, depending on their gas phase proton affinity.

SESI-MS offers several advantages for breath analysis. It is a soft ionization technique<sup>222</sup> and since the ionization takes place at ambient pressure, a SESI source can be coupled to any ambient inlet mass spectrometer. Therefore, HRMS and tandem MS capabilities can be exploited. Further, SESI-MS covers a wide  $m/z$  range<sup>223</sup> and since ions of both polarities can be generated, a wide range of compounds can be analyzed. In addition, high sensitivity, down to pptv, has been reported for SESI-MS<sup>224</sup> and recent studies have shown its applicability for the discovery of putative biomarkers for various diseases<sup>225-228</sup> as well as for pharmacokinetic studies.<sup>229,230</sup> The main drawback of SESI-MS is that the technique still lacks options for absolute quantification, which complicates standardization efforts.



# 4

Rapid and reversible control of human  
metabolism by individual sleep states

This chapter is adapted from :

Nora Nowak, Thomas Gaisl, Djordje Miladinovic, Ricards Marcinkevics, Martin Oswald, Stefan Bauer, Joachim Buhmann, Renato Zenobi, Pablo Sinues, Steven A. Brown, Malcolm Kohler, RAPID AND REVERSIBLE CONTROL OF HUMAN METABOLISM BY INDIVIDUAL SLEEP STATES. *Manuscript submitted for publication.*

M.K, S.A.B., P.S, R.Z., N.N, and T.G. designed the study. T.G., M.K., P.S. wrote the protocol for the ethics. N.N., T.G. and M.O. performed the experiments. N.N. analyzed all MS data and performed statistical analysis. T.G. analyzed the PSG data. D.M., R.M., S.B. and J.B. developed the algorithm based on Granger causality. M.K, S.A.B. P.S, N.N., T.G. and R.Z. contributed to the discussion and interpretation of the results. N.N., R.M, S.A.B. and M.K wrote the manuscript with input from the other co-authors.

## Summary

Sleep is crucial to restore body functions, performance, psychological wellbeing and metabolism across nearly all tissues and cells, and is known to be regulated by an endogenous circadian clock. Both circadian disruption and sleep restriction are linked to a wide range of metabolic dysfunctions in humans. Using exhaled breath analysis by secondary electrospray ionization high-resolution mass spectrometry (SESI-HRMS), here we measured for the first time the human exhaled metabolome at ten seconds resolution across a night of sleep in combination with conventional polysomnography. Our subsequent analysis of more than a thousand metabolites demonstrates rapid, reversible control of major metabolic pathways by the individual vigilance states of slow-wave sleep (SWS), rapid eye movement (REM) sleep, and wake. Within this framework, whereas a switch to wake increases fatty acid oxidation, a switch to SWS reduces it, and the subsequent transition to REM sleep results in elevation of TCA cycle intermediates preparing for mitochondrial oxidation. We demonstrated a similar stepwise logic for numerous other pathways implicated in macromolecular synthesis. Thus, in addition to daily regulation of metabolism, there exists a surprising and complex underlying orchestration across sleep and wake. Both likely play an important role in optimizing metabolic circuits for human performance and health.

## 4.1. Introduction

At the most basic level, humans spend daytime awake, moving and feeding, and nighttime asleep, quiescent and fasting. Considerable research has established that metabolism across the brain and body is regulated in daily “circadian” fashion, complementing this pattern. Even in the absence of daily cues, most aspects of this metabolic control persist, directed by an endogenous molecular clockwork.<sup>46</sup> However, systematic disruption of circadian patterns of activity – for example by shiftwork – results in considerable disruptions to normal metabolic patterns, and such disruption is believed to underlie the linkage between shiftwork and metabolic syndrome (a spectrum of disorders, including obesity, diabetes, and cardiovascular morbidity, that is associated with metabolic dysfunction).<sup>231</sup>

Overlaying this daily pattern is the sleep-wake cycle itself, a complex repetitive cycle of distinct brain states. Mammalian sleep is divided into rapid eye movement (REM) sleep and non-REM (NREM) sleep based on electroencephalogram (EEG) and electromyogram (EMG) measurements. In humans, within NREM sleep, three different stages are further differentiated: N1 and N2 sleep are considered as gradual changes from wakefulness towards slow-wave or deep sleep (N3).<sup>232</sup> Sleep amount is driven both by circadian influences, and by a separate homeostatic process, with increasing time awake favoring increased sleep.<sup>90</sup> Independently of circadian disruptions, impaired sleep is also associated with major physiological and psychological sequelae such as impaired glucose and lipid metabolism, cardiovascular disease, impaired psychological and social functioning with enormous socioeconomic consequences.<sup>233</sup> In general, circadian disruption is usually associated with sleep disturbance as well.

Much of our knowledge of the control of metabolism by circadian clocks and sleep in humans comes from metabolomics, the systematic study of small molecules produced by

anabolic and catabolic reactions, which can be sampled periodically across the day from blood, urine, and saliva.<sup>76,234–238</sup> These have been complemented by sampling accessible tissues such as blood and adipose tissue across time, and analyzing the temporal pattern of RNAs (transcriptomics) or proteins (proteomics) therein.<sup>239–242</sup> From these studies up to 20 % of all metabolites vary with time of day, and this oscillation can be disrupted by circadian misphasing (shiftwork),<sup>76</sup> and by sleep restriction<sup>235</sup> or sleep deprivation.<sup>237</sup> Multiple overarching and logical themes emerge: e.g. carbon energy storage as glycogen during wake/daytime, and its breakdown during sleep/nighttime; and energy expenditure-related pathways during wake, followed by synthesis and regeneration during sleep.<sup>243</sup>

An ever-growing body of evidence emerges that sleep is essential for health. Although global metabolic rate (for example oxygen consumption and CO<sub>2</sub> production as a measure of differences in energy expenditure and glucose utilization) has been measured across sleep,<sup>129,130,135</sup> changes in metabolic regulation on a molecular level across different sleep stages remain unexplored. This is mainly due to a lack of sufficient sampling rates for biofluids or tissues. Taking advantage of secondary electrospray ionization coupled to a high-resolution mass spectrometer (SESI-HRMS),<sup>223</sup> our groups have overcome these difficulties by analyzing exhaled breath. Breath analysis provides real-time information within seconds in a non-invasive fashion. Hundreds of metabolites have been reported from breath including fatty acids, amino acids and tricarboxylic acid (TCA) cycle intermediates.<sup>216,219</sup> We have pioneered the use of these technologies for circadian measurements across the day<sup>185,186</sup> and for identification of molecular alterations present in various diseases during daytime.<sup>226,227,244,245</sup> Here, we have modified a conventional constant positive airway pressure (CPAP) mask commonly used in sleep apnea to deliver breath to our SESI-HRMS across the night. In this way, we provide a glimpse of the human exhaled metabolome at unprecedented ten seconds resolution across a night of sleep.

## 4.2. Methods

### 4.2.1. Study participants

A group of 14 healthy volunteers (12 non-smokers, 1 ex-smoker, 1 active smoker) in the age of  $29.2 \pm 8.3$  years was recruited for this study. 57 % of the study subjects were male and mean BMI  $\pm$  SD was  $22 \pm 3$  kg/m<sup>2</sup>. They did not take any medication. The participants were asked to refrain from eating, drinking (except water), chewing gum, brushing their teeth and using any facial cosmetics (such as lip balm) during at least one hour prior to the measurements. Each individual spent two nights in the laboratory. In the first night, SESI-HRMS measurements were carried out in positive ionization mode, in the second night in negative ionization mode. A full polysomnography was performed in both nights. One participant could not be measured due to dysfunction of the MS and one quit the study after the first night. Therefore, the final numbers of included participants are  $n = 13$  for measurements in positive ion mode and  $n = 12$  for measurements in negative ion mode. The measurements were conducted in accordance with the Declaration of Helsinki and written informed consent was obtained from all participants. The study was approved by the local ethical committee (KEK-ZH 2016-00384).

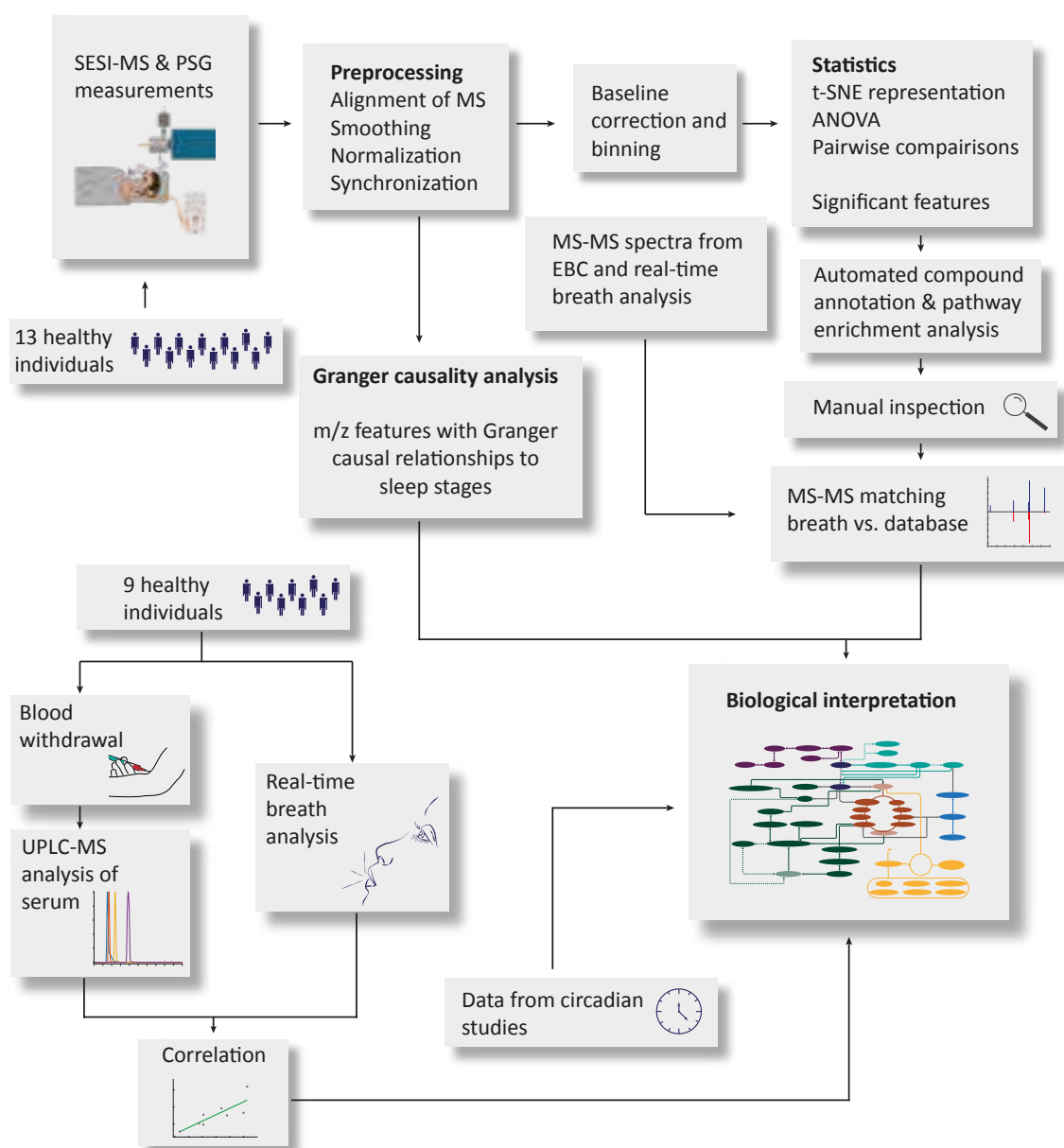


**Figure 4.1.: Workflow of the whole study.** SESI-HRMS and PSG measurements resulted in two large datasets, deposited in a curated data archive at ETH Zurich (DOI 10.3929/ethz-b-000422459). In a first step of data preprocessing, mass spectra were aligned, time traces were smoothed and normalized and mass spectra were synchronized with PSG data. The resulting dataset was analysed by inferring non-linear Granger causality with neural networks yielding a set of  $m/z$  features with Granger causal relationships to N3 sleep, REM sleep and wakefulness. Further, the preprocessed data was baseline corrected and within each subject, data was binned per sleep stage. Then, conventional statistics were applied resulting in sets of  $m/z$  features showing significant differences between sleep stages. These results were used for automated compound annotation and pathway enrichment analysis. After manual inspection this analysis yielded in a subset of metabolites mapped on pathways with potential sleep-related regulation. The identity of some of these metabolites could be confirmed with MS/MS data obtained from exhaled breath condensate or real-time breath analysis. In combination with the information about Granger causal relations between metabolites and sleep stages, we interpreted the obtained results biologically. We also took into account data from circadian studies reported elsewhere and correlation between metabolite levels in blood and breath.

**Table 4.1.: Sleep characteristics of our study participants and reference values.**<sup>246</sup> These results show that sleep architecture was not significantly altered by the setup. Sleep efficiency and amounts of REM sleep were comparable to reference values. Slow-wave sleep (N3) was even more abundant and less arousals occurred compared to reference. Hence, sleep behavior in this study can be considered as normal.

Variable (TST)	Study subjects (n=13) Mean $\pm$ SD	Reference values for <50 years old Mean $\pm$ 2 SD
Total sleep time, hours	5.9 $\pm$ 1.5	–
Number of leg movements	104 $\pm$ 82	–
Heart rate, per minute	56.4 $\pm$ 12.3	–
Sleep efficiency, %	84 $\pm$ 20	85 (64-100)
Stadium N1, %	8 $\pm$ 8	6 (0-15)
Stadium N2, %	51 $\pm$ 9	63 (42-84)
Stadium N3, %	22 $\pm$ 9	10 (0-30)
REM %	17 $\pm$ 7	19 (7-32)
Arousal Index	8 $\pm$ 11	17 (1-32)
Apnea Hypopnea Index	0 $\pm$ 0	1 (0-8)

#### 4.2.2. SESI-HRMS measurements during sleep

In order to sample exhaled breath continuously, we modified a continuous positive airway pressure (CPAP) mask with a hole (inner  $\varnothing$  = 12 mm), through which the individuals could inhale and exhale freely. 0.2 L/min were drawn into the ionization chamber by a vacuum pump installed at the exhaust of the ionization source. The flow was controlled by a mass flow controller. The mask was connected to the SESI source via a flexible stainless steel tube, which was coated with SilcoNert 2000 (SilcoTek GmbH, Bad Homburg, Germany) and heated to 130 °C in order to prevent adsorption and condensation. The flexibility of this tube allowed the participants to move and sleep in different body positions. Real-time breath analysis was performed with a commercial SESI source (SEADM, Spain) coupled to a TripleTOF 5600+ high-resolution mass spectrometer (AB Sciex, Concord, ON, Canada). The spray solution consisted of 0.2 % formic acid (99-100 %, VWR chemicals) in water (LC-MS grade, Fisher Scientific) and a voltage of 5.5 kV was applied in positive ion mode and -4.5 kV in negative mode. Full scan mass spectra were recorded with an accumulation time of 10 s in a mass range from 50 to 500 Da in positive mode and 50 to 450 Da in negative ion mode respectively. The ion source was heated to 130 °C, curtain gas was set to 10, collision gas was set to 0, collision energy to (-)10 eV, declustering potential (-)20 V

#### 4.2.3. Polysomnography

In parallel to the SESI-HRMS measurements full polysomnography was performed in all participants using an Alice 6 system (Philips Respironics, PA USA). For the setup as well as the scoring the recommendations from the American Academy of Sleep Medicine from 2007 were applied (AASM 2007 criteria, version B).<sup>191</sup>

#### 4.2.4. Data preprocessing

Raw mass spectra were converted into .mzXML format using MSConvert (ProteoWizard)<sup>247</sup> and polysomnography data was exported to .edf files. Further data processing was performed in Matlab R2018b, R 3.6.1 and python 3.7.1. First, mass spectra were aligned across all scans and all subjects. Then, a peaklist was generated by interpolation and averaging every 50<sup>th</sup> scan of all spectra. For positive ion mode spectra, the obtained peaklist was recalibrated with a list of known reference peaks. All peaks were centroided by integration yielding time traces of all peaks (1458 in positive ion mode, 1028 in negative ion mode) for each subject. In order to reduce the number of features, the following filtering criteria were applied: Only features that were higher in exhaled breath than dry room air in at least 50 % of the subjects were kept. Further, features with median intensities below 30 counts per second in at least 50 % of the subjects were removed. Since sleep stages have been determined from PSG only in 30 s intervals, but mass spectra were recorded every 10 seconds, we interpolated sleep stage information. MS time traces were smoothed by Savitzky Golay filtering (smoothing window of 19 data points). In order to reduce technical noise, such as spray instabilities, but also to account for breathing variations, we normalized our data. The humidity of breath is supposed to be constant.<sup>248</sup> Therefore, we used the water cluster signal ( $[(\text{H}_2\text{O})_3+\text{H}]^+$ ,  $m/z$  55.03897) for normalization in positive ion mode and the signal of a water-formic acid cluster ( $[\text{HCOOH}+\text{H}_2\text{O}]^-$ ,  $m/z$  63.00877) for normalization in negative ion mode. MS times and PSG times were synchronized, data points during lights on period as well as data points, where only MS or only PSG data was available, were removed. Moreover, very short sleep stages (< 70 s) were annotated with the previous one.

#### 4.2.5. Statistics

##### 4.2.5.1. Detrending

In order to separate gradual changes in metabolic profiles across the night from acute changes across sleep stages, we subtracted a baseline prior to statistical analysis, which we obtained from Savitzky-Golay filtering (smoothing window of 1001 datapoints).

##### 4.2.5.2. One-way ANOVA

We fitted our data for each metabolite with linear mixed effects models with a fixed effect for sleep stage and a random effect for person using the Satterthwaite's degrees of freedom method.<sup>249</sup> We then performed an  $\chi^2$  test to assess, whether the model with the different levels for the different sleep stages performs better than the simplest model with only an intercept. The obtained p-values were corrected for multiple hypothesis testing using Storey's procedure.<sup>250</sup>

##### 4.2.5.3. Pairwise comparisons

We calculated average spectra per sleep stage for each subject and performed pairwise comparisons of the different sleep stages using a two-sided Wilcoxon signed ranked test. Again,

we corrected for multiple hypothesis testing using Storey's procedure.<sup>250</sup> In addition, we calculated pairwise effect sizes (Cohen's  $d$ <sup>251</sup>) between sleep stages for each metabolite.

#### 4.2.5.4. Inferring non-linear Granger causality with neural networks

To discover metabolic features that are Granger-caused by different sleep stages, we trained feedforward neural networks with a specially tailored architecture (see figure 4.1) with sparsity-inducing penalty terms in the loss function. Technical details are provided in the supplementary information. After the above mentioned preprocessing, we performed training on positive and negative mode MS time series for three stages of sleep separately: wakefulness, N3 and REM. All sequences were time-reversed<sup>252</sup> to infer Granger causal relationships from sleep stage transitions to metabolism. We used a bootstrap procedure<sup>253</sup> to identify significant interactions between variables (see Algorithm 1). Implementation details, values of hyperparameters and the results of simulation experiments and cross-validation are provided in the supplementary information section.

#### 4.2.6. Pathway enrichment analysis and compound identification

Automated compound information using metabolic pathway information was performed using the mummichog algorithm.<sup>215,254</sup> The algorithm was run with the q-values obtained from pairwise comparisons described above. Significance threshold was set to  $q = 0.05$  and the manually curated human genome-scale metabolic model from the mummichog python package ("MFN") was used as pathway library. Adducts were restricted to  $[M+H]^+$  and  $[M-H]^-$ . Since mostly protonated or deprotonated species are formed in SESI,<sup>221</sup> we removed all radicals from the list of annotated compounds. We did further manual investigation on metabolites involved in the pathways with the highest numbers of significant hits and we thus reduced the selection to a few key pathways. We selected only pathways with very high metabolite coverage and pathways, in which key metabolites were significant hits. Carboxylic acids, where protonated species were significant hits, but not the deprotonated forms, were neglected. When pathway coverage was only high, because one mass resulted in several significant hits due to different isomers in one pathway, those were also ignored. For compounds involved in those pathways of interest, MS/MS spectra obtained from exhaled breath condensate (EBC) were compared to database spectra. Experimental details of EBC collection and ultra-high performance liquid chromatography-tandem MS methods are described elsewhere.<sup>255</sup> If features were not detected in EBC, real-time SESI-MS/MS spectra were recorded using an Orbitrap QExactive Plus mass spectrometer (Thermo Fisher, Germany) with a commercial SESI source (SuperSESI, Fossil Ion Tech, Spain). Breath was sampled at 0.3 L/min. The sampling line of the ion source was heated to 130 °C, the ionization chamber was heated to 90 °C and a spray solution of 0.1 % formic acid in water was used. A spray voltage of (-)3500 V was applied. The mass spectrometer was operated at 140,000 resolution in data dependent acquisition mode with an isolation window of 0.4 m/z. The automated gain control was set to  $1e6$  at MS1 level and to  $1e5$  at MS/MS level and a maximal injection time of 500ms was used. MS/MS library spectra were obtained from the spectral library with all publicly available MS/MS records available for MSDial.<sup>214,256</sup>



## 4.2.7. Blood breath comparison experiments

### 4.2.7.1. Study participants

Nine healthy volunteers in the age of  $30.6 \pm 7.8$  years, 44 % female, were studied to compare metabolite levels in breath and blood. All participants were non-smokers and did not take any medication. The participants underwent real-time breath analysis by SESI-HRMS and whole blood has been withdrawn simultaneously. Participants were asked to refrain from eating, drinking (except water), chewing gum, brushing their teeth and using any facial cosmetics (such as lip balm) during at least one hour prior to the measurements. The experiments were conducted in accordance with the Declaration of Helsinki and written informed consent was obtained from all participants. The study was approved by the local ethical committee (KEK-ZH 2016-00384).

### 4.2.7.2. Real-time SESI-HRMS breath analysis

Real-time breath measurements were performed similar to breath measurements during sleep. Instead of the flexible tube and the mask a single-use mouthpiece was connected to the sampling line. The flow through the ion source was controlled to 0.2 L/min by a low- $\Delta p$  mass flow controller (Bronkhorst, Switzerland) at the exhaust of the source. The participants were exhaling with a pressure drop of 12 mbar and to enable sampling of end-tidal breath, a flow-splitter was installed front-end. No vacuum pump was used in this setup. Full scan mass spectra were recorded in the range of 50 to 500 Da in positive mode with an accumulation time of 1 s. At least six exhalations were measured per person. All other parameters were as described for the measurements during sleep.

### 4.2.7.3. UPLC-tandem-MS measurements of serum

Whole blood was left at room temperature for 10-30 min for clotting. To obtain serum, it was then centrifuged for 15 min at 1500 rpm. Aliquots of 200  $\mu\text{L}$  were taken, 200  $\mu\text{L}$  of 1 mg/mL  $^{15}\text{N}_2$ -tryptophan (Cambridge Isotope Laboratories, Inc., Tewksbury, USA) in water were added as internal standard and proteins were precipitated by the addition of 600  $\mu\text{L}$  of methanol (LC-MS grade, Fisher Scientific, Pittsburgh, USA). Samples were incubated on ice for 10 minutes and centrifuged at 4  $^\circ\text{C}$  and 15800 g for 15 min. The supernatant was filtered using a 0.2  $\mu\text{m}$  reversed cellulose membrane filter, 400  $\mu\text{L}$  were aliquoted and solvents were removed in a vacuum dryer. The residual was resuspended in 75 mL of a mixture of water and methanol (95/5, v/v, both LC-MS grade, Fisher Scientific, Pittsburgh, USA), sonicated (10 min) and centrifuged (15 min, 15800 g) and transferred to LC vials with glass inserts. 10  $\mu\text{L}$  were injected for analysis. One sample per person has been analysed, analytical reproducibility was verified with quality control samples.

Chromatographic separation was performed on an ACQUITY UPLC system (I-Class, Waters, MA, USA) using an ACQUITY UPLC BEH C18 column (1.7  $\mu\text{m}$ , 2.1  $\times$  150 mm, Waters) with a corresponding precolumn filter. The flow rate was set to 240  $\mu\text{L}/\text{min}$  using a binary mixture of solvent A (water with 0.5 % methanol and 0.1 % formic acid) and solvent B (methanol with 0.1 % formic acid). The following gradient was used: 5 % B (1 min), 5 to 95 %

B (9 min), 100 % B (2 min), and 5 % B (2 min). The column temperature was set to 30 °C and the autosampler was kept at 5 °C.

Mass spectra were recorded on a quadrupole-time-of-flight high-resolution mass spectrometer (TripleTOF 5600+, AB Sciex, Concord, ON, Canada) with a heated electrospray ionization source in positive ion mode. Full-scan mass spectra ( $m/z$  range 50 to 650 Da) and data dependent MS/MS acquisitions ( $m/z$  range 50 to 650 Da) were performed. Curtain gas was set to 30, GS1 and GS2 were set to 50, a spray voltage of 5 kV was applied and the ion source was heated to 500 °C. The total cycle time was kept at 800 ms to obtain at least 12 points/peak (minimal LC peak width = 9 s) with 150 ms for full scan MS and 85 ms for seven product ion scans acquired with a collision energy of 10/20/30 eV.

#### 4.2.7.4. Data analysis.

Data preprocessing of breath spectra was performed as described elsewhere.<sup>226</sup> Signal intensities were normalized to the water cluster signal ( $[(\text{H}_2\text{O})_3+\text{H}]^+$ ,  $m/z$  55.03897). Raw data obtained from blood was converted to .mzXML format with MSConvert (ProteoWizard)<sup>247</sup> and further processed in Matlab R2018b, R 3.6.1. After centroiding, chromatographic peaks of target compounds were integrated. Robust linear regression<sup>257</sup> was performed with the intensities obtained from blood and breath. In addition, we calculated Pearson's and Spearman's correlation coefficients. As described above, we compared MS/MS spectra from blood and exhaled breath condensate with database spectra, to confirm the identities of the detected acylcarnitines.

Table 4.2.: Summary of identified metabolites with differential regulation across different stages of vigilance.

m/z	sum formula	mass error (ppm)	compound name	identified based on	adduct	q-value				effect size				Granger causal for			
						q-value ANOVA	N3 vs. REM WK	N3 vs. WK	N3 vs. REM WK	N3 vs. REM WK	N3 vs. WK	N3 vs. REM WK	N3 vs. WK	N3 vs. REM WK	N3 vs. WK	N3 vs. REM WK	N3 vs. WK
160.0971	C <sub>7</sub> H <sub>13</sub> NO <sub>3</sub>	1.77	dehydrocarnitine	exact mass & pathway mapping	[M+H] <sup>+</sup>	5.23E-149	0.105	0.076	0.291	0.85	1.31	0.3	yes	no	yes		
104.0705	C <sub>4</sub> H <sub>9</sub> NO <sub>2</sub>	0.76	aminobutanoate	MS/MS spectrum from EBC	[M+H] <sup>+</sup>	5.10E-62	0.063	0.046	0.31	1.22	0.88	-0.42	yes	no	no		
162.1125	C <sub>7</sub> H <sub>15</sub> NO <sub>3</sub>	0.21	carnitine	MS/MS spectrum from EBC	[M+H] <sup>+</sup>	1.66E-108	0.126	0.042	0.233	0.79	1.07	0.47	yes	no	no		
204.123	C <sub>9</sub> H <sub>17</sub> NO <sub>4</sub>	0.19	acetylcarnitine	MS/MS spectrum from EBC	[M+H] <sup>+</sup>	2.37E-99	0.095	0.043	0.31	0.84	1.32	0.43	yes	no	yes		
216.1233	C <sub>10</sub> H <sub>17</sub> NO <sub>4</sub>	1.32	acryloylcarnitine	exact mass & pathway mapping	[M+H] <sup>+</sup>	1.60E-47	0.187	0.043	0.31	0.6	0.99	0.28	yes	no	no		
218.1385	C <sub>10</sub> H <sub>19</sub> NO <sub>4</sub>	0.73	propionylcarnitine	MS/MS spectrum from EBC	[M+H] <sup>+</sup>	1.17E-101	0.251	0.039	0.233	0.5	1.45	0.38	no	no	yes		
232.1545	C <sub>11</sub> H <sub>21</sub> NO <sub>4</sub>	0.56	butyrylcarnitine	exact mass & pathway mapping	[M+H] <sup>+</sup>	8.21E-09	0.115	0.04	0.31	0.53	1.24	0.58	no	no	no		
179.0553	C <sub>6</sub> H <sub>12</sub> O <sub>6</sub>	4.68	hexose	MS/MS spectrum from EBC	[M+H] <sup>-</sup>	1.12E-06	0.075	0.024	0.054	-0.65	1.13	1.19	no	yes	yes		
133.0498	C <sub>5</sub> H <sub>10</sub> O <sub>4</sub>	6.47	deoxypentose	exact mass & pathway mapping	[M+H] <sup>-</sup>	2.30E-150	0.247	0.04	0.012	-0.57	1.35	1.5	no	no	yes		
149.0448	C <sub>5</sub> H <sub>10</sub> O <sub>5</sub>	4.86	pentose	real-time MS/MS spectrum	[M-H] <sup>-</sup>	6.50E-25	0.02	0.038	0.022	-1.53	1.91	2.59	no	yes	yes		
177.0395	C <sub>6</sub> H <sub>10</sub> O <sub>6</sub>	5.24	hexonolactone	exact mass & pathway mapping	[M-H] <sup>-</sup>	8.69E-20	0.156	0.048	0.11	-0.17	0.94	0.57	no	yes	yes		
195.0505	C <sub>6</sub> H <sub>12</sub> O <sub>7</sub>	2.73	hexonate	exact mass & pathway mapping	[M+H] <sup>-</sup>	3.80E-03	0.173	0.014	0.021	-1.62	1.47	2.33	no	yes	yes		
105.0186	C <sub>3</sub> H <sub>6</sub> O <sub>4</sub>	7.15	glycerate	exact mass & pathway mapping	[M-H] <sup>-</sup>	9.87E-169	0.141	0.056	0.138	0.72	1.32	0.93	no	no	yes		
103.003	C <sub>3</sub> H <sub>4</sub> O <sub>4</sub>	7.1	hydroxypyruvate	exact mass & pathway mapping	[M-H] <sup>-</sup>	7.04E-03	0.49	0.227	0.111	0.43	-0.69	-0.76	no	no	no		
72.993	C <sub>2</sub> H <sub>2</sub> O <sub>3</sub>	1.05	glyoxylate	exact mass & pathway mapping	[M-H] <sup>-</sup>	1.17E-09	0.03	0.509	0.154	1.02	-0.02	-0.83	no	yes	no		
88.9876	C <sub>2</sub> H <sub>2</sub> O <sub>4</sub>	4.62	oxalate	exact mass & pathway mapping	[M+H] <sup>-</sup>	1.23E-18	0.156	0.035	0.019	0.53	-0.96	-0.89	no	no	yes		
131.0342	C <sub>3</sub> H <sub>8</sub> O <sub>4</sub>	6.18	acetolactate	exact mass & pathway mapping	[M-H] <sup>-</sup>	2.72E-30	0.289	0.227	0.042	0.38	0.63	0.34	no	no	no		
87.0083	C <sub>3</sub> H <sub>4</sub> O <sub>3</sub>	5.94	pyruvate	exact mass & pathway mapping	[M-H] <sup>-</sup>	4.17E-53	0.03	0.557	0.047	0.82	-0.15	-0.89	no	yes	yes		
101.0237	C <sub>4</sub> H <sub>6</sub> O <sub>3</sub>	7.59	acetoacetate	exact mass & pathway mapping	[M+H] <sup>-</sup>	3.49E-73	0.049	0.267	0.506	1.13	0.66	0.06	no	no	no		
89.0241	C <sub>3</sub> H <sub>6</sub> O <sub>3</sub>	3.56	lactate	exact mass & pathway mapping	[M+H] <sup>-</sup>	1.67E-17	0.141	0.155	0.023	0.64	-0.62	-0.99	no	yes	yes		
130.9977	C <sub>4</sub> H <sub>4</sub> O <sub>5</sub>	6.98	oxaloacetate	described elsewhere68	[M-H] <sup>-</sup>	5.37E-02	0.018	0.405	0.098	0.87	-0.17	-0.84	no	no	yes		
133.0134	C <sub>4</sub> H <sub>6</sub> O <sub>5</sub>	6.05	malate	described elsewhere68	[M-H] <sup>-</sup>	1.38E-55	0.02	0.447	0.047	0.71	-0.1	-0.74	yes	yes	no		
115.003	C <sub>4</sub> H <sub>4</sub> O <sub>4</sub>	6.18	fumarate	described elsewhere68	[M+H] <sup>-</sup>	1.57E-05	0.075	0.508	0.286	0.93	0.17	-0.54	no	no	no		
117.0185	C <sub>4</sub> H <sub>6</sub> O <sub>4</sub>	6.93	succinate	described elsewhere68	[M-H] <sup>-</sup>	3.62E-03	0.406	0.561	0.487	0.47	0.22	-0.17	no	no	no		
145.0133	C <sub>5</sub> H <sub>6</sub> O <sub>5</sub>	6.44	oxoglutarate	described elsewhere68	[M-H] <sup>-</sup>	3.41E-11	0.141	0.155	0.486	0.87	0.65	-0.04	no	no	no		
191.0183	C <sub>6</sub> H <sub>8</sub> O <sub>7</sub>	7.5	(iso)citrate	described elsewhere68	[M-H] <sup>-</sup>	4.81E-12	0.065	0.508	0.201	1.01	0.11	-0.75	no	no	no		
173.0081	C <sub>6</sub> H <sub>6</sub> O <sub>6</sub>	6	aconitate	described elsewhere68	[M+H] <sup>-</sup>	1.70E-17	0.025	0.289	0.244	1.19	0.47	-0.61	no	no	no		
205.0347	C <sub>7</sub> H <sub>10</sub> O <sub>7</sub>	3.28	methylcitrate	exact mass & pathway mapping	[M-H] <sup>-</sup>	3.97E-48	0.113	0.289	0.505	1.16	0.62	-0.12	no	no	no		
187.0238	C <sub>7</sub> H <sub>8</sub> O <sub>6</sub>	5.18	methylaconitate	exact mass & pathway mapping	[M-H] <sup>-</sup>	7.35E-22	0.025	0.332	0.201	1.26	0.5	-0.62	no	no	no		
101.0237	C <sub>4</sub> H <sub>6</sub> O <sub>3</sub>	7.59	succinate semialdehyde	exact mass & pathway mapping	[M+H] <sup>-</sup>	3.49E-73	0.049	0.267	0.506	1.13	0.66	0.06	no	no	no		
103.0393	C <sub>4</sub> H <sub>8</sub> O <sub>3</sub>	7.15	hydroxybutyrate	exact mass & pathway mapping	[M+H] <sup>-</sup>	3.06E-53	0.127	0.355	0.467	0.96	0.5	-0.08	no	no	yes		
73.0293	C <sub>3</sub> H <sub>6</sub> O <sub>2</sub>	2.63	propanoate	exact mass & pathway mapping	[M-H] <sup>-</sup>	7.20E-127	0.333	0.016	0.028	0.14	1.2	1.17	yes	no	yes		
89.0241	C <sub>3</sub> H <sub>6</sub> O <sub>3</sub>	3.56	hydroxypropanoate	real-time MS/MS spectrum	[M-H] <sup>-</sup>	1.67E-17	0.141	0.155	0.023	0.64	-0.62	-0.99	no	yes	yes		
87.0083	C <sub>3</sub> H <sub>4</sub> O <sub>3</sub>	5.94	malonate semialdehyde	exact mass & pathway mapping	[M+H] <sup>-</sup>	4.17E-53	0.03	0.557	0.047	0.82	-0.15	-0.89	no	yes	yes		
181.0708	C <sub>6</sub> H <sub>14</sub> O <sub>6</sub>	5.24	hexitol	MS/MS spectrum from EBC	[M-H] <sup>-</sup>	1.68E-03	0.014	0.016	0.022	-1.47	1.41	2.16	no	yes	yes		
193.0347	C <sub>6</sub> H <sub>10</sub> O <sub>7</sub>	3.74	hexuronate	exact mass & pathway mapping	[M+H] <sup>-</sup>	1.04E-05	0.041	0.035	0.016	-1.15	1.14	1.77	no	yes	yes		
163.0602	C <sub>6</sub> H <sub>12</sub> O <sub>5</sub>	6.4	deoxyhexose	exact mass & pathway mapping	[M+H] <sup>-</sup>	9.77E-04	0.018	0.074	0.047	-1.71	0.45	1.28	no	no	yes		
151.06	C <sub>5</sub> H <sub>12</sub> O <sub>5</sub>	7.64	pentitol	real-time MS/MS spectrum	[M+H] <sup>-</sup>	4.91E-22	0.015	0.019	0.022	-1.69	1.53	2.52	no	yes	yes		

## 4.3. Results

### 4.3.1. Breath analysis during sleep

We analyzed exhaled breath of healthy individuals while they were sleeping in order to access metabolic pathway activity during different states of vigilance (see workflow, figures 4.2a, 4.1). Making use of the non-invasive and very high sampling frequency of SESI-HRMS breath analysis, we were able to access the human metabolome with an average depth of about 2000 metabolites per timepoint during sleep with a time resolution of ten seconds, while performing polysomnography in parallel (figure 4.2a). In total 13 healthy individuals with a normal sleep architecture (table 4.1) were analysed and we were able to detect traces of 1996  $m/z$  features over time. These traces were baseline-subtracted in order to remove confounding gradual changes in metabolite time profiles due to the unequal distribution of NREM sleep and REM sleep across the night, and then correlated with individual sleep stages (figure 4.2 b,c; heat maps for all individuals are given in supplementary figures B.1 and B.2, Dataset 1). In each subject, clear indications of families of sleep-regulated metabolites were visible as vertical stripes in these heat maps.

### 4.3.2. Sleep stage-specific metabolic patterns

In order to access whether there is noteworthy differential metabolic regulation globally across different stages of sleep, we first visualized median mass spectra of each sleep stage of all study subjects after dimension reduction. We found that spectral data of different people belonging to the same stage of vigilance cluster together (figure 4.3a), whereas we did not observe clustering according to subjects (figure 4.3b). Using analysis of variance individually for each metabolite, we then tested how a model considering sleep states to affect metabolite levels in breath performs compared to the null hypothesis of a model that does not consider sleep stages, and generated  $q$ -value distributions of all metabolites (figure 4.4a). Remarkably, for most of the detected  $m/z$  features (1277 features), a significant association with sleep state,  $q < 0.001$ , is observed across major sleep states (NREM, REM, WK (figure 4.4b-d). By contrast, far fewer differences were observed among metabolites across related sleep states (N1, N2, N3; 4.4e-g). Therefore, we did not consider N1 and N2 sleep in our further analysis.

### 4.3.3. Immediate metabolic regulation

To further investigate the nature of these sleep state-dependent metabolic patterns, we followed two approaches of analysis. First, we performed pairwise comparisons of breath metabolite levels during different sleep stages using Wilcoxon signed rank tests in order to detect rapid changes in levels of individual metabolites (An example from three individuals is shown in figure 4.5a, b. Numerical comparisons across all subjects and features are summarized in figure 4.5c, with individual metabolites listed in table B.2. Sample boxplots across all subjects and sleep stages are shown in figure 4.5d.). We found significant differences ( $q < 0.05$ ) between REM sleep and wakefulness for 842  $m/z$  features. Relative concentrations of 411 features differed between N3 sleep and wakefulness and 312 features had different levels during REM sleep and N3 sleep (figure 4.5c, supplementary figure B.3).

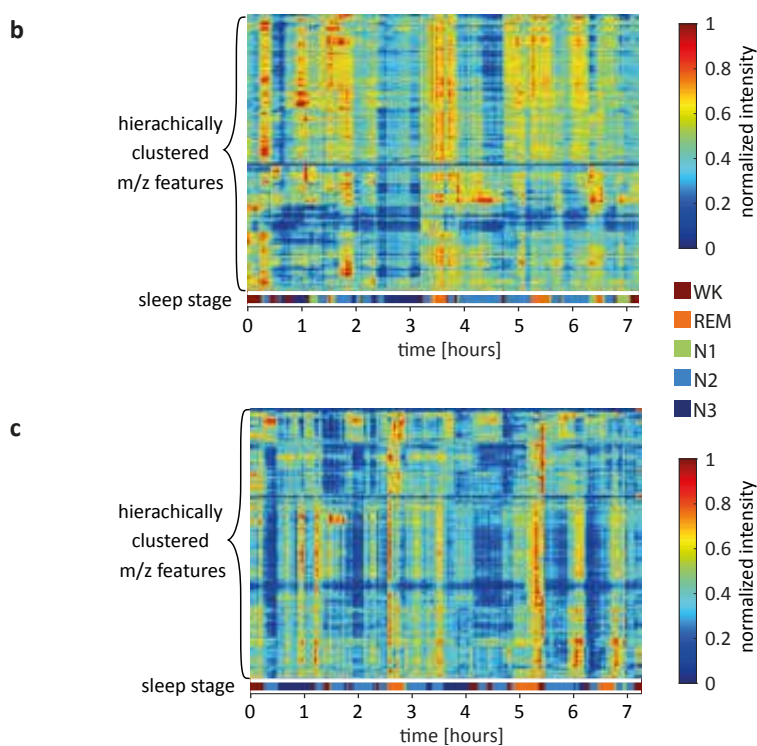
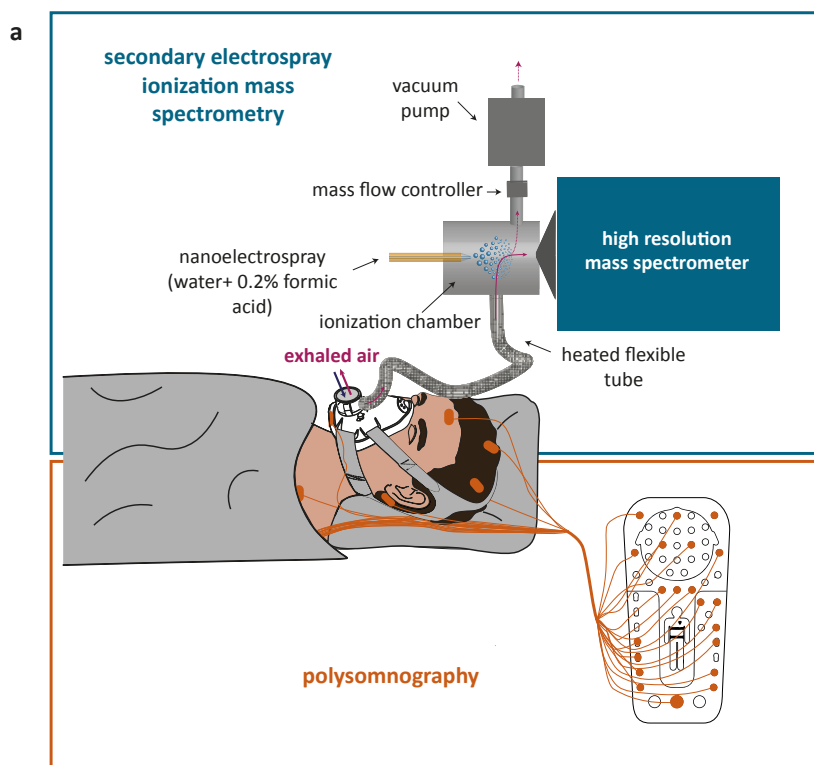


**Figure 4.2.: Real-time breath analysis during sleep by SESI-HRMS. a** Experimental Setup. Exhaled breath was sampled continuously with a mask, which was connected directly to the ionization source via a heated flexible tube. Molecules were ionized in the electrospray consisting of water and formic acid. Sample flow was controlled at the exhaust of the SESI source. Ions were detected with a high-resolution time-of-flight mass spectrometer. In parallel a full polysomnography was performed. **b,c** Heat map of 1271 m/z features detected in positive ionization mode (**b**) and 725 m/z features detected in negative ionization mode (**c**) over time in one subject after feature-wise baseline subtraction. Sleep stages are labeled on the bottom of the heat maps.

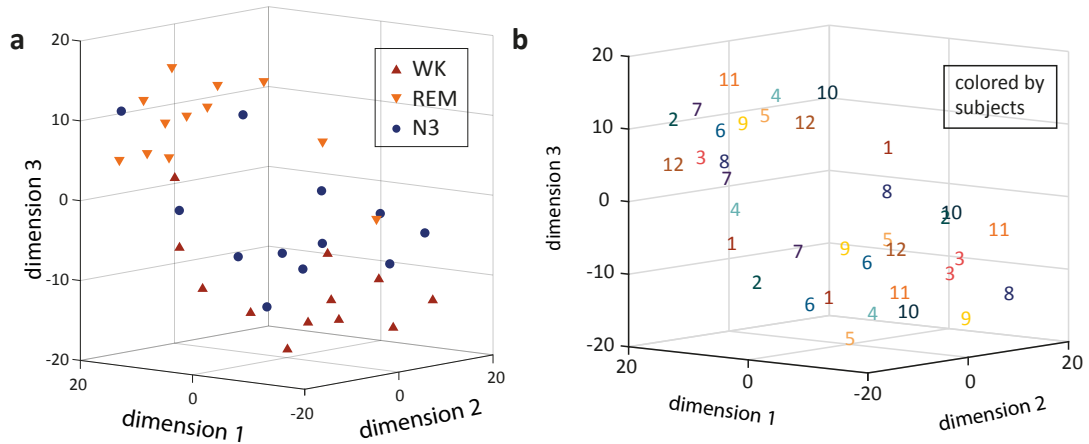


**Figure 4.3.:** Visualization of median breath spectra during N3 sleep, REM sleep and wakefulness after dimension reduction by t-distributed stochastic neighbor embedding. **a** Data points are colored by sleep stage. **b** Data points are colored and numbered by subjects. In contrast to sleep stage labeled data, here no subject-wise clustering is recognizable. This supports the hypothesis that instantaneous metabolic changes occur across different stages of vigilance.

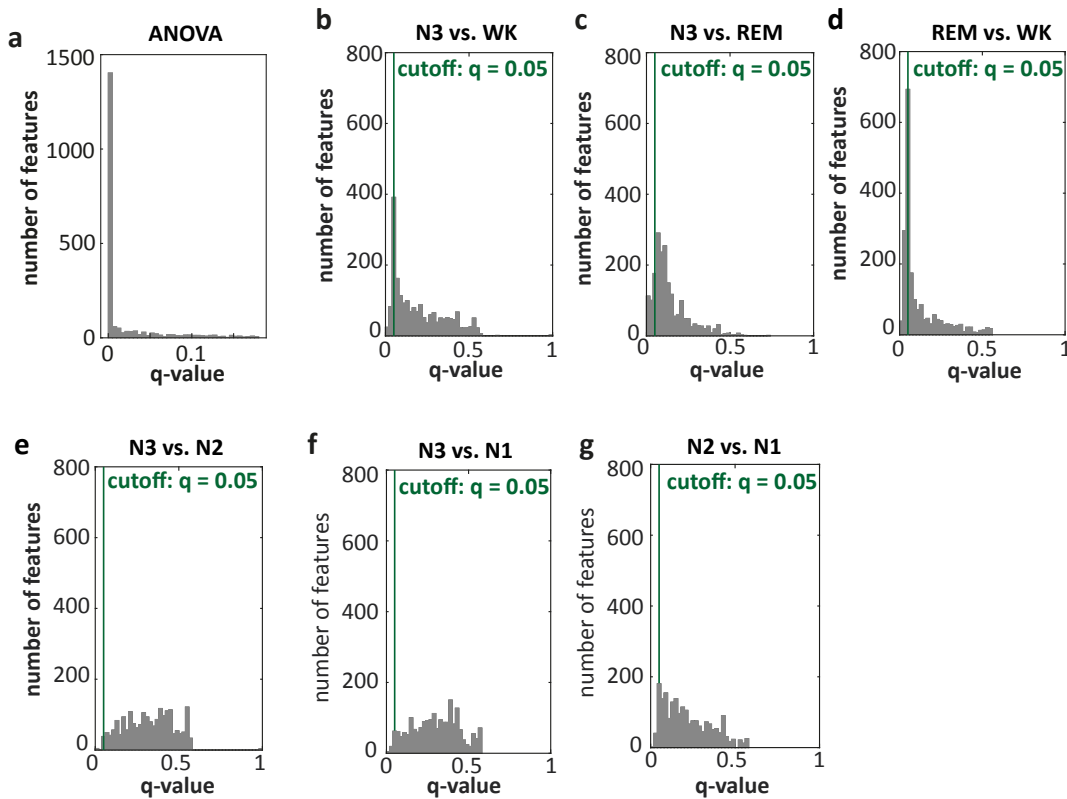


**Figure 4.4.:** a Q-value distribution of ANOVA testing for differences between a model accounting for different effects of sleep stages and a model not accounting for these differences. For 1277 features we obtained q-values below 0.001. This indicates sleep stage specific regulation of a major part of the metabolome. **b-g** Q-value distributions from pairwise comparisons using Wilcoxon signed rank tests. While comparisons of N3 sleep, REM sleep and wakefulness revealed metabolic differences between these states, flat q-value distributions obtained from comparisons between N1, N2, N3 suggest similarity between those stages also on a metabolic level.

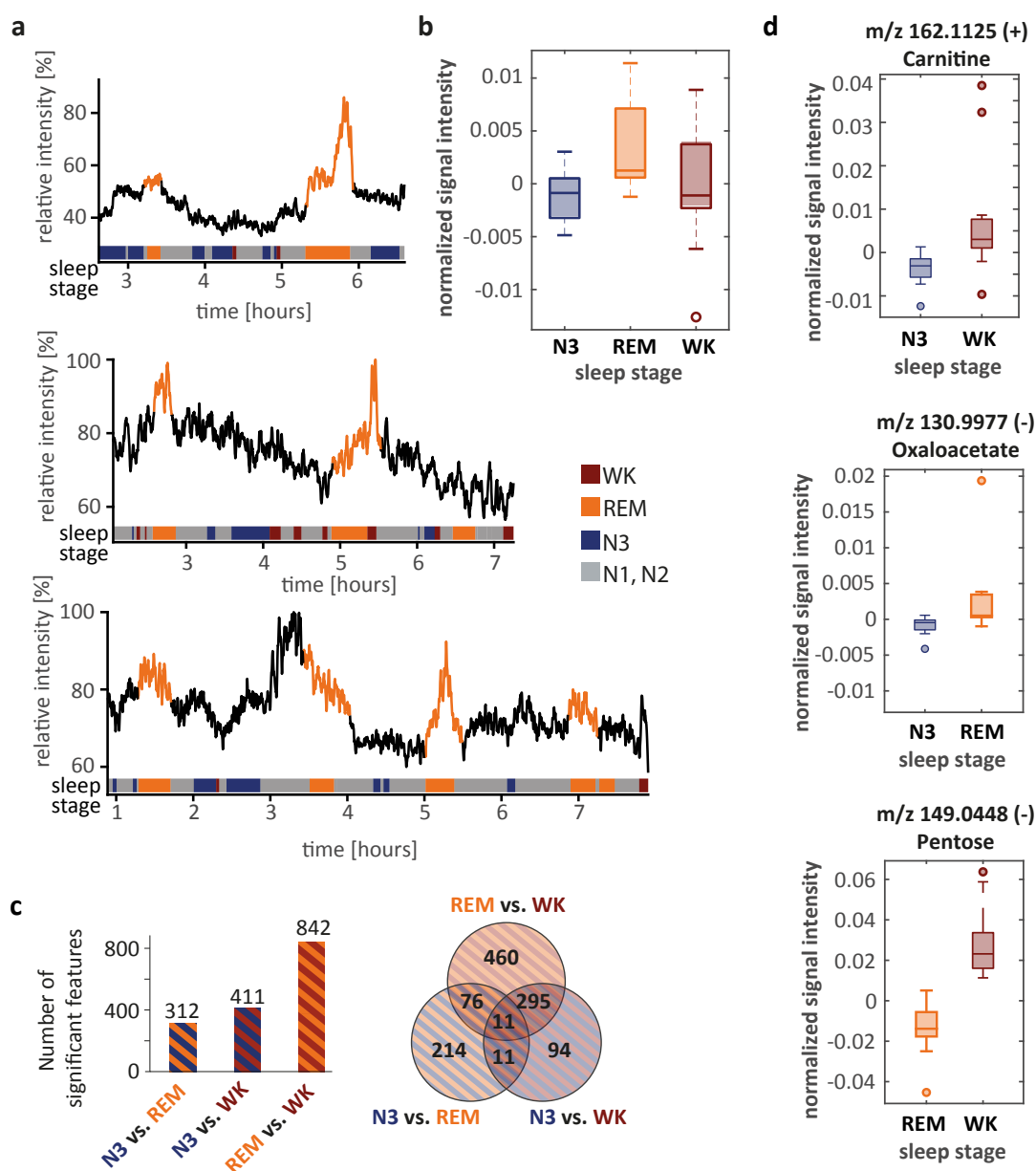


**Figure 4.5.:** **a** Time traces of m/z 149.0237 (negative mode, hereafter abbreviated as “-“) in three individuals, showing the direct increase of metabolite levels with REM sleep. We detected such metabolites using conventional comparative statistics. **b** Resulting boxplot (center line: median, box limits: 25<sup>th</sup> and 75<sup>th</sup> percent quantile, whisker length: 1.5 interquartile range) of metabolite shown in a. **c** Pairwise comparisons of mean breath spectra in Wilcoxon signed ranked tests suggest significantly differential regulation of hundreds of metabolites across different stages of sleep as presented in the bar plot. The Venn diagram shows that also here, there are overlaps between the sets of significant m/z features. **d** Boxplots (center line: median, box limits: 25<sup>th</sup> and 75<sup>th</sup> percent quantile, whisker length: 1.5 interquartile range) of three metabolites identified as carnitine, oxaloacetate and pentose showing significantly different levels in breath during N3 sleep and wakefulness, during N3 and REM sleep and during REM sleep and wakefulness, respectively.

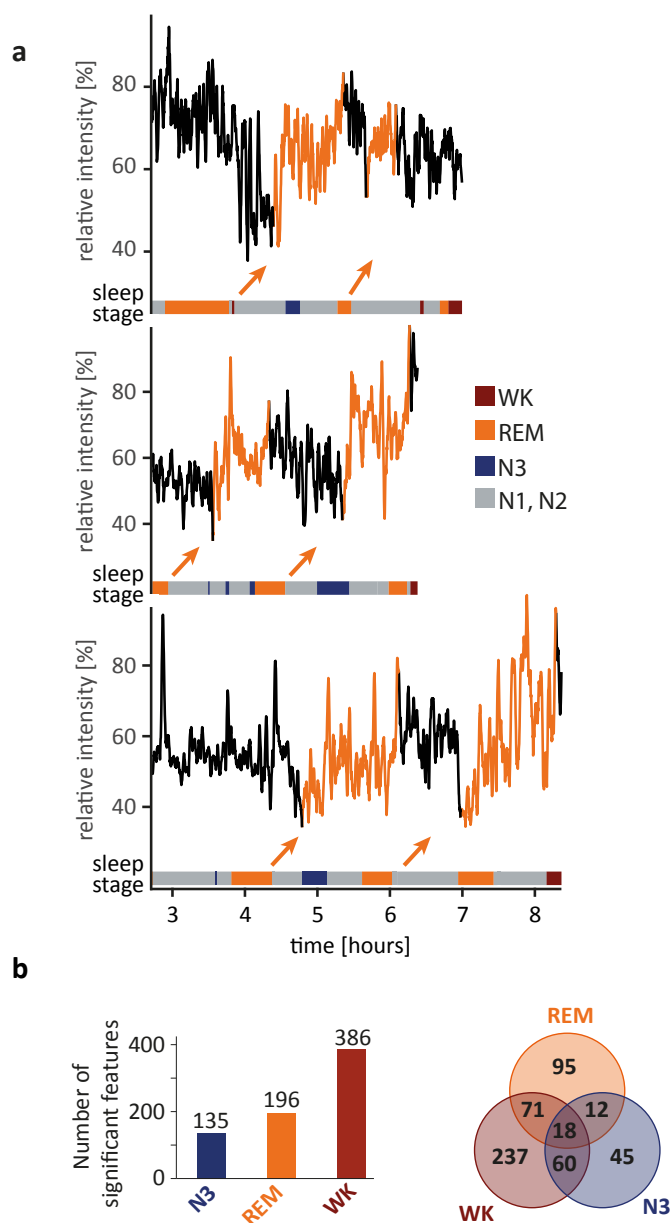


**Figure 4.6.:** **a** Time traces of  $m/z$  181.06 (-) in three individuals. Metabolite levels were rising slowly after the occurrence of REM sleep. Our analysis based on Granger causality unraveled such more complex temporal relationships. **b** Results from inferring non-linear Granger causality with neural networks suggest causal relationships between several hundreds of  $m/z$  features and N3 sleep, REM sleep and wakefulness as shown in the bar plot. The Venn diagram shows that these sets of features are overlapping.



In order to move beyond conventional analysis and the discovery of pairwise correlations of time-series variables (in our case a particular metabolite and a particular sleep stage), towards identifying directed (“causal”) interactions which could characterize functional circuits relating sleep and metabolism, we developed a neural network-based method to infer Granger causal relationships. The concept of Granger causality was previously very successfully applied in the domains of economics<sup>258</sup> and neuroscience.<sup>259</sup> Our Granger causality framework (fully described in the supplementary information) offers an alternative view of our data, based upon the concept of predictability: the idea is that the most significant sleep-related metabolites can be used to predict sleep states. Other technical advantages, such as modeling of nonlinear and time-delayed relationships are extensively discussed in the supplementary information. An example from three individuals is shown in figure 4.6a. Numerical comparisons across all subjects and features are summarized in figure 4.6b, with individual metabolites listed in table B.2. Our analysis based on Granger causality resulted in 386, 196 and 135 features associated with wakefulness, REM sleep and N3 sleep respectively, many of which (182, 60, 59) were not identified by our initial conventional approach.

#### 4.3.4. Pathway mapping of MS features

To understand the biology behind the metabolic regulation triggered by sleep stages, we performed compound identification and pathway analysis. Compound identification is still the biggest challenge in the field of metabolomics. Nevertheless, more and more tools are being developed for automated compound annotation.<sup>260</sup> We used an annotation algorithm that combines information about elemental composition obtained from the accurately measured mass with metabolic pathway mapping and enrichment analysis.<sup>254</sup> In this way, possible errors in the identification of any individual compound are “averaged out” against the expectation that quantitative differences would be observed across multiple metabolites within a given pathway. Since automated annotation is still prone to false positives, we further investigated top pathway hits further manually and confirmed the identities of several compounds with tandem mass spectrometry data from liquid chromatography – mass spectrometry measurements of exhaled breath condensate or from real-time breath measurements (figure 4.7).

#### 4.3.5. Sleep stages control axes of metabolism

Ontological analyses suggest that major axes of metabolism, such as lipid metabolism, carbohydrate metabolism and TCA cycle activity are in fact strongly sleep state-dependent (overview in figure 4.8, boxplots in figure B.4, quantitative results in table 4.2).

For example, we were able to identify short-chain acylcarnitines in exhaled breath for the first time (figure 4.10a-d), and we found breath levels of short-chain acylcarnitines to be highest during wakefulness and lowest during N3 sleep. For most of them, we additionally found Granger causal relationships to wakefulness and/or N3 sleep. We did not detect significant differences in carnitine levels between N3 and REM sleep. Thus, systemic changes in fatty acid oxidation are occurring across sleep and wake (yellow quadrant, figure 4.8): whereas a switch to wake increases fatty acid oxidation, a switch to NREM sleep reduces it.

Similarly, we found several metabolites involved in propanoate and butanoate metabolism

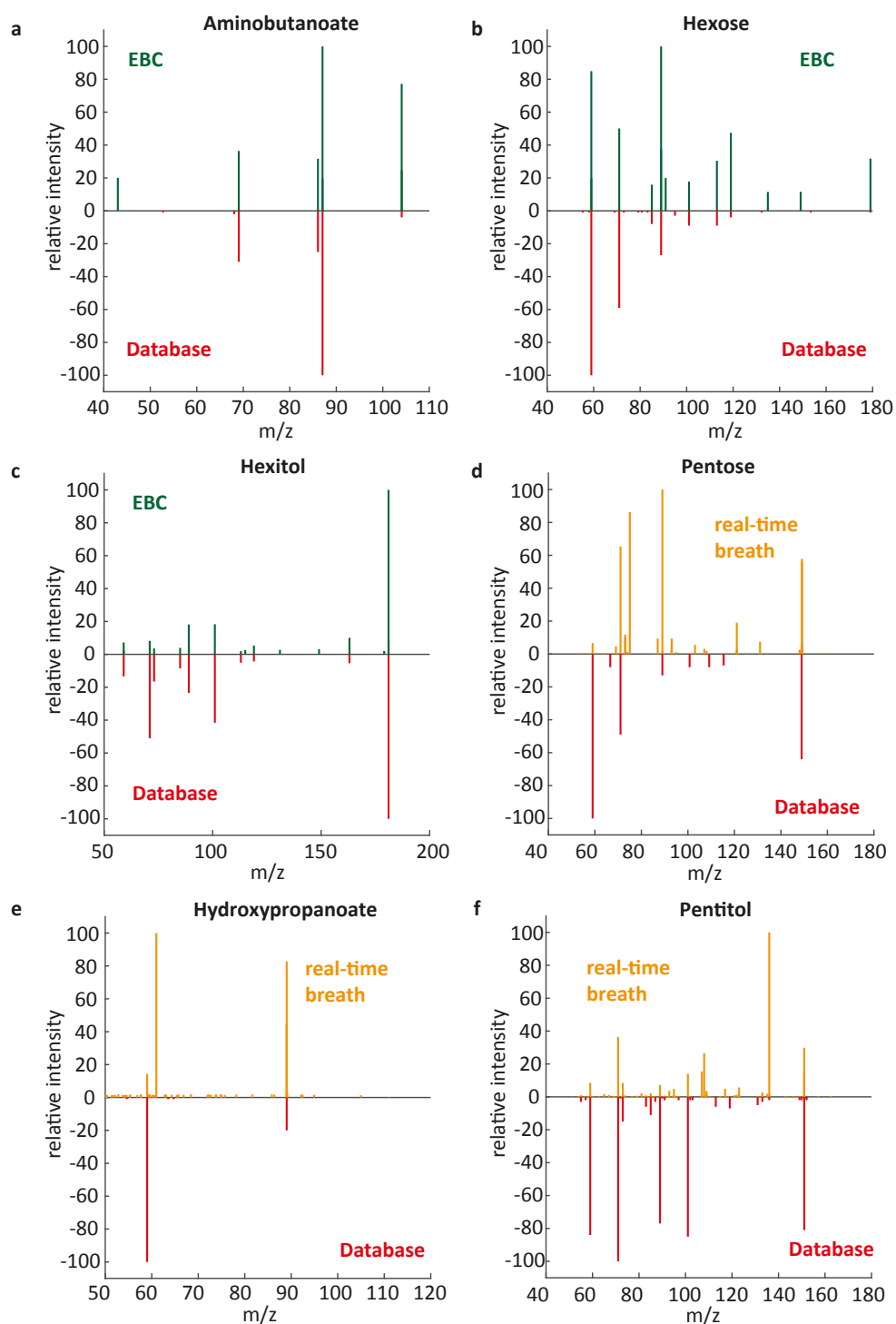


**Figure 4.7.:** MS/MS spectra from exhaled breath condensate (EBC) (a-c) and from real-time breath measurements (d-f) in comparison with database spectra. Database spectra were obtained from MS-DIAL<sup>256</sup> (all publicly available MS/MS records).

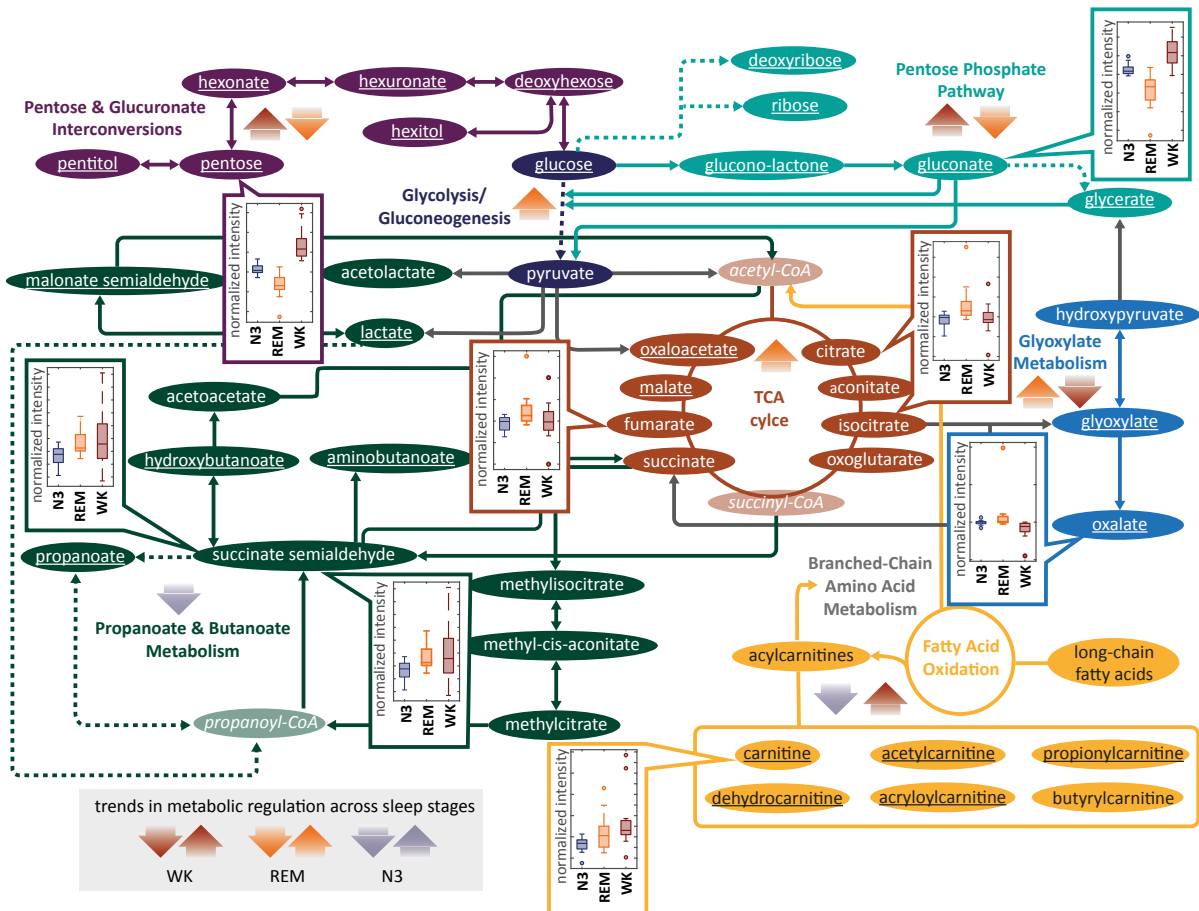


**Figure 4.8.: Metabolic pathways with differential regulation across different stages of vigilance.** Metabolites in *italic font* in transparent ovals are not detected. Solid ovals: metabolites showing significant differences. Boxplots are shown for a subset of these (center line: median, box limits: 25<sup>th</sup> and 75<sup>th</sup> percent quantile, whisker length: 1.5 interquartile range); Boxplots of all indicated compounds are provided in supplementary figure B.4, and numeric results in table 4.2. Underlined compounds additionally exhibit a Granger causal relationship between metabolite level and at least one sleep stage. Metabolic up- or downregulation during sleep stages are indicated for each pathway with arrows. Dashed lines indicate omitted molecules.

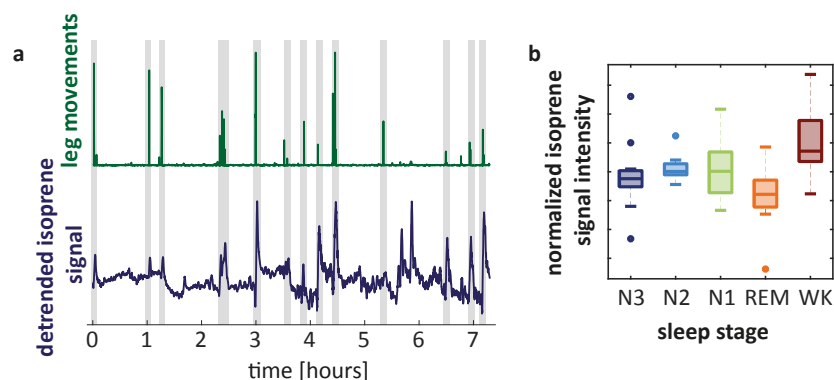


**Figure 4.9.: Breath levels of isoprene during sleep.** **a** The isoprene level in breath increases instantaneously with leg movements measured by EMG. **b** During REM sleep acute decrease of isoprene is observed. These findings are in good agreement with a study by King *et al.*<sup>261</sup> where isoprene levels were measured during sleep using proton transfer reaction mass spectrometry (PTR-MS). Thus, we were able to validate data recorded with a different technique, at a different time, with a different sample cohort and at a different laboratory. As described before,<sup>261</sup> this behavior can be explained by the fact that isoprene is mainly reflecting muscle activity. Muscles are the main compartment where isoprene is stored.<sup>262</sup> Therefore, during REM sleep, characterized by muscle atony,<sup>263</sup> lower isoprene levels in blood and thus also in breath are expected. During leg movements, in contrast, muscle perfusion is increased explaining higher isoprene levels in breath.

to be downregulated during NREM sleep and for propanoate and aminobutanoate we also found Granger causal indications of this connection (green quadrant, figure 4.8). These molecules are natural byproducts of fat and protein metabolism.

We observed increased levels of several TCA cycle intermediates during REM sleep (brown quadrant, figure 4.8). We also found malate and oxaloacetate to be Granger causally related with REM sleep. (Succinate was not upregulated during REM sleep.) Since normally REM sleep can only follow NREM sleep, a transition to REM sleep results in elevation of TCA cycle intermediates, possibly preparing for mitochondrial oxidation later in wake.

Finally, examining glycolysis, we found highest glucose levels in breath during wakefulness and lowest levels during REM sleep. We observed a similar behavior for several other metabolites involved in pentose phosphate pathway and pentose and glucuronate interconversions. For most of them, we also find Granger causal relationships with REM sleep and wakefulness. In contrast, we found opposite trends for pyruvate levels. They were increased during REM sleep and lowest during wakefulness. In addition, for many metabolites involved in carbohydrate metabolism, we observed significant differences between REM sleep and N3 sleep (purple and turquoise quadrants, figure 4.8).

## 4.4. Discussion

By taking advantage of metabolites present in human breath, our studies measure the human metabolome noninvasively at the unprecedented resolution of ten seconds across the night. Such exhaled metabolites are mainly the product of diffusion across the lung alveolar membrane, and therefore are thought to resemble the composition of the blood metabolome, with additional contributions from the upper airways.<sup>264</sup> We have separately verified this in

nine subjects, comparing the results of the metabolome in blood draws during wakefulness to that obtained from breath at the same time point. Levels of these carnitines correlate well with blood levels (figure 4.10e-i and figure 4.11a-d), indicating that breath levels are reflecting systemic carnitine levels. We also verified this relation between breath and blood metabolites for representatives of other metabolic pathways such as the TCA cycle (fumarate), glycolysis (lactate), propionate metabolism (lactate) and the pentose phosphate pathway (glycerate) (figure 4.11e-g).

Our results imply that a major part of the human metabolome is subjected to sleep stage-specific regulation. As mentioned above, this question has been hitherto difficult to address due to issues of sampling rate vs. sleep stage duration. However, our studies are in agreement with other existing data as we note below. For example, isoprene has been studied previously with respect to leg movements during sleep.<sup>261</sup> Amongst the detected molecules, we identified isoprene and observed decreased isoprene levels during REM sleep and spikes in exhaled isoprene associated with leg movements (figure 4.9).

Newly in our study, we found an extensive and immediate metabolic response to REM sleep, N3 sleep and wakefulness as well as metabolites with a more complicated temporal relationship to vigilance states. Metabolic patterns of N1, N2 and N3 sleep did not differ significantly, indicating that the gradual transition from wakefulness to deep sleep is reflected as well on a metabolic level.

Carnitines are rate-limiting for the transport of long-chain fatty acids across the mitochondrial membrane to be oxidized<sup>266</sup> and supplementation with carnitines is even able to increase fatty acid oxidation directly.<sup>267</sup> Our findings of decreased acylcarnitine levels during N3 sleep compared to wakefulness therefore suggest that energy consumption by fatty acid degradation is higher during wakefulness than during sleep. This is in agreement with findings from Davies *et al.*,<sup>237</sup> reporting increased carnitine levels during sleep deprivation compared to sleep, and with the ability of L-carnitine to decrease daytime sleepiness in narcolepsy patients.<sup>268</sup>

From our results for pathways involved in carbohydrate metabolism, we hypothesize increased glucose utilization via glycolysis during REM sleep. This assumption is in line with the previously reported decrease in glucose utilization during NREM sleep compared to REM sleep.<sup>269</sup> Increased pyruvate production via glycolysis during REM sleep goes along with increased TCA cycle activity during REM sleep induced by increased feeding from pyruvate via oxaloacetate, suggested by our findings on TCA cycle intermediates. This increase in TCA cycle activity might be a preparation for subsequent mitochondrial oxidation. Furthermore, there is evidence that the TCA cycle is involved in immune reprogramming.<sup>270</sup> Macrophage activation and cytokine production can be triggered by breaks in the TCA cycle, most notably after citrate/isocitrate and after succinate.<sup>271</sup> In addition, sleep is associated with anti-inflammatory function.<sup>147</sup> Our failure to see upregulated succinate during REM sleep in combination with our finding of upregulation of its successors fumarate and malate suggests that this checkpoint is not activated, making REM sleep anti-inflammatory.

Sleep loss has been associated with impaired glucose metabolism.<sup>128</sup> Recently, circulating propanoate levels have been associated positively with insulin sensitivity.<sup>272</sup> Thus, our findings of downregulated propanoate and butanoate metabolism during N3 sleep suggest SCFAs (short-chain fatty acids) as mediators for decreased insulin sensitivity during SWS.

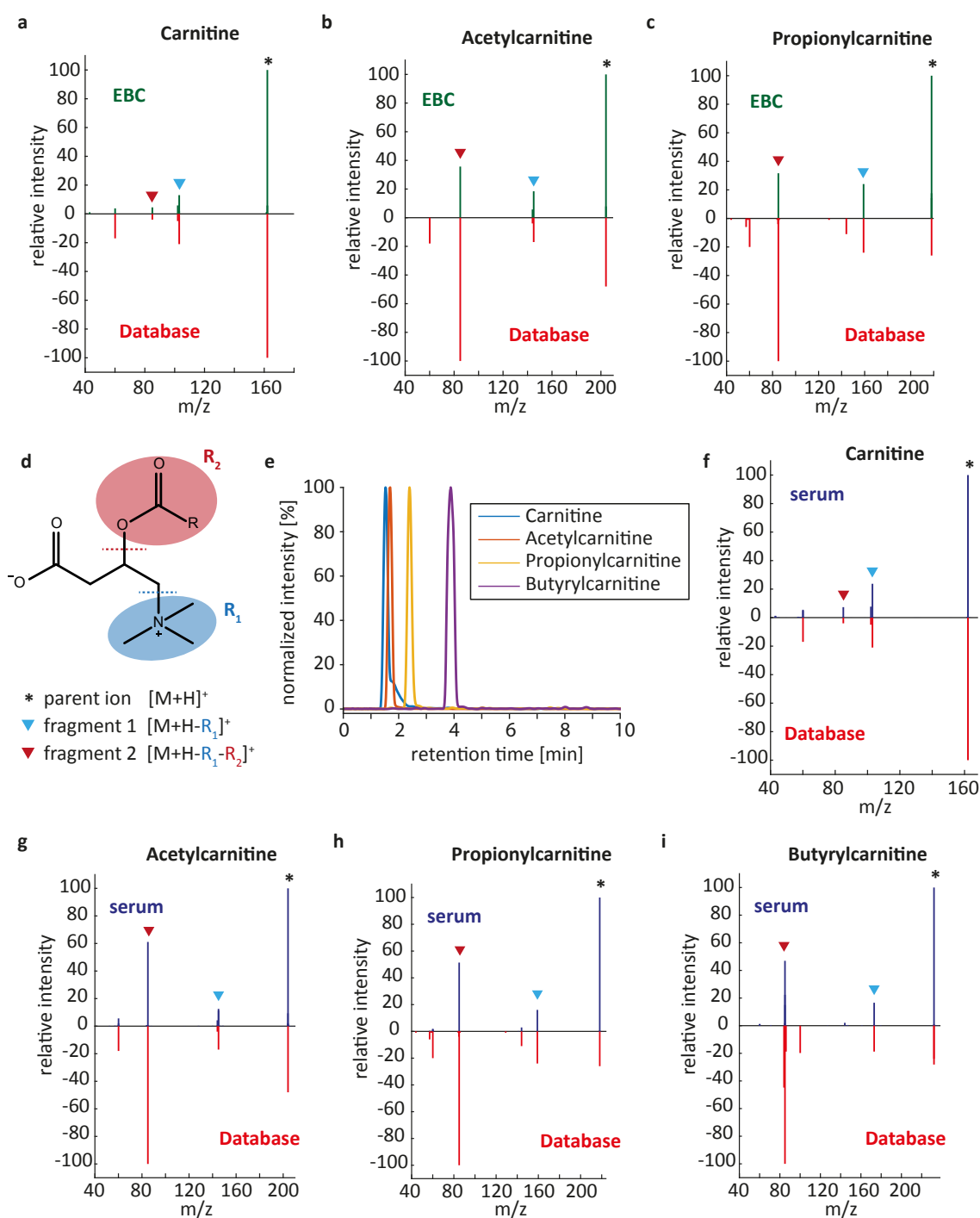


**Figure 4.10.: Identification of acylcarnitines in breath and serum.** a-c MS/MS spectra of acylcarnitines obtained from exhaled breath condensate in comparison with database MS/MS spectra. d Fragmentation pattern of acylcarnitines reported in literature.<sup>265</sup> e Chromatographic peaks of the carnitines measured in serum. As expected, retention times increase with increasing size of the alkyl chain. f-i MS/MS spectra of acylcarnitines obtained from serum in comparison with database MS/MS spectra.

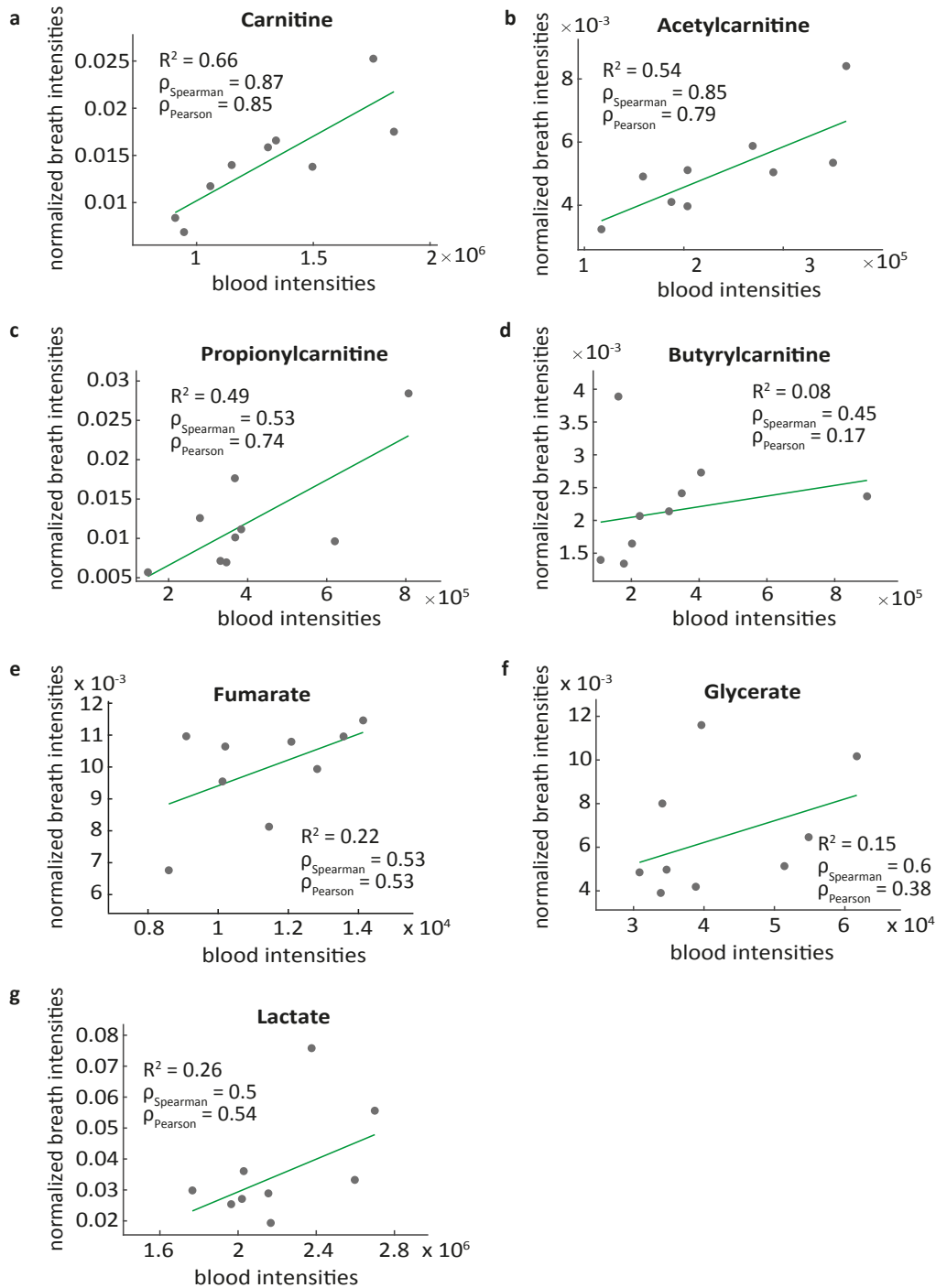


**Figure 4.11.: Correlation of metabolite levels in exhaled breath and serum.** a-d Correlation between blood and breath levels of carnitine, acetylcarnitine, propionylcarnitine and butyrylcarnitine and linear fits obtained from robust linear regression. These results indicate that short-chain acylcarnitine levels in exhaled breath reflect systemic levels. e-g Correlation between blood and breath levels of representatives of glycolysis (lactate), propionate metabolism (lactate), TCA cycle (fumarate) and pentose phosphate pathway (glycerate) and linear fits obtained from robust linear regression. These results indicate that metabolite levels in exhaled breath reflect systemic levels.

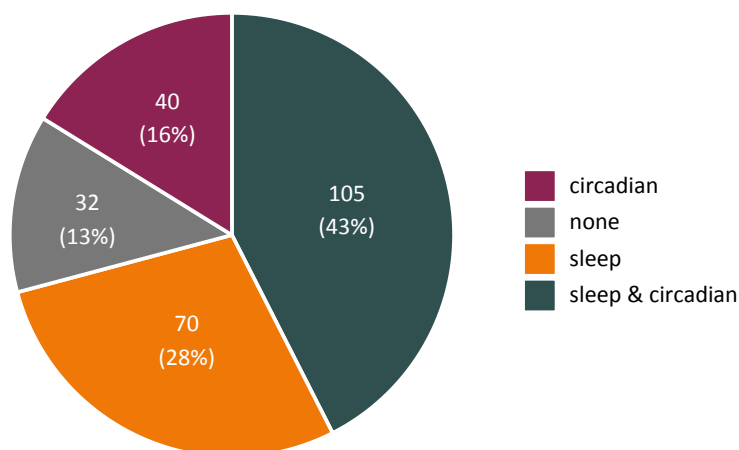


**Figure 4.12.: Comparison of sleep-related compounds and compounds under circadian control.** In total, 247 m/z features of the features we detected in this study have also been reported from circadian studies.<sup>55,76,185,236,273</sup> For 43 % of these features, we found an association with wakefulness, REM sleep or N3 sleep, and they are reported to be also under circadian control.<sup>55,76,185,236,273</sup> 28 % are associated with sleep only, and 16 % are only under circadian control. This suggests that many circadian metabolic pathways are also acutely sleep-controlled.

Sleep is a major output of circadian clock and disruption of both is associated with metabolic diseases.<sup>3,274</sup> Metabolic regulation by the circadian clock has been studied previously.<sup>55,76,185,236,273</sup> Here, we could show that metabolism is also controlled by sleep stages. Despite different samples types and different analysis techniques, we detected 247 of the m/z features reported in circadian studies also in our study in exhaled breath during sleep (figure 4.12). Amongst these commonly detected metabolites, the major part (42.5 %) is regulated by both sleep stages and circadian clocks. 16.2 % are controlled by circadian clocks only and 28.3 % are only associated with sleep states. Thus, circadian and sleep-dependent regulation of metabolism represent an interlocked network of metabolic control, analogous to the overlapping layers of control that we have described recently for the sleep- and circadian-dependent transcriptome.<sup>27</sup>

The orchestration between sleep architecture and metabolism, which we discovered here, might be essential for human health. To further investigate its clinical relevance, we evaluated breath levels of sleep-state dependent metabolites in a cohort of patients suffering from obstructive sleep apnea (OSA) and control subjects (Participant data and detailed methods are provided in Chapter 5). Many of the sleep state-regulated compounds displayed significant differences between the two groups. The functionality of those metabolites being influenced by both, OSA and sleep stages, is remarkably homogeneous. Most of the compounds are related to mitochondrial synthesis of acetyl CoA (figure 4.13). These findings indicate that especially for mitochondrial respiration, a healthy sleep architecture properly synchronized with metabolism, is of importance.

Although our dataset identifies over a thousand sleep state-regulated m/z features, the path-



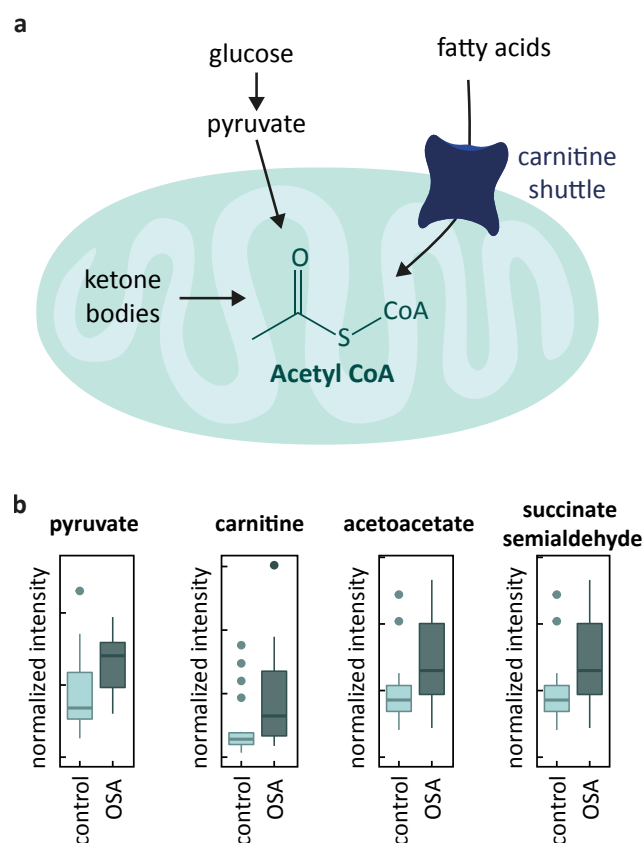


**Figure 4.13:** **a** Metabolites involved in mitochondrial synthesis of acetyl CoA are regulated by sleep states and also influenced by OSA, a disease associated with frequent sleep disruptions. **b** Boxplots (center line: median, box limits: 25<sup>th</sup> and 75<sup>th</sup> percent quantile, whisker length: 1.5 interquartile range) of some examples, for which significant differences were found between OSA patients and control subjects.

ways subject to sleep-dependent regulation found in this study are probably only scratching the surface of such metabolic regulation. Further studies will improve the identification of unknown compounds and thus enlarge pathway coverage. Moreover, the techniques that we have pioneered here could equally be employed to investigate how metabolic regulation is altered in individuals with sleep-related diseases.

## 4.5. Conclusion

In conclusion, by analysing exhaled breath during sleep, we found unprecedented evidence for sleep states as drivers of body metabolism. Not only circadian patterns but also sleep-wake patterns dynamically program metabolism, providing precise timing for carbohydrate metabolism, fatty acid oxidation, and the mitochondrial TCA cycle. Thereby, they directly connect sleep patterns to metabolic homeostasis and health.



# 5

Validation of breath biomarkers for  
obstructive sleep apnea

This chapter is adapted from:

Nora Nowak, Anna Engler, Sira Thiel, Anna S. Stöberl, Pablo Sinues, Renato Zenobi, Malcolm Kohler, VALIDATION OF BREATH BIOMARKERS FOR OBSTRUCTIVE SLEEP APNEA. *Manuscript submitted for publication.*

M.K, P.S and R.Z. designed the study. A.E. wrote the protocol for the ethics. A.E, S.T. and A.S, recruited study participants and assessed clinical parameters. N.N. performed the SESI-MS experiments and all data analysis. M.K, N.N. and R.Z. contributed to the discussion and interpretation of the results. N.N. wrote the manuscript with input from the other co-authors.

## Summary

Obstructive sleep apnea (OSA) is a widespread respiratory disease with negative metabolic and cardiovascular effects. The current gold standard for diagnosing OSA is polysomnography in the sleep laboratory, a time-consuming and costly procedure, which is inconvenient for the patient. Recent studies revealed evidence for the potential of breath analysis for the diagnosis of OSA based on a disease-specific metabolic pattern. However, none of these findings was validated in a larger and broader cohort, an essential step for its application in clinics.

In the present study, we validated a panel of breath biomarkers in a cohort of patients with possible OSA (N = 149). These markers were previously identified in our group by secondary electrospray ionization high-resolution mass spectrometry (SESI-HRMS). Here, we could confirm significant differences between metabolic patterns in exhaled breath from OSA patients compared to control subjects without OSA as well as the association of breath biomarker levels with disease severity. Our prediction of the diagnosis for the patients from this completely independent validation study using a classification model trained on the data from the previous study resulted in an area under the receiver operating characteristic curve of 0.66, which is comparable to questionnaire-based OSA screenings.

Thus, our results suggest that breath analysis by SESI-HRMS may be used to screen for OSA. Its true predictive power should be tested in combination with OSA screening questionnaires.

## 5.1. Introduction

Obstructive sleep apnea (OSA) is a highly prevalent sleep-related breathing disorder.<sup>275</sup> The repeated partial or complete collapse of the pharynx during sleep provokes apnea or hypopnea events, which may lead to repetitive oxygen desaturations. Frequent sleep disruptions and increased activity of the sympathetic nervous system are accompanying these apnea/hypopnea events and result in poor sleep quality and increased daytime sleepiness.<sup>276</sup> Several metabolic and cardiovascular consequences, such as an increased risk for cardiovascular diseases, arterial hypertension, diabetes, vascular dysfunction, as well as depression and car accidents, are well known.<sup>277-280</sup> OSA can be effectively treated i.e. with continuous positive airway pressure (CPAP).<sup>281-283</sup>

The conventional diagnosis of OSA is carried out by polysomnography or respiratory polygraphy,<sup>284,285</sup> which are time-consuming, costly and inconvenient for patients. In addition, there is emerging evidence for a high night-to-night variability of OSA, posing another challenge for diagnostics.<sup>286</sup> Thus, for a reliable diagnosis, testing during several nights would be required. Screening for OSA is conventionally based on questionnaires, such as the STOP-bang,<sup>287</sup> Berlin<sup>288</sup> or NoSAS score.<sup>289</sup> However, the results from such questionnaires are by nature subjective.

Exhaled breath contains several hundreds of metabolites and thus provides insights into biochemical processes of the human body.<sup>216</sup> Many of the metabolites in breath do not originate from the lungs but are transported from blood to the airways via gas exchange in the lung. Therefore, breath metabolite levels mostly reflect systemic metabolic processes. Furthermore, consistent alterations of the molecular fingerprint of exhaled breath in patients

with a certain disease may indicate disease specific metabolic changes. Such disease specific biomarkers detected in exhaled breath, could be the basis for an objective and non-invasive diagnostic procedure, which is fast and easy to perform for patients.

So far, many studies with small sample sizes have obtained promising results, suggesting a great diagnostic potential of exhaled breath analysis for various diseases. However, larger validation studies are missing and, to date, exhaled breath analysis is applied in clinical routine only for very few applications, such as the evaluation of bronchial inflammation by measuring fractional exhaled nitric oxide (FeNO).<sup>290</sup> To achieve a more widespread clinical application of breath analysis for disease diagnosis and monitoring, the validation of preliminary findings in large cohorts of patients is essential.

The investigation of exhaled breath in OSA patients using different technical approaches revealed convincing results for diagnosing this disease and for monitoring patients' compliance to CPAP therapy.<sup>277</sup> In some studies, electronic sensors (e-noses) were used to recognize OSA specific patterns in exhaled breath.<sup>291–294</sup> In their attempts of diagnosing OSA against the gold-standard (polysomnography), areas under the receiver operating characteristic curves (AUROCs) in the range from 0.84 (no 95% CI provided) to 0.87 (95% CI 0.61-1.00) were reported, suggesting future diagnostic applicability of breath analysis. However, e-noses do not allow for compound identification and thus do not provide mechanistic insights into the disease, but merely produce a complex “signal” whose statistical evaluation can give some valuable output. Furthermore, these data from studies with e-noses were not validated in larger and broader cohorts of patients with possible OSA.

Our untargeted investigation of an extensive spectrum of molecules in exhaled breath using secondary electrospray ionization high-resolution mass spectrometry (SESI-HRMS) revealed specific markers, allowing identification of a disease specific molecular profile of exhaled breath in patients with OSA recurrence after two weeks of CPAP therapy withdrawal.<sup>227</sup> In that randomized controlled trial, we found significant correlations between metabolite levels in breath and change in oxygen desaturation index (ODI, a clinical parameter for the severity of OSA) upon CPAP withdrawal, and significant differences between the CPAP withdrawal and treatment group. Further, we achieved a successful classification (AUROC = 0.87) between the withdrawal group and the group that continued the treatment. In order to transfer our exciting findings into the diagnostic algorithm of OSA, this observational study aims to validate these metabolic breath profiles in a larger treatment naive cohort of patients with possible OSA.

## 5.2. Methods

### 5.2.1. Study participants

This study includes 149 participants with possible OSA in the age of  $53.3 \pm 13.7$  years with a BMI of  $30.1 \pm 6.6$  kg/m<sup>2</sup> (table 5.1). The study protocol was approved by the local ethical committee (KEK-ZH 2016-00384). The experiments were conducted in accordance with the Declaration of Helsinki and written informed consent was obtained from all participants before participation. The clinical trial was registered at ClinicalTrials.gov (NCT02810158).

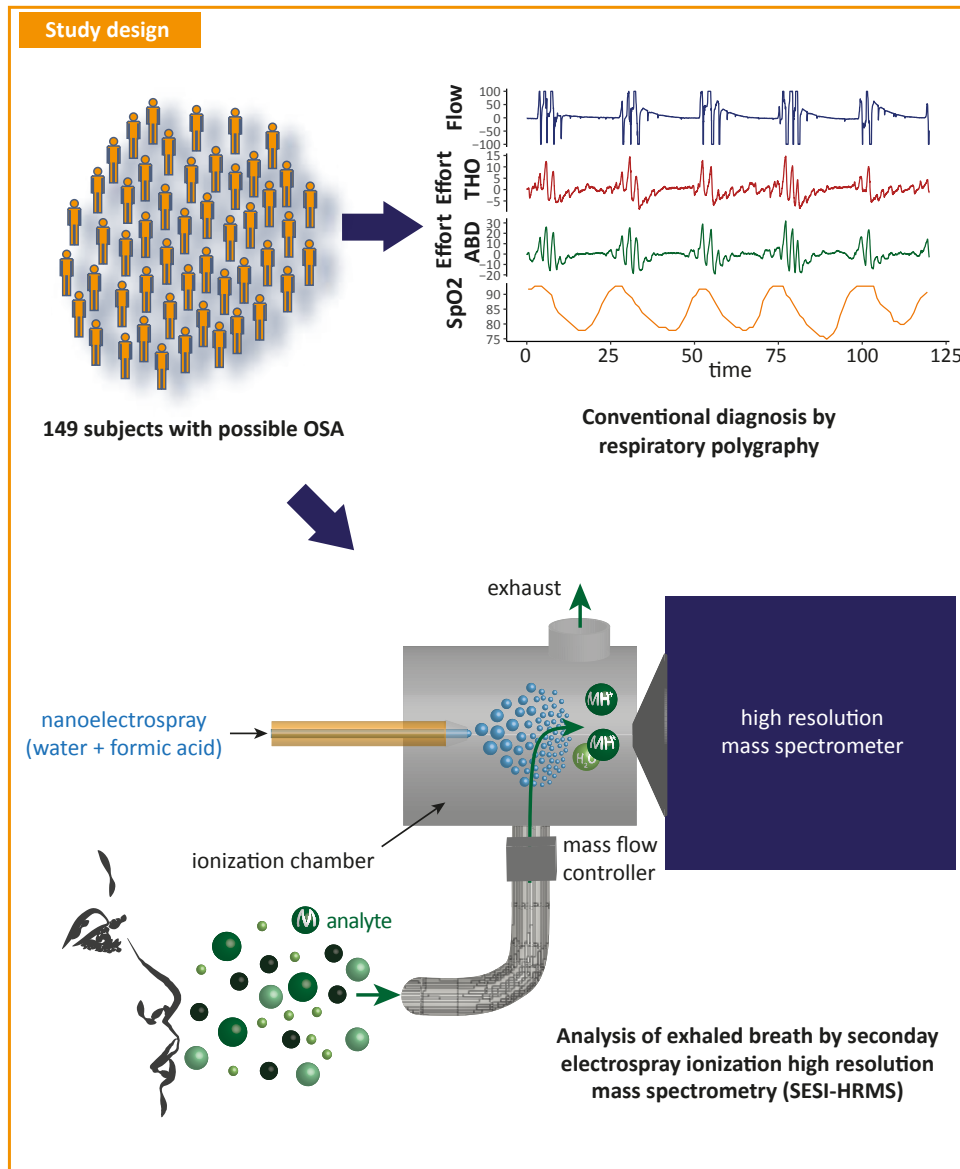


**Figure 5.1.: Study design.** 149 study subjects with possible OSA underwent conventional diagnosis by respiratory polygraphy in the sleep laboratory and exhaled breath analysis by SESI-HRMS.

All patients underwent in-hospital respiratory polygraphy (RP). Inpatient RPs were recorded by Alice 6 Diagnostic System (Philips Respironics, PA, USA), scored with validated Somnolyzer 24x7 software (Philips Respironics, PA, USA), and reviewed manually. The obtained data was evaluated according to the guidelines of the American Academy of Sleep Medicine.<sup>295</sup>

Furthermore, the participants were asked to fill in Epworth Sleepiness Scale (ESS) questionnaires.

### 5.2.2. SESI-HRMS measurements

Participants were asked to refrain from eating, drinking, chewing gum, alcohol, tobacco, caffeine use or brushing their teeth at least 1 hour prior to the SESI-HRMS measurements. Exhaled breath of 149 patients was analyzed by SESI-HRMS using a commercial SESI source (SEADM, Spain) coupled to a high-resolution TripleTOF 5600+ mass spectrometer (AB Sciex, Concord, Ontario, Canada). The participants were sitting in upright position in front of the mass spectrometer and exhaled at least six times with a pressure drop of 12 mbar through a disposable mouth piece into the heated sampling line, which was connected to the SESI source. A flow-splitter at the front-end enabled sampling of end-tidal breath. The flow through the ion source was set to 0.2 L/min. Full scan mass spectra were recorded in positive ion mode with an accumulation time of 1 s in the range of 50-500 Da.

### 5.2.3. Data preprocessing

All mass spectral data was analyzed with MATLAB R2020a and R 4.0.0. Mass spectra obtained from exhaled breath were preprocessed as described elsewhere.<sup>226</sup> In short, mass spectra were interpolated, aligned, exhalation time windows were chosen and peak picking was performed on the average breath spectrum. As in the pilot study,<sup>227</sup> breath signal intensities were normalized to the median intensity of the total ion current and then autoscaled.

### 5.2.4. Statistical analysis

Further, the  $m/z$  features were filtered for markers, which have been associated with OSA previously.<sup>227</sup> The  $m/z$  tolerance was set to 0.005 Da. The remaining 78  $m/z$  features were first tested for normality in a Shapiro-Wilk's test. Since the data was not normally distributed ( $p$ -value distribution from Shapiro-Wilk's test for normality is provided in supplementary figure B.16), we performed a correlation analysis between signal intensity and ODI as well as between signal intensity and ESS using Spearman correlation.

Moreover, we tested for differences in signal intensities between individuals without OSA and OSA patients by performing two-sided Mann-Whitney-U tests. Here, we first applied stratification criteria as they are commonly applied in the clinics: OSA ODI > 30/h or ODI > 10/h & ESS > 10 points, control ODI < 5/h or ODI < 10/h & ESS < 11 points (stratification 1). We then also tested for between-group differences with stricter stratification criteria (OSA: ODI > 30/h & ESS > 10 points, control: ODI < 10/h & ESS < 11 points, stratification 2) in order to remove individuals with ambiguous diagnosis. We also calculated  $\log_2$  fold



changes between the groups. To account for multiple hypothesis testing, false discovery rates (q-values) were calculated for all obtained p-values using Storey's procedure.<sup>250</sup>

### 5.2.5. Classification procedure

We combined the breath intensities obtained for the above mentioned 78 m/z features of the previously reported pilot study and this validation study. We used the data of the pilot study as training set and used the MATLAB classification learner app to find the best classification algorithm. For model evaluation we used a 7-fold cross validation. We defined the OSA and control group with the above mentioned criteria of stratification 1. In order to obtain balanced group sizes we only used the before and after measurements of the 9 individuals of the placebo group, who developed OSA in the pilot study. A gaussian support vector machine model performed best. We thus trained such model on the training data and predicted the validation data set obtained from this study.

### 5.2.6. Attempts of improvement of classification performance

Since both data sets were acquired on different mass spectrometers and with different generations of SESI sources, we assessed by principal component analysis the comparability of both data sets. A slight shift between both data sets was observed. We therefore performed a batch correction based on an empirical Bayes algorithm<sup>296</sup> and repeated the classification procedure described above.

We also repeated the classification procedure with stratification criteria, which are more similar to the ones used in the pilot study. For the validation data set we defined the groups as follows: OSA: ODI > 30/h, control: ODI < 10/h. In order to get balanced group sizes in the training set, we reduced the control group to ODI < 2/h.

## 5.3. Results

### 5.3.1. Study design and patient characteristics

149 participants between 19 and 83 years with possible OSA have been examined by respiratory polygraphy and their exhaled breath was analyzed by SESI-HRMS directly after the sleep study (figure 5.1). Patient characteristics and results from respiratory polygraphy are shown in table 5.1. Depending on the applied stratification criteria, the mean ODI in the OSA group varies between 38.3 and 46.8 events per hour. The control group had a mean ODI between 4.4 and 5.2 events per hour. The mean Epworth Sleepiness Scale score (obtained from a questionnaire estimating the extend of daytime sleepiness) in the OSA group ranged from 10 to 11 points and in the control group from 6 to 9.4 points.

**Table 5.1.:** Study participant characteristics. (AHI: apnea-hypopnea-index; BMI: body mass index; ESS: Epworth Sleepiness Scale; ODI: oxygen desaturation index; FVC: expiratory forced vital capacity; FEV1: forced expiratory volume in one second)

	all participants						OSA			healthy			
		stratification 1 ODI>30 or (ODI>10 & ESS>10)		stratification 2 ODI>30 & ESS>10		stratification 3 ODI>30		stratification 1 ODI<5 or (ODI<10 & ESS<11)		stratification 2 ODI<10 & ESS<11		stratification 3 ODI<10	
Number of subjects (N)	149	51		18		36		33		26		47	
Age, mean (SD), years	53.3 (13.7)	55 (13.4)		51.6 (10.2)		53.6 (13)		48.5 (14.6)		49.7 (14.3)		49.3 (14.6)	
male sex, n (%)	108 (72.5%)	35 (68.6%)		13 (72.2%)		26 (72.2%)		20 (60.6%)		17 (65.4%)		30 (63.8%)	
BMI, mean (SD), kg/m <sup>2</sup>	30.1 (6.6)	33 (6.5)		33.1 (6.7)		34 (6.5)		27.2 (6.1)		28 (6.4)		27.1 (5.5)	
active smoker, n (%)	31 (20.8%)	17 (33.3%)		7 (38.9%)		14 (38.9%)		6 (18.2%)		5 (19.2%)		10 (21.3%)	
former smoker, n (%)	53 (35.6%)	16 (31.4%)		4 (22.2%)		9 (25%)		11 (33.3%)		10 (38.5%)		16 (34%)	
AHI at diagnosis, mean (SD), events per hour	19.6 (17)	34.8 (18)		42.9 (15)		42.7 (15)		5.9 (5)		5.3 (3)		6.4 (5)	
ODI at diagnosis, mean (SD), events per hour	20.8 (17.5)	38.3 (17.5)		46.5 (14.7)		46.8 (13.2)		4.4 (2.7)		5 (2.6)		5.2 (2.6)	
ESS at diagnosis, mean (SD), points	8.9 (4.5)	11 (4.8)		14.2 (2.8)		10 (5.2)		7.4 (3.4)		6 (2.4)		9.4 (4.5)	
FEV1/FVC, mean (SD)	78.5 (7.7)	77.6 (8.7)		79.1 (7.9)		78.5 (7.6)		78 (5.5)		78 (5.6)		78.1 (5.5)	
FVC, mean (SD), % predicted	101 (16.7)	97.5 (18.7)		96.1 (15)		96.2 (17.2)		108.5 (15.5)		106.3 (16.1)		105.4 (16)	
FEV1, mean (SD), % predicted	99 (17.6)	95.3 (20.8)		94.9 (18.5)		94.5 (19.1)		103.9 (14.5)		102.4 (15)		101.2 (14.4)	

### 5.3.2. Metabolic patterns in exhaled breath associated with OSA

The data obtained in this validation study from SESI-HRMS measurements was pre-processed in the same way as it was done in our previous study,<sup>227</sup> which we refer to as pilot study in the following, i.e. the signal intensities were normalized to the median of total ion current and then autoscaled. We continued our analysis in a targeted fashion focusing only on the  $m/z$  features that have previously been associated with OSA in our pilot study. However, we were not able to detect all of them, which is most likely due to technical changes that have been made in the meantime. Nevertheless, 78 of the features that have been reported either as significantly different between the CPAP and the withdrawal group or as correlating with the change in ODI or as predictive for OSA previously, were also detected in this validation study. For those 78  $m/z$  features, we tested for significant differences between controls without OSA and OSA patients and for correlation with ODI and ESS. Moreover, we trained a classification model with the data from the pilot study and predicted the OSA diagnosis of the validation cohort from this study.

### 5.3.3. Significant differences in metabolic breath patterns between OSA patients and individuals without OSA

We tested for significant differences in metabolite intensities in exhaled breath between OSA patients and controls without OSA (Mann-Whitney-U test). We assigned the participants to two groups (OSA and control) based on the following criteria, which are commonly applied in clinics: ODI > 30/h or ODI > 10/h & ESS > 10 points (definitive OSA); and ODI < 5/h or ODI < 10/h & ESS < 11 points (definitive without relevant OSA; control) (stratification 1). All subjects in between were assigned to an “unclear” group, since no unambiguous OSA diagnosis could be stated. For 19 features we found significant ( $p < 0.05$ ) differences between the two groups (figure 5.2 and figure 5.3a and b, boxplots of two examples are shown in figure 5.3c and d, all boxplots are provided in supplementary figure B.6).

When we used stricter grouping criteria (OSA: ODI > 30/h & ESS > 10 points, control: ODI < 10/h & ESS < 11 points, stratification 2) in order to consider only patients with an unambiguous diagnosis, significance increases as shown in supplementary figure B.7 and supplementary figure B.8 (all boxplots are given in supplementary figure B.9). All numeric results are provided in supplementary tables B.4 and B.5.

Hence, our results from this validation study confirm our previous findings of a specific metabolic pattern in exhaled breath in OSA patients.

### 5.3.4. Association between disease severity and breath signal intensity

To test whether in this larger and more diverse cohort of patients, breath patterns do not only differ between the control and OSA group, but signal intensities are also correlating with the severity of OSA, we performed a Spearman correlation analysis. For 21 features, we found a significant correlation between breath levels and ODI ( $p < 0.05$ ) (figure 5.4a, correlation plots for two examples are shown in figure 5.4b, all correlation plots are provided in supplementary

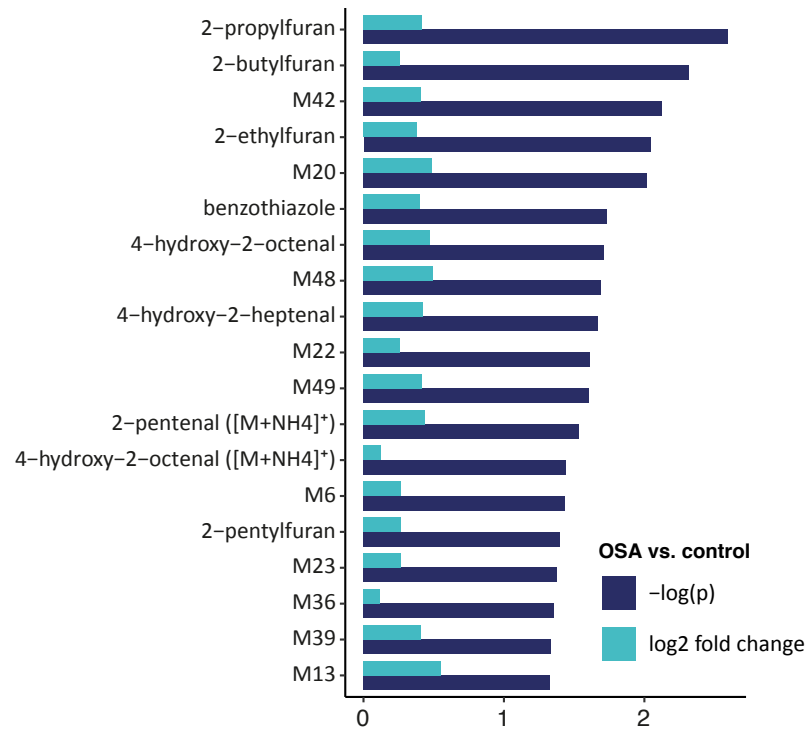


**Figure 5.2.: Significant differences in metabolic breath patterns between subjects with and without OSA** (OSA: ODI > 30/h or ODI > 10/h & ESS > 10 points; control: ODI < 5/h or ODI < 10/h & ESS < 11 points; unclear: in between; stratification 1). P-values and fold changes of significant features sorted by significance. Not identified features are labelled with Mxx.

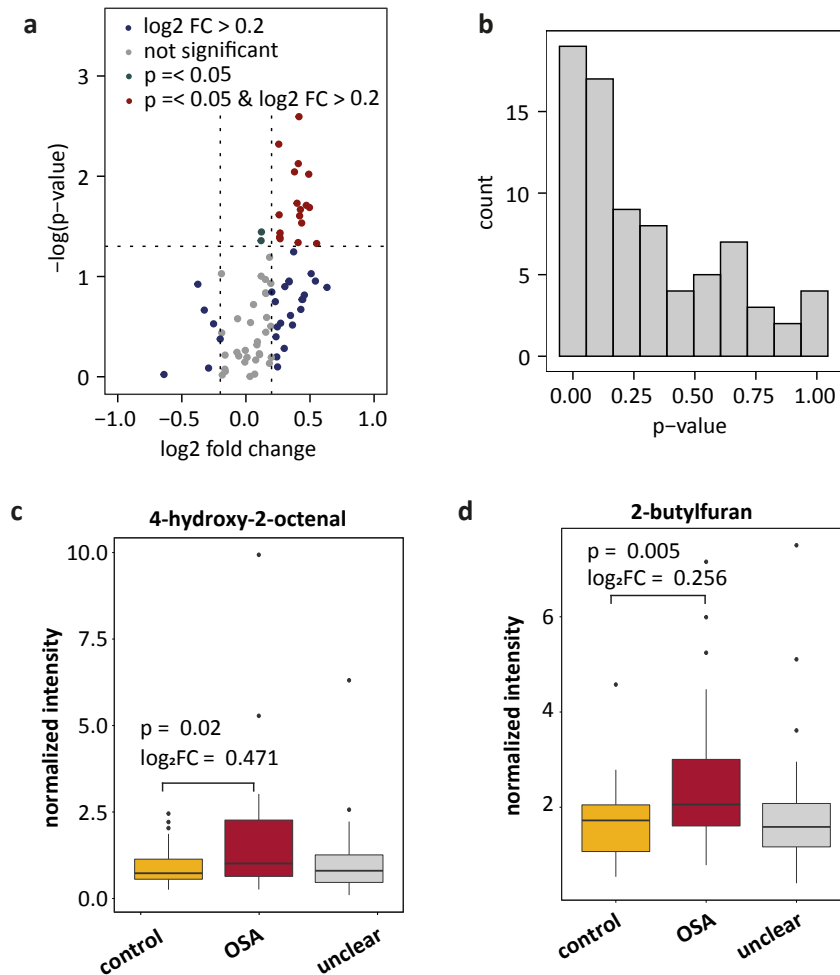


**Figure 5.3.: Significant differences in metabolic breath patterns between subjects with and without OSA** (OSA: ODI > 30/h or ODI > 10/h & ESS > 10 points; control: ODI < 5/h or ODI < 10/h & ESS < 11 points; unclear: in between; stratification 1). **a** volcano plot for all 78 metabolites. **b** p-value distribution for between-group differences from Mann-Whitney-U test. **c, d** Exemplary boxplots (center line: median, box limits: 25th and 75th percent quantile, whisker length: 1.5 interquartile range) of 4-hydroxy-2-octenal and 2-butylfuran. The Boxplots for all significant features are provided in supplementary figure B.6, numeric results for significant features are summarized in table 5.2 and 5.3 and numeric results of all 78 features are given in supplementary table B.4 and B.5.

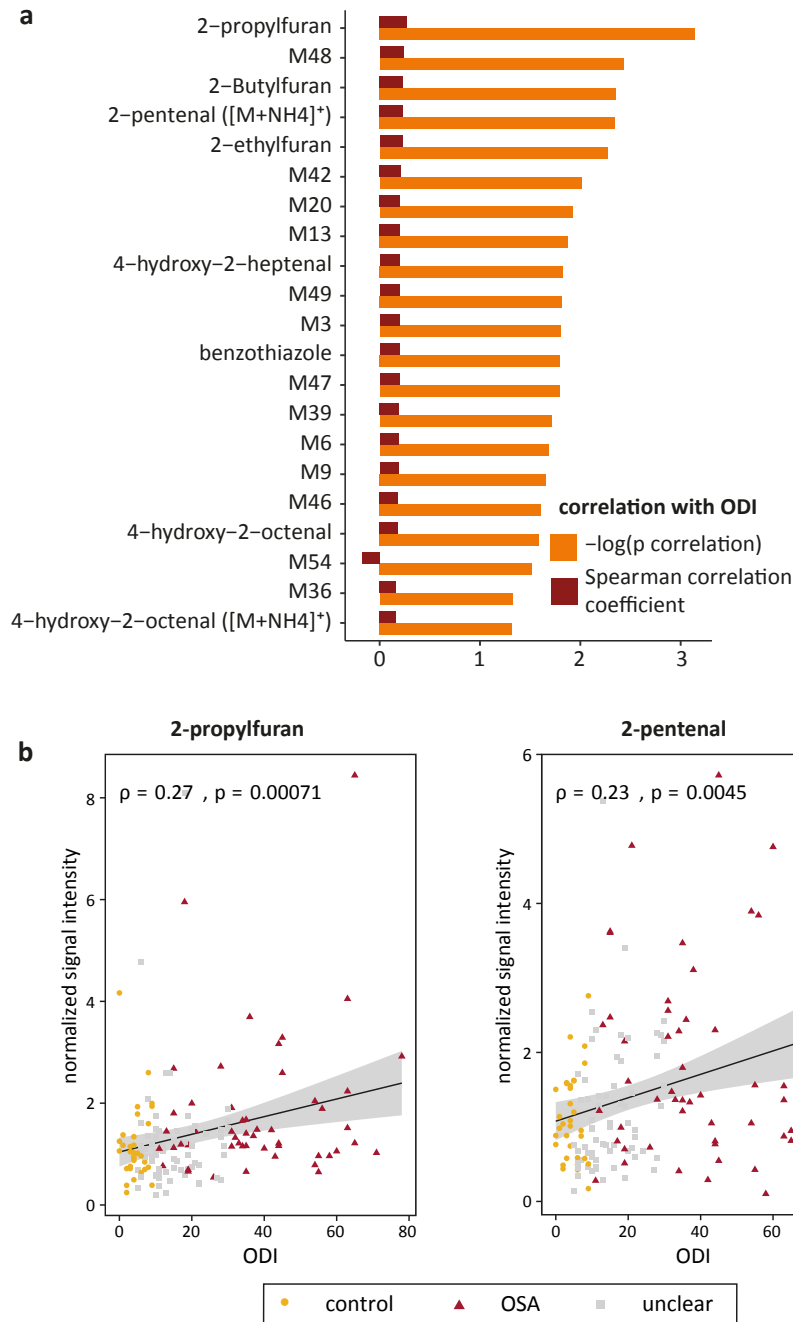


**Figure 5.4.: Correlations between metabolite levels in breath and OSA severity.** **a** p-values and correlation coefficients of features from exhaled breath with significant correlations with the ODI. **b** Exemplary regression lines for 2-propylfuran and 2-pentenal. Regression lines for all features with significant correlations with the ODI are provided in supplementary figure B.10. Numeric results for features with significant correlations are summarized in table 5.2 and 5.3 and numeric results of all 78 features are given in supplementary table B.4 and B.5. (OSA: ODI > 30/h or ODI > 10/h & ESS > 10 points; control: ODI < 5/h or ODI < 10/h & ESS < 11 points; unclear: in between; stratification 1)

figure B.10). All except one show higher intensities for an increased ODI, suggesting that oxygen desaturation correlates with an enrichment of these metabolites. This supports the association of these metabolites with apnea-related nocturnal hypoxemia. Amongst these metabolites correlating with the ODI are several unsaturated aldehydes as well as furanes and benzothiazole that have been identified before.<sup>297-299</sup> Thus, we could confirm the previously reported association between disease severity and breath signal intensity.

### 5.3.5. Association between sleepiness and breath signal intensity

For 9 features we found a significant correlation between their breath intensities and the ESS ( $p < 0.05$ ) (figure 5.5a). Amongst them, 4 are also correlating with the ODI, such as 2-pentylfuran and 4-hydroxy-2-octenal. Correlation plots for these two examples are shown in figure 5.5b (all correlation plots are provided in supplementary figure B.11). These findings suggest that not only hypoxia but also sleepiness is reflected in the metabolic breath pattern.

### 5.3.6. Classification

To assess to applicability of metabolite levels measured in exhaled breath using SESI-HRMS for the clinical diagnosis of OSA, we trained a classification model with the data from our pilot study and predicted the diagnosis of OSA or control in the validation cohort measured in this study. The classification procedure is shown schematically in figure 5.6.

First, we grouped the patients again as described above by the clinical criteria of stratification 1. In order to obtain balanced group sizes in the training set, we used only the “before” and “after” measurements of those patients in the CPAP withdrawal group, who developed significant OSA under placebo treatment (figure 5.7a). With the training data, we estimated the performance of the classification model in a 7-fold cross-validation. This resulted in an AUROC of 0.59 (figure 5.7b, the confusion matrix is provided in figure 5.7c). The prediction of the diagnosis for the validation data (figure 5.7a) yielded in an AUROC of 0.66 (figure 5.7b, confusion matrix is given in figure 5.7c). The accuracy of the prediction was 63% with a sensitivity of 76% and a specificity of 42%.

## 5.4. Discussion

To the best of our knowledge, this is the first report of a validation of breath biomarkers for OSA. Previous studies using e-noses, offline gas-chromatography coupled to mass spectrometry, or enzyme immunoassays to analyze exhaled breath condensate have achieved promising results regarding the distinction between OSA patients and controls without OSA from exhaled breath.<sup>277</sup> However, sample sizes in all these studies were limited and none of the results has been validated in an independent cohort of patients. In this study, we could confirm in a large and independent cohort that breath intensities of many of our previously discovered potential biomarkers for OSA differ significantly between OSA patients and controls without OSA. Most of them are consistently increased in OSA patients. We could also confirm a correlation between breath signal intensity and disease severity (represented by the ODI) for several metabolites. These findings suggest that the 33 metabolites shown in tables 5.2 and

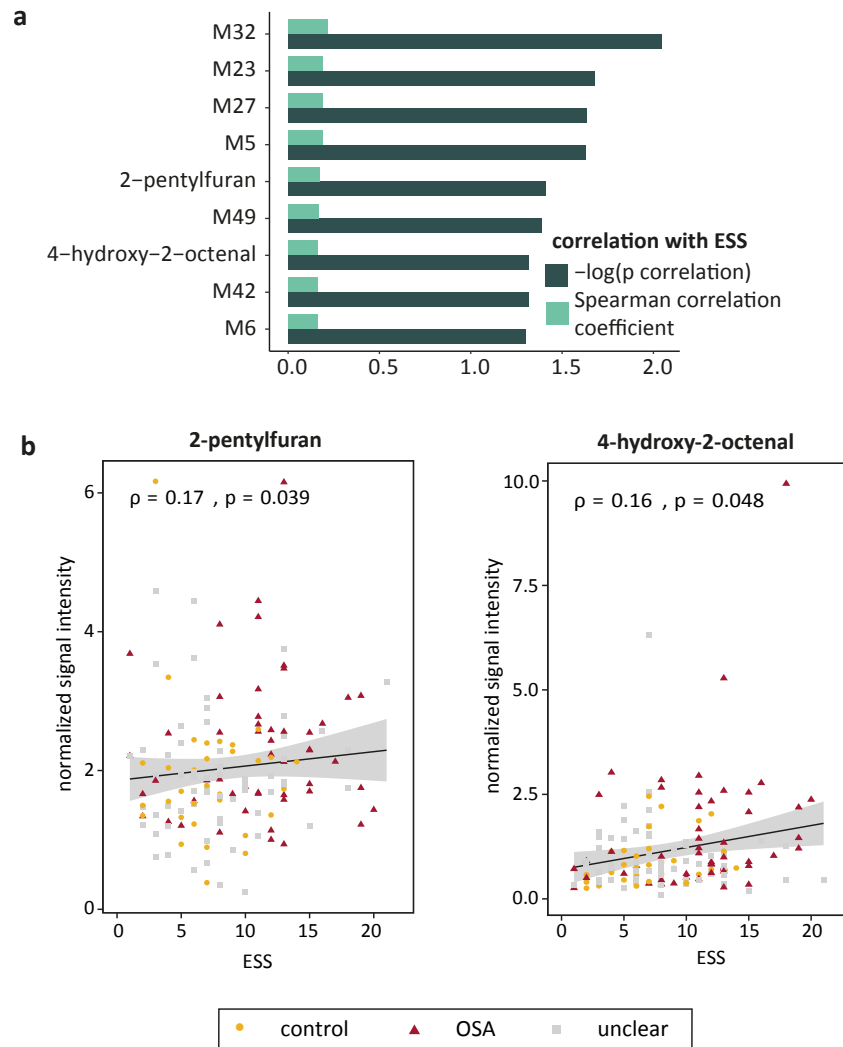


**Figure 5.5.: Correlations between metabolite levels in breath and sleepiness. a** p-values and correlation coefficients of features from exhaled breath with significant correlations with the ESS. **b** Exemplary regression lines for 2-pentylfuran and 4-hydroxy-2-octenal. Regression lines for all features with significant correlations with the ESS are provided in supplementary figure B.11. Numeric results for features with significant correlations are summarized in table 5.2 and 5.3 and numeric results of all 78 features are given in supplementary table B.4 and B.5. (OSA: ODI > 30/h or ODI > 10/h & ESS > 10 points; control: ODI < 5/h or ODI < 10/h & ESS < 11 points; unclear: in between; stratification 1)



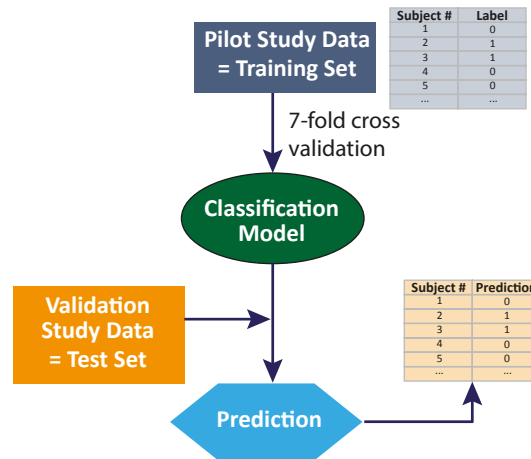


**Figure 5.6.: Classification procedure.** A classification model was trained with the data from our pilot study and its performance was estimated in a 7-fold cross validation. Subsequently, the diagnosis of the patient cohort from this validation study was predicted.

5.3 represent a panel of biomarkers, which are robust enough towards inter-individual variability to form a promising diagnostic tool. Inter-individual differences are the most likely reason for the lower correlation coefficients between signal intensities in breath and ODI that we observed in this diverse validation cohort compared to the correlations between the signal intensities and the within-subject change of ODI upon CPAP withdrawal, which we reported previously.

It is unlikely that there is one single biomarker that is sufficient for diagnosing a disease like OSA potentially associated with complex metabolic and cardiovascular consequences. In contrast, a pattern of several biomarkers is more likely to be disease-specific. Therefore, classification algorithms based on machine learning are convenient tools for making clinical diagnoses based on biomarker patterns. Here, we achieved a classification of the validation data set with an AUROC of 0.66, 76% sensitivity and 42% specificity, when we trained the model with the data from the independent patient cohort of our previously reported study.

Since the patient cohort of this study was much more diverse than the one in our pilot study, a lower classification performance would be expected. However, the support vector machine (SVM) model, which we used here, performed already worse in the cross validation with the training data ( $AUC_{CV} = 0.59$ ) compared to the model presented in the pilot study. This is likely to be due to different stratification criteria used in both studies, since with such small training sets, few samples can have a considerable influence. To test this hypothesis, we applied different stratification criteria. When we stratified the training data only based on ODI (as it was done in the pilot study), the model performance becomes comparable with the results that were reported previously ( $AUC_{CV} = 0.79$ , supplementary figure B.12a-c). This result supports our choice of an SVM model. However, the prediction of the validation data, which was then also stratified only based on the ODI, not only did not improve, but even declined slightly ( $AUC = 0.62$ , supplementary figure B.12d-f). This indicates that groups that are defined based on ODI and ESS can be distinguished better from the breath pattern with this biomarker panel than groups that are defined by ODI only. This is desirable, since a combination of ODI and ESS better reflects the clinical picture of significant OSA than only the

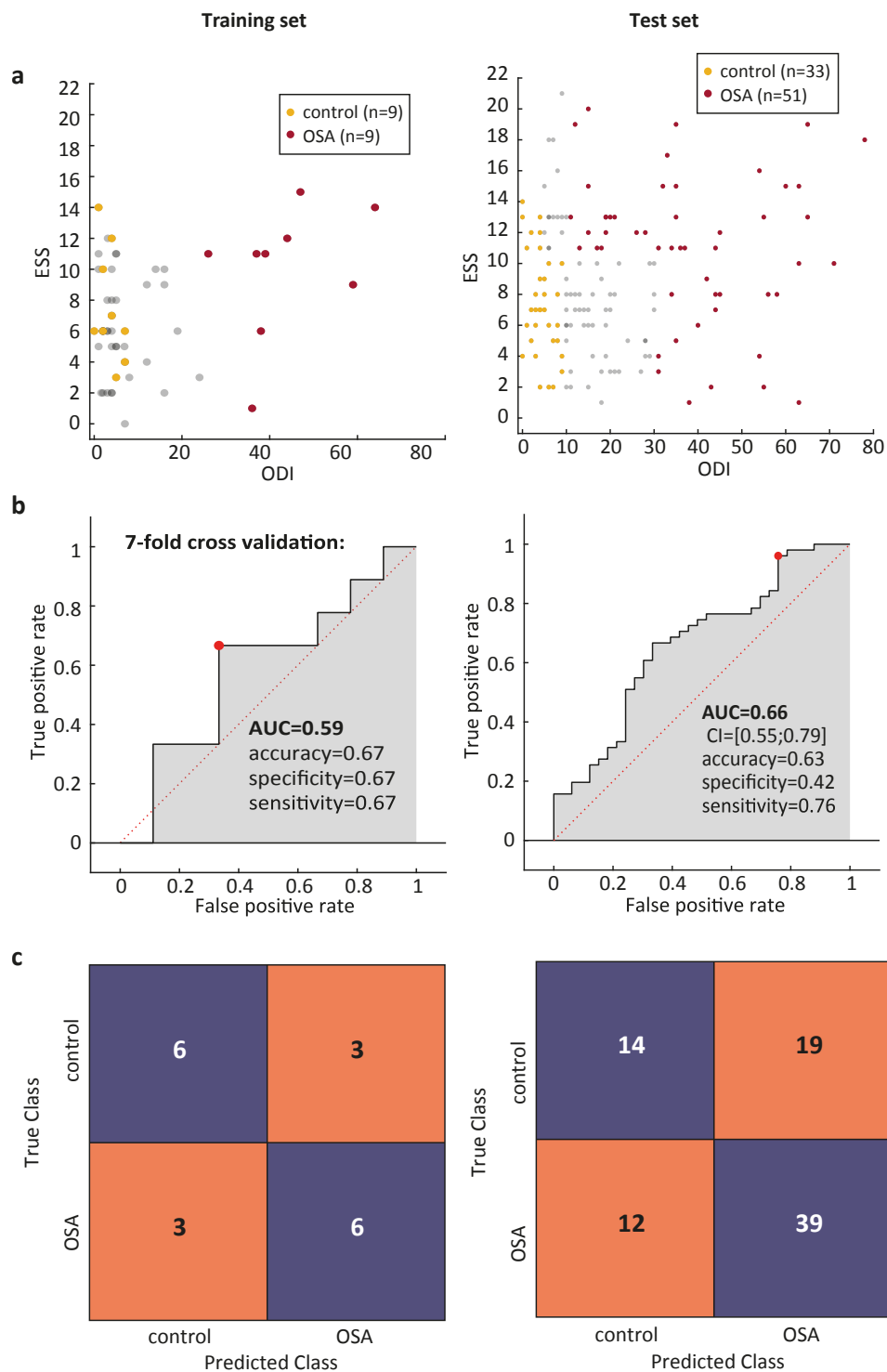


**Figure 5.7.: Classification results.** **a** ESS and ODI of samples in the training set (left) and test set (right). **b** ROC curve from 7-fold cross validation of the classification model with the training set (left) and from predictions of the validation cohort. **c** corresponding confusion matrices. (OSA: ODI > 30/h or ODI > 10/h & ESS > 10 points; control: ODI < 5/h or ODI < 10/h & ESS < 11 points; stratification 1)

ODI. All performance measures of this classification procedure (classification 2) are reported in the supplementary results and are summarized in supplementary table B.6.

SESI is still a rather novel technique and its performance is constantly improving. Also, between the pilot study and this validation study, technical improvements have been implemented. For example, a new ion source, which is more robust, has been developed, and we adapted collision gas settings of the MS in order to prevent fragmentation, although this leads to increased cluster formation. This is most likely the reason why we did no longer detect all of the previously reported markers in this study. The comparison of our data before and after batch correction between the data sets from both studies indicated that the data for the 78 potential biomarkers detected in both data sets are comparable and there is only a very small batch effect. A negligible change of the results from the classification procedure applied after batch correction confirmed this observation. (classification 3, PCA plot and classification outcome are shown in supplementary figure B.13 and supplementary figure B.14, and classification results are described in supplementary results and supplementary table B.6)

Another factor that might impair the classification results is a lack of standardization of SESI-HRMS and the lack of real-time breath quality control samples, respectively at the time when the study was conducted. Instrumental drifts are a common issue in large scale metabolomics studies, which is overcome in offline-techniques with quality controls.<sup>211</sup> These samples are then used for normalization, i.e., to separate the biological variation of interest from unwanted technical variation or other confounding factors, such as exogenous influences. Since such samples are not yet available for real-time breath analysis, a higher degree of standardization of sampling and methodology is required.<sup>300</sup> In future studies, a reference gas mixture could be established, to check the instrument performance and thereby reduce technical noise. This might improve the effectiveness of SESI-HRMS for screening for OSA. Ideally in a next step, calibration with standards of validated and identified biomarkers, such as the ones identified in this study, could be applied using standard addition. The standard addition procedure brings the advantage that in addition to technical fluctuations, matrix effects and thereby the influence of humidity on ionization efficiency and ion suppression effects can also be eliminated. However, the biggest challenge here is the availability of gaseous standards as well as the bottleneck of identification of metabolites. One possible approach is the use of permeation tubes.<sup>301</sup> Another confounding factor that might compromise the results are isobaric compounds since no separation step, such as chromatography, is used in real-time SESI-HRMS. To overcome this challenge, a targeted detection of the validated and identified biomarkers could involve MS-MS quantification or a coupling to ion mobility spectrometry and thereby provide a higher molecular specificity.

To date, different scores are derived from questionnaires for an initial approach to OSA screening. Our classification performance is comparable with the performances of the STOP-bang<sup>287</sup> and Berlin scores,<sup>288</sup> which are obtained from questionnaires and currently used for OSA screening. The NoSAS score performs slightly better, AUROCs of 0.74 and 0.81 have been reported from two different patient cohorts. However, in terms of sensitivity our results are comparable with the NoSAS score.<sup>289</sup> For a screening, this is the most relevant parameter, since ideally no subjects with OSA are missed. The false negatives that we observed are discussed in the supplementary discussion. It has been shown previously that the combination of NoSAS and metabolomics data can improve predictive performance remarkably.<sup>302</sup> Here,

**Table 5.2.: A panel of validated OSA biomarkers.** 33 of the previously detected<sup>227</sup> biomarkers for OSA show a significant correlation with the ODI or ESS or significant differences between OSA patients and control subjects in the validation cohort (significance level:  $p < 0.05$ ). (unsat. aldehydes: unsaturated aldehydes)

metabolite name	metabolite class	m/z	significant difference between groups	correlation with delta ODI	Pearson correlation coefficient	selected as predictor for classification
2-pentenal ( $[M+NH_4]^+$ )	unsat aldehydes	102.0913	yes	no		yes
4-hydroxy-2-heptenal	unsat. aldehydes	129.0908	yes	yes	0.48	no
4-hydroxy-2-octenal ( $[M+NH_4]^+$ )	unsat. aldehydes	143.1063	no	yes	0.42	no
4-hydroxy-2-octenal	unsat. aldehydes	160.1329	yes	yes	0.42	no
2-undecenal	unsat. aldehydes	169.1584	no	yes	0.38	no
2-ethylfuran	furanes	97.0647	yes	no		yes
2-propylfuran	furanes	111.0803	yes	yes	0.4	yes
2-butylfuran	furanes	125.0958	yes	yes	0.44	no
2-pentylfuran	furanes	139.1116	yes	yes	0.38	yes
benzothiazole	thiazoles	136.0216	yes	no		no
4-(hexyloxy)phenol	benzenoids	195.1379	no	yes	0.38	no
M1	unknown	53.0391	no	no		yes
M3	unknown	79.0409	no	no		yes
M5	unknown	81.0525	yes	no		no
M6	unknown	83.0854	no	no		yes
M9	unknown	93.0574	no	no		yes
M13	unknown	103.0943	no	no		yes
M20	unknown	122.0835	yes	no		no
M22	unknown	124.0835	yes	no		no
M23	unknown	128.0701	no	no		yes
M27	unknown	136.0471	yes	no		yes
M32	unknown	149.0971	yes	no		no
M34	unknown	152.0699	yes	yes	0.42	no
M36	unknown	158.1241	yes	no		no
M39	unknown	165.1272	no	no		yes
M42	unknown	175.1117	yes	no		yes
M43	unknown	182.0897	no	yes	0.38	no
M44	unknown	207.1378	no	yes	0.38	no
M46	unknown	209.1168	no	yes	0.4	no
M47	unknown	209.1536	yes	no		no
M48	unknown	210.1568	no	no		yes
M49	unknown	211.1325	no	yes	0.38	no
M54	unknown	228.0686	no	no		yes

**Table 5.3.: A panel of validated OSA biomarkers.** 33 of the previously detected<sup>227</sup> biomarkers for OSA show a significant correlation with the ODI or ESS or significant differences between OSA patients and control subjects in the validation cohort (significance level:  $p < 0.05$ ). (unsat. aldehydes: unsaturated aldehydes).

metabolite name	m/z	Spearman correlation coefficient ODI	p correlation ODI	q correlation ODI	Spearman correlation coefficient ESS	p correlation ESS	q correlation ESS	p between groups (stratification 1)	q between groups (stratification 1)	log <sub>2</sub> fold change between groups (stratification 1)	p between groups (stratification 2)	q between groups (stratification 2)	log <sub>2</sub> fold change between groups (stratification 2)
2-pentenal ([M+NH <sub>4</sub> ] <sup>+</sup> )	102.0912	0.23	0.005	0.017	0.07	0.43	0.34	0.029	0.087	0.43	0.003	0.004	0.75
4-hydroxy-2-heptenal	129.0908	0.2	0.015	0.02	0.13	0.11	0.26	0.022	0.081	0.42	0.003	0.004	0.83
4-hydroxy-2-octenal ([M+NH <sub>4</sub> ] <sup>+</sup> )	143.1064	0.16	0.048	0.036	0.13	0.11	0.26	0.036	0.088	0.12	0.006	0.005	0.25
4-hydroxy-2-octenal	160.1331	0.18	0.026	0.023	0.16	0.05	0.19	0.02	0.081	0.47	0.001	0.003	0.85
2-undecenal	169.1586	0.11	0.17	0.072	0.09	0.3	0.34	0.36	0.246	0.16	0.04	0.018	0.33
2-ethylfuran	97.0646	0.23	0.005	0.017	0.1	0.25	0.34	0.009	0.068	0.38	0.005	0.004	0.8
2-propylfuran	111.0803	0.27	0.001	0.011	0.1	0.21	0.34	0.003	0.068	0.41	0.004	0.004	0.56
2-butylfuran	125.0961	0.23	0.004	0.017	0.13	0.13	0.28	0.005	0.068	0.26	0.001	0.004	0.48
2-pentylfuran	139.1116	0.11	0.197	0.074	0.17	0.04	0.19	0.04	0.088	0.26	0.002	0.004	0.57
benzothiazole	136.0213	0.2	0.016	0.02	-0.04	0.62	0.35	0.019	0.081	0.4	0.025	0.014	0.5
4-(hexyloxy)phenol	195.1379	0.15	0.076	0.048	0.06	0.45	0.34	0.111	0.143	0.34	0.01	0.008	0.62
M1	53.0374	0.1	0.237	0.079	0.08	0.37	0.34	0.314	0.223	0.19	0.032	0.015	0.48
M3	79.0392	0.2	0.016	0.02	-0.06	0.49	0.34	0.094	0.143	0.51	0.067	0.024	0.71
M5	81.0525	0.06	0.466	0.12	0.19	0.02	0.19	0.153	0.152	0.46	0.051	0.021	0.74
M6	83.0853	0.19	0.021	0.022	0.16	0.05	0.19	0.037	0.088	0.27	0.03	0.015	0.48
M9	93.0548	0.19	0.022	0.022	-0.1	0.24	0.34	0.213	0.184	0.43	0.179	0.051	0.52
M13	103.0952	0.2	0.013	0.02	0.05	0.55	0.34	0.047	0.088	0.55	0.019	0.011	0.95
M20	122.0806	0.21	0.012	0.02	0.03	0.68	0.37	0.01	0.068	0.49	0.005	0.004	0.8
M22	124.0838	0.14	0.09	0.053	0.15	0.06	0.22	0.024	0.081	0.26	0.036	0.017	0.41
M23	128.0703	0.13	0.114	0.058	0.19	0.02	0.19	0.042	0.088	0.27	0.002	0.004	0.35
M27	136.0511	-0.06	0.485	0.123	0.19	0.02	0.19	0.96	0.446	-0.18	0.401	0.084	-0.03
M32	149.0959	0.11	0.176	0.072	0.21	0.01	0.19	0.126	0.144	0.3	0.019	0.011	0.38
M34	152.0705	0.13	0.104	0.055	0.02	0.82	0.41	0.178	0.164	0.23	0.045	0.02	0.55
M36	158.125	0.16	0.048	0.036	0.14	0.09	0.25	0.044	0.088	0.12	0.003	0.004	0.67
M39	165.1273	0.19	0.019	0.022	0.1	0.24	0.34	0.046	0.088	0.41	0.005	0.004	0.54
M42	175.1134	0.21	0.01	0.02	0.16	0.05	0.19	0.007	0.068	0.41	0.001	0.003	0.64
M43	182.0809	0.12	0.146	0.071	0.14	0.09	0.25	0.064	0.11	0.18	0.001	0.004	0.55
M44	207.1381	0.15	0.065	0.043	0.02	0.82	0.41	0.245	0.204	0.35	0.028	0.015	0.58
M46	209.1173	0.18	0.025	0.023	-0.03	0.69	0.37	0.111	0.143	0.54	0.026	0.014	0.75
M47	209.1536	0.2	0.016	0.02	0.03	0.72	0.37	0.057	0.102	0.37	0.012	0.008	0.68
M48	210.1568	0.24	0.004	0.017	0.02	0.83	0.41	0.02	0.081	0.5	0.014	0.01	0.67
M49	211.1328	0.2	0.015	0.02	0.17	0.04	0.19	0.025	0.081	0.42	0.002	0.004	0.67
M54	228.0642	-0.18	0.03	0.025	-0.05	0.58	0.34	0.119	0.143	-0.37	0.119	0.04	-0.4

real-time breath analysis could speed up diagnosis and make it even less bothersome for the patients. We think that the combination of exhaled breath analysis and the NoSAS score might provide an objective and easy-to-perform assay for screening patients with possible OSA. Only positively tested patients would then need to undergo the time-consuming, costly and inconvenient respiratory polygraphy to confirm or refute the screening result. During the screening even multiple testing would be possible, since the breath test is fast and non-invasive. This might help to overcome the problem of a considerable night-to-night variation of OSA. Further studies, looking at the combination of the NoSAS score and SESI-HRMS are needed.

In addition, exhaled breath metabolomics can provide biological information because compounds can be identified. Here, we could confirm the association of unsaturated aldehydes, furans and benzothiazole with OSA. These findings are strengthening the hypotheses from our pilot study of increased oxidative stress levels and altered gut microbiota in OSA patients. Moreover, our findings of metabolites such as 2-pentylfuran and 4-hydroxy-2-octenal, correlating with both, ESS and ODI, suggest an association of those metabolites with the sleep deprivation going along with OSA leading to increased sleepiness.

## 5.5. Conclusion

In conclusion, we could confirm our previous findings of an OSA specific metabolic breath pattern and confirm a panel of 33 biomarkers in a larger and broader cohort of patients with possible OSA. This is the first validation study for breath analysis by SESI-HRMS, bringing this technique an important step closer to its application in clinics. However, before it can be implemented for clinical use, the added value of SESI-HRMS measurements to conventional OSA screening questionnaires, such as NoSAS, should be evaluated in further studies.

# 6

Multi-omics correlates of insulin signaling  
and circadian function

The work presented in this chapter was performed in collaboration with Ngoc-Hien Du<sup>1</sup>, Flore Sinturel<sup>2</sup>, Pauline Gosselin<sup>2</sup>, Camille Saini<sup>2</sup>, Charna Dibner<sup>2</sup>, François R. Jornayvaz<sup>3</sup>, Jacques Philippe<sup>3</sup>, Guillaume Rey<sup>2</sup>, Emmanouil T. Dermitzakis<sup>2</sup> and Steven A. Brown<sup>1</sup> (<sup>1</sup>University of Zurich, <sup>2</sup>University of Geneva, <sup>3</sup>University Hospital of Geneva). A manuscript for publication is in preparation.

S.A.B, C.D., J.P. and E.T.D. designed the study. C.S., F.R.J. and J.P. conducted subject enrolment and sampling. F.S. and P.G. carried out cell culture experiments. NH.D. carried out the GWAS analysis. N.N. performed the mass spectrometry measurements and the corresponding data analysis. N.N., NH.D. and F.S. carried out the combined data analysis and wrote the manuscript with input from all co-authors.



## Summary

There is major evidence for a complex cross-talk between circadian clocks and metabolism. Moreover, circadian disruption is associated with an increased risk for metabolic diseases, such as type 2 diabetes, obesity and metabolic syndrome. Since shift work and social jetlag are common phenomena in modern society, this association with adverse health effects has become a major issue of public health. While several studies investigated the effect of disrupted circadian clocks on metabolism, the influence of metabolite profiles related to metabolic diseases on circadian clock parameters remains largely unexplored.

In this study, we therefore measured the expression of the circadian reporter gene *Bmal1-luc* in U2OS cells in the presence of serum from patients with and without type 2 diabetes and or obesity. Moreover, we assessed clinical parameters and carried out metabolic profiling by ultra-high performance liquid chromatography coupled to high-resolution mass spectrometry with the serum samples.

In obese patients suffering from metabolic syndrome, we detected an association between elevated levels of metabolites related to insulin resistance and elongation of *Bmal1-luc* period length. Furthermore, our results from a genome wide association study using circadian period length as a trait suggest *March1* as genetic origin of these metabolic factors.

Thus, our findings indicate that insulin resistance might be a driving force in the vicious cycle of metabolic syndrome and circadian clock dysfunction.

## 6.1. Introduction

In virtually all light-sensitive organisms, circadian clocks govern most aspects of physiology, including metabolism,<sup>58</sup> to synchronize them with the external environment.<sup>303</sup> In mammals, a master pacemaker in the brain, located in the suprachiasmatic nuclei (SCN), drives this circadian control of behavior and physiology. The SCN receives external light stimuli and conveys this information to peripheral clocks, which are present in nearly every cell.<sup>304</sup> The circadian clocks can also be entrained by other stimuli such as feeding, exercising or resting/activity cycles.<sup>305</sup> On a molecular level, the circadian timing system consists of transcriptional-translational feedback loops of clock genes and clock proteins, for example CLOCK, BMAL1, PER and CRY, which result in oscillations with a period length of roughly 24 hours.<sup>306</sup>

In a modern 24/7 society, shift work is common and social jetlag has become a public issue. There is strong evidence from epidemiologic studies that this circadian disruption is associated with an increased incidence of metabolic diseases, such as type 2 diabetes (T2D), obesity and metabolic syndrome, but also cardiovascular diseases.<sup>307-309</sup> In mice as well as in humans, an interplay between circadian clocks and metabolism is considered to be crucial for metabolic health.

Studies with rodents suggest that there is bidirectional cross talk between clocks and metabolism. Whereas forced circadian misalignment in mice leads to disruption of metabolic pathways, high fat diet induces the alteration of circadian oscillations.<sup>63,66</sup> Several relationships between clock gene function and metabolic functions have been unraveled. Weitz et al. found that rather *BMAL1* rhythmicity than overall *BMAL1* function is essential for

glucose homeostasis.<sup>310</sup> Other studies showed that the core clock gene *Rev-erb $\alpha$*  is crucial for proper lipid and carbohydrate metabolism.<sup>311–313</sup> In addition, epigenetic factors were identified to play a role in the connection between clocks and metabolism in mice. The histone deacetylase HDAC3, for example, is necessary for proper metabolic regulation by *Rev-erb $\alpha$* <sup>35</sup> and the NAD cofactor-dependent histone deacetylase SIRT1 is needed for circadian acetylation of PER2 and BMAL1.<sup>46,314</sup>

In humans, sleep restriction has been shown to trigger increased caloric intake and weight gain despite increased energy expenditure during wakefulness compared to sleep.<sup>151</sup> Moreover, mutations in the core clock genes *Clock* and *Bmal1* have been associated with metabolic disorders in humans.<sup>315,316</sup> In adipose tissue of patients suffering from severe obesity, decreased amplitudes of several rhythmically expressed cytokines was observed.<sup>317</sup> Recently, an inverse correlation between the cellular circadian period length and glycated hemoglobin (HbA1c) was reported in T2D patients, underpinning the relevance of circadian clocks for metabolic health.<sup>70</sup> However, even though there is clear evidence for a direct link between circadian clocks and metabolic syndrome, genetic and biochemical links remain largely unknown in humans. Therefore, there is no ability yet to use this knowledge in a clinically relevant fashion.

Circadian oscillations measured *in vitro* in human fibroblasts were shown to reflect overall *in vivo* circadian clock properties.<sup>196</sup> Further, experiments with human cells cultured in human serum suggest that circulating factors can alter circadian properties. Serum factors from elder persons, for example, caused period shortening and phase shifting towards earlier phases.<sup>318</sup> While there are many studies on the effect of circadian disruption on metabolism, the other direction, i.e., how metabolic factors can affect circadian clocks, remains much less explored. Since obesity and T2D are known to provoke metabolic alterations of blood chemistry testing effects of these serum metabolites on cellular function of the circadian clock could unravel insights into the connection between metabolic health and proper clock function. This can make the assessment of clock properties an interesting tool for the detection of disease-related changes of serum composition.

In this study, we used a combinatorial approach of metabolomics and circadian measurements of human osteosarcoma U2OS cells in the presence of human serum to gain insights into molecular factors in serum that might modify circadian properties in obese patients. Further, we performed a genome wide association study using circadian period length as a trait to search for genetic origin of these metabolic factors.

## 6.2. Methods

### 6.2.1. Participant characteristics and study design

308 participants were enrolled in this study, divided into four categories: non-diabetic non obese volunteers, non-diabetic obese volunteers, obese volunteers with type 2 diabetes and non-obese volunteers with type 2 diabetes. All participants gave informed consent and the study had ethics committee approval (CER11-015). Participants were included according to the criteria listed in supplementary table B.7, based on a detailed questionnaire completed during the pre-selection process. The study was registered at ClinicalTrials.gov (registration

no. NCT02384148). A list of the baseline characteristics of the participants in each group is presented in supplementary table B.8. The participant age and sex were comparable between the groups, and differences between the groups stemmed from diagnose of Type 2 diabetes, HbA1c and BMI values (supplementary table B.8). A detailed list of medications taken by the participants is presented in supplementary table B.9. All study participants filled out the Munich Chronotype Questionnaire (MCTQ), allowing calculation of MSF<sub>sc</sub> values that characterize an individual's chronotype. The participants were asked to follow a moderate diet without excess fat or alcohol intake, 24 hours prior to the testing day.

### 6.2.2. Harvesting of sera

Blood samples for all study participants were collected between 08:00 and 10:00 hours, following overnight fasting from 10 pm onwards. Blood samples were collected in clot-activator vacutainers and immediately analyzed by the Geneva University Hospital laboratory for blood analysis including glucose, HbA1c, hormones, lipids, liver and kidney functions measurements (detailed list of the measured clinical parameters in the blood is reported in supplementary table B.10). Serum was immediately prepared from blood samples by centrifugation (10 min, 1650 x g, 4 °C) and stored at -80 °C until circadian measurements.

### 6.2.3. Primary dermal fibroblast culture, in vitro synchronization and DNA extraction

Cutaneous biopsies were taken from each participant's shoulder between 8.00 and 9 AM and processed as described previously.<sup>195</sup> Cells in culture were synchronized with a 100 nM dexamethasone pulse, and collected 24 h later. DNA was extracted using QIAamp DNA Mini Kit (Qiagen AG) and eluted in a final volume of 15 µL.

### 6.2.4. Lentivector production

*Bmal1-luc* lentiviral particles [Brown et al. 2005] were produced at the Viral Vector Facility of the University of Zurich. Transient transfection in 293T cells was performed using the polyethylenimine method.<sup>319</sup> Lentiviral particles were harvested at 48 h post-transfection, PEG precipitated, titred and used for the transduction of the U2OS cells with multiplicity of infection (MOI) of 3.

### 6.2.5. U2OS cell culture, in vitro synchronization and real-time bioluminescence recording

U2OS cells (ATCC) were cultured in DMEM low glucose (GIBCO) supplemented with 1% Penicillin/Streptomycin (GIBCO), 0.5% Amphotericin B (life Diagnostic), 0.5% Gentamycin (Merck) and 10% FCS (GIBCO). Cells were transduced with the *Bmal1* (also known as *Arntl*)-*luciferase* (*luc*) lentivector, and selected with Blasticidin S (Invitrogen) at 25 µg/mL final concentration. The same batch of transduced U2OS cells has been used for all the circadian measurements. After synchronization of the cells with a 100 nmol/l dexamethasone pulse,

the circadian bioluminescence recording is performed in DMEM low glucose without phenol red (GIBCO) supplemented with 1% Penicillin/Streptomycin (GIBCO), 0.5% Amphotericine B (Life Diagnostic), 0.5% Gentamycin (Merck), 1  $\mu\text{L}/\text{mL}$  of luciferin (Prolume 13nM pH7.4) and in the presence of 10% of the individual's sera. Bioluminescence was monitored by a home-made robotic device equipped with photomultiplier tube detector assemblies, allowing the recording of technical triplicates in 24-well plates (Gerber et al., 2013) for 1 week. After removing the first oscillation cycle (to avoid a potential bias stemming from the immediate early response to synchronization), raw data were processed in parallel graphs by moving average with a window of 24 h, allowing to analyze the period of time series without the variability of magnitudes.

## 6.2.6. Metabolomics by UPLC-MS

### 6.2.6.1. Sample preparation and measurements

200  $\mu\text{L}$  of serum were thawed on ice, 200  $\mu\text{L}$  of 1 mg/mL  $^{15}\text{N}_2$ -tryptophan (Cambridge Isotope Laboratories, Inc., Tewksbury, USA) in water (LC-MS grade, Fisher Scientific, Pittsburgh, USA) were added as internal standard and proteins were precipitated by the addition of 600  $\mu\text{L}$  of methanol (LC-MS grade, Fisher Scientific, Pittsburgh, USA). The samples were incubated on ice for 10 minutes and centrifuged at 4  $^\circ\text{C}$  and 15800 g for 15 min. The supernatant was filtered using a 0.2  $\mu\text{m}$  reversed cellulose membrane filter. 10  $\mu\text{L}$  of the metabolite extract were injected directly for chromatographic separation on an ACQUITY UPLC BEH AMIDE column (1.7  $\mu\text{m}$ , 2.1  $\times$  150 mm, Waters) with a corresponding precolumn filter. 400  $\mu\text{L}$  of the metabolite extract were aliquoted and solvents were removed in a vacuum dryer. The residual was resuspended in 75 mL of a mixture of water and methanol (95/5, v/v, both LC-MS grade, Fisher Scientific, Pittsburgh, USA), sonicated (10 min) and centrifuged (15 min, 15800 g) and transferred to LC vials with glass inserts for chromatographic separation on an ACQUITY UPLC BEH C18 column (1.7  $\mu\text{m}$ , 2.1  $\times$  150 mm, Waters). Also there, 10  $\mu\text{L}$  were injected for analysis. One sample per person were analyzed, analytical reproducibility was verified with quality control (QC) samples (pool of all samples). The samples were measured in batches of 60 samples and QC samples were measured across each batch.

Chromatographic separation was performed on an ACQUITY UPLC system (I-Class, Waters, MA, USA). With the RP column, the flow rate was set to 240  $\mu\text{L}/\text{min}$  using a binary mixture of solvent A (water with 0.5 % methanol and 0.1 % formic acid) and solvent B (methanol with 0.1 % formic acid). The following gradient was used: 5 % B (1 min), 5 to 95 % B (9 min), 100 % B (2 min), and 5 % B (2 min). The column temperature was set to 30  $^\circ\text{C}$  and the autosampler was kept at 5  $^\circ\text{C}$ . For the AMIDE column a flow rate of 400  $\mu\text{L}/\text{min}$  was used with a binary mixture of solvent A (water with 0.1% formic acid) and solvent B (acetonitrile with 0.1% formic acid). The following gradient was applied: 99-30% B (7 min), 99% B (3 min). The column was kept at 45  $^\circ\text{C}$  and the autosampler at 5  $^\circ\text{C}$ .

Mass spectra were recorded on a quadrupole-time-of-flight high-resolution mass spectrometer (TripleTOF 5600+, AB Sciex, Concord, ON, Canada) with a heated electrospray ionization source in positive and negative ion mode. Full-scan mass spectra ( $m/z$  range 50 to 650 Da) and data dependent MS-MS acquisitions ( $m/z$  range 40 to 650 Da) were performed. Curtain

gas flow was set to 30 au, GS1 and GS2 were set to 60 au, a spray voltage of 5 kV (-4.5 kV) was applied and the ion source was heated to 500 °C. For the RP measurements, the total cycle time was kept at 800 ms to obtain at least 12 points/peak (minimal LC peak width = 9 s) with 150 ms for full scan MS and 85.7 ms for seven data dependent product ion scans acquired with a collision energy of 10/20/30 eV. For the AMIDE measurements, the total cycle time was kept at 550 ms to obtain at least 12 points/peak (minimal LC peak width = 6 s) with 150 ms for full scan MS and 87.5 ms for four data dependent product ion scans acquired with a collision energy of 10/20/30 eV.

#### 6.2.6.2. Measurements of reference standards

In addition, reference standards were measured for a certain number of metabolites. Four different mixtures of non-isobaric compounds at a concentration of 10 µg/mL, 5 µg/mL and 1 µg/mL in 5% methanol for RP measurements and 75% methanol for AMIDE measurements were produced (compositions of the four mixtures are given in table 6.1). Moreover, 10 µg/mL solutions were produced separately for linoleic acid, arachidonic acid, docosapentaenoic acid, myristic acid and ethanolamine. 10 µL of each sample were injected for UPLC-MS measurements. Mass spectra were recorded in full scan and product ion mode. For measurements on the RP column, each acquisition cycle consisted of a full scan with an acquisition time of 150 ms and six product ion scans with an acquisition time of 100 ms. For measurements on the AMIDE column, each acquisition cycle consisted of a full scan with an acquisition time of 100 ms and four product ion scans with an acquisition time of 100 ms. Collision energies are stated in table 6.1, the other instrument parameters were set as described above for the data dependent acquisitions.

#### 6.2.6.3. Data preprocessing

Raw data files were converted into .mzXML files and centroided using MSConvert (Proteowizard).<sup>247</sup> Further preprocessing was conducted with XCMS<sup>320,321</sup> in R (v3.6.1). For each measurement batch, peak picking, peak alignment, integration and annotation was performed. The applied parameter settings are given in table 6.2.

Subsequently, data obtained from the QC samples was used to correct for instrumental drift using *statTarget* in R.<sup>322</sup> We applied the QCRLSC method (parameter settings: *Frule* = 0.8, *QCspan* = 0.5, *degree* = 2, *imputeM* = KNN) and removed all features that were detected in less than half of the QC samples as well as features, which had a relative standard deviation above 50% in the QCs after drift correction. Features identified as isotopes have also been removed. To confirm whether the drift correction did also remove inter-batch effects successfully, we compared the results of a principle component analysis before and after correction (figure 6.1).

Finally, the features obtained from the different measurement batches were combined automatically (*m/z* tolerance: 0.001 Da, retention time tolerance: 15 s). This automatic merging failed for isomers with small differences in retention time, when large shifts in retention time occurred between batches. We therefore reviewed the merging by visual inspection of all extracted ion chromatograms and corrected manually for wrong assignments.

**Table 6.1.:** Composition of standard mixtures of reference compounds and collision energies used for the acquisition of product ion scans.

Compound Name	column	polarity	Mixture #	Collision energy (eV)
3-(4-hydroxyphenyl)propionic acid	RP	neg	1	-20
3-methyl-2-oxobutyric acid	RP	neg	1	-20
8-hydroxyoctanoic acid	RP	neg	1	-20
citric acid	RP	neg	1	-10
cortisol	RP	pos	1	20
cortisone	RP	pos	1	30
D-pantothenic acid	RP	neg	1	-20
glycodeoxycholic acid	RP	neg	1	-20
L-isoleucine	RP	pos	1	15
lauroylcarnitine	RP	pos	1	-10
succinic acid	RP	neg	1	-10
3-hydroxybutyric acid	RP	neg	2	-10
4-hydroxyphenylacetic acid	RP	neg	2	-10
4-methyl-2-oxovaleric acid	RP	neg	2	-30
alpha-ketobutyric acid	RP	neg	2	-10
glycocholic acid	RP	pos	2	15
hexadecanedioic acid	RP	neg	2	-20
hippuric acid	RP	neg	2	-20
L-(-)-phenyllactic acid	RP	neg	2	-20
L-tryptophan	RP	neg	2	-20
L-tyrosine	RP	neg	2	-20
levulinic acid	RP	neg	2	-10
N-acetylmethionine	RP	neg	2	-20
tetradecanedioic acid	RP	neg	2	-20
5-oxoproline	RP	pos	3	20
creatinine	AMIDE	pos	3	30
DL-citrulline	AMIDE	pos	3	15
L-4-hydroxyproline	AMIDE	pos	3	20
L-alanine	AMIDE	pos	3	10
L-cysteine	AMIDE	pos	3	10
L-glutamic acid	AMIDE	pos	3	10
L-proline	AMIDE	pos	3	10
L-serine	AMIDE	pos	3	10
L-threonine	AMIDE	pos	3	10
N,N-dimethylglycine	AMIDE	pos	3	10
pipecolic acid	RP	pos	3	20
choline chloride	AMIDE	pos	4	30
creatine	AMIDE	pos	4	20
cystathionine	AMIDE	pos	4	10
glycine	AMIDE	pos	4	10
L-(+)-ornithine	AMIDE	pos	4	10
L-arginine	AMIDE	pos	4	15
L-aspartic acid	AMIDE	pos	4	10
L-histidine	AMIDE	pos	4	15
L-lysine	AMIDE	pos	4	10
pelargonic acid	RP	neg	4	-30
serotonin	RP	pos	4	15

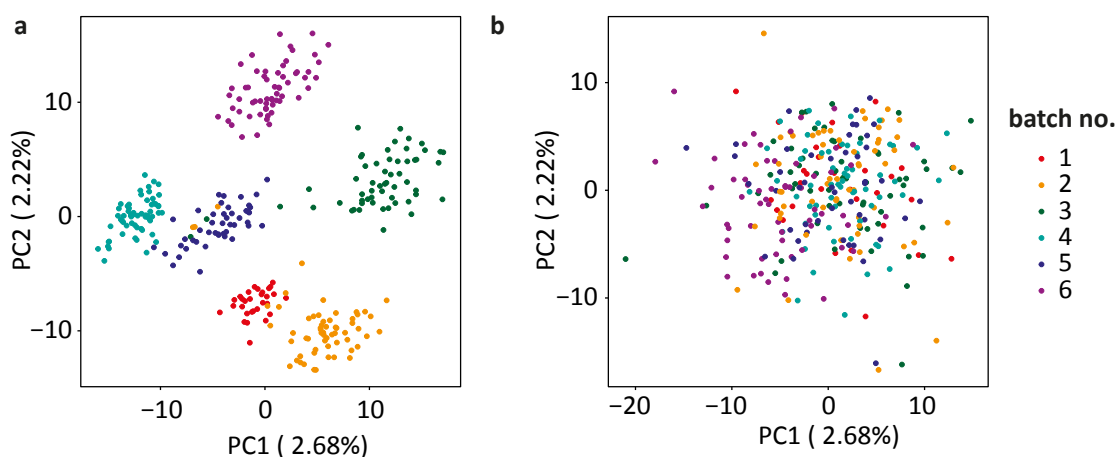


**Figure 6.1.:** Principal component analysis before (a) and after (b) instrumental drift correction.

In addition to this untargeted peak extraction, we performed targeted analysis for metabolites, of which we measured reference standards. We used the peakPanther R package<sup>323</sup> with the target list given in table 6.3. Retention time windows for isoleucine, pipercolinic acid, citric acid, 4-methyl-2-oxovaleric acid, phenyllactic acid, tetradecanedioic acid and docosapentaenoic acid were adapted for each batch, due to the presence of isomers at similar retention times. We applied drift correction with QC samples as described above.

Data from untargeted and targeted peak extraction were combined and only features detected in all samples were further considered. We removed features from the untargeted peak extraction approach, which were already covered by the targeted approach, in order to avoid duplicates. This resulted in 372 remaining features. Peak areas were log-transformed and autoscaled.

### 6.2.7. Statistical analysis

All data analysis was conducted in R (v3.6.1). In order to assess the relation between the circadian period length measured in U2OS cells cultured in patient's serum and clinical parameters or metabolite levels in serum, we performed two-sided Kolmogorow-Smirnow (KS) tests between the first and the fourth data quartile. We performed these comparisons within the different patient groups (obese, T2D and healthy).

### 6.2.8. Metabolic pathway analysis and compound annotation

We made use of two different tools for automated compound annotation in order to annotate the peaks from our untargeted metabolic approach. We used MSDial<sup>256</sup> for MS/MS library matching with the spectra we obtained from data dependent MS/MS acquisition. Moreover, we applied the mummichog algorithm<sup>254</sup> in MetaboAnalyst for R,<sup>215</sup> which infers metabolic pathway information and biological activity. We employed the *homo sapiens* Kegg database, set the mass tolerance to 10 ppm and the p-value threshold to 0.2. We subsequently reviewed the annotations for biologically relevant features manually and confirmed metabolite identities with reference standards, if available.

**Table 6.2.:** Parameter settings for preprocessing of LC-MS data using XCMS in R.

	<b>parameter</b>	<b>RP pos</b>	<b>RP neg</b>	<b>AMIDE pos</b>	<b>AMIDE neg</b>
<b>peak detection (centWave)</b>	ppm	10	10	10	10
	peakwidth	c(5,12)	c(5,12)	c(5,12)	c(5,12)
	mzdiff	-0.001	-0.001	-0.001	-0.001
	snthresh	6	3	3	3
	integrate	1	1	1	1
	noise	0	0	0	0
	prefilter	c(3,100)	c(3,100)	c(3,100)	c(3,100)
	fitgauss	FALSE	FALSE	FALSE	FALSE
<b>alignment (peakGroups)</b>	minFraction	0.5	0.5	0.5	0.5
	binSize	0.01	0.01	0.01	0.01
	minSamples	1	1	1	1
	bw	5	5	5	5
	span	0.6	0.6	0.6	0.6
<b>annotation</b>	perfwhm	0.6	0.6	0.6	0.6
	mzabs	0.001	0.001	0.001	0.001
	cor_eic_th	0.75	0.75	0.75	0.75

### 6.2.9. Genotyping

Fibroblasts were genotyped using the Illumina CoreExome 24 v1.3 array. Only samples with variant calling rate > 98 % were considered. Population stratification was done by principal component analysis using the phase 3 1000 genome variants to select for European subjects. This left 269 subjects went into genome wide association analysis. Variants were then filtered to choose only variants from the European panel. Next, variants were filtered using vcftools with the following parameters:  $-\text{mac } 2$ ,  $-\text{max-missing } 0.95$ ,  $-\text{hwe } 0.000001$ . This yielded 290867 genotyped variants. Genotyped were then imputed using the Michigan Imputation Server with the phase 3 1000 genome genotypes as reference. Imputed variants were filtered out according to these criteria: imputation quality > 0.5, MAF > 0.05, Hardy-Weinberg probability <  $1e-6$ . A total of 5630127 variants were left after filtering these steps.

### 6.2.10. Genome wide association analysis

Genome wide association analysis was performed on circadian period length using PLINK 1.90. Sex, age, disease (control, obese non T2D, non obese T2D, and obese T2D), date of circadian measurement, experimenter, and the first 10 MDS dimensions of the genotypes were included as covariates.



**Table 6.3.:** Target list for targeted peak extraction.

Name	m/z	m/z <sub>min</sub>	m/z <sub>max</sub>	tR	tR <sub>min</sub>	tR <sub>max</sub>	column	polarity
L-isoleucine (M+H)	132.1019	132.1009	132.1029	160.2	145.2	175.2	RP	positive
lauroylcarnitine (M+H)	344.2795	344.2785	344.2805	615.6	600.6	630.6	RP	positive
cortisone (M+H)	361.2009	361.1999	361.2019	507	492	522	RP	positive
cortisol (M+H)	363.2166	363.2156	363.2176	526.2	511.2	541.2	RP	positive
glycocholic acid (M+H)	466.3163	466.3153	466.3173	628.2	613.2	643.2	RP	positive
5-oxoproline (M+H)	130.0499	130.0489	130.0509	128.4	113.4	143.4	RP	positive
pipecolinic acid (M+H)	130.0863	130.0853	130.0873	103.2	88.2	118.2	RP	positive
serotonin (M+H-NH <sub>3</sub> )	160.0757	160.0747	160.0767	159	144	174	RP	positive
3-methyl-2-oxobutyric acid (M-H)	115.0401	115.0391	115.0411	245.4	230.4	260.4	RP	negative
succinic acid (M-H)	117.0193	117.0183	117.0203	148.8	133.8	163.8	RP	negative
8-hydroxyoctanoic acid (M-H)	159.1027	159.1017	159.1037	430.2	415.2	445.2	RP	negative
3-(4-hydroxyphenyl)propionic acid (M-H)	165.0557	165.0547	165.0567	379.2	364.2	394.2	RP	negative
citric acid (M-H)	191.0197	191.0187	191.0207	129	114	144	RP	negative
D-pantothenic acid (M-H)	218.1034	218.1024	218.1044	247.2	232.2	262.2	RP	negative
glycodeoxycholic acid (M-H)	448.3068	448.3058	448.3078	667.8	652.8	682.8	RP	negative
L-tyrosine (M-H)	180.0666	180.0656	180.0676	136.2	121.2	151.2	RP	negative
4-methyl-2-oxovaleric acid (M-H)	129.0557	129.0547	129.0567	372.6	357.6	387.6	RP	negative
hippuric acid (M-H)	178.0510	178.0500	178.0520	328.2	313.2	343.2	RP	negative
N-acetylmethionine (M-H)	190.0543	190.0533	190.0553	300	285	315	RP	negative
L-(-)-phenyllactic acid (M-H)	165.0557	165.0547	165.0567	413.4	398.4	428.4	RP	negative
L-tryptophan (M-H)	203.0826	203.0816	203.0836	289.2	274.2	304.2	RP	negative
alpha-ketobutyric acid (M-H)	101.0244	101.0234	101.0254	160.2	145.2	175.2	RP	negative
4-hydroxyphenylacetic acid (M-H)	151.0401	151.0391	151.0411	334.2	319.2	349.2	RP	negative
tetradecanedioic acid (M-H)	257.1758	257.1748	257.1768	640.2	625.2	655.2	RP	negative
hexadecanedioic acid (M-H)	285.2071	285.2061	285.2081	0	-15	15	RP	negative
myristic acid (M-H)	227.2017	227.2007	227.2027	744.6	729.6	759.6	RP	negative
3-hydroxybutyric acid (M-H)	103.0401	103.0391	103.0411	156	141	171	RP	negative
levulinic acid (M-H)	115.0401	115.0391	115.0411	193.8	178.8	208.8	RP	negative
linoleic acid (M-H)	279.2330	279.2320	279.2340	754.8	739.8	769.8	RP	negative
arachidonic acid (M-H)	303.2330	303.2320	303.2340	750	735	765	RP	negative
pelargonic acid (M-H)	157.1234	157.1224	157.1244	649.2	634.2	664.2	RP	negative
L-alanine (M+H)	90.0550	90.0540	90.0560	232.8	202.8	262.8	AMIDE	positive
N,N-dimethylglycine (M+H)	104.0706	104.0696	104.0716	231	201	261	AMIDE	positive
L-serine (M+H)	106.0499	106.0489	106.0509	264.6	234.6	294.6	AMIDE	positive
creatinine (M+H)	114.0662	114.0652	114.0672	165.6	135.6	195.6	AMIDE	positive
L-proline (M+H)	116.0706	116.0696	116.0716	229.2	199.2	259.2	AMIDE	positive
L-threonine (M+H)	120.0655	120.0645	120.0665	256.2	226.2	286.2	AMIDE	positive
5-oxoproline (M+H)	130.0499	130.0489	130.0509	254.4	224.4	284.4	AMIDE	positive
L-4-hydroxyproline (M+H)	132.0655	132.0645	132.0665	258.6	228.6	288.6	AMIDE	positive
L-(+)-ornithine (M+H-NH <sub>3</sub> )	116.0706	116.0696	116.0716	292.8	262.8	322.8	AMIDE	positive
L-glutamic acid (M+H)	148.0604	148.0594	148.0614	254.4	224.4	284.4	AMIDE	positive
DL-citrulline (M+H-NH <sub>3</sub> )	159.0764	159.0754	159.0774	265.8	235.8	295.8	AMIDE	positive
ethanolamine (M+Na)	84.0420	84.0410	84.0430	254.4	224.4	284.4	AMIDE	positive
L-cysteine (2M+H)	243.0468	243.0458	243.0478	331.2	301.2	361.2	AMIDE	positive
glycine (M+H)	76.0393	76.0383	76.0403	249	219	279	AMIDE	positive
choline chloride (M+H)	105.1148	105.1138	105.1158	64.8	34.8	94.8	AMIDE	positive
pipecolinic acid (M+H)	130.0863	130.0853	130.0873	217.8	187.8	247.8	AMIDE	positive
creatine (M+H)	132.0768	132.0758	132.0778	195.6	165.6	225.6	AMIDE	positive
L-aspartic acid (M+H)	134.0448	134.0438	134.0458	272.4	242.4	302.4	AMIDE	positive
L-lysine (M+H)	147.1128	147.1118	147.1138	288	258	318	AMIDE	positive
L-histidine (M+H)	156.0768	156.0758	156.0778	289.8	259.8	319.8	AMIDE	positive
L-arginine (M+H)	175.1190	175.1180	175.1200	284.4	254.4	314.4	AMIDE	positive
serotonin (M+H-NH <sub>3</sub> )	160.0757	160.0747	160.0767	165	135	195	AMIDE	positive
cystathionine (M+H)	223.0747	223.0737	223.0757	324	294	354	AMIDE	positive
pelargonic acid (M-H)	157.1234	157.1224	157.1244	84	54	114	AMIDE	negative
docosapentaenoic acid (M-H)	329.2486	329.2476	329.2496	64.2	34.2	94.2	AMIDE	negative

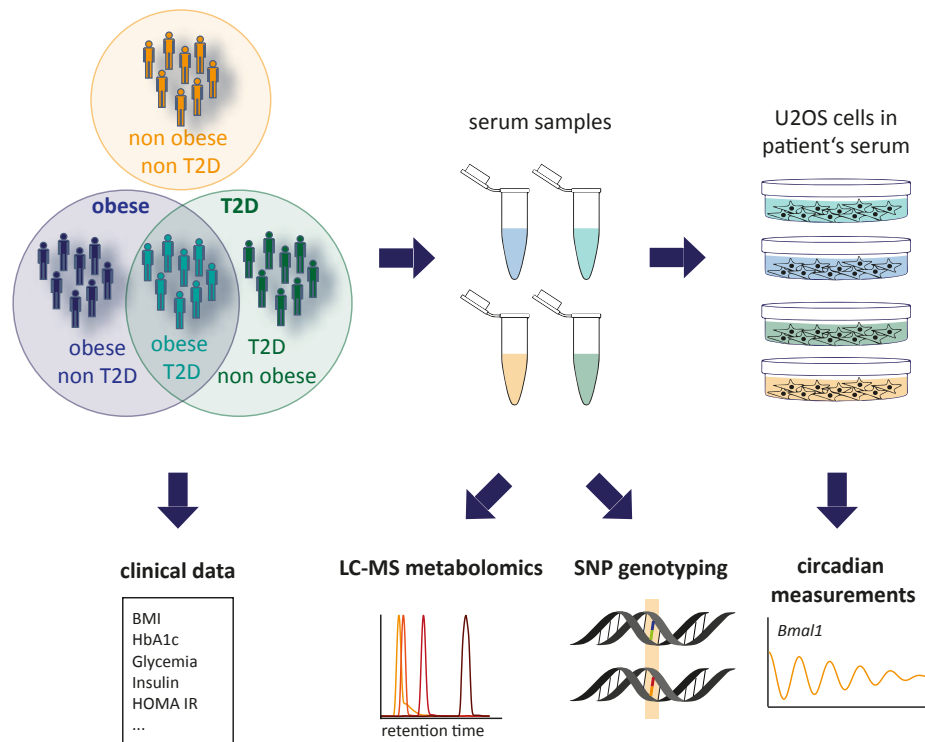


**Figure 6.2.:** Study overview. Groups of healthy persons, obese and type II diabetes (T2D) patients have been recruited and clinical parameters were assessed. Serum samples were taken and used for metabolite profiling by liquid chromatography coupled to mass spectrometry (LC-MS) and single nucleotide polymorphism (SNP) genotyping. Moreover, U2OS cells were cultured in the serum and circadian clock parameters were measured in a bioluminescence assay.

## 6.3. Results

### 6.3.1. Study design

We recruited 144 obese patients, 49 amongst them were also suffering from T2D. In addition, we included 52 non-obese T2D patients and 112 non-obese non-diabetic controls. Baseline characteristics, medication and blood parameters for the patient cohort are summarized in Table 4, Table 5 and Table 6 and our workflow is presented in figure 6.2. Due to a relatively high variability in the data and in order to not reduce statistical power, we did not divide the T2D group into obese and lean subjects in our further analysis. We obtained serum samples from all participants and subjected them to metabolomics analysis by liquid chromatography coupled to mass spectrometry (LC-MS) and performed SNP genotyping after DNA extraction from skin biopsies. Further, we measured circadian reporter gene expression of U2OS cells in the presence of the patient's sera in a bioluminescence assay.<sup>a</sup> We then looked for associations of the measured circadian period length with clinical parameters, metabolites and genotypes in order to get further insights into the link between circadian clocks and metabolic health.

<sup>a</sup> Every time, we mention period length or circadian clock property throughout this chapter, we refer to the this *Bmal1*-luc expression.

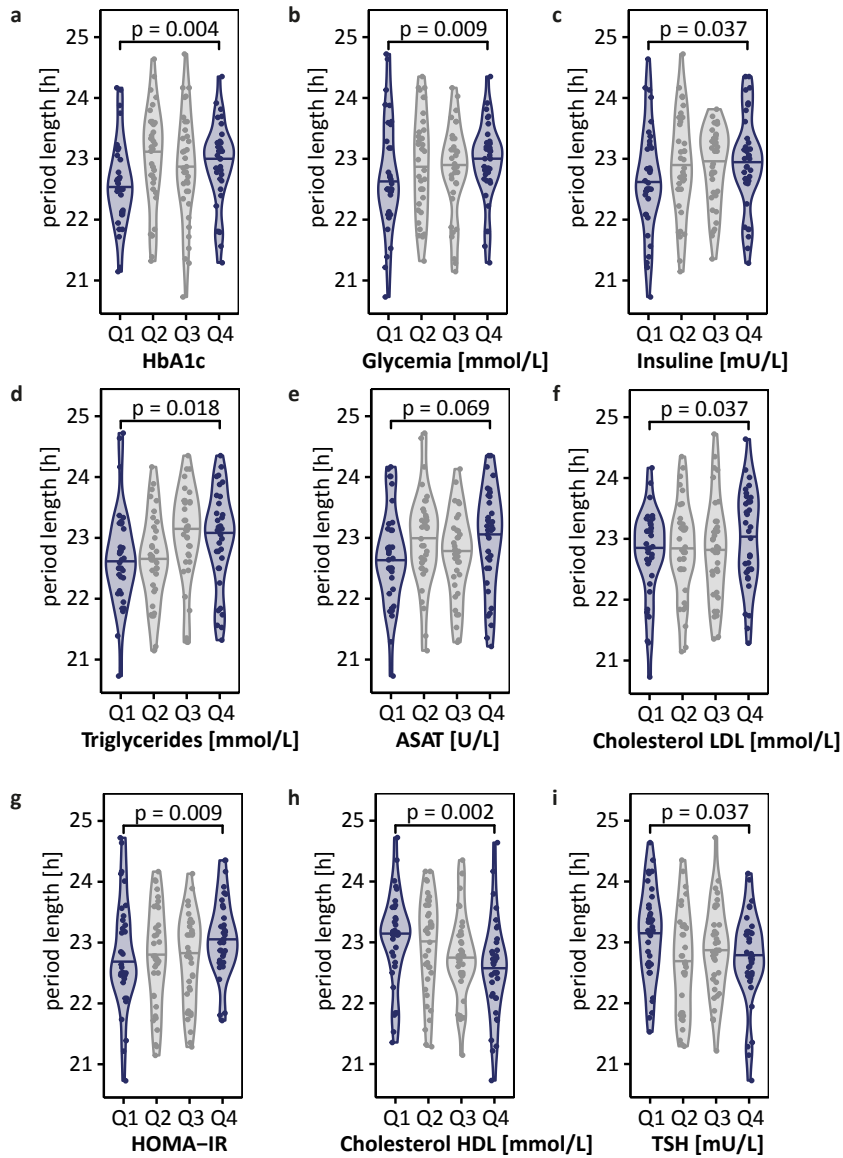


**Figure 6.3:** Association of circadian period length measured in U2OS cells cultured in human serum with clinical parameters of obese patients. Violin plots for data split in quartiles based on the clinical variables. Given p-values were obtained from two-sided Kolmogow-Smirnow test. Medians are indicated with horizontal lines. (HbA1c: glycated hemoglobin, ASAT: aspartate-aminotransferase, HOMA-IR: index for insulin resistance, TSH: thyroid stimulating hormone)

### 6.3.2. Circadian period length increases with severity of obesity

First, we tested for association between clinical parameters that are typically assessed in the diagnosis of obesity and T2D, and the circadian period length measured in U2OS cells grown in serum. For each variable, we considered only the extreme cases, comparing only the first and the fourth quartile of the data by means of a Kolmogorow-Smirnow test.

We found an increase in the circadian period length with increased severity of obesity (figure 6.3). We observed a prolonged period length for increased levels of glycosylated hemoglobin (HbA1c), fasting glucose, insulin, triglyceride levels, low-density lipoprotein (LDL) cholesterol, aspartate-aminotransferase (ASAT) and insuline resistance represented by the HOMA-IR index.<sup>324</sup> In contrast, for high-density lipoprotein (HDL) cholesterol, which is known to be decreased in obese subjects,<sup>325</sup> we detected an inverse correlation with period length. Most of these differences between the two outer quartiles were significant in both, obese subjects with and without T2D. However, they were not significant in non-obese non-diabetics. In the non-obese T2D group, we found only for few variables significant differences and the effect size was much lower as compared to the obese group. This points towards obesity being the most important aspect for the period elongation. The numeric results for all groups are summarized in table 6.4.

Interestingly, within the obese group, the circadian period lengthening did not correlate with the body mass index (BMI). This indicates that only serum from metabolically unhealthy patients with severe obesity contains factors, which can modify circadian clock properties.

### 6.3.3. Branched-chain amino acid pathway activity associated with circadian period elongation

In order to get further understanding of those metabolic factors, we compared the period length of U2OS cells grown in serum with low and high levels of the metabolites, which we measured by LC-MS. For a range of compounds, we found an association between period length and metabolite levels in serum of obese patients. Numeric data for the most significant features ( $p \leq 0.2$ ) are provided in table 6.6. We were able to identify a subset of these metabolites (table 6.5), for which the difference of the median period length between the first and fourth quartile is summarized in figure 6.4a. While some metabolites had a prolonging effect on the circadian period length others were accelerating the circadian clock. Metabolic pathway enrichment analysis suggested branched-chain amino acid (BCAA) degradation and biosynthesis as most involved metabolic pathways. We found elevated levels of three representatives (isoleucine, ketoleucine and 3-methyl-2-oxobutyric acid) of BCAA metabolism to be associated with an elongation of the period length. Violin plots are shown for these metabolites in figure 6.4b-d. Violin plots for all metabolites of figure 6.4a are provided in supplementary figure B.17 and supplementary figure B.18.

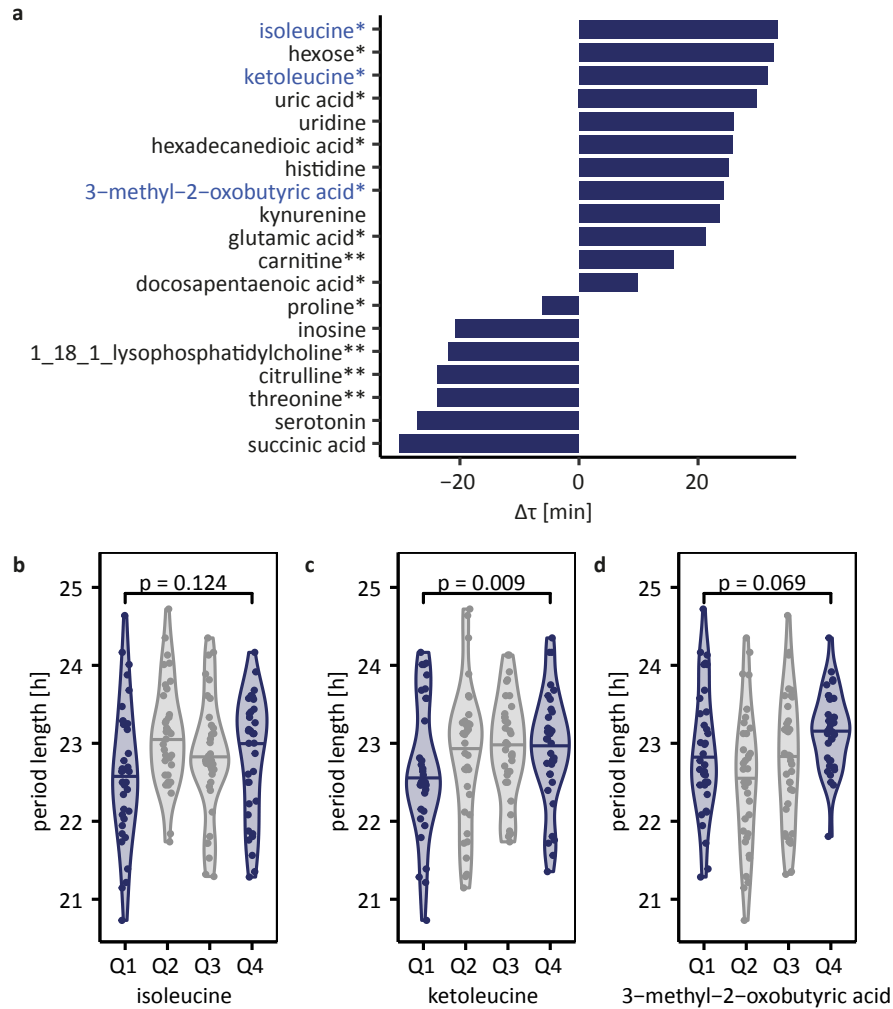


**Figure 6.4:** **a** Identified metabolites, which have an influence on the circadian period length of U2OS cells sorted by difference in period length between the median of quartile 1 (Q1) and quartile 4 (Q4). Metabolites, for which we also found significant differences ( $p_{\text{KS-test}} \leq 0.2$ ) in insulin resistance (HOMA-IR) between Q1 and Q4 are marked with asterisks (\* for positive association, \*\* for inverse association). **b,c** Violin plots for representatives of branched-chain amino acid (BCAA) metabolism. Data points are split in quartiles based on the metabolite levels and given p-values were obtained from two-sided Kolmogorov-Smirnov test. Medians are indicated with horizontal lines. Violin plots for all metabolites are provided in supplementary figures B.17 and B.17.

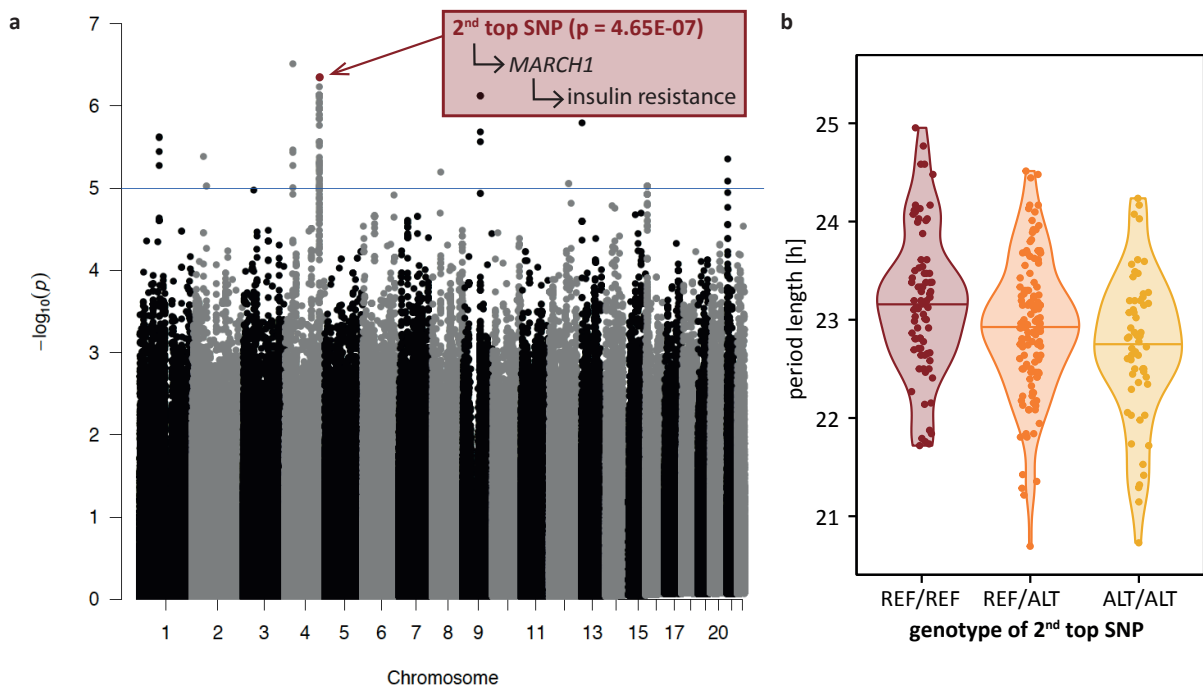


**Figure 6.5:** **a** Manhattan plot from genome-wide association analysis of circadian period length measured in U2OS cells cultured in patient's serum and patient's genotype. The second most significant single nucleotide polymorphism (SNP) is located at the *MARCH1* gene, which is involved in insulin signalling. **b** The circadian period length of U2OS cells differs for the different genotypes of this SNP found in the patient's, in whose serum *bmal1-luc* expression was measured. The reference allele is G, the alternative allele is T.

#### 6.3.4. *March1* as genetic origin of the link between serum composition and period length in obese subjects

From genome-wide association analysis we found the second most significant SNP ( $p = 4.6510^{-7}$ ) to be located on the *MARCH1* gene, which is involved in insulin resistance (figure 6.5a).<sup>326</sup> By evaluating the period length for the three different genotypes of this SNP, we observed a significantly longer period length for the REF/REF genotype compared to the two genotypes with the ALT allele (the reference allele is G, the alternative allele is T, figure 6.5b). Since the SNP is associated with insulin resistance, we also compared the HOMA-IR between the different genotypes of this SNP. For all subjects together, we did not find significant differences in insulin resistance between the different genotypes (figure 6.6a). However, in the presence of the reference allele, we found a bigger difference in insulin resistance between obese and non-obese subjects (figure 6.6b, c, while for T2D (obese and non-obese) versus non-T2D subjects, the genotype had no influence on the difference in insulin resistance (figure 6.6d, e). This supports our hypothesis of obesity being the main factor for this link to circadian clock properties and suggests insulin resistance to be involved in this connection.

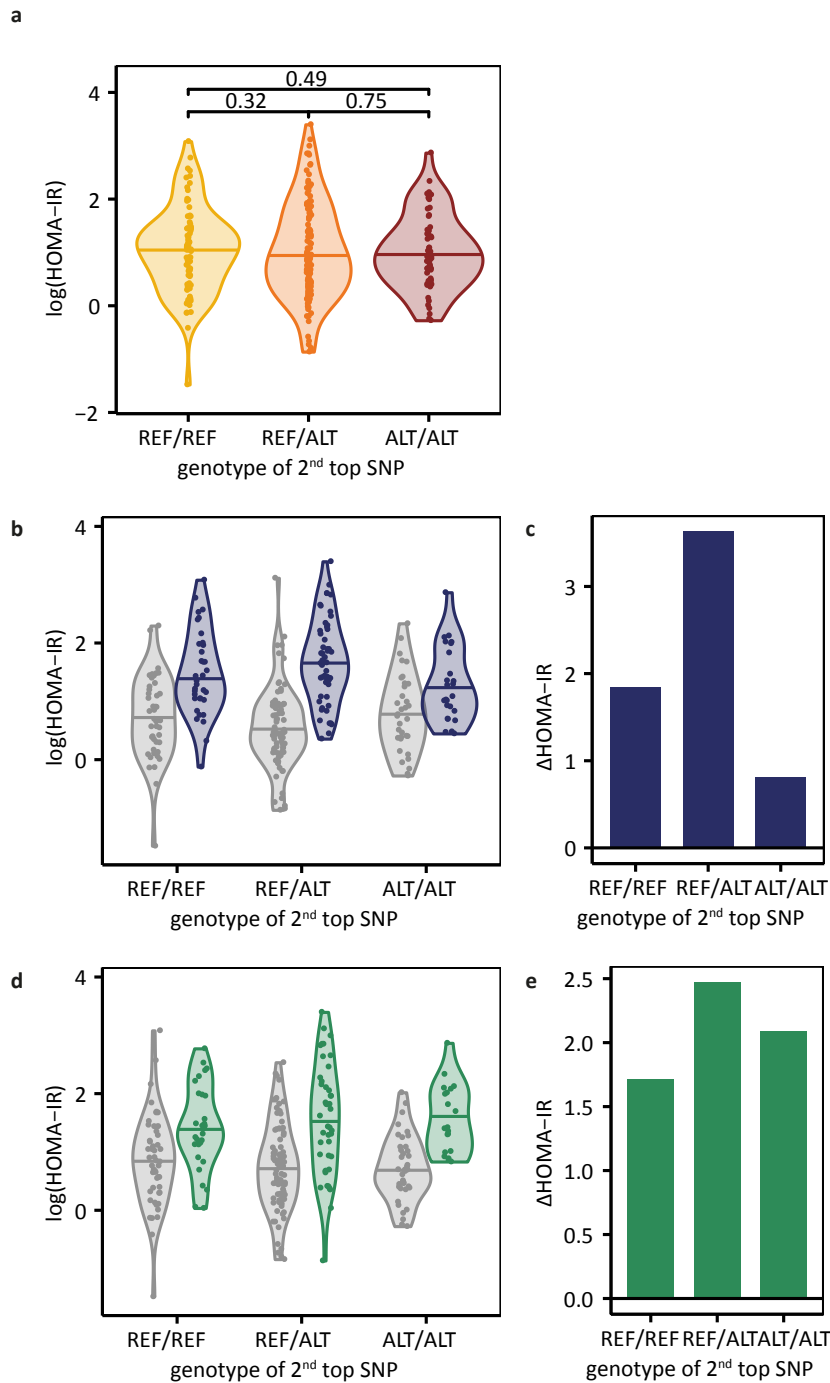


**Figure 6.6.:** **a** Violin plot showing the HOMA-IR for the different genotypes of the second most significant SNP associated with the circadian period length, medians are represented by horizontal lines. No significant differences were observed. However, when data was split by obesity (**b**), we observed a bigger difference between healthy and obese subjects in presence of the reference allele (**c**). The genotype had no influence on the difference between T2D patients and healthy individuals (**d,e**).

## 6.4. Discussion

Obesity, i.e. the weight gain as a result of a positive energy balance, can occur despite a metabolically normal state (metabolically healthy obesity), but it is often accompanied by metabolic syndrome as a comorbidity.<sup>327</sup> Indications for this metabolic disorder are abdominal obesity, high blood pressure, high blood sugar, high serum triglyceride levels and low HDL cholesterol. Moreover, metabolic syndrome is closely related to insulin resistance and prediabetes and is considered as one of the major risk factors for T2D.<sup>324</sup>

Our data from this study suggests that metabolic alterations in serum of obese patients suffering from metabolic syndrome have a lengthening effect on the circadian period length. The more the blood chemistry is altered, the more pronounced the elongation of the circadian period length in U2OS cells. Our findings are in agreement with the results Kohsaka *et al.* obtained from mice. They found longer period lengths in mice fed a high-fat diet compared to regular chow fed mice.<sup>66</sup> Notably, we did not find a correlation between period length and BMI, supporting that not only weight gain, but rather metabolic factors associated with metabolic syndrome are responsible for the circadian changes.

To the best of our knowledge, mechanisms behind this effect of metabolic processes on the circadian clock remain unexplored so far. From metabolite profiling by UPLC-MS we were able to identify a panel of metabolites, which are involved in this interaction with the circadian clock. Remarkably, for most of those metabolites, an association with insulin resistance has been reported in literature. Accordingly, we found significant differences in the HOMA-IR index between the outer quartiles of the majority of these metabolites (figure 6.4, table 6.6). A correlation between uridine levels in urine and HOMA-IR have been observed in humans before<sup>328</sup> and injection of uridine in obese mice induced deterioration of glucose tolerance.<sup>329</sup> Moreover, we found a positive correlation between uric acid and glutamic acid levels in serum and insulin resistance, corroborating results reported in literature.<sup>330,331</sup> Also, upregulation of the kynurenine pathway has been related to insulin resistance in obesity. Tryptophan can be metabolized either to kynurenines or to serotonin. It has been suggested that inflammation in obesity induces upregulation of the tryptophan-kynurenine route.<sup>332</sup> Activation of this pathway results in increased levels of xanthurenic acid, which can form complexes with insulin that are less active than insulin itself.<sup>333</sup> In line with these findings, serotonin was reported to enhance insulin secretion<sup>333</sup> and we observed an inverse relation between serotonin levels in serum and circadian period length. Similarly, for succinic acid,<sup>334</sup> citrulline,<sup>335</sup> inosine<sup>336,337</sup> and lysophosphatidylcholine<sup>337</sup> enhancing effects on insulin release have been reported. We found for increased serum levels of all of them a shortening of the circadian period length. This further indicates insulin resistance being a key factor in the alteration of circadian clock properties.

Metabolic pathway analysis indicated disturbed BCAA metabolism to be a major contributor for the period length elongation. For high serum levels of the three representatives isoleucine, keto(iso)leucine and 3-methyl-2-oxobutyric acid, we also found increased HOMA-IR values. Within the last decade, evidence for circulating BCAAs promoting insulin resistance in obesity has emerged. It has been suggested that elevated BCAA levels lead to hyperactivation of the nutrient sensing mammalian target of rapamycin complex 1 (mTORC1) followed by activation of the ribosomal kinase S6K1. This leads to phosphorylation and thereby



inhibition of insulin receptor substrate 1 (IRS-1) resulting in insulin resistance. Another mechanism, which has been proposed, is mitochondrial dysfunction triggered by increased BCAA levels, which is also associated with insulin resistance.<sup>338–341</sup> mTOR is also involved in the regulation of the circadian clock and might thus provide a link between insulin resistance and clock properties. Seghal and co-workers found circadian period lengthening upon mTORC1 activation in *Drosophila*.<sup>342</sup> Moreover, insulin is known to have a period lengthening effect in mice, possibly via mTORC1 activation.<sup>343</sup> This suggests the activation of mTORC due to elevated BCAA levels in obese subjects suffering from insulin resistance as plausible mechanism for the elongation of period length, which we observed.

Our results from the GWA analysis indicate that a genetic aspect might determine the serum composition in obese patients, which elongates circadian period length. Notably, *March1*, where the second top SNP is located, is involved in the regulation of insulin sensitivity. In insulin resistance, overexpression of the E3 ubiquitin ligase MARCH1 leads to degradation of insulin receptors on cell surfaces.<sup>326</sup> Thus, also these results support our hypothesis of insulin resistance being a main contributor to the alterations of serum chemistry of obese patients, which can alter circadian clock properties.

In this study, we gained further evidence for metabolism being able to influence circadian clocks, which has been studied much less so far than the regulation of metabolism by circadian clocks. In addition, our results showcase how the circadian clock may be used as a sensor that can be genetically exploited to make discoveries about a disease, since the clock is intimately connected to many cellular processes. Even though our sample size is rather small for studying GWA and therefore the expected statistical significance is as expected not very high, we think the strength of this study lies in the interdisciplinary approach of genetics, metabolomics and circadian assays. And the results of all experiments point towards insulin resistance as a major contributor for circadian period lengthening. Maintaining a more metabolically healthy obesity would therefore be helpful to prevent this circadian period effect. However, at this point it remains unclear if this rather small change in period length has any harmful effect or if it is rather a physiological adaptation to metabolic changes.

## 6.5. Conclusion

In conclusion, we found that metabolic factors in serum of obese patients, can prolong circadian clock *bmal1-luc* period length. Insulin resistance might play a crucial role in this interaction and might therefore be a driving force in the vicious cycle of metabolic disorders and circadian clocks: The altered blood chemistry in patients suffering from obesity with metabolic syndrome disrupts the circadian clocks, which is well-known to have negative effects on metabolic health. The identified metabolic and genetic factors could constitute promising drug targets for restoring metabolic health and circadian alignment.

**Table 6.4.:** Differences in period length between quartile 1 and 4 of various clinical parameters that are associated with obesity. The given p-values are obtained from a two-sided Kolmogorow-Smirnow test carried out between the first and fourth data quartile,  $\Delta\tau$  is the difference between the median period length of these two quartiles.

clinical parameter	obese		obese T2D		obese non T2D		T2D (obese & non obese)		non T2D non obese	
	p	$\Delta\tau$	p	$\Delta\tau$	p	$\Delta\tau$	p	$\Delta\tau$	p	$\Delta\tau$
<b>Cholesterol HDL</b> [mmol/L]	0.002	-35.1	0.162	-18.8	0.003	-40.1	0.417	-12.5	0.996	3.5
<b>HbA1c</b>	0.004	31.7	0.174	30.2	0.092	34	0.668	4.2	0.928	-1.4
<b>Glycemia</b> [mmol/L]	0.009	31.7	0.42	22.2	0.086	22.6	0.154	19	0.324	-12.8
<b>HOMA-IR</b>	0.009	30.6	0.075	28.1	0.017	25	0.076	14.9	0.928	2.8
<b>Triglycerides</b> [mmol/L]	0.018	30.6	0.187	21.9	0.094	37.5	0.147	13.5	0.518	11.1
<b>Cholesterol LDL</b> [mmol/L]	0.037	13.5	0.807	2.1	0.808	-11.1	0.61	-4.2	0.996	0.8
<b>Insuline</b> [mU/L]	0.037	30.1	0.075	28.1	0.174	22.2	0.431	8.9	0.744	6.9
<b>TSH [mU/L]</b>	0.037	-26	1	-3.3	0.007	-44.7	0.867	8	0.744	-7.6
<b>ASAT [U/L]</b>	0.069	29.2	0.174	33	0.328	16.7	0.018	22.4	0.928	2.1
<b>BMI</b>	0.878	2	0.982	6.7	0.907	-8.3	0.684	-3.6	0.049	-30.6

**Table 6.5.:** Identification of m/z features, for which significant effects on the period length of U2OS cells were observed in the obese group.

metabolite name	m/z	tR	column	polarity	adduct	ID level
serotonin	160.0756	157.32	RP	pos	[M+H-NH3] <sup>+</sup>	standard
ketoleucine	129.0562	335.29	RP	neg	[M-H] <sup>-</sup>	mummichog annotation
F1	338.3423	811.59	RP	pos		
hexose	203.0526	90.19	RP	pos	[M+Na] <sup>+</sup>	mummichog annotation
F2	310.3109	777.43	RP	pos		
F3	383.1164	90.48	RP	pos		
F4	546.72	388.31	RP	pos		
succinic acid	117.0197	134.55	RP	neg	[M-H] <sup>-</sup>	standard
F8	219.0264	88.14	RP	pos		
F9	225.0344	90.18	RP	pos		
F5	504.858	82.56	RP	pos		
F6	539.7725	374.55	RP	pos		
F7	546.2188	388.18	RP	pos		
3-methyl-2-oxobutyric acid	115.0406	224.29	RP	neg	[M-H] <sup>-</sup>	standard
F10	147.0571	286.78	RP	pos		
glutamic acid	148.0602	258.55	AMIDE	pos	[M+H] <sup>+</sup>	standard
carnitine	162.1123	90.69	RP	pos	[M+H] <sup>+</sup>	MS/MS library match
uric acid	169.0356	111.28	RP	pos	[M+H] <sup>+</sup>	mummichog annotation
citrulline	176.1028	274.55	AMIDE	pos	[M+H] <sup>+</sup>	standard
carnitine	184.0942	89.19	RP	pos	[M+Na] <sup>+</sup>	mummichog annotation
kynurenine	192.0655	214.28	RP	pos	[M-NH3+H] <sup>+</sup>	mummichog annotation
kynurenine	209.0921	214.29	RP	pos	[M+H] <sup>+</sup>	MS/MS library match
hexadecanedioic acid	285.207	679.95	RP	neg	[M-H] <sup>-</sup>	standard
F13	302.9691	248.69	AMIDE	pos		
F14	313.1549	172.21	AMIDE	pos		
docosapentaenoic acid	329.2486	761.54	RP	neg	[M-H] <sup>-</sup>	standard
F15	372.7382	237.3	AMIDE	pos		
F11	378.2409	689.16	RP	pos		
lysophosphatidylcholine (18:1)	522.3561	738.79	RP	pos	[M+H] <sup>+</sup>	MS/MS library match
F12	546.3559	730.6	RP	pos		
proline	116.0706	250.58	AMIDE	pos	[M+H] <sup>+</sup>	standard
threonine	120.0655	260.04	AMIDE	pos	[M+H] <sup>+</sup>	standard
isoleucine	132.1022	149.12	RP	pos	[M+H] <sup>+</sup>	standard
histidine	156.0767	292.88	AMIDE	pos	[M+H] <sup>+</sup>	standard
citrulline	159.0763	274.22	AMIDE	pos	[M+H-NH3] <sup>+</sup>	standard
F20	203.1502	264.73	AMIDE	pos		
F27	206.8936	87.3	RP	pos		
F16	229.1546	100.71	RP	pos		
F23	234.9814	248.63	AMIDE	pos		
F17	237.1123	585.03	RP	pos		
F18	251.0811	323.7	RP	pos		
F26	252.0777	260.13	AMIDE	pos		
uridine	267.0589	103.28	RP	pos	[M+Na] <sup>+</sup>	mummichog annotation
F19	279.0847	447.59	RP	pos		
inosine	291.0703	156.53	RP	pos	[M+Na] <sup>+</sup>	mummichog annotation
F28	370.9567	248.71	AMIDE	pos		
F29	430.6968	237.4	AMIDE	pos		
F30	440.7256	235.21	AMIDE	pos		
F21	539.2712	374.62	RP	pos		
F22	540.2739	374.61	RP	pos		
F24	604.7954	378.3	RP	pos		
F25	638.7271	464.58	RP	pos		

**Table 6.6.:** Summary of m/z features, for which significant ( $p \leq 0.2$ ) effects on the period length of U2OS cells were observed in the obese group. The given p-values are obtained from a two-sided Kolmogorow-Smirnow test between the first and the fourth data quartile,  $\Delta\tau$  is the difference between the median period length of quartile 1 and 4. For the obese group, differences in insulin resistance (HOMA-IR) of Q1 and Q4 are also provided.

Metabolite name	obese		obese T2D		obese non T2D		T2D		healthy		obese	
	p	$\Delta\tau$	p	$\Delta\tau$	p	$\Delta\tau$	p	$\Delta\tau$	p	$\Delta\tau$	$P_{\text{HOMA-IR}}$	$\Delta\text{HOMA-IR}$
serotonin	0.004	-27.1	0.65	-3.8	0.008	-30.6	0.833	2.4	0.744	-8.3	0.699	2.6
ketoleucine	0.009	31.7	0.928	20.8	0.006	38.9	0.853	-7.4	0.928	7.6	0	205.3
F1	0.009	-31.6	0.064	-31.6	0.189	-25	0.239	-16	0.1	20.8	0.504	-14.2
hexose	0.018	32.6	0.075	30.9	0.017	37.5	0.079	13.5	0.928	2.8	0	401.1
F2	0.018	-32.1	0.075	-27.4	0.32	-34	0.019	-20.8	0.187	11.8	0.699	39.9
F3	0.018	32.6	0.075	35.1	0.039	30.6	0.154	13.9	0.187	28.5	0	401.9
F4	0.018	23	0.064	17.1	0.799	20.1	0.417	8.3	0.518	5.4	0.037	102.6
succinic acid	0.037	-30.2	0.397	-13.5	0.097	-30.6	0.475	5.1	0.744	16.7	0.211	-70.1
F8	0.037	24.1	0.334	3.8	0.343	25.7	0.376	9.7	0.324	-0.7	0	423.5
F9	0.037	27.7	0.354	24.3	0.523	25.6	0.66	7.5	0.928	-7.8	0	373.8
F5	0.037	-13.3	0.894	-3.3	0.474	11.1	0.586	-7.4	0.518	-5.6	0.979	-12.3
F6	0.037	-33.8	0.14	-22.2	0.328	-38.2	0.602	-8.4	0.928	-3.8	0.878	-14.6
F7	0.037	21.3	0.375	9.4	0.189	30.6	0.41	7.4	0.744	3.8	0.037	153.2
3-methyl-2-oxobutyric acid	0.069	24.2	0.024	29.2	0.078	26.8	0.417	10.3	0.324	8.3	0.018	218.4
F10	0.069	22	0.623	-0.3	0.184	38.9	0.781	0.7	0.744	-12.5	0.878	-33.3
glutamic acid	0.069	21.3	0.596	17.1	0.199	26.4	0.833	1.4	0.996	3.8	0.001	264.2
carnitine	0.069	15.8	0.443	9	0.184	22.2	0.157	19.1	0.928	0.4	0.069	-117.8
uric acid	0.069	29.9	0.998	-2.4	0.019	47.2	0.985	-2.8	0.518	-5.6	0.069	51
citruilline	0.069	-23.8	0.397	-12.5	0.523	-26.4	0.446	-8	0.1	-5.6	0.018	-202.3
carnitine	0.069	24.5	0.397	20.3	0.328	33.3	0.908	1.4	0.996	-0.7	0.211	136.3
kynurenine	0.069	24.4	1	6.9	0.043	38.9	0.796	7.6	0.049	-12.8	0.336	36.9
kynurenine	0.069	23.6	0.988	0.3	0.045	34.7	0.954	5.6	0.324	-2.2	0.699	19.2
hexadecanedioic acid	0.069	25.8	0.029	30.9	0.503	8.2	0.02	18.9	0.324	15	0.069	58.6
F13	0.069	29.5	0.894	5.9	0.189	37.5	0.992	-0.4	0.744	2.8	0.504	4.8
F14	0.069	20.4	0.187	17.1	0.966	9	0.635	8.3	0.744	9	0.003	214.3
docosapentaenoic acid	0.069	9.9	0.151	-24.1	0.081	35.7	0.28	-9	0.928	2.1	0.124	83.4
F15	0.069	0	0.596	15.1	0.284	7.6	0.376	4.8	0.744	-10.4	0.037	-122.1
F11	0.069	-31.9	0.174	-27.4	0.543	-33	0.977	3.5	0.1	-20.8	0.211	-116.3
lysophosphatidylcholine (18:1)	0.069	-22	0.2	-27.1	0.513	-17.4	0.453	-2.8	0.187	-12.2	0.069	-95.1
F12	0.069	-20.8	0.081	-26	0.719	-13.8	0.04	-17.8	0.744	-10.4	0.124	-42
proline	0.124	-6.2	0.075	-19.1	0.384	4.2	0.61	11.5	0.928	-13.9	0.069	74.3
threonine	0.124	-23.8	0.024	-18.7	0.739	-6.5	0.61	-6.7	0.518	-12.1	0.004	-201.9
isoleucine	0.124	33.3	0.966	9	0.553	14.6	0.994	2.1	0.1	-11.8	0	246.7
histidine	0.124	25.1	0.982	-0.9	0.043	37.4	0.961	8.3	0.187	16.7	0.336	-19.8
citruilline	0.124	-21.8	0.894	-10.9	0.853	0.7	0.291	8.2	0.324	0.7	0.018	-161.7
F20	0.124	27.5	0.334	15.3	0.199	39.5	0.23	11.7	0.744	-6.9	0.069	-125.3
F27	0.124	-18.1	0.596	-8.7	0.335	22.9	0.475	-4.9	0.744	1.4	0	-283.8
F16	0.124	2.8	0.779	2.8	0.16	11.8	0.954	2.1	0.1	-25	1	-7
F23	0.124	30	0.912	5.4	0.045	37.5	0.95	-0.8	0.744	1.4	0.336	8.4
F17	0.124	19.4	0.65	-0.7	0.359	-3.8	0.61	-4.2	0.928	-2.2	0.885	25.8
F18	0.124	17.1	0.623	-11.3	0.523	25.6	0.602	-4.2	0.023	-22.2	0.124	77.4
F26	0.124	-13.8	0.742	9.4	0.017	-38.2	0.818	4.9	0.928	-0.6	0.124	127.5
uridine	0.124	26	0.623	4.9	0.043	30.8	0.125	10.8	0.518	-10.4	0.211	-107.6
F19	0.124	-22	0.623	-11.8	0.048	-39.1	0.84	-6.3	0.744	-8.3	0.004	-150.2
inosine	0.124	-20.8	0.73	-20.8	0.174	-23.6	0.41	-14.4	0.518	-10.4	0.878	-9.2
F28	0.124	29.2	0.912	5.4	0.1	37.5	0.999	-4.2	0.928	6.3	0.069	35.7
F29	0.124	13.2	0.912	-4.5	0.474	18.8	0.376	7.3	0.744	-6.9	0.211	-60.3
F30	0.124	22.6	0.73	-16.7	0.573	31.6	0.773	5.1	0.518	9	0	-260.1
F21	0.124	-31	0.14	-16.6	0.328	-38.2	0.725	0	0.928	0.7	0.504	-78
F22	0.124	-28.2	0.314	-14.4	0.543	-32.6	0.891	3.5	0.518	-6.3	0.878	34.7
F24	0.124	-12.1	0.314	-3.8	0.914	-17.9	0.125	-14.9	0.996	-2.8	0.336	-61.2
F25	0.124	21.5	0.807	-12.4	0.351	26.4	0.403	9.7	0.744	-7.6	0.211	28.5

# 7

Understanding metabolic effects of  
seasonal light schedules in arctic reindeer

The work presented in this chapter was performed in collaboration with Sara Meier<sup>1</sup>, Gabriela Wagner<sup>2</sup>, Melanie Furrer<sup>3</sup>, Reto Huber<sup>3</sup> and Steven A. Brown<sup>1</sup> (<sup>1</sup>University of Zurich, <sup>2</sup>Arctic University of Norway, <sup>3</sup>University Children's Hospital). A manuscript for publication is in preparation.

S.A.B., G.W., R.H. and S.M. designed the study. S.M., G.W. and M.F. carried out the experiments with the animals in Tromsø. S.M. performed all cell culture experiments. N.N. and S.M. performed the mass spectrometry measurements, data analysis and wrote the manuscript with input from all co-authors.

## Summary

In humans, metabolism is widely controlled by circadian clocks and disruption of the circadian clock is associated with health issues, such as type 2 diabetes, obesity, metabolic syndrome or cardiovascular diseases. In arctic species, such as reindeer, which have always been seasonally exposed to constant light conditions, circadian biology is poorly understood. So far, it has been reported that during midnight sun and polar night, arctic reindeer lose rhythmicity in their activity patterns and blood levels of melatonin. However, daily patterns in metabolic regulation remain completely unexplored.

In this study, we investigated diurnal rhythms in metabolic regulation in four Norwegian reindeer (*Rangifer tarandus tarandus*) across all four seasons. In addition we recorded actigraphy data from the animals and evaluated clock gene expression in reindeer fibroblasts in a bioluminescence assay. By metabolic profiling of blood samples, which were taken in two-hour intervals, using ultra high performance liquid chromatography coupled to mass spectrometry, we were able to extract 794 metabolic features. In a large percentage of those features, we detected 24-hour rhythms in at least one reindeer in one season. While corresponding to the arrhythmic behavior, less metabolites displayed circadian rhythms in summer, surprisingly many metabolites were rhythmic in winter. Despite a high inter-individual variability, we found metabolic pathways related to ruminal microbial nitrogen metabolism to be regulated in a circadian fashion consistently throughout the whole year.

Our findings suggest that in arctic reindeer, behavioral circadian rhythmicity can be uncoupled from metabolic circadian rhythmicity.

## 7.1. Introduction

Most aspects of physiology, amongst them metabolism<sup>58</sup> are synchronized with the external environment by circadian clocks in almost all living organisms.<sup>303</sup> In mammals, the clock machinery is organized in a hierarchical fashion. The suprachiasmatic nucleus (SCN) in the brain acts as master pacemaker. It receives external light stimuli from melanopsin-containing retinal ganglion cells in the eye and forwards this information to peripheral clocks.<sup>304,344</sup> While light is the most prominent input, also other stimuli such as feeding, exercising or resting/activity cycles can act as Zeitgeber and entrain the circadian clock.<sup>305</sup> On a molecular level, the circadian timing system is based on the rhythmical expression of the clock genes *Clock*, *Bmal1*, *Per* and *Cry*, which is regulated by a transcriptional-translational feedback loop.<sup>306</sup>

There is significant evidence that metabolism is largely controlled by circadian clocks<sup>185,236,273</sup> and circadian disruption is associated with negative consequences on metabolic health. Numerous epidemiologic studies have demonstrated an increased risk for metabolic diseases, such as diabetes or metabolic syndrome, but also cardiovascular diseases and cancer when the endogenous clock and the environment are desynchronized.<sup>71,345,346</sup> Since shift work has become essential in a modern 24/7 society and social jetlag is a common problem, strategies for the handling of this public health issue are highly demanded. However, this is not a modern phenomenon, but arctic species have always dealt with seasonal conditions of constant light (LL) during midnight sun and constant darkness (DD) during

polar night. Understanding their evolutionary optimized strategies could therefore provide breakthrough insights for human health.

To date, it remains unclear if arctic species have developed new mechanisms to control their circadian clock, if they are able to disconnect their clock from the rest of their physiology, or if they are even lacking a circadian clock.<sup>347</sup> Several aspects of circadian rhythms have been investigated in reindeer in the last decade and the results suggest that the animals have developed remarkable evolutionary strategies. Van Oort *et al.* studied seasonal changes in activity patterns of the Norwegian reindeer (*Rangifer tarandus tarandus*) and the Svalbard reindeer (*Rangifer tarandus platyrhynchus*).<sup>348,349</sup> They found that both species lost their circadian activity during midnight sun, while during polar night only the Svalbard reindeer lost rhythmic activity. The authors explained these findings with the higher latitude of the habitat of Svalbard reindeer (78°N) compared to 70°N for the Norwegian, where still some twilight exists during polar night. Furthermore, they observed for ruminants typical ultradian rhythms, which were most visible during summer and winter. In addition, the loss of circadian oscillations of blood melatonin levels in reindeer during midnight sun and polar light has been observed, while in other mammals, melatonin oscillations continued under constant conditions.<sup>350,351</sup> Moreover, Lu *et al.* found no or only limited circadian oscillations in the expression of the clock gene *Bmal1* in reindeer fibroblasts.<sup>352</sup> Therefore, they hypothesized that reindeer have lost their circadian clock in adaptation to their arctic habitat. From a recent genomics study there is evidence for reindeer-specific mutations of genes involved in circadian clock function. For example, a mutation of *Per2* was observed, which prevents binding to CRY1 proteins.<sup>353</sup>

In contrast to the findings described above, which point towards no or little endogenous circadian control in reindeer, in a recent study, circadian rhythms in rumen temperature were found throughout the year in Svalbard reindeer indicating a persisting circadian metabolism.<sup>354</sup> In this study, we investigated diel metabolic regulation in Norwegian reindeer across all four seasons with an untargeted metabolomics approach in combination with the assessment of behavior and clock gene expression.

## 7.2. Methods

### 7.2.1. Animals

Samples for this study were collected from four adult reindeer born in 2017 (3 females, 1 castrated male, paternal half-siblings) in the Department of Arctic and Marine Biology (AAB) at the University of Tromsø (UiT) 69° N, 18° E. There, the animals were kept for research purposes under the regulation of the Norwegian Food Safety Authority *Mattilsynet* in the animal facility of the AAB. They roamed in big outside enclosures throughout the year and were fed *ad libitum* with reindeer food pellets (Felleskjøpet #13541).

For each experiment, the animals were captured and brought into an indoor stable. There, each animal was tethered by its halter into a separate stall with enough space to lie down, access food pellets (*ad libitum*) and water (figure 7.1). In the stable, natural light came in through a big window at one side of the room. Programmable ceiling lamps provided additional light following the outside natural light-dark schedule. In winter, all windows were



covered to avoid artificial light exposure.

The animals had been habituated to the stable and human handling for earlier experiments. Further habitation was performed by daily human presence in the stable, physical contact to humans, outdoor walks and reindeer lichens (*Cladonia rangiferina*) and salix twigs (*Salix sp*) as food reward.



**Figure 7.1.:** The four reindeer tethered in the stable before the experiment in March. The left picture shows the 3 female reindeer #3, #2 and #1 (left to right). The right picture shows the castrated male #4. The silver package attached to their antlers are the Actiwatches wrapped in duct tape. Each animal has access to an automatically refilling drinking trough and a food trough providing food pellets ad libitum.

### 7.2.2. Actigraphy

Each animal was equipped with a Motionwatch 8 Actiwatch (CamNtech #132764), which measures activity counts at a 1 min interval. In spring the Actiwatches were attached to the antlers of the animals and to their halters in all other seasons. They were attached from March 12 to April 21 in spring, from June 19 to July 21 in summer, from September 5 to October 29 in autumn and from December 9 to January 16 in winter.

The data was normalized by dividing the counts for each interval by the 99. percentile of all the counts per minute collected across the year. All values above 1 were considered as outliers and set to 0. The lower threshold was set to 0.1 setting all values below to 0 as well. In figure 7.4, 30-day intervals including the days of the blood sampling were chosen. The actograms were plotted, and periodicity analysis was performed using the ActogramJ<sup>355</sup> plug-in in ImageJ (version 1.53a, Wayne Rasband, USA).

### 7.2.3. Catheterization and skin biopsy under anesthesia

For serial blood collection, the four animals received a polyurethane catheter into the jugular vein (EQUIVET HiFlow long-term IV catheter, KRUISE # 122005) on the left side of their neck. Catheterization was performed by a certified veterinary under full anesthesia using Rompun vet (20mg/mL, Bayer vital GmbH, vNr 023446). A 3-way-stopcock with 10 cm tubing was attached to the catheter and the catheterized area was covered with a gauze patch and fixed by a bandage.

After catheterization, a small skin patch (approximately 4x 4 cm) behind the reindeer's ear was clipped disinfected with 70% Ethanol and one biopsy per animal was taken with a biopsy punch needle ( $\varnothing = 2\text{mm}$ , Stiefel #600208). Each biopsy was immediately transferred into 1.5 mL of cold advanced Dulbecco's Modified Eagle Medium (advanced DMEM, Gibco #12491) containing 50% fetal calf serum (FCS, Bioswisstec #S60500), 1% GlutaMAX (200mM, Gibco #3505061), 0.1% Gentamycin (50 mg/mL, Sigma-Aldrich #G1397) and 0.1% Amphotericin B (250  $\mu\text{g}/\text{mL}$ , Sigma-Aldrich #A2942) and stored at 4°C. After biopsy taking, the wound was disinfected with iodine.

The animals were injected with the anti-anesthetic Antisedan (5mg/mL, Zoetis, vNr 471953) into the thigh, given time to wake up until they could stand stably and brought back into the stable for recovery. It was made sure all animals were standing and awake after the catheterization.

### 7.2.4. Primary fibroblast culture from skin biopsy

All procedures described in this section were performed in a biosafety 2 (BSL-2) cell culture laboratory.

Each skin biopsy was digested for 4 h in 1.8 mL of warm advanced DMEM containing 10% FCS, 1% GlutaMAX and 0.1% Gentamycin (below referred to as culture medium) and supplemented with 0.2 mL the digestion enzyme Liberase TM (1.125 mg/mL, Roche #05401119001). The content of each well was pipetted 9 mL of Dulbecco's Phosphate Buffered Saline (PBS) (Sigma-Aldrich # D8537) and then centrifuged for 5 minutes at 1200 rpm. The PBS was aspirated and each biopsy was resuspended in 1 mL of warm culture medium containing 0.1% of Amphotericin B and placed into a fresh well of a 6-well plate.

For each biopsy, one Millicell culture insert (Millipore #PICMORG50) was prepared by cutting off its plastic legs and placed on each biopsy. The inside of the insert was filled with 1.5 mL and the surrounding with 1 mL of warm culture medium (+ 0.1% Amphotericin B). This setup facilitates fibroblast growth due to the biopsies being pressed against the cell culture. The culture was then stored in a cell culture incubator at 37°C, 5% CO<sub>2</sub>. After 24 h the first fibroblasts started growing out of the biopsy.

The culture medium of the biopsies was changed every 3 - 4 days. In the first week, the culture medium was supplemented with 0.1% Amphotericin B to prevent mold infection of the cultures. The Millicell culture insert was removed after 1 week. When the fibroblasts reached  $\geq 50\%$  confluency in the original culture, they were replated into one fresh well of a 6-well plate (passaging). Once they had reached 80% confluency, the fibroblasts were split in a 1:2 ratio for all further passages as follows:

The culture medium was aspirated and the cells were washed with 2 mL of PBSToTo to detach them from the plate, the cells were incubated in 200  $\mu$ L of 0.05% Trypsin (Trypsin-EDTA, Life Technologies #15400054) enzyme for 5 min in the cell culture incubator. After 5 min, the Trypsin had detached most fibroblasts and culture medium was added to stop the enzyme activity. By pipetting the medium up and releasing it over the plate surface 5 - 8 times thoroughly, all cells were resuspended in the medium. The cell suspension was then distributed to the fresh well(s) of a 6-well plate. By moving the plates gently back and forth and left to right 4 times each, the cells were distributed evenly across the dish surface.

After 1 to 2 months in culture, the fibroblasts were frozen at passage 3 to 5. Therefore, the fibroblasts were trypsinized as for passaging, resuspended in freezing medium (culture medium containing 10% Dimethyl sulfoxide (DMSO, Sigma-Aldrich #D8418), transferred to a cryotube for freezing cultured cells and frozen at  $-80^{\circ}$ . The next day they were transferred to a liquid nitrogen tank. For circadian measurements the cells were brought to Zurich on dry ice.

### 7.2.5. Bioluminometry of *Bmal1* expression in reindeer skin fibroblasts

All procedures described in this section were performed in a BSL-2 cell culture laboratory.

#### 7.2.5.1. Virus production and titration

The *Bmal1:Luciferase* plasmid was packaged into lentiviral particles using the well-established protocol of calcium phosphate transfection for second generation transfer plasmids<sup>356</sup> with one small modification: Step 15, adding of 20% sucrose before concentrating the virus by ultracentrifugation, was omitted.

The produced *Bmal1:Luciferase* lentivirus was titrated on human cells of the S2 osteosarcoma cell line (U2OS) and *Bmal1* expression was measured by bioluminometry as described for reindeer skin fibroblasts in the following sections. Therefore, four wells of a black 24-well measurement plate (BERTHOLD TECHNOLOGIES #41082) of U2OS were infected with 5, 7, 10 and 15  $\mu$ L of *Bmal1:Luciferase* lentivirus.

#### 7.2.5.2. Infection of skin fibroblasts with *Bmal1:Luciferase* lentivirus

Reindeer fibroblasts were thawed in a  $37^{\circ}$  C warm water bath and the thawed cell suspension was transferred to warm culture medium. The mixture was centrifuged for 5 minutes at 1'200 rpm. The supernatant was removed and the cells were resuspended in 1 mL warm culture medium and evenly distributed to fresh wells of preferred size containing warm culture medium. The next day the medium was changed to fresh warm culture medium. As before, the culture medium was changed every 3 to 4 days and cell confluency assessed twice a week. Once the fibroblasts reached  $\geq 50\%$  confluency, the culture medium was changed to 1 mL of culture medium supplemented with 0.1% 8 mM protamine sulfate (8mg/mL, Sigma-Aldrich #P438) and the fibroblasts were infected with 15  $\mu$ L *Bmal1:Luciferase* lentivirus (20 times concentrated by Ultracentrifugation, see Salmon *et al.*<sup>356</sup> . After 6 h of incubation, the culture medium was refreshed.

Three days after the infection by *Bmal1:Luciferase* lentivirus, the fibroblasts in the 12-well plate were split 1:1 to 2 wells of a 24-well measurement plate. Since, low survival of fibroblasts was noticed after splitting, the above-mentioned splitting protocol was slightly adapted: Instead of using 200  $\mu$ L of 0.05% Trypsin, only two drops of 0.5% Trypsin were used. Using such a small volume ensured more efficient subsequent blocking of Trypsin activity and improved fibroblast survival.

### 7.2.5.3. Synchronization and bioluminometry of *Bmal1* expression

For synchronization and measurement, clear DMEM (DMEM 1x, no phenol red, Gibco #31053028) supplemented with 10% FCS, 1% GlutaMAX and 0.1% Gentamycin was used (referred to as clear medium in the following section). The following procedures were additionally performed on a 24-well measurement plate of U2OS cells as technical control.

To synchronize clock gene expression of the fibroblasts the culture medium was changed to 0.5 mL/well of clear medium containing 0.01% of the corticosteroid Dexamethasone (10mM, Sigma-Aldrich #D4902) were added. The exposure was stopped by aspirating the medium. Any residual dexamethasone was removed by washing twice with 1 mL of PBS. Then, 1mL of clear medium supplemented with 0.5% 20 mM Luciferin (20mM, Regis Technologies #360202) was added to each well and the plates were sealed with parafilm. Bioluminescence was recorded for one week in a custom-made lumicycler device measuring bioluminescence signals for 1 min/well returning to the same well every 48 min (LumiCycle, Actimetrics, USA).

The raw bioluminometry data was plotted in Rstudio (R version 3.6.1, The R Foundation for Statistical Computing). Time-series analysis was performed using the Lumicycler Analysis program (Actimetrics), where period and amplitude were predicted by fitting a cosine function to the raw data.

## 7.2.6. Blood metabolomics

### 7.2.6.1. Blood sampling

Blood samples were collected for 24 h in 2-hour intervals. The exact time schedules are provided in figure 7.2. With a 2.5 mL syringe, 2 - 2.5 mL of blood were withdrawn from the 3-way stopcock from each reindeer at each timepoint. The blood was immediately transferred into a heparinized vacutainer (VACUETTE® RÖHRCHEN 4 mL Natrium Heparin, Greiner Bio-One #454030), tilted back and forth 4 times and put on ice. Then 5 mL of Ringer solution (Sodium chloride 9mg/mL, Baxter #2B0043) were injected through the 3-way stopcock into the tubing to fill its dead volume. After that 1 - 2 mL of Ringer solution supplemented with 2% Heparin solution (Heparin Leo 5000 IE/mL, Leo Pharma, Vnr 064927) were injected into the tubing as clotting prevention. Before the next sample was taken, the previously injected solution was aspirated from the tubing and discarded. Subsequently, the blood was centrifuged at 10 rpm for 15 min and the plasma (supernatant) was stored in 200  $\mu$ L aliquots at 20°C. Later, the samples were brought to Zurich and stored at -80° until metabolomic analysis.

After the last blood collection, the catheters were removed, the wound disinfected with Iodine and the animals were released into a small outside enclosure, where the wound was

observed for one week. Afterwards, they were released into their usual outside enclosure.

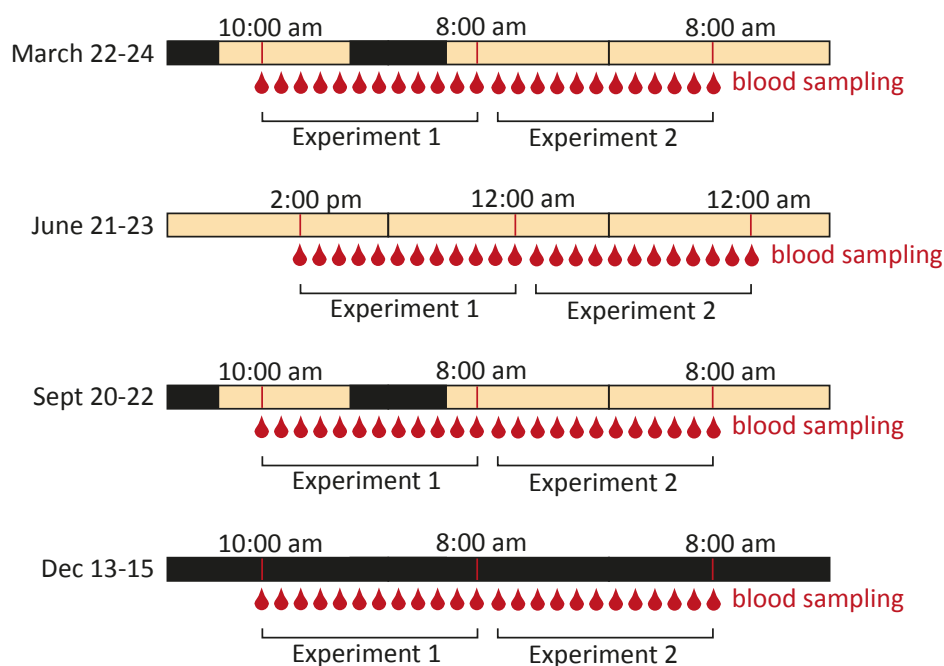


**Figure 7.2.:** Schematic of the experimental design of the blood sampling in the four seasons. Yellow bars indicate the lights were on, black bars indicate the lights were off. Blood samples were taken in two-hour intervals. The first sample was taken at 10:00 am, except for June, when it was taken at 2:00 pm.

### 7.2.6.2. Randomization and quality control samples

Samples were prepared and measured in randomized order and split into batches of approximately 60 samples. In addition, quality control samples (QC) were made by pooling all samples from spring and summer. The pooled sample was aliquoted to 200  $\mu\text{L}$  again. Further sample preparation was done as described below. QC samples were mixed and re-aliquoted prior to measurements to assess only analytical reproducibility. They were prepared as described below, measured across all batches and used later on for batch correction.

### 7.2.6.3. Plasma sample preparation

200  $\mu\text{L}$  aliquots of reindeer plasma samples were thawed on ice and 200  $\mu\text{L}$  of 1 mg/mL  $^{15}\text{N}_2$ -Tryptophan (Cambridge Isotope Laboratories, Inc. #PR-23263) in water (LC-MS grade water, Fisher Scientific #W6500) as Internal Standard (IS) and 600  $\mu\text{L}$  of MeOH were added. After vortexing (2 min), the samples were incubated on ice for 10 min. Then, they were centrifuged at 15'000 g for 15 min at 4°C to precipitate the proteins and all residual solid components. The metabolite extract (supernatant) was removed and filtered with a 0.2  $\mu\text{m}$  reversed cellulose membrane filter. Then, 200  $\mu\text{L}$  of the samples were transferred into a HPLC glass vials with glass insert (BGB #080401 and #110500) for MS measurement on the AMIDE column (see next section). To evaporate the solvent 400  $\mu\text{L}$  of the samples were put into a vacuum dryer and the residuals were resuspended in 75  $\mu\text{L}$  water with 5% MeOH. To fully resuspend all solid

particles, the samples were sonicated for 10 minutes and were centrifuged for 15 min at room temperature. The supernatant was transferred into a HPLC glass vial with glass insert for measurement on the C18 column (see next section).

#### 7.2.6.4. UPLC-MS measurements

Chromatographic separation was performed on an ACQUITY UPLC system as described in Chapter 6.

Mass spectra were recorded on an Orbitrap mass spectrometer (Orbitrap QExactive Plus, Thermo Fisher Scientific) with a heated electrospray ionization source.

Full scan spectra in the  $m/z$  range of  $m/z = 50 - 750$  were recorded in positive and negative ion mode at a resolving power of 140,000 full width half maximum (fwhm). The automatic gain control (AGC) target was set to  $2 \cdot 10^5$  charges and a maximal injection time (IT) of 200 ms was used. The ion source parameters were optimized for the measurements with the different UPLC columns separately. For the C18 measurements, sheath gas flow rate was set to 50 units, aux gas flow rate to 5 units and sweep gas flow rate to 0. A capillary temperature of 360 °C was used, the aux gas heater temperature was set to 300 °C and a S-lens RF level of 60 was applied. For the AMIDE measurements, sheath gas flow rate was set to 60 units, aux gas flow rate to 10 units and sweep gas flow rate to 0. A capillary temperature of 380 °C was used, the aux gas heater temperature was set to 350°C in positive mode and 360 °C in negative mode and a S-lens RF level of 60 was applied. In both methods a spray voltage of 3.7 kV was used in positive mode and -3.3 kV in negative mode.

At the beginning, the middle and the end of each batch, a mix of standards was injected for a quick performance check. Mass calibration was performed prior to each batch to ensure a mass accuracy of better than 5 ppm.

In addition, data dependent acquisition (DDA) was carried out with the QC samples and used later for MS/MS matching. The DDA methods consist of one full scan MS (resolution: 140,000 fwhm, AGC target:  $2 \cdot 10^5$  charges, maximum IT: 100 ms, mass range:  $m/z = 50 - 750$ ) followed by three data dependent MS/MS scans (resolution: 70,000 fwhm, AGC target:  $2 \cdot 10^5$  charges, maximum IT: 50 ms, isolation window: 0.4  $m/z$ , stepped collision energy: 10/20/30 eV) with a minimum AGC target of  $8 \cdot 10^3$  for scan initiation and 10 s of dynamic exclusion.

#### 7.2.7. Data analysis

All data analysis was carried out in R (v3.6 and v4.0). Data preprocessing was done as described in Chapter 6. The applied parameter settings for the XCMS preprocessing are provided in table 7.1. In total, we obtained 794  $m/z$  features. Peak areas were  $\log_2$ -transformed and z-scored across all seasons within each reindeer separately.

Rhythmicity analysis was performed with the R package *LimoRhyde*<sup>357</sup> for each animal in each season separately. Subsequently, phase and amplitude were predicted with *ZeitZeiger*.<sup>358</sup>

**Table 7.1.:** Parameter settings for preprocessing of LC-MS data using XCMS in R.

	parameter	RP pos	RP neg	AMIDE pos	AMIDE neg
<b>peak detection (centWave)</b>	ppm	5	5	5	5
	peakwidth	c(5,12)	c(5,12)	c(5,12)	c(5,12)
	mzdiff	-0.001	-0.001	-0.001	-0.001
	snthresh	10	10	10	10
	integrate	1	1	1	1
	noise	900000	900000	900000	900000
	prefilter	c(4,200000)	c(4,200000)	c(4,200000)	c(4,200000)
	fitgauss	FALSE	FALSE	FALSE	FALSE
<b>alignment (peakGroups)</b>	minFraction	0.5	0.5	0.5	0.5
	binSize	0.01	0.01	0.01	0.01
	minSamples	1	1	1	1
	bw	5	5	5	5
	span	0.6	0.6	0.6	0.6
<b>annotation</b>	perfwHM	0.6	0.6	0.6	0.6
	mzabs	0.001	0.001	0.001	0.001
	cor_eic_th	0.75	0.75	0.75	0.75

### 7.2.8. Metabolic pathway enrichment analysis and compound annotation

We applied two different tools for automated compound annotation in order to annotate the peaks from our untargeted metabolic approach. We used MSDial<sup>256</sup> for MS/MS library matching with the spectra we obtained from data dependent MS/MS acquisition. Moreover, we applied the mummichog algorithm<sup>254</sup> in MetaboAnalyst for R,<sup>215</sup> which infers metabolic pathway information and biological activity. We employed the *bos taurus* Kegg database, set the mass tolerance to 5 ppm and the p-value threshold to 0.05. Only pathways with at least two significant hits were considered further.

## 7.3. Results

### 7.3.1. Study design

We performed experiments on four Norwegian reindeer (*Rangifer tarandus tarandus*) during summer and winter solstice and during spring and autumn equinox (figure 7.3). For each experiment, the reindeer were brought into a stable, where they were fed *ad libitum* (figure 7.1). Under anesthesia, skin biopsies were taken for fibroblast cultivation and subsequent assessment of *Bmal1* expression and the animals were catheterized. The light in the stable was programmed according to the natural light schedule in each season. Then, blood samples were taken in two-hour intervals for 48 hours (figure 7.2). Here, we only report the results from the first 24 hours. During the second day, the light schedule was modified for a different experiment. After the blood sampling, the reindeer were released. In addition to the

metabolomics experiment, we recorded their activity with Actiwatches for a longer period.

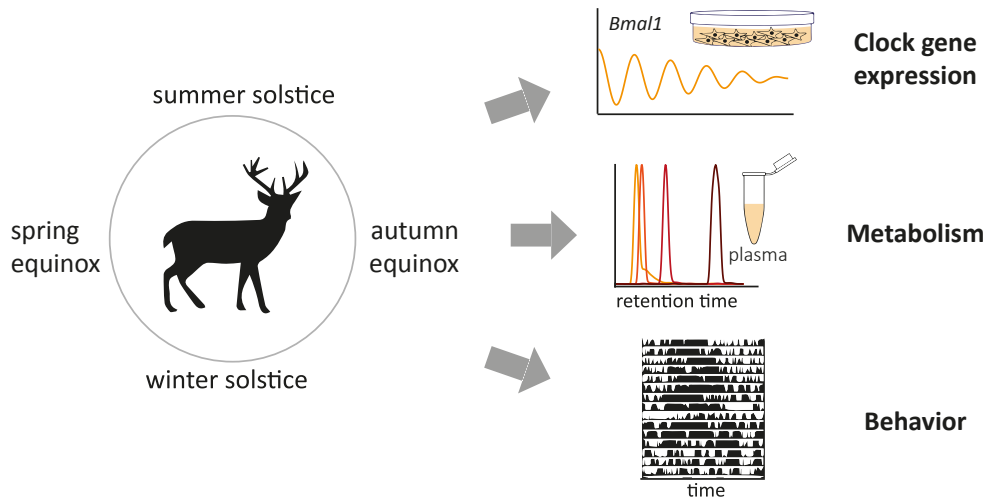


**Figure 7.3.: Study design.** We assessed daily rhythms in four Norwegian reindeer across all four seasons. We measured clock gene expression in a bioluminescence assay, metabolic profiles by LC-MS analysis of plasma samples and we recorded activity patterns by actigraphy.

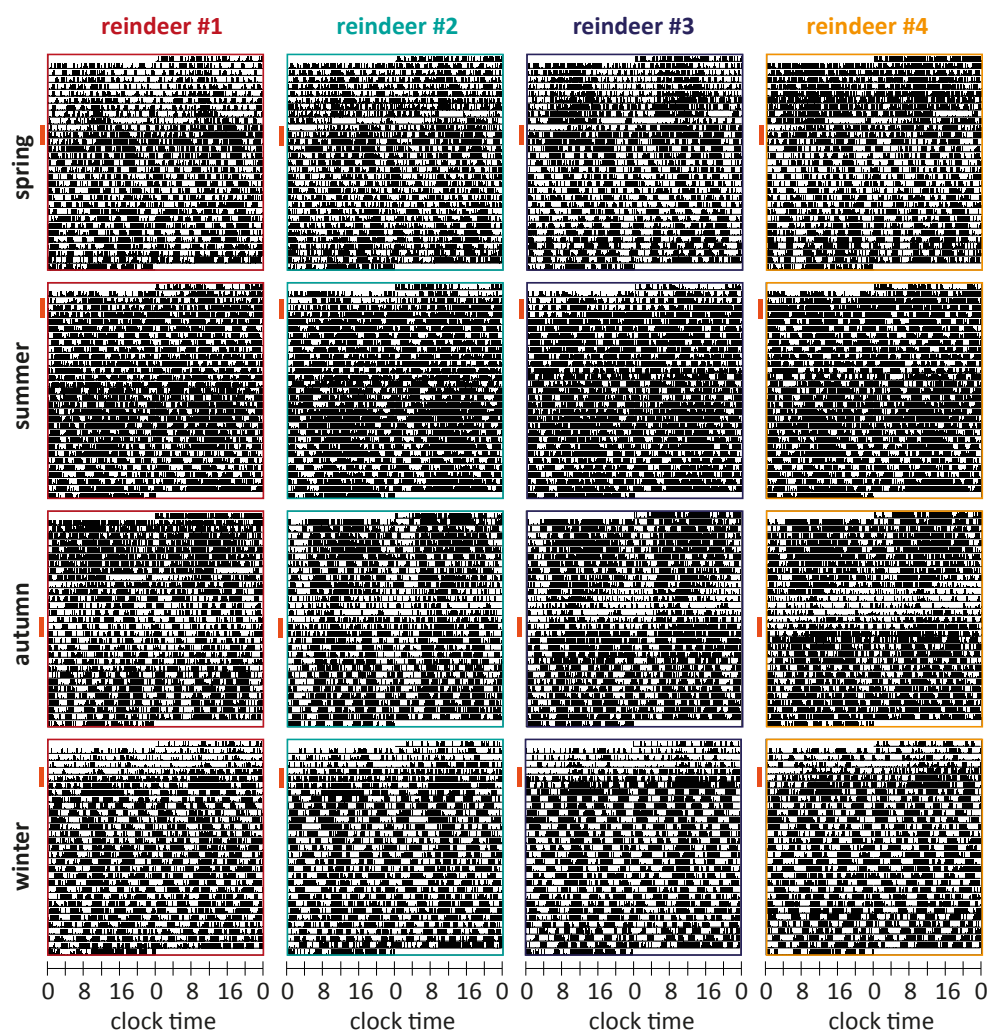
### 7.3.2. Circadian behavior in spring, autumn and winter

The activity of the animals across the four seasons is shown in the actograms in figure 7.4. We selected time intervals of 30 days including the time of the experiments as well as one or two days before and several days after. Visual inspection of the actograms already suggests a much higher activity of the reindeer during summer compared to the other seasons. This observation was confirmed by calculation of the 24-h-average activity, shown in figure 7.5. We further performed Fourier transformation to compute periodograms (figure 7.6). In spring and autumn, when the reindeer experienced alternating light-dark (LD) periods, we detected circadian rhythms in their activity patterns with period lengths of roughly 24 hours (ranging from 24.05 to 24.23 h). In summer, these circadian patterns disappeared completely, instead, ultradian rhythms with period lengths below 12 hours became much more pronounced. These ultradian rhythms were also detected in the other seasons, but were less dominant. In winter, the animals did not show any circadian behavior. Note that the animals were kept in complete darkness in winter already for a week prior to the experiment. However, when they were released after the experiment, they experienced civil twilight alternating with complete darkness.

### 7.3.3. Metabolism under circadian control in spring, autumn and winter with high inter-individual variability

From UPLC-MS analysis of the blood plasma samples, we extracted 794  $m/z$  features after removing noisy peaks, peaks not detected in all samples and duplicates. In order to get a first overview of our data, we performed principal component analysis. The results shown in

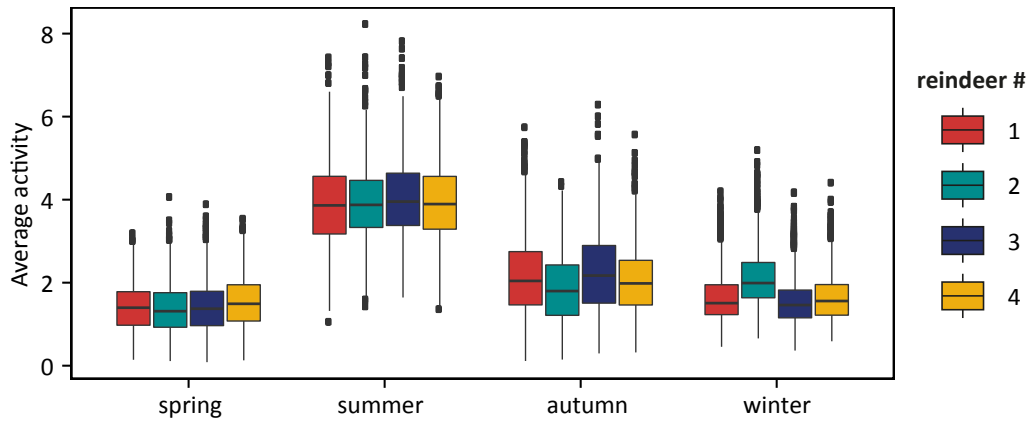




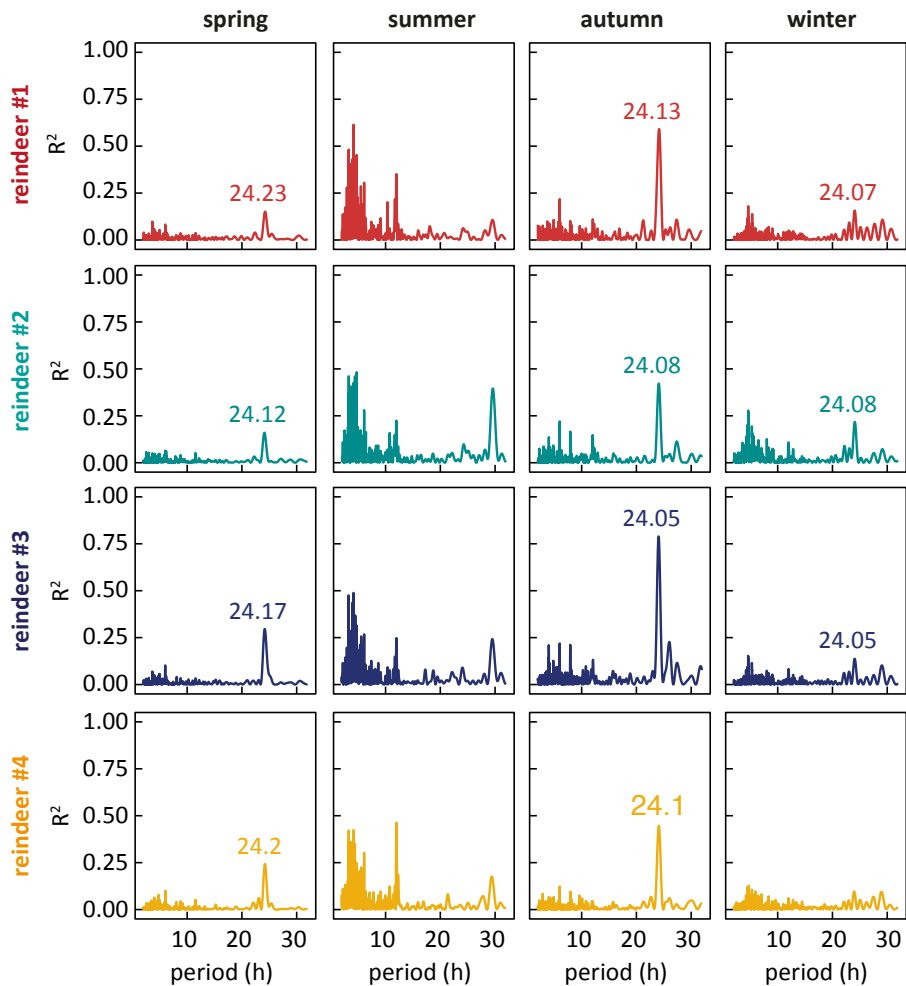
**Figure 7.4.:** Double-plotted actograms (smoothed with Kernel = 25) of the individual reindeer for 30 days in each season. The days when blood sampling was performed are marked with orange bars.

figure 7.7 suggest that the first two principal components represent differences in metabolic profiles between the four seasons (figure 7.7a) rather than between the individual animals (figure 7.7b).

Since we observed a relatively high variability in the time profiles of various metabolites between the four animals, we performed rhythmicity analysis for each animal and each season separately. The resulting p-value distributions for 24-hour rhythms are provided in figure 7.8 and all numeric results are given in the supplementary table B.12. Being aware of the high probability for false positives, we decided to use raw p-values instead of q-values to keep as many metabolites as possible for pathway enrichment analysis. In reindeer #4, the only male, we found by far the highest overall number of rhythmic m/z features. Surprisingly, we found the highest number of circadian features in winter, while as expected in summer, the fewest features displayed circadian rhythms. The numbers of rhythmic features in spring and autumn are comparable. Similar to the male reindeer, for the female reindeer we found mainly arrhythmic metabolic features in summer and a significant number of rhythmic fea-



**Figure 7.5.:** Boxplots representing the average activity per period of 24 h obtained from the activity patterns shown in figure 7.4 (center line: median, box limits: 25th and 75th percent quantile, whisker length: 1.5 interquartile range).



**Figure 7.6.:** Periodograms obtained by Fourier transformation of the activity patterns shown in figure 7.4.

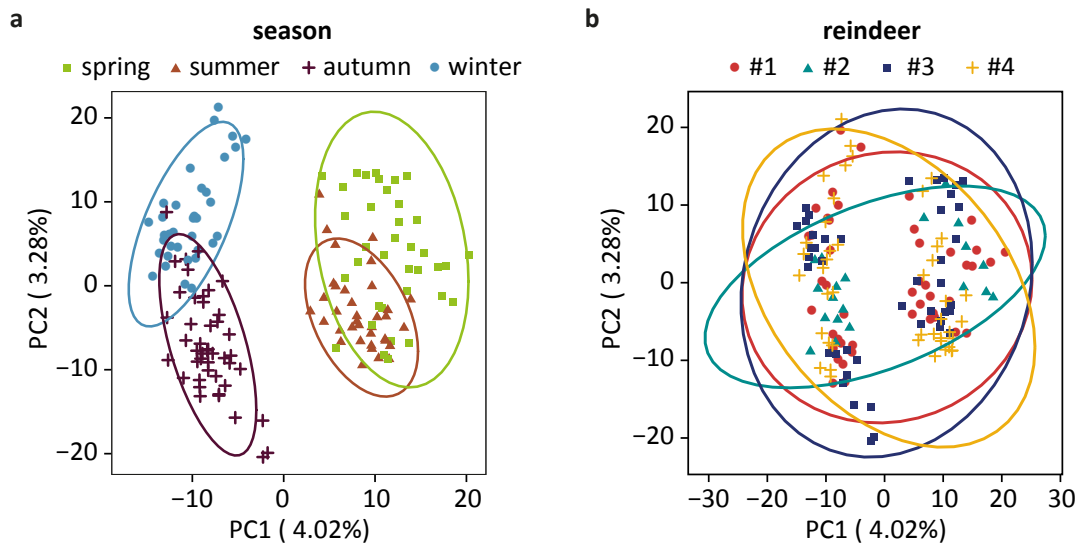


**Figure 7.7.:** Results from principal component analysis of all metabolic features. Data points are colored by season (a) and individuals (b).

tures during winter. Whereas #1 and #3 show also many rhythmic features in spring, they had surprisingly few circadian features in autumn. In reindeer #2, in contrast, we detected far less rhythmic features during spring, probably resulting from catheter problems.

To further investigate differences in rhythmicity of the metabolome between the individuals and across the different seasons, we evaluated the overlap between rhythmic features and displayed them in Venn diagrams (figure 7.9). For a large fraction of all 794 detected  $m/z$  features, we found circadian rhythms in at least one animal in at least one season. In spring, 54% of all detected features were rhythmic in at least one animal, in summer 31%, in autumn 45% and in winter 60% respectively. 119 features (15%) were rhythmic in all seasons in at least one animal. The comparison between the individual animals shows that inter-individual differences in rhythmicity are most pronounced in autumn, but they exist across the whole year.

We visualized the time course of all metabolic features, for which we detected circadian rhythms in at least one animal in at least one season, in a heat map (figure 7.10). We grouped them by their rhythmicity detected in reindeer #4, which showed the highest number of rhythmic features and sorted them by circadian phase within the groups. In most groups, a cluster of features peaking at night and one peaking during the day can be detected. In the group of features, which are rhythmic in spring, autumn and winter, a phase shift seems to happen across the year. Moreover, for some of these features, there are indications for ultradian rhythms in summer.

### 7.3.4. Phase and amplitude distribution of circadian metabolic features

Moreover, we predicted amplitude and phase for the circadian metabolic features (numeric results are provided in the supplementary table B.12). The predicted phases are visualized in

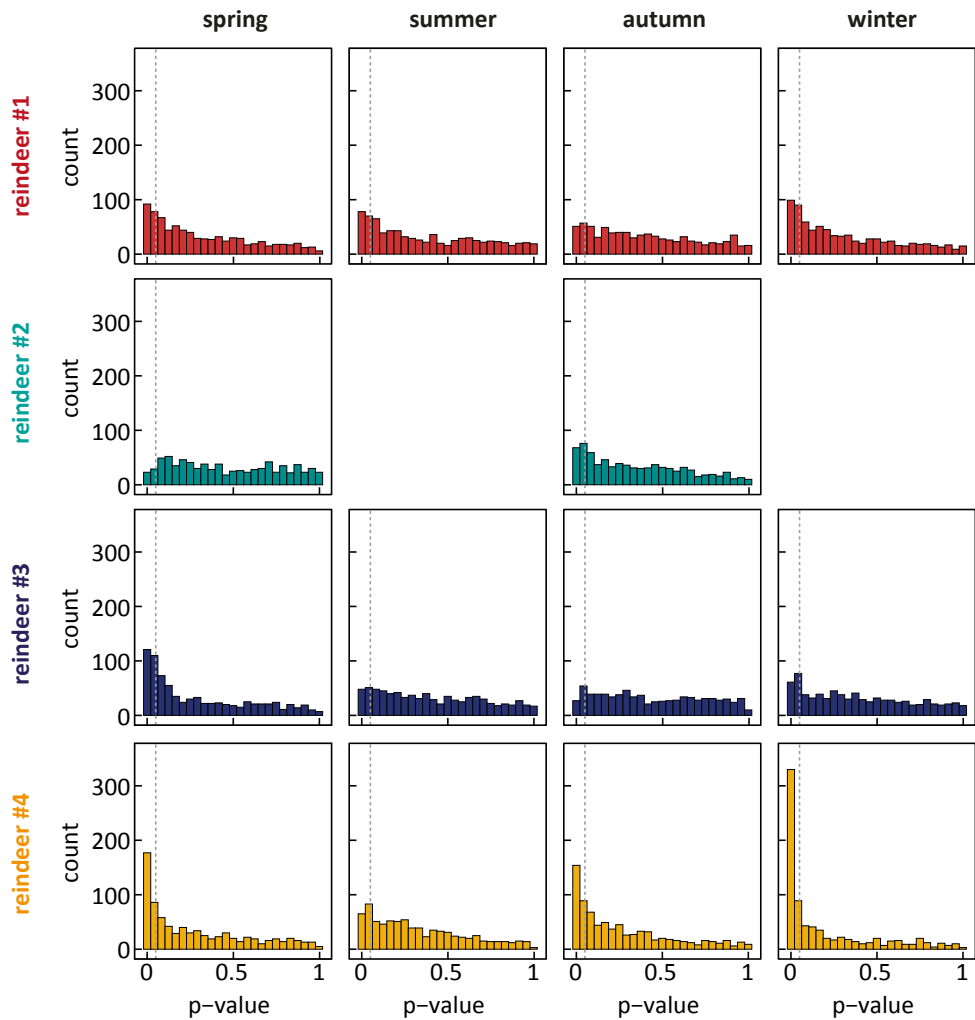


**Figure 7.8.:** P-value distributions from rhythmicity analysis (period length = 24 h) of all metabolic features shown for each individual in each season. Dashed grey lines represent the chosen p-value cutoff ( $p = 0.05$ ) for significant rhythmicity. For reindeer #2 in summer and winter no samples could be collected due to catheter clogging.

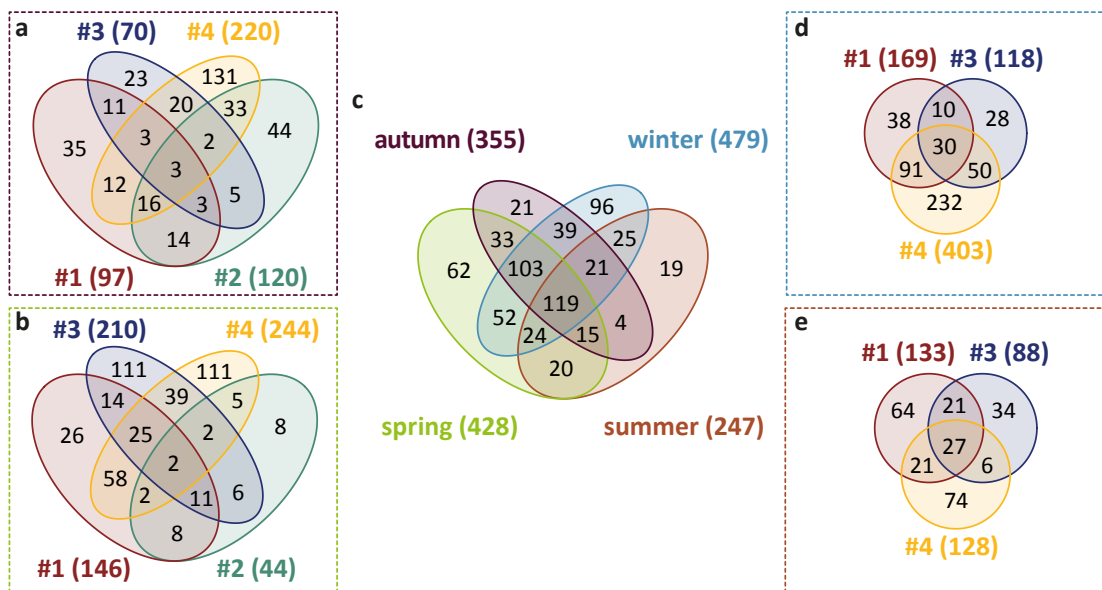


**Figure 7.9:** Venn diagrams are presenting inter-seasonal (c) and inter-individual differences (a autumn, b spring, d winter, e summer) in metabolic circadian rhythms between the four reindeer (#1, #2, #3, #4) within the seasons. In spring, 428 features showed circadian rhythms in at least one animal, 247 in summer, 355 in autumn and 479 in winter accordingly. The colored numbers in brackets in a, b, d and e represent the number of circadian features in the correspondent animal in the according season.

rose plots in figure 7.11. Also here, we observed significant differences between the individuals, nevertheless some overall trends are visible.

In spring, most rhythmic features peak during noon (12 am to 2 pm) or before dawn (2 am to 6 am) in the female reindeer. In contrast, in the male reindeer, we found most features to display a peak at night (0 am to 2 am). In autumn and winter, we detected a group of metabolites with a peak at noon (12 am to 2 pm) in all animals. Moreover, in autumn, in reindeer #1 another group of metabolites peaked around dawn, while in reindeer #2 a group of metabolites peaked after dawn (6 am to 8 am). In the male reindeer, we observed additionally major peaks after dusk (8 pm to 10 pm) and before dawn (2 am to 4 am). In all reindeer many circadian features displayed rhythms with peaks spread around the “usual dawn” (2 am to 10 am) despite constant darkness. During summer we did not observe the major peak at noon, but still many metabolites showed peaks around the “usual dawn” (2 am to 6 am). Moreover in reindeer #3 and #4 a group of metabolites peaked during “usual dusk” (6 pm to 8 pm).

Thus, even though phase distributions vary among the individuals and across the seasons, major peaks are always detected around dawn, dusk and/or noon, even under constant light conditions.

As shown in figure 7.12, the amplitudes of the rhythmic features did not change much between the four seasons and the small changes, which we observed are not consistent among the individual animals.

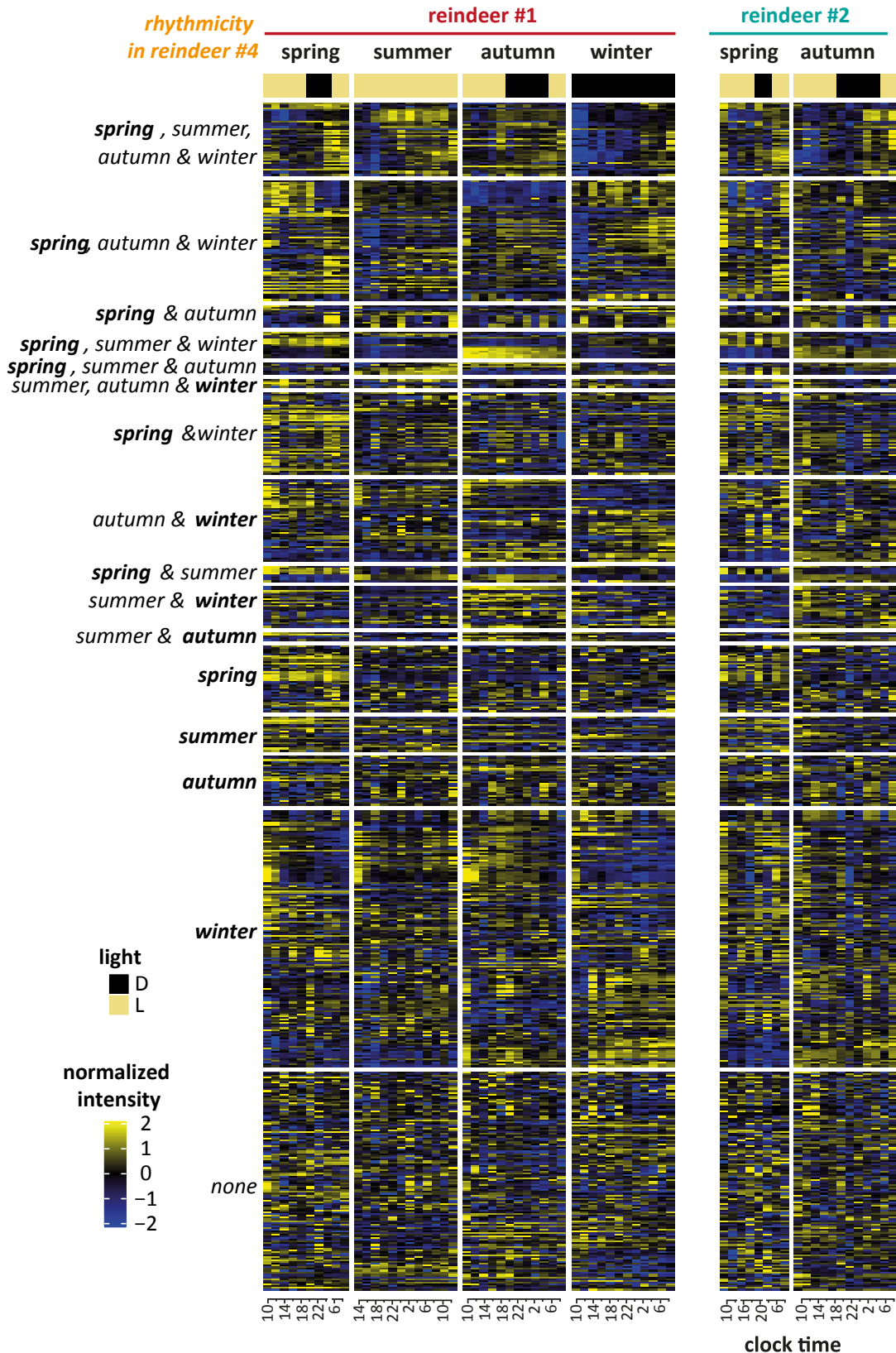
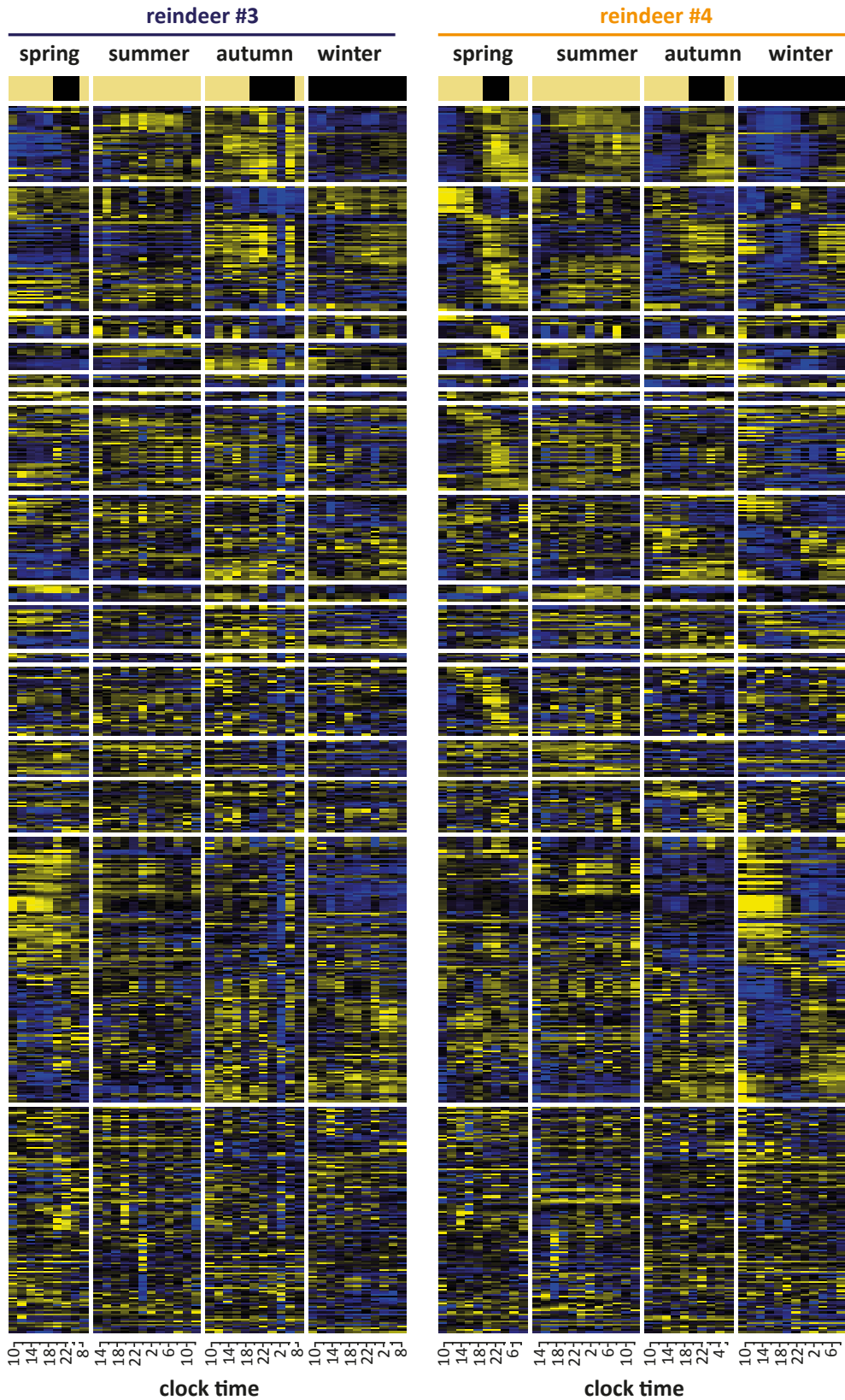


**Figure 7.10.:** Heatmaps showing the time course of the intensity of all metabolic features, for which significant circadian rhythms were found in at least one animal in at least one season. The features are grouped by their rhythmicity in reindeer #4 as indicated on the left.



Within the groups they are sorted by their circadian phase of reindeer #4 during the season shown in bold on the left. The given times are local clock times. Intensities were normalized and  $\log_2$ -transformed for each animal separately.

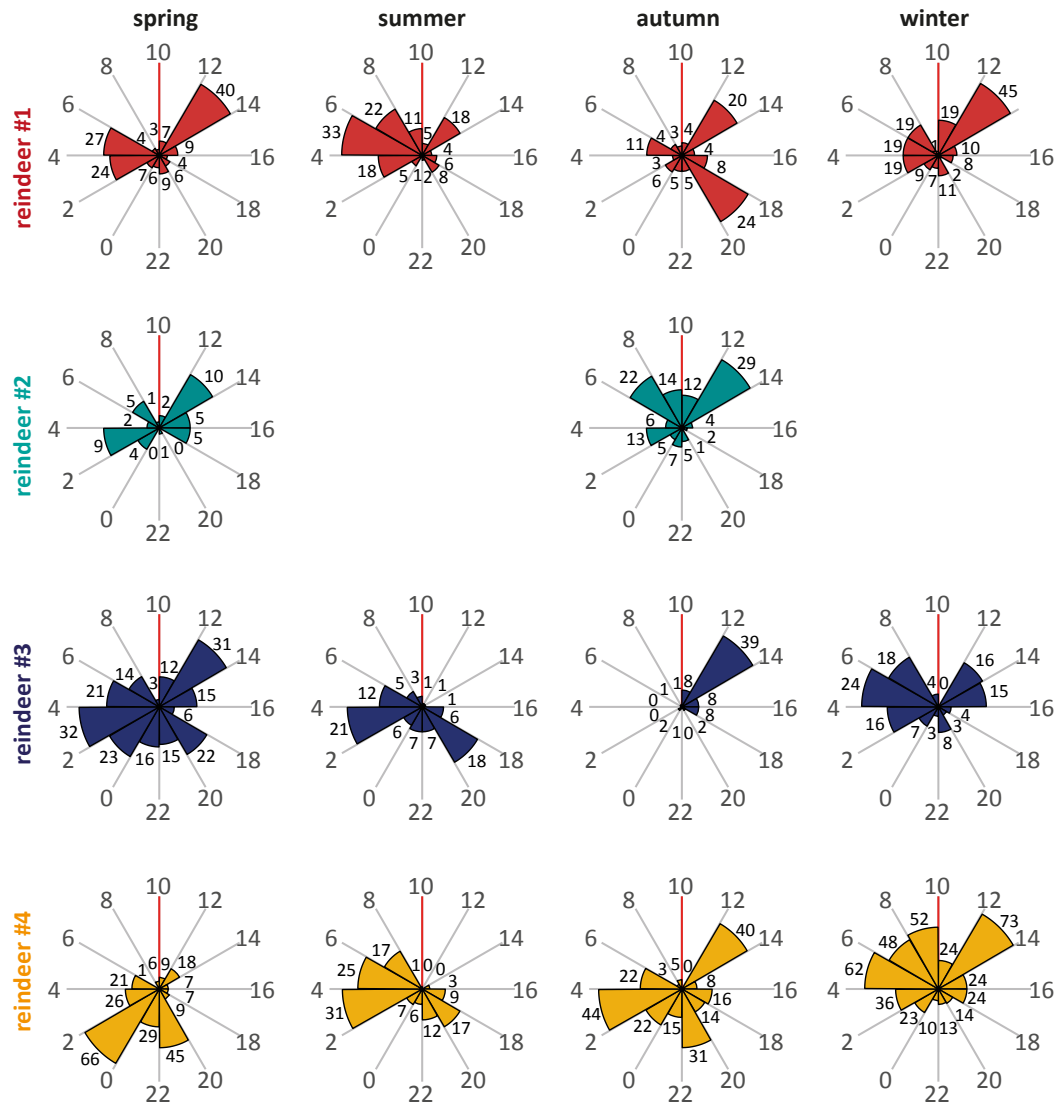


**Figure 7.11.:** Roseplots representing the phase distribution of circadian metabolic features in each reindeer in all seasons. Grey numbers represent local clock time, black number represent counts of features peaking in the corresponding time interval. The starting time of the bleeding experiment is indicated by the red lines.



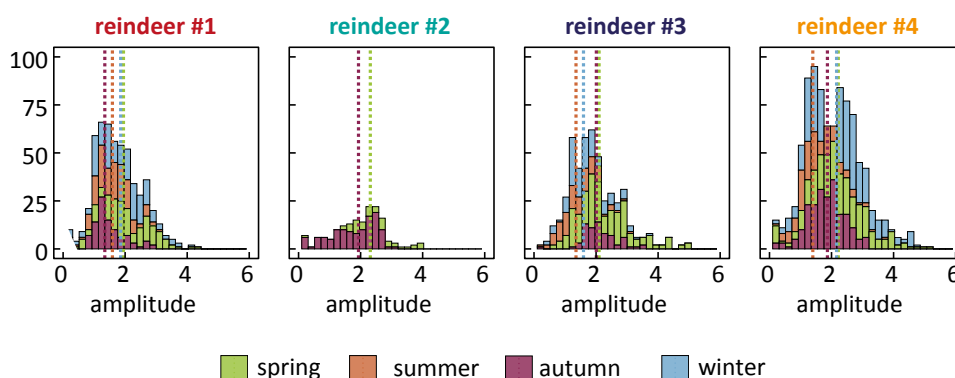


**Figure 7.12.:** Amplitude distributions of circadian metabolic features in each reindeer across the different seasons. Vertical dashed lines represent the median amplitude of the according season.

### 7.3.5. Metabolic pathway enrichment analysis reveals consistent circadian regulation of certain pathways across the whole year

To get some idea about which metabolic pathways are regulated in a circadian fashion, we tried to annotate or identify as many  $m/z$  features as possible. For compounds for which we knew retention times from the measurements described in Chapter 6, we performed targeted peak extraction directly. For the features, which we obtained from untargeted peak extraction, we used automatic annotation by data base matching of MS/MS spectra in MS DIAL.<sup>214</sup> Further we used the mummichog algorithm,<sup>215,254</sup> a combined approach of compound annotation and metabolic pathway enrichment analysis. We carried out this analysis for each animal in each season separately. Identified metabolite names and the corresponding method of annotation are given in the supplementary table B.12. Results from pathway enrichment analysis are summarized in the supplementary table B.13. Despite the inter-seasonal and inter-individual differences reported above, the results from pathway enrichment analysis point towards similar pathways being regulated in a circadian fashion across all seasons and animals. Amino acid related pathways, purine metabolism, pantothenate and CoA biosynthesis and pyrimidine metabolism were enriched among the rhythmic metabolites consistently. Moreover, in spring and winter, glycerol(phospho)lipid metabolism was enriched across several animals. In spring, fatty acid synthesis was additionally suggested to be under circadian control and in winter, propanoate and butanoate metabolism representatives displayed circadian patterns.

## 7.4. Discussion

While Larsen *et al.*<sup>353</sup> observed seasonal changes in blood levels of metabolites involved in lipid metabolism, to the best of our knowledge, circadian regulation of metabolism has not been investigated in reindeer so far. In this study we found circadian pattern for a variety of metabolites in all four seasons, despite the different light conditions. Surprisingly, these rhythms did not all follow the behavioral patterns, which we observed.

Our findings on the reindeer's behavior are consistent with results reported by van Oort

*et al.*<sup>348</sup> We found robust circadian activity patterns in spring and autumn, while none of the animals did display circadian rhythms in their behavior during summer. Instead, we also found more ultradian patterns in summer. In summer, the reindeer were generally more active throughout the day, which is in good agreement with previous findings.<sup>349</sup> The reindeer are supposed to maximize food intake during midnight sun to extensively exploit the short vegetative phase in the Arctic and build up energy deposits. Interestingly, the average activity was similar in autumn, winter and spring. This is in accordance with findings from Arnold *et al.*, who reported that animals start to become really active only in the second half of spring, when vegetation period starts and only until late summer.<sup>354</sup> Even though the animals experienced civil twilight upon release after the blood sampling, they remained behaviorally arrhythmic.

On a metabolic level, we found daily rhythms across all seasons. In summer the lowest percentage of metabolic features displayed circadian rhythms (11-17% of all detected features), while surprisingly, the highest number of rhythmic features was observed in winter (15-51% of all detected features). Hence, most rhythmic patterns in metabolism do not follow the behavioral patterns we observed in the reindeer.

The low number of rhythmic metabolites observed in summer suggests that constant light and the absence of other Zeitgebers, such as rhythmic feeding or activity dampen rhythmicity of metabolic regulation. Nevertheless, we did also find circadian patterns for a certain amount of metabolites in summer, indicating that there is no complete abolishment of circadian clock during midnight sun. The surprisingly high number of rhythmic metabolites in winter despite complete darkness points towards a functional clock in winter. In addition, our findings of rather similar phase distributions in the seasons with and without rhythmic light conditions and the consistent results from metabolic pathway enrichment analysis across all four seasons, support the hypothesis of a circadian clock, which is ticking and influencing metabolism around the whole year.

In the group of metabolites, which were rhythmic in spring, autumn and winter in reindeer #4 (figure 7.10), 3 clusters are detectable in summer. i) A first cluster of features displaying indications for ultradian rhythms, which might reflect ruminant activity. In order to clearly distinguish between ultradian patterns and noise a sampling with increased frequency is needed. ii) A second cluster of features staying constantly low in summer as in the light phases during spring and autumn, while they seem to be in free-run in winter. Thus, they might reflect circadian regulation with light as main Zeitgeber. iii) A third cluster of metabolites, which stay constantly high during summer, while they are high during the dark phases and low during the light phases in spring and autumn. During winter they are constantly rather low and the amplitudes of rhythms seems dampened. We hypothesize that these metabolites might be driven by sleep pressure, as in spring and autumn, sleep pressure accumulates during the day, in summer sleep pressure is constantly high due to the increased activity of the reindeer and in winter it is constantly rather low due to their decreased activity. This hypothesis could be tested in a sleep deprivation experiment.

Notably, the metabolic rhythms we found in reindeer #4 only during winter are much less pronounced or not at all detected in the three female reindeer. This points towards a sex-dependent effect. In winter, male reindeer are digging in the snow to make forage available for the females.<sup>359</sup> It might be that the males can therefore afford the comfort of rhythmic

patterns, while the females need to feed upon occasion and therefore display less rhythms.

We observed large inter-individual differences in metabolic rhythms among the four animals regarding rhythmicity itself but also regarding circadian phase. In humans, different circadian metabolic phenotypes have been reported.<sup>360</sup> Certainly, larger sample sizes would help to further confirm our findings and to clearly distinguish between stochastic effects of noise upon determination of rhythmicity and different circadian metabolic phenotypes in reindeer. However, this is very difficult to achieve for this kind of experiment, since reindeer husbandry is reserved to Saami families with very few exceptions.<sup>361</sup>

Despite the large inter-individual differences, our results from pathway enrichment are surprisingly consistent across the animals and also across the seasons. Many of the top pathway hits are related to amino acid metabolism and purine and pyrimidine metabolism and displayed rhythms across the whole year. Amino acids, pyrimidines and purines are all known sources for microbial nitrogen in ruminants. Amino acids can be deaminated and excreted as ammonia by ruminal bacteria.<sup>362,363</sup> Ammonia also serves as a nitrogen source for microbial synthesis of amino acids and peptides, which are necessary for their growth.<sup>364</sup> Moreover, in dairy cows, purines and pyrimidines are the origin of roughly 20% of the ruminal microbial nitrogen.<sup>365</sup> Therefore, we hypothesize that the metabolic pathways, which are under circadian control across the whole year might reflect primarily nitrogen metabolism of ruminal microbial populations. Further confirmation of the compound annotations obtained automatically, by measuring reference standards and MS/MS spectra, could provide further evidence for this hypothesis.

Our experiments on circadian clock gene expressions are still ongoing. Therefore, no final conclusions can be made here, yet. However, our preliminary findings indicated an intact circadian clock in spring (figure 7.13). Thus against conclusions from earlier studies,<sup>352</sup> we found that at least the clock mechanism exists at a cellular level.

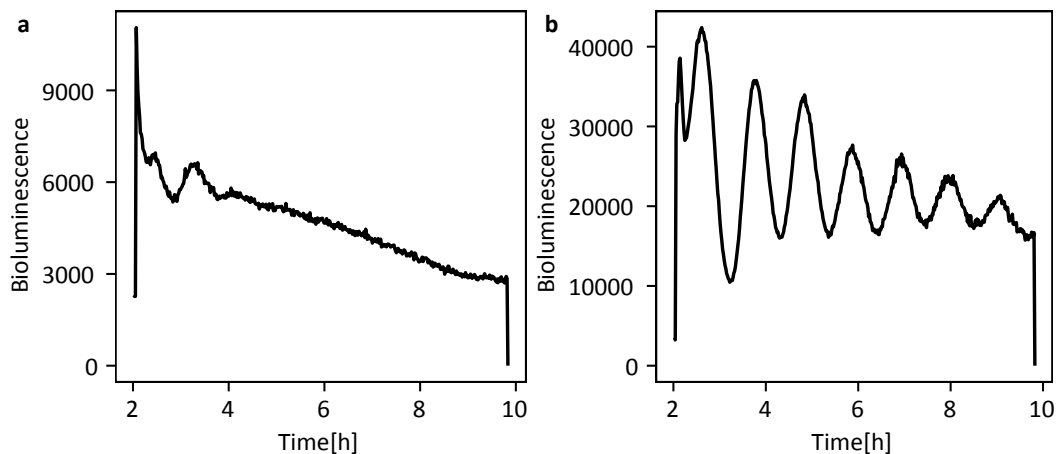


**Figure 7.13:** Bioluminescence recordings reflecting the expression levels of the circadian reporter gene *Bmal1:luc*. **a** *Bmal1:luc* expression in reindeer fibroblasts collected in March. Circadian rhythms were detected in the beginning. **b** *Bmal1:luc* expression in U2OS cells as control.

## 7.5. Conclusion

In conclusion, we found evidence for circadian regulation of metabolism in Norwegian reindeer throughout the year, despite their arrhythmic behavior in constant light and constant darkness. This suggests that behavioral circadian rhythmicity can be uncoupled from metabolic circadian rhythmicity. While the metabolic rhythms were less pronounced during summer, a high degree of rhythmicity was observed in the metabolome during winter. Thus, even in constant darkness, circadian metabolic regulation seems favorable for the animals.

# 8

## Conclusions and outlook

Within the scope of this thesis, novel insights into the complex interplay between sleep, circadian clocks and metabolism were unraveled with cutting-edge techniques, including high-resolution mass spectrometry (HRMS). On the one hand, the virtually unlimited sampling frequency, the non-invasiveness and the real-time information provided by breath analysis was exploited. On the other hand, blood was used as a biological sample, which is less prone to exogenous influences and can be analyzed efficiently by liquid chromatography coupled to HRMS, adding a dimension of separation.

For the first time, metabolome-wide regulation during sleep was monitored using breath analysis by secondary electrospray ionization (SESI) coupled to HRMS (Chapter 4). A setup for analyzing exhaled breath during sleep using SESI-MS with a ten-second time resolution was developed and paves the way for the investigation of metabolic processes associated with sleep itself or with sleep-related diseases. Major axes of metabolism were found to undergo rapid and reversible modifications upon sleep stage changes. While fatty acid oxidation was increased during wakefulness, this metabolic process was decreased after a switch to slow wave sleep. A subsequent switch to rapid eye movement sleep activated TCA cycle activity in preparation for mitochondrial oxidation. This complex orchestration and synchronization of metabolism and sleep architecture might play an important role for human health and performance that has been underestimated until now.

Besides these novel biological findings, breath analysis by SESI-HRMS was brought a step closer to its clinical application as a diagnostic tool. A panel of obstructive sleep apnea (OSA) breath biomarkers was validated in a large and independent group of patients (Chapter 5). During this validation study, the previously stated association between breath levels of these markers and OSA severity was confirmed despite a much higher diversity in this validation cohort. The obtained results suggest that breath analysis by SESI-MS may add an objective value for OSA screening and its combination with conventional questionnaires, such as for the NoSAS score, might thereby improve sensitivity and accuracy of the screening.

Interestingly, 13 of the 33 OSA biomarkers, which were validated here, showed increased levels during REM sleep compared to the other sleep stages in the healthy individuals, who were measured continuously during sleep. Amongst those metabolites are furans and unsaturated hydroxy-aldehydes. Since both, REM sleep and OSA, are associated with increased sympathetic activity,<sup>366</sup> this suggests that these metabolites are regulated by the autonomous nervous system.

In addition to these biomarkers, a broader range of compounds, for which the above mentioned sleep state-dependent changes were detected in healthy individuals, was also differentially regulated between OSA patients and control subjects in this cohort. Remarkably, most of these compounds were involved in mitochondrial respiration, more precisely in the synthesis of acetyl CoA. This indicates that acetyl CoA regulation might be especially affected by a disrupted sleep architecture. These findings further highlight the importance of a synchronization between sleep architecture and metabolism for metabolic health and will inform future hypothesis-driven research in this area.

While breath analysis unraveled metabolic processes related to sleep architecture and obstructive sleep apnea, metabolic profiling in blood provided insights into the connection between circadian clocks and metabolism. In a multi-omics approach, certain metabolic factors in serum from metabolically unhealthy obese patients were discovered to have a lengthening

---

effect on the circadian period length of the expression of the reporter gene *Bmal1-luc* in U2OS cells (Chapter 6). Thanks to the molecular information provided by HRMS, a further investigation of the function of these metabolites was possible. This analysis revealed that most of them were associated with insulin resistance and in addition, the results from a GWAS analysis indicated a genomic origin of these metabolic factors. These findings lead to the hypothesis that insulin resistance might play a central role in the vicious cycle that has been postulated regarding the connection between the circadian clock and obesity in humans.

Furthermore, this connection between metabolic factors associated with insulin resistance and circadian period length showcases the potential use of circadian measures for diagnostic purposes. Since the circadian clock is intimately connected to many cellular processes, it may be used as a sensor that can be genetically exploited to make discoveries about a disease, and the points at which it acts may provide novel treatment ideas.

Circadian disruption is associated with negative consequences on metabolic health in humans, whereas arctic species, such as Norwegian reindeer (*Rangifer tarandus tarandus*), have always been exposed to seasonally occurring conditions of constant light. Metabolic profiling of reindeer blood samples revealed 24-hour rhythms in a large percentage of the detected metabolites during spring, autumn and surprisingly, even under constant darkness in winter, when the animals displayed arrhythmic behavior (Chapter 7). During summer, when the animals experienced constant light and were active throughout the whole day and night, this metabolic rhythmicity was reduced. Nevertheless, a significant number of metabolites still showed circadian patterns. These results suggest that arctic reindeer have developed mechanisms to decouple circadian metabolic regulation from behavioral rhythms. The rhythmic behavior seems to be driven mostly by the light schedule. In contrast, the origin of metabolic rhythms, especially in constant darkness during winter, remain to be discovered.

While this thesis adds some pieces to the complex puzzle that is the interaction between metabolic regulation, sleep and circadian clocks, many other pieces remain to be addressed. Future research ideas emerging from the results obtained in this work are described in the following paragraphs.

### **Pursuing mechanistic understanding of sleep stage-dependent metabolic regulation**

Our unprecedented findings on sleep-stage specific metabolic regulation provoke questions about the underlying mechanisms. We hypothesize that sympathetic activation may be an important mechanism for orchestrating sleep architecture and metabolism. Therefore, it would be interesting to investigate the responses of metabolic pathways upon sympathetic activation. In humans, sympathetic activity can be triggered by the immersion of hands in ice-cold water.<sup>367</sup> In addition, mice models with chronic sympathetic hyperactivity<sup>368</sup> could be investigated. Another possible approach to get further mechanistic insights into sleep stage-dependent metabolic regulation would be to study effects on the metabolome upon REM sleep deprivation.

In general, thanks to its powerful combination of high resolution in the dimension of mass and time, the setup we developed here opens further possibilities for research on metabolic regulation during sleep. For example, metabolic changes upon arousals from different sleep

stages may be studied to find out whether the metabolic or physiological effect of an arousal is influenced by the preceding sleep state. Likewise, metabolic profiling during sleep may be performed in patients suffering from sleep-related diseases, such as narcolepsy or OSA, to investigate immediate metabolic consequences.

### **Further investigation of metabolic regulation under arctic light conditions**

Besides metabolites regulated in a circadian fashion, metabolic profiling in Norwegian reindeer revealed indications for groups of metabolite being mainly controlled by sleep deprivation. In addition, a preliminary proof of principle for the assessment of sleep parameters in reindeer has been achieved in our group. Therefore, a logical follow-up experiment is the combination of metabolomics and sleep recordings and the investigation of the metabolic effect of sleep deprivation. Eventually, even breath analysis could be performed on the animals, similar to our sleep study in humans. However, this would require an on-site mass spectrometer, a sampling device for reindeer breath and a way of avoiding confounding signals from excretions and environment.

Another aspect calling for further investigation are the ultradian patterns, which became apparent in summer for certain metabolites. An experiment where blood is sampled in shorter intervals may provide further evidence here.

### **Further studies on metabolic interactions between circadian clocks and obesity**

Our observation of a prolonged circadian period length in U2OS cells in the presence of certain metabolic serum factors related to insulin resistance in obesity, raises the following questions: are the circadian clocks in these patients slowed down? Or did they develop some kind of compensatory mechanism to keep the clock machinery still running at the same pace? To tackle these questions, the circadian expression of clock genes may be measured in fibroblasts originating from obese patients. The bioluminescence assay could be performed in presence as well as in absence of the patients own serum. These experiments might reveal if clock properties have changed in these patients and if they show the same period lengthening effect in presence of the metabolic factors in serum.

### **Pushing SESI-HRMS towards clinical routine**

While various clinical trials with rather small study cohorts indicated the diagnostic potential of breath analysis recently, the transition of breath analysis by SESI-HRMS to a clinical setting is still in its infancy. It is absolutely essential to validate biomarker candidates in independent and large sample cohorts, e.g. for diseases such as chronic obstructive pulmonary disease or cystic fibrosis, as was presented here for OSA. Moreover, the OSA biomarkers that were validated in this thesis, should be further validated in a longitudinal study as well.

In addition to large-cohort studies, further technical development of SESI-MS can bring the technique closer to its application in clinical routines. Here, the main focus should lie on standardization and ideally even on strategies for absolute quantification. Recent advances of using reference gas mixtures for monitoring instrument performance should be incorporated in all future studies. Besides, one should aim for gaseous standards of as many of the



---

validated OSA biomarkers as possible in order to establish targeted quantification methods for them. Ideally, those methods should rely on the principle of standard addition to account for matrix effects. Multiple reaction monitoring methods on triple quadrupole mass spectrometers are a reasonable instrumentation option for a targeted approach providing quantitative information with high sensitivity and, due to MS/MS involvement, high specificity as well. The transition to such instruments would additionally reduce costs and instrument size tremendously, which would further facilitate their widespread incorporation in future clinical routines.

All in all, the advances in the use of SESI-HRMS achieved in this thesis paved the way for further exploitation of this promising method for clinical applications as well as fundamental research. Intriguing novel interactions between metabolism and both, sleep architecture and circadian clocks, were uncovered by metabolic profiling with high-resolution mass spectrometry techniques.



## References

- [1] T. Roenneberg, K. V. Allebrandt, M. Merrow, and C. Vetter. “Social jetlag and obesity”. *Current Biology* 22.10 (2012), 939–943.
- [2] C. P. Coomans, E. A. Lucassen, S. Kooijman, et al. “Plasticity of circadian clocks and consequences for metabolism”. *Diabetes, Obesity and Metabolism* 17.S1 (2015), 65–75.
- [3] R. M. Kelly, U. Healy, S. Sreenan, J. H. McDermott, and A. N. Coogan. “Clocks in the clinic: circadian rhythms in health and disease”. *Postgraduate Medical Journal* 94.1117 (2018), 653–658.
- [4] S. Sahar and P. Sassone-Corsi. “Metabolism and cancer: The circadian clock connection”. *Nature Reviews Cancer* 9.12 (2009), 886–896.
- [5] L. D. Asarnow, A. M. Soehner, and A. G. Harvey. “Circadian rhythms and psychiatric illness”. *Current Opinion in Psychiatry* 26.6 (2013), 566–571.
- [6] O. Castanon-Cervantes, M. Wu, J. C. Ehlen, et al. “Dysregulation of Inflammatory Responses by Chronic Circadian Disruption”. *The Journal of Immunology* 185.10 (2010), 5796–5805.
- [7] P. Codoñer-Franch and M. Gombert. “Circadian rhythms in the pathogenesis of gastrointestinal diseases”. *World Journal of Gastroenterology* 24.38 (2018), 4297–4303.
- [8] S. A. Brown. “Circadian Metabolism: From Mechanisms to Metabolomics and Medicine”. *Trends in Endocrinology and Metabolism* 27.6 (2016), 415–426.
- [9] J. S. O’Neill, E. S. Maywood, and M. H. Hastings. “Cellular mechanisms of circadian pacemaking: beyond transcriptional loops”. *Handbook of experimental pharmacology* 217 (2013), 67–103.
- [10] A. Balsalobre, F. Damiola, and U. Schibler. “A serum shock induces circadian gene expression in mammalian tissue culture cells”. *Cell* 93.6 (1998), 929–937.
- [11] R. Y. Moore and N. J. Lenn. “A retinohypothalamic projection in the rat”. *Journal of Comparative Neurology* 146.1 (1972), 1–14.
- [12] R. M. Buijs and A. Kalsbeek. “Hypothalamic integration of central and peripheral clocks”. *Nature Reviews Neuroscience* 2.7 (2001), 521–526.
- [13] U. Albrecht. “Timing to Perfection: The Biology of Central and Peripheral Circadian Clocks”. *Neuron* 74.2 (2012), 246–260.

- [14] U. Albrecht and G. Eichele. “The mammalian circadian clock”. *Current opinion in genetics & development* 13.3 (2003), 271–7.
- [15] L. S. Mure, H. D. Le, G. Benegiamo, et al. “Diurnal transcriptome atlas of a primate across major neural and peripheral tissues”. *Science* 359.6381 (2018).
- [16] S. Ramamoorthy and J. A. Cidlowski. “Corticosteroids: Mechanisms of Action in Health and Disease”. *Rheumatic Disease Clinics of North America* 42.1 (2016), 15–31.
- [17] C. Vollmers, S. Gill, L. DiTacchio, S. R. Pulivarthy, H. D. Le, and S. Panda. “Time of feeding and the intrinsic circadian clock drive rhythms in hepatic gene expression”. *Proceedings of the National Academy of Sciences of the United States of America* 106.50 (2009), 21453–21458.
- [18] F. Damiola, N. Le Minli, N. Preitner, B. Kornmann, F. Fleury-Olela, and U. Schibler. “Restricted feeding uncouples circadian oscillators in peripheral tissues from the central pacemaker in the suprachiasmatic nucleus”. *Genes and Development* 14.23 (2000), 2950–2961.
- [19] C. Saini, A. Liani, T. Curie, et al. “Real-time recording of circadian liver gene expression in freely moving mice reveals the phase-setting behavior of hepatocyte clocks”. *Genes and Development* 27.13 (2013), 1526–1536.
- [20] K. L. Eckel-Mahan, V. R. Patel, R. P. Mohny, K. S. Vignola, P. Baldi, and P. Sassone-Corsi. “Coordination of the transcriptome and metabolome by the circadian clock”. *Proceedings of the National Academy of Sciences* 109.14 (2012), 5541–5546.
- [21] Y. Nakahata, S. Sahar, G. Astarita, M. Kaluzova, and P. Sassone-Corsi. “Circadian Control of the NAD<sup>+</sup> Salvage Pathway by CLOCK-SIRT1”. *Science* 324.5927 (2009), 654–657.
- [22] Y. Zhang, B. Fang, M. J. Emmett, et al. “Discrete functions of nuclear receptor Rev-erb $\alpha$  couple metabolism to the clock”. *Science* 348.6242 (2015), 1488–1492.
- [23] I. Schmutz, J. A. Ripperger, S. Baeriswyl-Aebischer, and U. Albrecht. “The mammalian clock component PERIOD2 coordinates circadian output by interaction with nuclear receptors”. *Genes and Development* 24.4 (2010), 345–357.
- [24] G. Asher, D. Gatfield, M. Stratmann, et al. “SIRT1 regulates circadian clock gene expression through PER2 deacetylation”. *Cell* 134.2 (2008), 317–328.
- [25] Y. Lee and E. K. Kim. “AMP-activated protein kinase as a key molecular link between metabolism and clockwork”. *Experimental and Molecular Medicine* 45.7 (2013), e33.
- [26] K. Schmitt, A. Grimm, R. Dallmann, et al. “Circadian Control of DRP1 Activity Regulates Mitochondrial Dynamics and Bioenergetics”. *Cell Metabolism* 27.3 (2018), 657–666.e5.
- [27] S. B. Noya, D. Colameo, F. Brüning, et al. “The forebrain synaptic transcriptome is organized by clocks but its proteome is driven by sleep”. *Science* 366.6462 (2019), eaav2642.

- [28] M. S. Robles, S. J. Humphrey, and M. Mann. “Phosphorylation Is a Central Mechanism for Circadian Control of Metabolism and Physiology”. *Cell Metabolism* 25.1 (2017), 118–127.
- [29] R. Aviram, G. Manella, N. Kopelman, et al. “Lipidomics Analyses Reveal Temporal and Spatial Lipid Organization and Uncover Daily Oscillations in Intracellular Organelles”. *Molecular Cell* 62.4 (2016), 636–648.
- [30] U. Loizides-Mangold, L. Perrin, B. Vandereycken, et al. “Lipidomics reveals diurnal lipid oscillations in human skeletal muscle persisting in cellular myotubes cultured in vitro”. *Proceedings of the National Academy of Sciences of the United States of America* 114.41 (2017), E8565–E8574.
- [31] K. A. Lamia, S. J. Papp, R. T. Yu, et al. “Cryptochromes mediate rhythmic repression of the glucocorticoid receptor”. *Nature* 480.7378 (2011), 552–556.
- [32] S. D. Jordan and K. A. Lamia. “AMPK at the crossroads of circadian clocks and metabolism”. *Molecular and Cellular Endocrinology* 366.2 (2013), 163–169.
- [33] J. O. Lipton, E. D. Yuan, L. M. Boyle, et al. “The circadian protein BMAL1 regulates translation in response to S6K1-mediated phosphorylation”. *Cell* 161.5 (2015), 1138–1151.
- [34] S. Masri, R. Orozco-Solis, L. Aguilar-Arnal, M. Cervantes, and P. Sassone-Corsi. “Coupling circadian rhythms of metabolism and chromatin remodelling”. *Diabetes, Obesity and Metabolism* 17.S1 (2015), 17–22.
- [35] D. Feng, T. Liu, Z. Sun, et al. “A circadian rhythm orchestrated by histone deacetylase 3 controls hepatic lipid metabolism”. *Science* 331.6022 (2011), 1315–1319.
- [36] M. Nakajima, K. Imai, H. Ito, et al. “Reconstitution of circadian oscillation of cyanobacterial KaiC phosphorylation in vitro”. *Science* 308.5720 (2005), 414–415.
- [37] J. S. O'Neill and A. B. Reddy. “Circadian clocks in human red blood cells”. *Nature* 469.7331 (2011), 498–504.
- [38] I. S. Kil, K. W. Ryu, S. K. Lee, et al. “Circadian Oscillation of Sulfiredoxin in the Mitochondria”. *Molecular Cell* 59.4 (2015), 651–663.
- [39] A. Korenčič, R. Košir, G. Bordyugov, R. Lehmann, D. Rozman, and H. Herzog. “Timing of circadian genes in mammalian tissues”. *Scientific Reports* 4.1 (2015), 5782.
- [40] M. Perelis, B. Marcheva, K. M. Ramsey, et al. “Pancreatic b cell enhancers regulate rhythmic transcription of genes controlling insulin secretion”. *Science* 350.6261 (2015), aac4250.
- [41] L. A. Sadacca, K. A. Lamia, A. S. DeLemos, B. Blum, and C. J. Weitz. “An intrinsic circadian clock of the pancreas is required for normal insulin release and glucose homeostasis in mice”. *Diabetologia* 54.1 (2011), 120–124.
- [42] G. K. Paschos, S. Ibrahim, W. L. Song, et al. “Obesity in mice with adipocyte-specific deletion of clock component Arntl”. *Nature Medicine* 18.12 (2012), 1768–1777.

- [43] L. Perrin, U. Loizides-Mangold, S. Skarupelova, et al. “Human skeletal myotubes display a cell-autonomous circadian clock implicated in basal myokine secretion”. *Molecular Metabolism* 4.11 (2015), 834–845.
- [44] B. J. Greenwell, A. J. Trott, J. R. Beytebiere, et al. “Rhythmic Food Intake Drives Rhythmic Gene Expression More Potently than the Hepatic Circadian Clock in Mice”. *Cell Reports* 27.3 (2019), 649–657.e5.
- [45] S. A. Brown, G. Zumbrunn, F. Fleury-Olela, N. Preitner, and U. Schibler. “Rhythms of Mammalian Body Temperature Can Sustain Peripheral Circadian Clocks”. *Current Biology* 12.18 (2002), 1574–1583.
- [46] H. Reinke and G. Asher. “Crosstalk between metabolism and circadian clocks”. *Nature Reviews Molecular Cell Biology* 20.4 (2019), 227–241.
- [47] G. Benegiamo, L. S. Mure, G. Erikson, H. D. Le, E. Moriggi, S. A. Brown, and S. Panda. “The RNA-Binding Protein NONO Coordinates Hepatic Adaptation to Feeding”. *Cell Metabolism* 27.2 (2018), 404–418.e7.
- [48] G. Asher, H. Reinke, M. Altmeyer, M. Gutierrez-Arcelus, M. O. Hottiger, and U. Schibler. “Poly(ADP-ribose) polymerase 1 participates in the phase entrainment of circadian clocks to feeding”. *Cell* 142.6 (2010), 943–953.
- [49] J. Qian and F. A. Scheer. “Circadian System and Glucose Metabolism: Implications for Physiology and Disease”. *Trends in Endocrinology and Metabolism* 27.5 (2016), 282–293.
- [50] A. Kalsbeek and E. Fliers. “Daily regulation of hormone profiles”. *Handbook of experimental pharmacology* 217 (2013), 185–226.
- [51] A. Leliavski, R. Dumbell, V. Ott, and H. Oster. “Adrenal clocks and the role of adrenal hormones in the regulation of circadian physiology”. *Journal of Biological Rhythms* 30.1 (2015), 20–34.
- [52] H. Oster, E. Challet, V. Ott, et al. “The functional and clinical significance of the 24-hour rhythm of circulating glucocorticoids”. *Endocrine Reviews* 38.1 (2017), 3–45.
- [53] F. A. Scheer, C. J. Morris, and S. A. Shea. “The internal circadian clock increases hunger and appetite in the evening independent of food intake and other behaviors”. *Obesity* 21.3 (2013), 421–423.
- [54] H. Hsueh, Y. Wang, G. G. Cornelissen-Guillaume, A. J. Kastin, E. Jang, F. Halberg, and W. Pan. “Diminished leptin signaling can alter circadian rhythm of metabolic activity and feeding”. *Journal of Applied Physiology* 115.7 (2013), 995–1003.
- [55] J. Cedernaes, W. Huang, K. M. Ramsey, et al. “Transcriptional Basis for Rhythmic Control of Hunger and Metabolism within the AgRP Neuron”. *Cell Metabolism* 29.5 (2019), 1078–1091.e5.
- [56] J. Qian, C. J. Morris, R. Caputo, M. Garaulet, and F. A. Scheer. “Ghrelin is impacted by the endogenous circadian system and by circadian misalignment in humans”. *International Journal of Obesity* 43.8 (2019), 1644–1649.

- [57] J. Cedernaes, N. Waldeck, and J. Bass. “Neurogenetic basis for circadian regulation of metabolism by the hypothalamus”. *Genes and Development* 33.17-18 (2019), 1136–1158.
- [58] J. Bass and J. S. Takahashi. “Circadian integration of metabolism and energetics”. *Science* 330.6009 (2010), 1349–1354.
- [59] J. Arendt. “Shift work: coping with the biological clock”. *Occupational Medicine* 60.1 (2010), 10–20.
- [60] T. Akerstedt. “Psychological and psychophysiological effects of shift work”. *Scandinavian journal of work, environment & health* 16 Suppl 1 (1990), 67–73.
- [61] J. Shilts, G. Chen, and J. J. Hughey. “Evidence for widespread dysregulation of circadian clock progression in human cancer”. *PeerJ* 6.1 (2018), e4327.
- [62] O. Ramos-Lopez, M. Samblas, F. I. Milagro, J. I. Riezu-Boj, A. B. Crujeiras, and J. A. Martinez. “Circadian gene methylation profiles are associated with obesity, metabolic disturbances and carbohydrate intake”. *Chronobiology International* 35.7 (2018), 969–981.
- [63] F. W. Turek, C. Joshu, A. Kohsaka, et al. “Obesity and Metabolic Syndrome in Circadian Clock Mutant Mice”. *Science* 308.5724 (2005), 1043–1045.
- [64] D. M. Arble, J. Bass, A. D. Laposky, M. H. Vitaterna, and F. W. Turek. “Circadian Timing of Food Intake Contributes to Weight Gain”. *Obesity* 17.11 (2009), 2100–2102.
- [65] M. Hatori, C. Vollmers, A. Zarrinpar, et al. “Time-Restricted Feeding without Reducing Caloric Intake Prevents Metabolic Diseases in Mice Fed a High-Fat Diet”. *Cell Metabolism* 15.6 (2012), 848–860.
- [66] A. Kohsaka, A. D. Laposky, K. M. Ramsey, et al. “High-Fat Diet Disrupts Behavioral and Molecular Circadian Rhythms in Mice”. *Cell Metabolism* 6.5 (2007), 414–421.
- [67] G. Beccuti, C. Monagheddu, A. Evangelista, G. Ciccone, F. Broglio, S. Laura, and S. Bo. “Timing of food intake: Sounding the alarm about metabolic impairments? A systematic review”. *Pharmacological Research* 125.Pt B (2017), 132–141.
- [68] T. Sun and X. Han. “Death versus dedifferentiation: The molecular bases of beta cell mass reduction in type 2 diabetes”. *Seminars in Cell and Developmental Biology* 103 (2020), 76–82.
- [69] J. Lee, K. Ma, M. Moulik, and V. Yechoor. “Untimely oxidative stress in beta-cells leads to diabetes – Role of circadian clock in beta-cell function”. *Free Radical Biology and Medicine* 119 (2018), 69–74.
- [70] F. Sinturel, A. M. Makhoulouf, P. Meyer, et al. “Cellular circadian period length inversely correlates with HbA1c levels in individuals with type 2 diabetes”. *Diabetologia* 62.8 (2019), 1453–1462.
- [71] A. Pan, E. S. Schernhammer, Q. Sun, and F. B. Hu. “Rotating night shift work and risk of type 2 diabetes: Two prospective cohort studies in women”. *PLoS Medicine* 8.12 (2011). Ed. by L. Groop, e1001141.

- [72] M. W. Greene. “Circadian rhythms and tumor growth”. *Cancer Letters* 318.2 (2012), 115–123.
- [73] M. C. B. Brum, F. F. D. Filho, C. C. Schnorr, G. B. Bottega, and T. C. Rodrigues. “Shift work and its association with metabolic disorders”. *Diabetology and Metabolic Syndrome* 7.1 (2015), 45.
- [74] E. S. Schernhammer, C. H. Kroenke, F. Laden, and S. E. Hankinson. “Night work and risk of breast cancer”. *Epidemiology* 17.1 (2006), 108–111.
- [75] D. Resuehr, G. Wu, R. L. Johnson, M. E. Young, J. B. Hogenesch, and K. L. Gamble. “Shift Work Disrupts Circadian Regulation of the Transcriptome in Hospital Nurses”. *Journal of Biological Rhythms* 34.2 (2019), 167–177.
- [76] L. Kervezee, N. Cermakian, and D. B. Boivin. “Individual metabolomic signatures of circadian misalignment during simulated night shifts in humans”. *PLOS Biology* 17.6 (2019). Ed. by M. F. Ceriani, e3000303.
- [77] D. J. Skene, E. Skorniyakov, N. R. Chowdhury, et al. “Separation of circadian- and behavior-driven metabolite rhythms in humans provides a window on peripheral oscillators and metabolism”. *Proceedings of the National Academy of Sciences of the United States of America* 115.30 (2018), 7825–7830.
- [78] C. A. Thaiss, D. Zeevi, M. Levy, et al. “Transkingdom control of microbiota diurnal oscillations promotes metabolic homeostasis”. *Cell* 159.3 (2014), 514–529.
- [79] J. H. Yu, C. H. Yun, J. H. Ahn, et al. “Evening chronotype is associated with metabolic disorders and body composition in middle-aged adults”. *Journal of Clinical Endocrinology and Metabolism* 100.4 (2015), 1494–1502.
- [80] K. L. Knutson and M. von Schantz. “Associations between chronotype, morbidity and mortality in the UK Biobank cohort”. *Chronobiology International* 35.8 (2018), 1045–1053.
- [81] E. Espitia-Bautista, M. Velasco-Ramos, I. Osnaya-Ramírez, M. Ángeles-Castellanos, R. M. Buijs, and C. Escobar. “Social jet-lag potentiates obesity and metabolic syndrome when combined with cafeteria diet in rats”. *Metabolism* 72 (2017), 83–93.
- [82] D. J. Stenvers, F. F. A. Scheer, P. Schrauwen, S. E. la Fleur, and A. Kalsbeek. “Circadian clocks and insulin resistance”. *Nat Rev Endocrinol* 15.2 (2019), 75–89.
- [83] C. Vetter, E. E. Devore, C. A. Ramin, F. E. Speizer, W. C. Willett, and E. S. Schernhammer. “Mismatch of sleep and work timing and risk of type 2 diabetes”. *Diabetes Care* 38.9 (2015), 1707–1713.
- [84] C. R. Cederroth, U. Albrecht, J. Bass, et al. “Medicine in the Fourth Dimension”. *Cell Metabolism* 30.2 (2019), 238–250.
- [85] M. Gorgoni, A. D’Atri, G. Lauri, P. M. Rossini, F. Ferlazzo, and L. De Gennaro. “Is sleep essential for neural plasticity in humans, and how does it affect motor and cognitive recovery?” *Neural Plasticity* 2013 (2013), 103949.
- [86] C. Puentes-Mestril, J. Roach, N. Niethard, M. Zochowski, and S. J. Aton. “How rhythms of the sleeping brain tune memory and synaptic plasticity”. *Sleep* 42.7 (2019).



- [87] G. Tononi and C. Cirelli. “Sleep and synaptic down-selection”. *European Journal of Neuroscience* 51.1 (2020), 413–421.
- [88] A Rechtschaffen and A Kales. “A manual of standardized terminology, technique and scoring system for sleep stages of human subjects”. *Public Health Service* (1968).
- [89] A. A. Borbély. “A two process model of sleep regulation”. *Human neurobiology* 1.3 (1982), 195–204.
- [90] A. A. Borbély, S. Daan, A. Wirz-Justice, and T. Deboer. “The two-process model of sleep regulation: A reappraisal”. *Journal of Sleep Research* 25.2 (2016), 131–143.
- [91] A. Laposky, A. Easton, C. Dugovic, J. Walisser, C. Bradfield, and F. Turek. *Deletion of the mammalian circadian clock gene BMAL1/Mop3 alters baseline sleep architecture and the response to sleep deprivation*. 2005.
- [92] G. M. Mang, F. La Spada, Y. Emmenegger, S. Chappuis, J. A. Ripperger, U. Albrecht, and P. Franken. “Altered sleep homeostasis in REV-ERB $\alpha$  knockout mice”. *Sleep* 39.3 (2016), 589–601.
- [93] E Rosenbaum. *Warum müssen wir schlafen? Eine neue Theorie des Schlafes*. Berlin: August Hirschwald, 1892.
- [94] C. H. C. Leenaars, S. A. Savelyev, S. Van der Mierden, R. N. J. M. A. Joosten, M. De-matteis, T. Porkka-Heiskanen, and M. G. P. Feenstra. “Intracerebral Adenosine During Sleep Deprivation: A Meta-Analysis and New Experimental Data”. *Journal of Circadian Rhythms* 16.1 (2018), 11.
- [95] C. W. Berridge, B. E. Schmeichel, and R. A. España. “Noradrenergic modulation of wakefulness/arousal”. *Sleep Medicine Reviews* 16.2 (2012), 187–197.
- [96] J. Oh, C. Petersen, C. M. Walsh, J. C. Bittencourt, T. C. Neylan, and L. T. Grinberg. “The role of co-neurotransmitters in sleep and wake regulation”. *Molecular Psychiatry* 24.9 (2019), 1284–1295.
- [97] G. H. Diering, R. S. Nirujogi, R. H. Roth, P. F. Worley, A Pandey, and R. L. Huganir. “Homer1a drives homeostatic scaling-down of excitatory synapses during sleep”. *Science* 355.6324 (2017), 511–515.
- [98] Z. Wang, J. Ma, C. Miyoshi, et al. “Quantitative phosphoproteomic analysis of the molecular substrates of sleep need”. *Nature* 558.7710 (2018), 435–439.
- [99] F. Brüning, S. B. Noya, T. Bange, et al. “Sleep-wake cycles drive daily dynamics of synaptic phosphorylation”. *Science* 366.6462 (2019), 201–+.
- [100] C. M. Muheim, A. Spinnler, T. Sartorius, et al. “Dynamic- and Frequency-Specific Regulation of Sleep Oscillations by Cortical Potassium Channels”. *Current Biology* 29.18 (2019), 2983–2992.e3.
- [101] F. Tatsuki, G. A. A. Sunagawa, S. Shi, et al. “Involvement of Ca(2+)-Dependent Hyperpolarization in Sleep Duration in Mammals”. *Neuron* 90.1 (2016), 70–85.
- [102] C. Mikhail, A. Vaucher, S. Jimenez, and M. Tafti. “ERK signaling pathway regulates sleep duration through activity-induced gene expression during wakefulness”. *Science Signaling* 10.463 (2017).

- [103] V. Crunelli and S. W. Hughes. “The slow (below 1 Hz) rhythm of non-REM sleep: a dialogue between three cardinal oscillators”. *Nature Neuroscience* 13.1 (2010), 9–17.
- [104] M. Kalia. “Neurobiology of sleep”. *Metabolism: Clinical and Experimental* 55.SUPPL. 2 (2006), S2–6.
- [105] D. McGinty and R. Szymusiak. “The sleep–wake switch: A neuronal alarm clock”. *Nature Medicine* 6.5 (2000), 510–511.
- [106] J. Lu, D. Sherman, M. Devor, and C. B. Saper. “A putative flip–flop switch for control of REM sleep”. *Nature* 441.7093 (2006), 589–594.
- [107] K. S. Chen, M. Xu, Z. Zhang, W. C. Chang, T. Gaj, D. V. Schaffer, and Y. Dan. “A Hypothalamic Switch for REM and Non-REM Sleep”. *Neuron* 97.5 (2018), 1168–1176.e4.
- [108] N. N. Aalling, M. Nedergaard, and M. DiNuzzo. “Cerebral Metabolic Changes During Sleep”. *Curr Neurol Neurosci Rep* 18.9 (2018), 57.
- [109] P. Mächler, M. T. Wyss, M. Elsayed, et al. “In Vivo Evidence for a Lactate Gradient from Astrocytes to Neurons”. *Cell Metabolism* 23.1 (2016), 94–102.
- [110] M. DiNuzzo and M. Nedergaard. “Brain energetics during the sleep–wake cycle”. *Current Opinion in Neurobiology* 47 (2017), 65–72.
- [111] D. Burdakov, L. T. Jensen, H. Alexopoulos, et al. “Tandem-Pore K<sup>+</sup> Channels Mediate Inhibition of Orexin Neurons by Glucose”. *Neuron* 50.5 (2006), 711–722.
- [112] C. Varin, A. Rancillac, H. Geoffroy, S. Arthaud, P. Fort, and T. Gallopin. “Glucose Induces Slow-Wave Sleep by Exciting the Sleep-Promoting Neurons in the Ventrolateral Preoptic Nucleus: A New Link between Sleep and Metabolism”. *Journal of Neuroscience* 35.27 (2015), 9900–9911.
- [113] A. Yamanaka, C. T. Beuckmann, J. T. Willie, et al. “Hypothalamic orexin neurons regulate arousal according to energy balance in mice”. *Neuron* 38.5 (2003), 701–713.
- [114] F. Tang, S. Lane, A. Korsak, J. F. Paton, A. V. Gourine, S. Kasparov, and A. G. Teschemacher. “Lactate-mediated glia-neuronal signalling in the mammalian brain”. *Nature Communications* 5.1 (2014), 3284.
- [115] G. A. Dienel and N. F. Cruz. “Aerobic glycolysis during brain activation: adrenergic regulation and influence of norepinephrine on astrocytic metabolism”. *Journal of Neurochemistry* 138.1 (2016), 14–52.
- [116] C. Cirelli, C. M. Gutierrez, and G. Tononi. “Extensive and Divergent Effects of Sleep and Wakefulness on Brain Gene Expression”. *Neuron* 41.1 (2004), 35–43.
- [117] J. M. Petit, I. Tobler, I. Allaman, A. A. Borbély, and P. J. Magistretti. “Sleep deprivation modulates brain mRNAs encoding genes of glycogen metabolism”. *European Journal of Neuroscience* 16.6 (2002), 1163–1167.
- [118] S. Chikahisa and H. Séi. “The Role of ATP in Sleep Regulation”. *Frontiers in Neurology* 2 (2011), 87.

- [119] P. Maquet, D. Dive, E. Salmon, et al. "Cerebral glucose utilization during sleep-wake cycle in man determined by positron emission tomography and [18F]2-fluoro-2-deoxy-d-glucose method". *Brain Research* 513.1 (1990), 136–143.
- [120] P. J. Boyle, J. C. Scott, A. J. Krentz, R. J. Nagy, E Comstock, and C Hoffman. "Diminished brain glucose metabolism is a significant determinant for falling rates of systemic glucose utilization during sleep in normal humans". *The Journal of Clinical Investigation* 93.2 (1994), 529–535.
- [121] P. Maquet. "Sleep function(s) and cerebral metabolism". *Behavioural Brain Research* 69.1 (1995), 75–83.
- [122] R. J. Berger and N. H. Phillips. "Energy conservation and sleep". *Behavioural Brain Research* 69.1-2 (1995), 65–73.
- [123] D. P. White, J. V. Weil, and C. W. Zwillich. "Metabolic rate and breathing during sleep". *Journal of Applied Physiology* 59.2 (1985), 384–391.
- [124] M. A. Elgar, M. D. Pagel, and P. H. Harvey. "Sleep in mammals". *Animal Behaviour* 36.5 (1988), 1407–1419.
- [125] K. V. Allebrandt, N Amin, B Müller-Myhsok, et al. "A KATP channel gene effect on sleep duration: from genome-wide association studies to function in Drosophila". *Molecular psychiatry* 18.1 (2013), 122–132.
- [126] H. M. Ollila, S. Utge, E. Kronholm, et al. "TRIB1 constitutes a molecular link between regulation of sleep and lipid metabolism in humans". *Translational Psychiatry* 2.3 (2012).
- [127] E. Van Cauter, J. D. Blackman, D. Roland, J. P. Spire, S. Refetoff, and K. S. Polonsky. "Modulation of glucose regulation and insulin secretion by circadian rhythmicity and sleep". *Journal of Clinical Investigation* 88.3 (1991), 934–942.
- [128] K. L. Knutson. "Impact of Sleep and Sleep Loss on Glucose Homeostasis and Appetite Regulation". *Sleep Medicine Clinics* 2.2 (2007), 187–197.
- [129] D. R. Brebbia and K. Z. Altshuler. "Oxygen Consumption Rate and Electroencephalographic Stage of Sleep". *Science* 150.3703 (1965), 1621–1623.
- [130] A. M. Fontvieille, R Rising, M Spraul, D. E. Larson, and E Ravussin. "Relationship between sleep stages and metabolic rate in humans". *American Journal of Physiology-Endocrinology and Metabolism* 267.5 (1994), E732–E737.
- [131] P Webb and M Hiestand. "Sleep metabolism and age". *Journal of Applied Physiology* 38.2 (1975), 257–262.
- [132] E. H. Haskell, J. W. Palca, J. M. Walker, R. J. Berger, and H. C. Heller. "Metabolism and thermoregulation during stages of sleep in humans exposed to heat and cold". *Journal of Applied Physiology Respiratory Environmental and Exercise Physiology* 51.4 (1981), 948–954.
- [133] J. W. Palca, J. M. Walker, and R. J. Berger. "Thermoregulation, metabolism, and stages of sleep in cold-exposed men". *Journal of Applied Physiology* 61.3 (1986), 940–947.

- [134] C. M. Jung, E. L. Melanson, E. J. Frydendall, L. Perreault, R. H. Eckel, and K. P. Wright. "Energy expenditure during sleep, sleep deprivation and sleep following sleep deprivation in adult humans". *Journal of Physiology* 589.1 (2011), 235–244.
- [135] M. Kayaba, I. Park, K. Iwayama, et al. "Energy metabolism differs between sleep stages and begins to increase prior to awakening". *Metabolism* 69 (2017), 14–23.
- [136] S. Sharma and M. Kavuru. "Sleep and metabolism: an overview". *International journal of endocrinology* 2010 (2010).
- [137] M. Kojima, H. Hosoda, Y. Date, M. Nakazato, H. Matsuo, and K. Kangawa. "Ghrelin is a growth-hormone-releasing acylated peptide from stomach". *Nature* 402.6762 (1999), 656–660.
- [138] J. C. Weikel, A. Wichniak, M. Ising, et al. "Ghrelin promotes slow-wave sleep in humans". *American Journal of Physiology - Endocrinology and Metabolism* 284.2 47-2 (2003), E407–E415.
- [139] S. M. Gale, V. D. Castracane, and C. S. Mantzoros. "Energy Homeostasis, Obesity and Eating Disorders: Recent Advances in Endocrinology". *The Journal of Nutrition* 134.2 (2004), 295–298.
- [140] C. Simon, C. Gronfier, J. L. Schlienger, and G. Brandenberger. "Circadian and ultradian variations of leptin in normal man under continuous enteral nutrition: Relationship to sleep and body temperature". *Journal of Clinical Endocrinology and Metabolism* 83.6 (1998), 1893–1899.
- [141] A. D. Laposky, J. Shelton, J. Bass, C. Dugovic, N. Perrino, and F. W. Turek. "Altered sleep regulation in leptin-deficient mice". *American Journal of Physiology-Regulatory, Integrative and Comparative Physiology* 290.4 (2006), R894–R903.
- [142] J. M. Siegel. "Hypocretin (OREXIN): Role in normal behavior and neuropathology". *Annual Review of Psychology* 55.1 (2004), 125–148.
- [143] J. A. Teske and V. Mavanji. "Energy expenditure: role of orexin". *Vitamins and Hormones* 89 (2012), 91–109.
- [144] J. F. Sassin, D. C. Parker, J. W. Mace, R. W. Gotlin, L. C. Johnson, and L. G. Rossman. "Human growth hormone release: Relation to slow-wave sleep and sleep-waking cycles". *Science* 165.3892 (1969), 513–515.
- [145] D. A. Schmid, A. Wichniak, M. Uhr, et al. "Changes of sleep architecture, spectral composition of sleep EEG, the nocturnal secretion of cortisol, ACTH, GH, prolactin, melatonin, ghrelin, and leptin, and the DEX-CRH test in depressed patients during treatment with mirtazapine". *Neuropsychopharmacology* 31.4 (2006), 832–844.
- [146] F. Latta, R. Leproult, E. Tasali, E. Hofmann, M. L'Hermite-Balériaux, G. Copinschi, and E. Van Cauter. "Sex Differences in Nocturnal Growth Hormone and Prolactin Secretion in Healthy Older Adults: Relationships With Sleep EEG Variables". *Sleep* 28.12 (2005), 1519–1524.

- [147] B. Gómez-González, E. Domínguez-Salazar, G. Hurtado-Alvarado, E. Esqueda-Leon, R. Santana-Miranda, J. A. Rojas-Zamorano, and J. Velázquez-Moctezuma. “Role of sleep in the regulation of the immune system and the pituitary hormones”. *Annals of the New York Academy of Sciences* 1261.1 (2012), 97–106.
- [148] L. Besedovsky, T. Lange, and J. Born. “Sleep and immune function”. *Pflugers Archiv European Journal of Physiology* 463.1 (2012), 121–137.
- [149] L. Imeri and M. R. Opp. “How (and why) the immune system makes us sleep”. *Nature Reviews Neuroscience* 10.3 (2009), 199–210.
- [150] J. R. Brestoff and D. Artis. “Immune regulation of metabolic homeostasis in health and disease”. *Cell* 161.1 (2015), 146–160.
- [151] R. R. Markwald, E. L. Melanson, M. R. Smith, J. Higgins, L. Perreault, R. H. Eckel, and K. P. Wright. “Impact of insufficient sleep on total daily energy expenditure, food intake, and weight gain”. *Proceedings of the National Academy of Sciences of the United States of America* 110.14 (2013), 5695–5700.
- [152] A. V. Nedeltcheva, J. M. Kilkus, J. Imperial, K. Kasza, D. A. Schoeller, and P. D. Penev. “Sleep curtailment is accompanied by increased intake of calories from snacks”. *American Journal of Clinical Nutrition* 89.1 (2009), 126–133.
- [153] S. M. Schmid, M. Hallschmid, K. Jauch-Chara, et al. “Short-term sleep loss decreases physical activity under free-living conditions but does not increase food intake under time-deprived laboratory conditions in healthy men”. *American Journal of Clinical Nutrition* 90.6 (2009), 1476–1482.
- [154] P. D. Penev. “Sleep deprivation and energy metabolism: To sleep, perchance to eat?”. *Current Opinion in Endocrinology, Diabetes and Obesity* 14.5 (2007), 374–381.
- [155] K. Spiegel, E. Tasali, P. Penev, and E. Van Cauter. “Brief communication: Sleep curtailment in healthy young men is associated with decreased leptin levels, elevated ghrelin levels, and increased hunger and appetite”. *Annals of Internal Medicine* 141.11 (2004), 846–850.
- [156] F. P. Cappuccio, L. D’Elia, P. Strazzullo, and M. A. Miller. “Quantity and Quality of Sleep and Incidence of Type 2 Diabetes”. *Diabetes Care* 33.2 (2010), 414–420.
- [157] C. M. Depner, E. L. Melanson, R. H. Eckel, et al. “Ad libitum Weekend Recovery Sleep Fails to Prevent Metabolic Dysregulation during a Repeating Pattern of Insufficient Sleep and Weekend Recovery Sleep”. *Current Biology* 29.6 (2019), 957–967.e4.
- [158] O. M. Buxton, M. Pavlova, E. W. Reid, W. Wang, D. C. Simonson, and G. K. Adler. “Sleep Restriction for 1 Week Reduces Insulin Sensitivity in Healthy Men”. *Diabetes* 59.9 (2010), 2126.
- [159] T. Anothaisintawee, S. Reutrakul, E. Van Cauter, and A. Thakkinstian. “Sleep disturbances compared to traditional risk factors for diabetes development: Systematic review and meta-analysis”. *Sleep Medicine Reviews* 30 (2016), 11–24.

- [160] F. P. Cappuccio, F. M. Taggart, N. B. Kandala, A. Currie, E. Peile, S. Stranges, and M. A. Miller. "Meta-analysis of short sleep duration and obesity in children and adults". *Sleep* 31.5 (2008), 619–626.
- [161] S. Reutrakul and E. Van Cauter. "Sleep influences on obesity, insulin resistance, and risk of type 2 diabetes". *Metabolism: Clinical and Experimental* 84 (2018), 56–66.
- [162] R. Carter and D. E. Watenpaugh. "Obesity and obstructive sleep apnea: Or is it OSA and obesity?" *Pathophysiology* 15.2 (2008), 71–77.
- [163] I. A. Harsch, P. C. Konturek, C. Koebnick, et al. "Leptin and ghrelin levels in patients with obstructive sleep apnoea: effect of CPAP treatment". *European Respiratory Journal* 22.2 (2003), 251.
- [164] L. Mallon, J. E. Broman, and J. Hetta. "High Incidence of Diabetes in Men With Sleep Complaints or Short Sleep Duration". *Diabetes Care* 28.11 (2005), 2762–2767.
- [165] S. D. West, D. J. Nicoll, and J. R. Stradling. "Prevalence of obstructive sleep apnoea in men with type 2 diabetes". *Thorax* 61.11 (2006), 945–950.
- [166] G. D. Foster, M. H. Sanders, R. Millman, et al. "Obstructive sleep apnea among obese patients with type 2 diabetes". *Diabetes Care* 32.6 (2009), 1017–1019.
- [167] M. T. Barone and L. Menna-Barreto. "Diabetes and sleep: A complex cause-and-effect relationship". *Diabetes Research and Clinical Practice* 91.2 (2011), 129–137.
- [168] M. Pallayova, V. Donic, and Z. Tomori. "Beneficial effects of severe sleep apnea therapy on nocturnal glucose control in persons with type 2 diabetes mellitus". *Diabetes Research and Clinical Practice* 81.1 (2008), e8.
- [169] M. Smurra, P. Philip, J. Taillard, C. Guilleminault, B. Bioulac, and H. Gin. "CPAP treatment does not affect glucose–insulin metabolism in sleep apneic patients". *Sleep Medicine* 2.3 (2001), 207–213.
- [170] L. Hecht, R. Möhler, and G. Meyer. "Effects of CPAP-respiration on markers of glucose metabolism in patients with obstructive sleep apnoea syndrome: a systematic review and meta-analysis". *German medical science : GMS e-journal* 9 (2011), Doc20–Doc20.
- [171] G. Pillar and N. Shehadeh. "Abdominal Fat and Sleep Apnea". *Diabetes Care* 31.Supplement 2 (2008), S303–S309.
- [172] Y. Dauvilliers, S. Rompré, J. F. Gagnon, M. Vendette, D. Petit, and J. Montplaisir. "REM sleep characteristics in narcolepsy and REM sleep behavior disorder". *Sleep* 30.7 (2007), 844–849.
- [173] N. Dahmen, J. Bierbrauer, and M. Kasten. "Increased prevalence of obesity in narcoleptic patients and relatives". *European Archives of Psychiatry and Clinical Neuroscience* 251.2 (2001), 85–89.
- [174] S. Yehuda, B. Sredni, R. L. Carasso, and D. Kenigsbuch-Sredni. "REM sleep deprivation in rats results in inflammation and interleukin-17 elevation". *Journal of Interferon and Cytokine Research* 29.7 (2009), 393–398.

- [175] S. Ryan, C. T. Taylor, and W. T. McNicholas. “Predictors of Elevated Nuclear Factor-kappaB-dependent Genes in Obstructive Sleep Apnea Syndrome”. *American Journal of Respiratory and Critical Care Medicine* 174.7 (2006), 824–830.
- [176] C. A. Everson and L. A. Toth. “Systemic bacterial invasion induced by sleep deprivation”. *American Journal of Physiology - Regulatory Integrative and Comparative Physiology* 278.4 47-4 (2000), R905–R916.
- [177] C. M. Carroll and S. L. Macauley. “The Interaction Between Sleep and Metabolism in Alzheimer’s Disease: Cause or Consequence of Disease?” *Frontiers in Aging Neuroscience* 11 (2019), 258.
- [178] L. Peter-Derex, P. Yammine, H. Bastuji, and B. Croisile. “Sleep and Alzheimer’s disease”. *Sleep Medicine Reviews* 19 (2015), 29–38.
- [179] B. P. Lucey, A. McCullough, E. C. Landsness, et al. “Reduced non-rapid eye movement sleep is associated with tau pathology in early Alzheimer’s disease”. *Science Translational Medicine* 11.474 (2019), eaau6550.
- [180] B. P. Lucey, A. M. Fagan, D. M. Holtzman, J. C. Morris, and R. J. Bateman. “Diurnal oscillation of CSF Abeta and other AD biomarkers”. *Molecular Neurodegeneration* 12.1 (2017), 36.
- [181] A. Gabelle, I. Jaussent, C. Hirtz, et al. “Cerebrospinal fluid levels of orexin-A and histamine, and sleep profile within the Alzheimer process”. *Neurobiology of Aging* 53 (2017), 59–66.
- [182] C. Holingue, A. Wennberg, S. Berger, V. Y. Polotsky, and A. P. Spira. “Disturbed sleep and diabetes: A potential nexus of dementia risk”. *Metabolism: Clinical and Experimental* 84 (2018), 85–93.
- [183] L. Xie, H. Kang, Q. Xu, et al. “Sleep drives metabolite clearance from the adult brain”. *Science* 342.6156 (2013), 373–377.
- [184] V. van der Vinne, S. J. Swoap, T. J. Vajtay, and D. R. Weaver. “Desynchrony between brain and peripheral clocks caused by CK1delta/e disruption in GABA neurons does not lead to adverse metabolic outcomes”. *Proceedings of the National Academy of Sciences of the United States of America* 115.10 (2018), E2437–E2446.
- [185] P. Martinez-Lozano Sinues, L. Tarokh, X. Li, M. Kohler, S. A. Brown, R. Zenobi, and R. Dallmann. “Circadian Variation of the Human Metabolome Captured by Real-Time Breath Analysis”. *PLoS ONE* 9.12 (2014). Ed. by N. Cermakian, e114422.
- [186] P. M.-L. Sinues, M. Kohler, and R. Zenobi. “Monitoring Diurnal Changes in Exhaled Human Breath”. *Analytical Chemistry* 85.1 (2013), 369–373.
- [187] C. N. Hor, J. Yeung, M. Jan, et al. “Sleep-wake-driven and circadian contributions to daily rhythms in gene expression and chromatin accessibility in the murine cortex”. *Proceedings of the National Academy of Sciences* 116.51 (2019), 25773–25783.
- [188] M. J. Kim, J. H. Lee, and J. F. Duffy. “Circadian rhythm sleep disorders”. *Journal of Clinical Outcomes Management* 20.11 (2013), 513–528.

- [189] Y. Dagan and L. Ayalon. "Case study: Psychiatric misdiagnosis of non-24-hours sleep-wake schedule disorder resolved by melatonin". *Journal of the American Academy of Child and Adolescent Psychiatry* 44.12 (2005), 1271–1275.
- [190] J. P. Wisor, B. F. O'Hara, A. Terao, et al. "A role for cryptochromes in sleep regulation". *BMC Neuroscience* 3 (2002), 20.
- [191] C Iber. *The AASM Manual for the Scoring of Sleep and Associated Events: Rules, Terminology and Technical Specifications*. American Academy of Sleep Medicine, 2007.
- [192] S. R. Pandi-Perumal, D. Warren Spence, and A. S. BaHammam. "Polysomnography: An Overview". In: *Primary Care Sleep Medicine: A Practical Guide*. Ed. by S. R. Pandi-Perumal and J. F. Pagel. Springer New York, 2014, pp. 29–42.
- [193] K. E. Bloch. "Polysomnography: a systematic review". *Technology and Health Care* 5.4 (1997), 285–305.
- [194] B. Jafari and V. Mohsenin. *Polysomnography*. 2010.
- [195] S. A. Brown, F. Fleury-Olela, E. Nagoshi, et al. "The Period Length of Fibroblast Circadian Gene Expression Varies Widely among Human Individuals". *PLoS Biology* 3.10 (2005). Ed. by E. Mignot, e338.
- [196] L. Pagani, E. A. Semenova, E. Moriggi, et al. "The physiological period length of the human circadian clock in vivo is directly proportional to period in human fibroblasts". *PLoS ONE* 5.10 (2010), e13376.
- [197] T. Arndt. "Luciferin-Luciferase-System". In: *Lexikon der Medizinischen Laboratoriumsdiagnostik*. Ed. by A. Gressner and T. Arndt. Springer, Berlin, Heidelberg, 2019, pp. 1535–1535.
- [198] S. B. Milne, T. P. Mathews, D. S. Myers, P. T. Ivanova, and H. A. Brown. "Sum of the Parts: Mass Spectrometry-Based Metabolomics". *Biochemistry* 52.22 (2013), 3829–3840.
- [199] C. Junot, F. Fenaille, B. Colsch, and F. Bécher. "High resolution mass spectrometry based techniques at the crossroads of metabolic pathways". *Mass Spectrometry Reviews* 33.6 (2014), 471–500.
- [200] K. Dettmer, P. A. Aronov, and B. D. Hammock. "Mass spectrometry-based metabolomics". *Mass Spectrometry Reviews* 26 (2007), 51–78. arXiv: NIHMS150003.
- [201] W. B. Dunn, A. Erban, R. J. M. Weber, et al. "Mass appeal: metabolite identification in mass spectrometry-focused untargeted metabolomics". *Metabolomics* 9 (2013), 44–66.
- [202] J. H. Gross. "Instrumentation". In: *Mass Spectrometry*. Cham: Springer, Cham, 2017, pp. 151–292.
- [203] M. Guilhaus. "Principles and instrumentation in time-of-flight mass spectrometry. Physical and instrumental concepts". *Journal of Mass Spectrometry* 30.11 (1995), 1519–1532.
- [204] A. Makarov. "Electrostatic Axially Harmonic Orbital Trapping: A High-Performance Technique of Mass Analysis". *Analytical Chemistry* 72.6 (2000), 1156–1162.



- [205] J. F. García-Reyes, D. Moreno-González, R. Nortes-Méndez, B. Gilbert-López, and A. Molina Díaz. “HRMS”. In: *Applications in High Resolution Mass Spectrometry*. Elsevier, 2017, pp. 15–57.
- [206] J. H. Gross. “Tandem Mass Spectrometry”. In: *Mass Spectrometry*. Cham: Springer International Publishing, 2017, pp. 539–612.
- [207] G. L. Andrews, B. L. Simons, J. B. Young, A. M. Hawkrigde, and D. C. Muddiman. “Performance Characteristics of a New Hybrid Quadrupole Time-of-Flight Tandem Mass Spectrometer (TripleTOF 5600)”. *Analytical Chemistry* 83.13 (2011), 5442–5446.
- [208] A. Michalski, E. Damoc, J.-P. Hauschild, et al. “Mass Spectrometry-based Proteomics Using Q Exactive, a High-performance Benchtop Quadrupole Orbitrap Mass Spectrometer”. *Molecular & Cellular Proteomics* 10.9 (2011), M111.011015.
- [209] N. Psychogios, D. D. Hau, J. Peng, et al. “The Human Serum Metabolome”. *PLoS ONE* 6.2 (2011). Ed. by D. Flower, e16957.
- [210] A. Roux, D. Lison, C. Junot, and J.-F. Heilier. “Applications of liquid chromatography coupled to mass spectrometry-based metabolomics in clinical chemistry and toxicology: A review”. *Clinical Biochemistry* 44.1 (2011), 119–135.
- [211] W. B. Dunn, D. Broadhurst, P. Begley, et al. “Procedures for large-scale metabolic profiling of serum and plasma using gas chromatography and liquid chromatography coupled to mass spectrometry”. *Nature Protocols* 6.7 (2011), 1060–1083.
- [212] M Churchwell, N Twaddle, L Meeker, and D Doerge. “Improving LC–MS sensitivity through increases in chromatographic performance: Comparisons of UPLC–ES/MS/MS to HPLC–ES/MS/MS”. *Journal of Chromatography B* 825.2 (2005), 134–143.
- [213] J. H. Gross. “Electrospray Ionization”. In: *Mass Spectrometry*. Cham: Springer Cham, 2017, pp. 721–778.
- [214] H. Tsugawa, T. Cajka, T. Kind, et al. “MS-DIAL: data-independent MS/MS deconvolution for comprehensive metabolome analysis”. *Nature Methods* 12.6 (2015), 523–526.
- [215] J. Chong, D. S. Wishart, and J. Xia. “Using MetaboAnalyst 4.0 for Comprehensive and Integrative Metabolomics Data Analysis”. *Current Protocols in Bioinformatics* 68.1 (2019), e86.
- [216] B de Lacy Costello, A Amann, H Al-Kateb, et al. “A review of the volatiles from the healthy human body”. *Journal of Breath Research* 8.1 (2014), 014001.
- [217] M. Simionescu. “Cellular components of the air-blood barrier”. *Journal of Cellular and Molecular Medicine* 5.3 (2001), 320–321.
- [218] J. Piiper. “Pulmonary Gas Exchange”. In: *Comprehensive Human Physiology*. Ed. by R. Greger and U. Windhorst. Berlin, Heidelberg: Springer Berlin Heidelberg, 1996, pp. 2037–2049.
- [219] T. Bruderer, T. Gaisl, M. T. Gaugg, et al. “On-Line Analysis of Exhaled Breath”. *Chemical Reviews* 119.19 (2019), 10803–10828.

- [220] C. Wu, W. F. Siems, and H. H. Hill. "Secondary electrospray ionization ion mobility spectrometry/mass spectrometry of illicit drugs". *Analytical Chemistry* 72.2 (2000), 396–403.
- [221] A. T. Rioseras, M. T. Gaugg, and P. Martinez-Lozano Sinues. "Secondary electrospray ionization proceeds via gas-phase chemical ionization". *Analytical Methods* 9.34 (2017), 5052–5057.
- [222] P. M.-I. Sinues, E. Criado, G. Vidal, P. Martinez-Lozano Sinues, E. Criado, and G. Vidal. "Mechanistic study on the ionization of trace gases by an electrospray plume". *International Journal of Mass Spectrometry* 313 (2012), 21–29.
- [223] M. T. Gaugg, D. G. Gomez, C. Barrios-Collado, G. Vidal-de Miguel, M. Kohler, R. Zenobi, and P. Martinez-Lozano Sinues. "Expanding metabolite coverage of real-time breath analysis by coupling a universal secondary electrospray ionization source and high resolution mass spectrometry—a pilot study on tobacco smokers". *Journal of Breath Research* 10.1 (2016), 016010.
- [224] D. Zamora, M. Amo-Gonzalez, M. Lanza, G. Fernández de la Mora, and J. Fernández de la Mora. "Reaching a Vapor Sensitivity of 0.01 Parts Per Quadrillion in the Screening of Large Volume Freight". *Analytical Chemistry* 90.4 (2018), 2468–2474.
- [225] P. Martinez-Lozano Sinues, L. Meier, C. Berchtold, et al. "Breath analysis in real time by mass spectrometry in chronic obstructive pulmonary disease". *Respiration* 87.4 (2014), 301–310.
- [226] M. T. Gaugg, Y. Nussbaumer-Ochsner, L. Bregy, et al. "Real-Time Breath Analysis Reveals Specific Metabolic Signatures of COPD Exacerbations". *Chest* 156.2 (2019), 269–276.
- [227] E. I. Schwarz, P. Martinez-Lozano Sinues, L. Bregy, et al. "Effects of CPAP therapy withdrawal on exhaled breath pattern in obstructive sleep apnoea". *Thorax* 71.2 (2016), 110–117.
- [228] M. T. Gaugg, A. Engler, L. Bregy, et al. "Molecular breath analysis supports altered amino acid metabolism in idiopathic pulmonary fibrosis". *Respirology* 24.5 (2019), 437–444.
- [229] M. T. Gaugg, A. Engler, Y. Nussbaumer-Ochsner, et al. "Metabolic effects of inhaled salbutamol determined by exhaled breath analysis". *Journal of Breath Research* 11.4 (2017), 046004.
- [230] X. Li, P. Martinez-Lozano Sinues, R. Dallmann, et al. "Drug Pharmacokinetics Determined by Real-Time Analysis of Mouse Breath". *Angewandte Chemie International Edition* 54.27 (2015), 7815–7818.
- [231] L. Kervezee, A. Kosmadopoulos, and D. B. Boivin. "Metabolic and cardiovascular consequences of shift work: The role of circadian disruption and sleep disturbances". *European Journal of Neuroscience* 51.1 (2020), 396–412.

- [232] A. Kales and A. Rechtschaffen. *A manual of standardized terminology, techniques and scoring system for sleep stages of human subjects*. no 204. Bethesda: U. S. National Institute of Neurological Diseases and Blindness, Neurological Information Network, 1968, 57 p.
- [233] G. Kecklund and J. Axelsson. “Health consequences of shift work and insufficient sleep”. *BMJ* 355 (2016), i5210.
- [234] J. E. Ang, V. Revell, A. Mann, et al. “Identification of Human Plasma Metabolites Exhibiting Time-of-Day Variation Using an Untargeted Liquid Chromatography-Mass Spectrometry Metabolomic Approach”. *Chronobiology International* 29.7 (2012), 868–881.
- [235] L. N. Bell, J. M. Kilkus, J. N. Booth, L. E. Bromley, J. G. Imperial, and P. D. Penev. “Effects of sleep restriction on the human plasma metabolome”. *Physiology & Behavior* 122 (2013), 25–31.
- [236] R. Dallmann, A. U. Viola, L. Tarokh, C. Cajochen, and S. A. Brown. “The human circadian metabolome”. *Proceedings of the National Academy of Sciences* 109.7 (2012), 2625–2629.
- [237] S. K. Davies, J. E. Ang, V. L. Revell, et al. “Effect of sleep deprivation on the human metabolome”. *Proceedings of the National Academy of Sciences* 111.29 (2014), 10761–10766.
- [238] L. K. Grant, S. Ftouni, B. Nijagal, et al. “Circadian and wake-dependent changes in human plasma polar metabolites during prolonged wakefulness: A preliminary analysis”. *Scientific Reports* 9.1 (2019), 4428.
- [239] S. N. Archer, E. E. Laing, C. S. Möller-Levet, et al. “Mistimed sleep disrupts circadian regulation of the human transcriptome”. *Proceedings of the National Academy of Sciences* 111.6 (2014), E682–E691.
- [240] S. Christou, S. M. T. Wehrens, C. Isherwood, et al. “Circadian regulation in human white adipose tissue revealed by transcriptome and metabolic network analysis”. *Scientific Reports* 9.1 (2019), 2641.
- [241] F. Spornl, S. Korge, K. Jurchott, et al. “Kruppel-like factor 9 is a circadian transcription factor in human epidermis that controls proliferation of keratinocytes”. *Proceedings of the National Academy of Sciences* 109.27 (2012), 10903–10908.
- [242] M. S. Robles and M. Mann. “Proteomic Approaches in Circadian Biology”. In: *Circadian Clocks*. Ed. by A. Kramer and M. Merrow. Berlin, Heidelberg: Springer Berlin Heidelberg, 2013, pp. 389–407.
- [243] J.-M. Petit, S. Burlet-Godinot, P. J. Magistretti, and I. Allaman. “Glycogen metabolism and the homeostatic regulation of sleep”. *Metabolic Brain Disease* 30.1 (2015), 263–279.
- [244] L. Bregy, Y. Nussbaumer-Ochsner, P. Martinez-Lozano Sinues, et al. “Real-time mass spectrometric identification of metabolites characteristic of chronic obstructive pulmonary disease in exhaled breath”. *Clinical Mass Spectrometry* 7 (2018), 29–35.

- [245] T. Gaisl, L. Bregy, N. Stebler, et al. “Real-time exhaled breath analysis in patients with cystic fibrosis and controls”. *Journal of Breath Research* 12.3 (2018), 036013.
- [246] S. Redline, H. L. Kirchner, S. F. Quan, D. J. Gottlieb, V. Kapur, and A. Newman. “The Effects of Age, Sex, Ethnicity, and Sleep-Disordered Breathing on Sleep Architecture”. *Archives of Internal Medicine* 164.4 (2004), 406.
- [247] D. Kessner, M. Chambers, R. Burke, D. Agus, and P. Mallick. “ProteoWizard: open source software for rapid proteomics tools development”. *Bioinformatics* 24.21 (2008), 2534–2536.
- [248] R. Burton. “Respiration”. In: *Physiology by Numbers: An Encouragement to Quantitative Thinking*. Cambridge University Press, 2000. Chap. 5, pp. 65–91.
- [249] A. Kuznetsova, P. B. Brockhoff, and R. H. B. Christensen. “lmerTest Package: Tests in Linear Mixed Effects Models”. *Journal of Statistical Software* 82.13 (2017), 1–26.
- [250] J. D. Storey. “A direct approach to false discovery rates”. *Journal of the Royal Statistical Society: Series B (Statistical Methodology)* 64.3 (2002), 479–498.
- [251] J. Cohen. *Statistical power analysis for the behavioral sciences*. Academic Press London, 1977.
- [252] I. Winkler, D. Panknin, D. Bartz, K.-R. Müller, and S. Haufe. “Validity of Time Reversal for Testing Granger Causality”. *IEEE Transactions on Signal Processing* 64.11 (2016), 2746–2760.
- [253] J. Fox. “Bootstrapping Regression Models”. In: *An R and S-Plus companion to applied regression*. Ed. by J. Fox and G. Monette. Sage, 2002.
- [254] S. Li, Y. Park, S. Duraisingham, et al. “Predicting Network Activity from High Throughput Metabolomics”. *PLoS Computational Biology* 9.7 (2013). Ed. by C. A. Ouzounis, e1003123.
- [255] M. T. Gaugg, T. Bruderer, N. Nowak, L. Eiffert, P. Martinez-Lozano Sinues, M. Kohler, and R. Zenobi. “Mass-Spectrometric Detection of Omega-Oxidation Products of Aliphatic Fatty Acids in Exhaled Breath”. *Analytical Chemistry* 89.19 (2017), 10329–10334.
- [256] H. Tsugawa. *MS-DIAL*. 2019.
- [257] P. W. Holland and R. E. Welsch. “Robust regression using iteratively reweighted least-squares”. *Communications in Statistics - Theory and Methods* 6.9 (1977), 813–827.
- [258] C. W. J. Granger. “Investigating Causal Relations by Econometric Models and Cross-spectral Methods”. *Econometrica* 37.3 (1969), 424.
- [259] A. K. Seth, A. B. Barrett, and L. Barnett. “Granger Causality Analysis in Neuroscience and Neuroimaging”. *Journal of Neuroscience* 35.8 (2015), 3293–3297.
- [260] R. Chaleckis, I. Meister, P. Zhang, and C. E. Wheelock. “Challenges, progress and promises of metabolite annotation for LC-MS-based metabolomics”. *Current Opinion in Biotechnology* 55 (2019), 44–50.

- [261] J. King, A. Kupferthaler, B. Frauscher, et al. “Measurement of endogenous acetone and isoprene in exhaled breath during sleep”. *Physiological Measurement* 33.3 (2012), 413–428.
- [262] J. King, H. Koc, K. Unterkofler, et al. “Physiological modeling of isoprene dynamics in exhaled breath”. *Journal of Theoretical Biology* 267.4 (2010), 626–637.
- [263] P. L. Brooks and J. H. Peever. “Unraveling the Mechanisms of REM Sleep Atonia”. *Sleep* 31.11 (2008), 1492–1497.
- [264] B. M. Ross and R. Babgi. “Volatile compounds in blood headspace and nasal breath”. *Journal of Breath Research* 11.4 (2017), 046001.
- [265] P. Giesbertz, J. Ecker, A. Haag, B. Spanier, and H. Daniel. “An LC-MS/MS method to quantify acylcarnitine species including isomeric and odd-numbered forms in plasma and tissues”. *Journal of Lipid Research* 56.10 (2015), 2029–2039.
- [266] N. Longo, M. Frigeni, and M. Pasquali. “Carnitine transport and fatty acid oxidation”. *Biochimica et Biophysica Acta (BBA) - Molecular Cell Research* 1863.10 (2016), 2422–2435.
- [267] L. C. Rodgers, J. Cole, K. M. Rattigan, M. P. Barrett, N. Kurian, I. B. McInnes, and C. S. Goodyear. “The rheumatoid synovial environment alters fatty acid metabolism in human monocytes and enhances CCL20 secretion”. *Rheumatology* 59.4 (2020), 869–878.
- [268] T. Miyagawa, H. Kawamura, M. Obuchi, et al. “Effects of Oral L-Carnitine Administration in Narcolepsy Patients: A Randomized, Double-Blind, Cross-Over and Placebo-Controlled Trial”. *PLoS ONE* 8.1 (2013). Ed. by M. Mazza, e53707.
- [269] E. Van Cauter, K. S. Polonsky, and A. J. Scheen. “Roles of Circadian Rhythmicity and Sleep in Human Glucose Regulation”. *Endocrine Reviews* 18.5 (1997), 716–738.
- [270] S. Galván-Peña and L. A. O’Neill. “Metabolic Reprograming in Macrophage Polarization”. *Frontiers in Immunology* 5 (2014), 420.
- [271] N. C. Williams and L. A. J. O’Neill. “A Role for the Krebs Cycle Intermediate Citrate in Metabolic Reprogramming in Innate Immunity and Inflammation”. *Frontiers in Immunology* 9 (2018), 141.
- [272] M. Müller, M. A. G. Hernández, G. H. Goossens, et al. “Circulating but not faecal short-chain fatty acids are related to insulin sensitivity, lipolysis and GLP-1 concentrations in humans”. *Scientific Reports* 9.1 (2019), 12515.
- [273] K. A. Dyar, D. Lutter, A. Artati, et al. “Atlas of Circadian Metabolism Reveals System-wide Coordination and Communication between Clocks”. *Cell* 174.6 (2018), 1571–1585.e11.
- [274] K. L. Knutson and E. Van Cauter. “Associations between Sleep Loss and Increased Risk of Obesity and Diabetes”. *Annals of the New York Academy of Sciences* 1129.1 (2008), 287–304.
- [275] A. Malhotra and D. P. White. “Obstructive sleep apnoea”. *The Lancet* 360.9328 (2002), 237–245.

- [276] P. Lévy, M. Kohler, W. T. McNicholas, et al. “Obstructive sleep apnoea syndrome”. *Nature Reviews Disease Primers* 1.1 (2015), 15015.
- [277] E. I. Schwarz, A. Engler, and M. Kohler. “Exhaled breath analysis in obstructive sleep apnea”. *Expert review of respiratory medicine* 11.8 (2017), 631–639.
- [278] S. Tregear, J. Reston, K. Schoelles, and B. Phillips. “Obstructive sleep apnea and risk of motor vehicle crash: systematic review and meta-analysis”. *Journal of clinical sleep medicine* 5.6 (2009), 573–81.
- [279] J. M. Marin, S. J. Carrizo, E. Vicente, and A. G. Agusti. “Long-term cardiovascular outcomes in men with obstructive sleep apnoea-hypopnoea with or without treatment with continuous positive airway pressure: an observational study”. *The Lancet* 365.9464 (2005), 1046–1053.
- [280] F. J. Nieto, T. B. Young, B. K. Lind, et al. “Association of Sleep-Disordered Breathing, Sleep Apnea, and Hypertension in a Large Community-Based Study”. *JAMA* 283.14 (2000), 1829.
- [281] J. G. Park, T. M. Morgenthaler, and P. C. Gay. “Novel and Emerging Nonpositive Airway Pressure Therapies for Sleep Apnea”. *Chest* 144.6 (2013), 1946–1952.
- [282] T. E. Weaver and R. R. Grunstein. “Adherence to Continuous Positive Airway Pressure Therapy: The Challenge to Effective Treatment”. *Proceedings of the American Thoracic Society* 5.2 (2008), 173–178.
- [283] N McArdle, G Devereux, H Heidarnjad, H. M. Engleman, T. W. Mackay, and N. J. Douglas. “Long-term use of CPAP therapy for sleep apnea/hypopnea syndrome”. *American journal of respiratory and critical care medicine* 159.4 Pt 1 (1999), 1108–14.
- [284] C. A. Kushida, M. R. Littner, T. Morgenthaler, et al. “Practice Parameters for the Indications for Polysomnography and Related Procedures: An Update for 2005”. *Sleep* 28.4 (2005), 499–523.
- [285] W. T. McNicholas. “Diagnosis of Obstructive Sleep Apnea in Adults”. *Proceedings of the American Thoracic Society* 5.2 (2008), 154–160.
- [286] M. Roeder, M. Bradicich, E. I. Schwarz, S. Thiel, T. Gaisl, U. Held, and M. Kohler. “Night-to-night variability of respiratory events in obstructive sleep apnoea: a systematic review and meta-analysis”. *Thorax* (2020), thoraxjnl–2020–214544.
- [287] F. Chung, B. Yegneswaran, P. Liao, et al. “STOP Questionnaire”. *Anesthesiology* 108.5 (2008), 812–821.
- [288] N. C. Netzer, R. A. Stoohs, C. M. Netzer, K. Clark, and K. P. Strohl. “Using the Berlin Questionnaire To Identify Patients at Risk for the Sleep Apnea Syndrome”. *Annals of Internal Medicine* 131.7 (1999), 485.
- [289] H. Marti-Soler, C. Hirotsu, P. Marques-Vidal, et al. “The NoSAS score for screening of sleep-disordered breathing: a derivation and validation study.” *The Lancet. Respiratory medicine* 4.9 (2016), 742–748.
- [290] J. Pereira, P. Porto-Figueira, C. Cavaco, et al. “Breath Analysis as a Potential and Non-Invasive Frontier in Disease Diagnosis: An Overview”. *Metabolites* 5.1 (2015), 3–55.

- [291] T. Greulich, A. Hattesoehl, A. Grabisch, et al. "Detection of obstructive sleep apnoea by an electronic nose." *The European respiratory journal* 42.1 (2013), 145–55.
- [292] P. Benedek, Z. Lázár, A. Bikov, L. Kunos, G. Katona, and I. Horváth. "Exhaled biomarker pattern is altered in children with obstructive sleep apnoea syndrome". *International journal of pediatric otorhinolaryngology* 77.8 (2013), 1244–7.
- [293] S. Dragonieri, F. Porcelli, F. Longobardi, et al. "An electronic nose in the discrimination of obese patients with and without obstructive sleep apnoea". *Journal of Breath Research* 9.2 (2015), 026005.
- [294] L. Kunos, A. Bikov, Z. Lazar, B. Z. Korosi, P. Benedek, G. Losonczy, and I. Horvath. "Evening and morning exhaled volatile compound patterns are different in obstructive sleep apnoea assessed with electronic nose". *Sleep and Breathing* 19.1 (2015), 247–253.
- [295] R. B. Berry, R. Budhiraja, D. J. Gottlieb, et al. "Rules for scoring respiratory events in sleep: update of the 2007 AASM Manual for the Scoring of Sleep and Associated Events. Deliberations of the Sleep Apnea Definitions Task Force of the American Academy of Sleep Medicine". *Journal of clinical sleep medicine* 8.5 (2012), 597–619.
- [296] W. E. Johnson, C. Li, and A. Rabinovic. "Adjusting batch effects in microarray expression data using empirical Bayes methods". *Biostatistics* 8.1 (2007), 118–127.
- [297] D. García-Gómez, L. Bregy, C. Barrios-Collado, G. Vidal-de Miguel, and R. Zenobi. "Real-Time High-Resolution Tandem Mass Spectrometry Identifies Furan Derivatives in Exhaled Breath". *Analytical Chemistry* 87.13 (2015), 6919–6924.
- [298] D. García-Gómez, P. Martínez-Lozano Sinues, C. Barrios-Collado, G. Vidal-de Miguel, M. Gaugg, and R. Zenobi. "Identification of 2-alkenals, 4-hydroxy-2-alkenals, and 4-hydroxy-2,6-alkadienals in exhaled breath condensate by UHPLC-HRMS and in breath by real-time HRMS." *Analytical chemistry* 87.5 (2015), 3087–93.
- [299] D. García-Gómez, L. Bregy, Y. Nussbaumer-Ochsner, T. Gaisl, M. Kohler, and R. Zenobi. "Detection and Quantification of Benzothiazoles in Exhaled Breath and Exhaled Breath Condensate by Real-Time Secondary Electrospray Ionization-High-Resolution Mass Spectrometry and Ultra-High Performance Liquid Chromatography." *Environmental science & technology* 49.20 (2015), 12519–24.
- [300] G. B. Hanna, P. R. Boshier, S. R. Markar, and A. Romano. "Accuracy and Methodologic Challenges of Volatile Organic Compound-Based Exhaled Breath Tests for Cancer Diagnosis". *JAMA Oncology* 5.1 (2019), e182815.
- [301] M. Guillevic, M. K. Vollmer, S. A. Wyss, et al. "Dynamic-gravimetric preparation of metrologically traceable primary calibration standards for halogenated greenhouse gases". *Atmospheric Measurement Techniques* 11.6 (2018), 3351–3372.
- [302] A. Lebkuchen, V. M. Carvalho, G. Venturini, et al. "Metabolomic and lipidomic profile in men with obstructive sleep apnoea: implications for diagnosis and biomarkers of cardiovascular risk". *Scientific Reports* 8.1 (2018), 11270.
- [303] D. Bell-Pedersen, V. M. Cassone, D. J. Earnest, S. S. Golden, P. E. Hardin, T. L. Thomas, and M. J. Zoran. *Circadian rhythms from multiple oscillators: Lessons from diverse organisms*. 2005.

- [304] J. A. Mohawk, C. B. Green, and J. S. Takahashi. “Central and peripheral circadian clocks in mammals”. *Annual review of neuroscience* 35 (2012), 445–62.
- [305] T. Hirota and Y. Fukada. “Resetting Mechanism of Central and Peripheral Circadian Clocks in Mammals”. *Zoological Science* 21.4 (2004), 359–368.
- [306] F. Gachon, E. Nagoshi, S. A. Brown, J. Ripperger, and U. Schibler. *The mammalian circadian timing system: From gene expression to physiology*. 2004.
- [307] J. Hernández-García, D. Navas-Carrillo, and E. Orenes-Piñero. “Alterations of circadian rhythms and their impact on obesity, metabolic syndrome and cardiovascular diseases”. *Critical Reviews in Food Science and Nutrition* 60.6 (2020), 1038–1047.
- [308] E. M. Scott. “Circadian clocks, obesity and cardiometabolic function”. *Diabetes, Obesity and Metabolism* 17.S1 (2015), 84–89.
- [309] U. Albrecht. “The circadian clock, metabolism and obesity”. *Obesity Reviews* 18 (2017), 25–33.
- [310] K. A. Lamia, K.-F. Storch, and C. J. Weitz. “Physiological significance of a peripheral tissue circadian clock”. *Proceedings of the National Academy of Sciences* 105.39 (2008), 15172–15177.
- [311] H. Cho, X. Zhao, M. Hatori, et al. “Regulation of circadian behaviour and metabolism by REV-ERB-alpha and REV-ERB-beta”. *Nature* 485.7396 (2012), 123–127.
- [312] J. Delezie, S. Dumont, H. Dardente, et al. “The nuclear receptor REV-ERBalpha is required for the daily balance of carbohydrate and lipid metabolism”. *The FASEB Journal* 26.8 (2012), 3321–3335.
- [313] G. Le Martelot, T. Claudel, D. Gatfield, et al. “REV-ERBalpha Participates in Circadian SREBP Signaling and Bile Acid Homeostasis”. *PLoS Biology* 7.9 (2009). Ed. by A. J. Vidal-Puig, e1000181.
- [314] Y. Nakahata, M. Kaluzova, B. Grimaldi, et al. “The NAD<sup>+</sup>-Dependent Deacetylase SIRT1 Modulates CLOCK-Mediated Chromatin Remodeling and Circadian Control”. *Cell* 134.2 (2008), 329–340.
- [315] M. J. Prasai, J. T. George, and E. M. Scott. “Molecular clocks, type 2 diabetes and cardiovascular disease”. *Diabetes and Vascular Disease Research* 5.2 (2008), 89–95.
- [316] E. M. Scott, A. M. Carter, and P. J. Grant. “Association between polymorphisms in the Clock gene, obesity and the metabolic syndrome in man”. *International Journal of Obesity* 32.4 (2008), 658–662.
- [317] P. Gomez-Abella/n, C. Gomez-Santos, J. A. Madrid, et al. “Circadian Expression of Adiponectin and Its Receptors in Human Adipose Tissue”. *Endocrinology* 151.1 (2010), 115–122.
- [318] L. Pagani, K. Schmitt, F. Meier, et al. “Serum factors in older individuals change cellular clock properties”. *Proceedings of the National Academy of Sciences* 108.17 (2011), 7218–7223.



- [319] J. R. Toledo, Y. Prieto, N. Oramas, and O. Sánchez. “Polyethylenimine-Based Transfection Method as a Simple and Effective Way to Produce Recombinant Lentiviral Vectors”. *Applied Biochemistry and Biotechnology* 157.3 (2009), 538–544.
- [320] C. A. Smith, E. J. Want, G. O’Maille, R. Abagyan, and G. Siuzdak. “XCMS: Processing Mass Spectrometry Data for Metabolite Profiling Using Nonlinear Peak Alignment, Matching, and Identification”. *Analytical Chemistry* 78.3 (2006), 779–787.
- [321] R. Tautenhahn, C. Böttcher, and S. Neumann. “Highly sensitive feature detection for high resolution LC/MS”. *BMC Bioinformatics* 9.1 (2008), 504.
- [322] H. Luan, F. Ji, Y. Chen, and Z. Cai. “statTarget: A streamlined tool for signal drift correction and interpretations of quantitative mass spectrometry-based omics data”. *Analytica Chimica Acta* 1036 (2018), 66–72.
- [323] A Wolfer and G Correia. *PeakPanther: Peak Picking and Annotation of High Resolution Experiments*. 2020.
- [324] K. G. M. Alberti, P. Zimmet, and J. Shaw. “The metabolic syndrome—a new worldwide definition”. *The Lancet* 366.9491 (2005), 1059–1062.
- [325] K. Bora, M. S. Pathak, P. Borah, and D. Das. “Association of Decreased High-Density Lipoprotein Cholesterol (HDL-C) With Obesity and Risk Estimates for Decreased HDL-C Attributable to Obesity”. *Journal of Primary Care & Community Health* 8.1 (2017), 26–30.
- [326] A. Nagarajan, M. C. Petersen, A. R. Nasiri, et al. “MARCH1 regulates insulin sensitivity by controlling cell surface insulin receptor levels”. *Nature Communications* 7.1 (2016), 12639.
- [327] M. Mongraw-Chaffin, M. C. Foster, C. A. Anderson, et al. “Metabolically Healthy Obesity, Transition to Metabolic Syndrome, and Cardiovascular Risk”. *Journal of the American College of Cardiology* 71.17 (2018), 1857–1865.
- [328] Y. Zhang, S. Guo, C. Xie, and J. Fang. “Uridine Metabolism and Its Role in Glucose, Lipid, and Amino Acid Homeostasis”. *BioMed Research International* 2020 (2020), 1–7.
- [329] Y. Deng, Z. V. Wang, R. Gordillo, et al. “An adipo-biliary-uridine axis that regulates energy homeostasis”. *Science* 355.6330 (2017), eaaf5375.
- [330] J. A. de Miranda, G. G. Almeida, R. I. L. Martins, et al. “The role of uric acid in the insulin resistance in children and adolescents with obesity”. *Revista paulista de pediatria : orgao oficial da Sociedade de Pediatria de Sao Paulo* 33.4 (2015), 431–6.
- [331] R. Seibert, F. Abbasi, F. M. Hantash, M. P. Caulfield, G. Reaven, and S. H. Kim. “Relationship between insulin resistance and amino acids in women and men”. *Physiological Reports* 3.5 (2015), e12392.
- [332] M. Favennec, B. Hennart, R. Caiazzo, et al. “The kynurenine pathway is activated in human obesity and shifted toward kynurenine monooxygenase activation”. *Obesity* 23.10 (2015), 2066–2074.

- [333] G. Oxenkrug. “Insulin Resistance and Dysregulation of Tryptophan-Kynurenine and Kynurenine-Nicotinamide Adenine Dinucleotide Metabolic Pathways”. *Molecular Neurobiology* 48.2 (2013), 294–301.
- [334] C. Alarcon, B. Wicksteed, M. Prentki, B. E. Corkey, and C. J. Rhodes. “Succinate Is a Preferential Metabolic Stimulus-Coupling Signal for Glucose-Induced Proinsulin Biosynthesis Translation”. *Diabetes* 51.8 (2002), 2496–2504.
- [335] H. Yoshitomi, M. Momoo, X. Ma, Y. Huang, S. Suguro, Y. Yamagishi, and M. Gao. “L-Citrulline increases hepatic sensitivity to insulin by reducing the phosphorylation of serine 1101 in insulin receptor substrate-1”. *BMC Complementary and Alternative Medicine* 15.1 (2015), 188.
- [336] K. Capito and C. J. Hedekov. “Inosine-stimulated insulin release and metabolism of inosine in isolated mouse pancreatic islets”. *Biochemical Journal* 158.2 (1976), 335–340.
- [337] O. A. Smiseth, P. Gunnes, T. Sand, and O. D. Mjøs. “Inosine causing insulin release and increased myocardial uptake of carbohydrates relative to free fatty acids in dogs”. *Clinical Physiology* 9.1 (1989), 27–38.
- [338] J. Lu, G. Xie, W. Jia, and W. Jia. “Insulin resistance and the metabolism of branched-chain amino acids”. *Frontiers of Medicine* 7.1 (2013), 53–59.
- [339] M.-S. Yoon. “The Emerging Role of Branched-Chain Amino Acids in Insulin Resistance and Metabolism”. *Nutrients* 8.7 (2016), 405.
- [340] C. J. Lynch and S. H. Adams. “Branched-chain amino acids in metabolic signalling and insulin resistance”. *Nature Reviews Endocrinology* 10.12 (2014), 723–736.
- [341] M. M. Adeva, J. Calviño, G. Souto, and C. Donapetry. “Insulin resistance and the metabolism of branched-chain amino acids in humans”. *Amino Acids* 43.1 (2012), 171–181.
- [342] X. Zheng and A. Sehgal. “AKT and TOR Signaling Set the Pace of the Circadian Pacing”. *Current Biology* 20.13 (2010), 1203–1208.
- [343] P. Crosby, R. Hamnett, M. Putker, et al. “Insulin/IGF-1 Drives PERIOD Synthesis to Entrain Circadian Rhythms with Feeding Time”. *Cell* 177.4 (2019), 896–909.e20.
- [344] S. M. Reppert and D. R. Weaver. “Coordination of circadian timing in mammals.” *Nature* 418.6901 (2002), 935–41.
- [345] A. Knutsson, T. Akerstedt, B. G. Jonsson, and K. Orth-Gomer. “Increased risk of ischaemic heart disease in shift workers”. *Lancet (London, England)* 2 (1986), 89–92.
- [346] E. S. Schernhammer, F. Laden, F. E. Speizer, W. C. Willett, D. J. Hunter, I. Kawachi, and G. A. Colditz. “Rotating Night Shifts and Risk of Breast Cancer in Women Participating in the Nurses’ Health Study”. *JNCI Journal of the National Cancer Institute* 93.20 (2001), 1563–1568.
- [347] M. J. Paul and W. J. Schwartz. “Circadian Rhythms: How Does a Reindeer Tell Time?” *Current Biology* 20.6 (2010), R280–R282.

- [348] B. E. H. van Oort, N. J. C. Tyler, M. P. Gerkema, L. Folkow, A. S. Blix, and K.-A. Stokkan. “Circadian organization in reindeer”. *Nature* 438.7071 (2005), 1095–1096.
- [349] B. E. H. van Oort, N. J. C. Tyler, M. P. Gerkema, L. Folkow, and K.-A. Stokkan. “Where clocks are redundant: weak circadian mechanisms in reindeer living under polar photic conditions”. *Naturwissenschaften* 94.3 (2007), 183–194.
- [350] D. Hazlerigg, A. S. Blix, and K.-A. Stokkan. “Waiting for the Sun: the circannual programme of reindeer is delayed by the recurrence of rhythmical melatonin secretion after the arctic night.” *The Journal of experimental biology* 220.Pt 21 (2017), 3869–3872.
- [351] K.-A. Stokkan, B. E. H. van Oort, N. J. C. Tyler, and A. S. I. Loudon. “Adaptations for life in the Arctic: evidence that melatonin rhythms in reindeer are not driven by a circadian oscillator but remain acutely sensitive to environmental photoperiod”. *Journal of Pineal Research* 43.3 (2007), 289–293.
- [352] W. Lu, Q.-J. Meng, N. J. Tyler, K.-A. Stokkan, and A. S. Loudon. “A Circadian Clock Is Not Required in an Arctic Mammal”. *Current Biology* 20.6 (2010), 533–537.
- [353] T. S. Larsen, H Lagercrantz, R. A. Riemersma, and A. S. Blix. “Seasonal changes in blood lipids, adrenaline, noradrenaline, glucose and insulin in Norwegian reindeer”. *Acta physiologica Scandinavica* 124.1 (1985), 53–9.
- [354] W. Arnold, T. Ruf, L. E. Loe, R. J. Irvine, E. Ropstad, V. Veiberg, and S. D. Albon. “Circadian rhythmicity persists through the Polar night and midnight sun in Svalbard reindeer”. *Scientific Reports* 8.1 (2018), 14466.
- [355] B. Schmid, C. Helfrich-Förster, and T. Yoshii. “A new ImageJ plug-in ActogramJ for chronobiological analyses”. *Journal of biological rhythms* 26.5 (2011), 464–7.
- [356] P. Salmon and D. Trono. “Production and Titration of Lentiviral Vectors”. *Current Protocols in Human Genetics* 54.1 (2007), 12.10.1–12.10.24.
- [357] J. M. Singer and J. J. Hughey. “LimoRhyde: A Flexible Approach for Differential Analysis of Rhythmic Transcriptome Data”. *Journal of biological rhythms* 34.1 (2019), 5–18.
- [358] J. J. Hughey, T. Hastie, and A. J. Butte. “ZeitZeiger: supervised learning for high-dimensional data from an oscillatory system”. *Nucleic Acids Research* 44.8 (2016), e80–e80.
- [359] J. Å. Riseth, H. Tømmervik, E. Helander-Renvall, et al. “Sámi traditional ecological knowledge as a guide to science: snow, ice and reindeer pasture facing climate change”. *Polar Record* 47.3 (2011), 202–217.
- [360] E. C.-P. Chua, G. Shui, I. T.-G. Lee, et al. “Extensive diversity in circadian regulation of plasma lipids and evidence for different circadian metabolic phenotypes in humans.” *Proceedings of the National Academy of Sciences of the United States of America* 110.35 (2013), 14468–73.
- [361] J.-L. L. Jernsletten and K. Klokov. *Sustainable Reindeer Husbandry*. Tech. rep. Centre for Saami Studies, University of Tromsø, 2002, pp. 1–7.

- [362] I. E. Beltran, P. Gregorini, J. Daza, O. A. Balocchi, A. Morales, and R. G. Pulido. “Diurnal Concentration of Urinary Nitrogen and Rumen Ammonia Are Modified by Timing and Mass of Herbage Allocation”. *Animals* 9.11 (2019), 961.
- [363] A. Bach, S. Calsamiglia, and M. Stern. “Nitrogen Metabolism in the Rumen”. *Journal of Dairy Science* 88 (2005), E9–E21.
- [364] F. Gachon, E. Nagoshi, S. A. Brown, J. Ripperger, and U. Schibler. “The mammalian circadian timing system: from gene expression to physiology.” *Chromosoma* 113.3 (2004), 103–12.
- [365] C. Stentoft, B. A. Røjen, S. K. Jensen, N. B. Kristensen, M. Vestergaard, and M. Larsen. “Absorption and intermediary metabolism of purines and pyrimidines in lactating dairy cows”. *British Journal of Nutrition* 113.4 (2015), 560–573.
- [366] R. P. Smith, D. Veale, a. L. Patrick, and B. Royal. “Obstrutive sleep apnoea and the autonomic nervous system”. *Sleep Medicine Reviews* 2.2 (1998), 69–92.
- [367] L. Janský, P. Šrámek, J. Šavlíková, B. Uličný, H. Janáková, and K. Horký. “Change in sympathetic activity, cardiovascular functions and plasma hormone concentrations due to cold water immersion in men”. *European Journal of Applied Physiology and Occupational Physiology* 74.1-2 (1996), 148–152.
- [368] J. D. Altman, A. U. Trendelenburg, L MacMillan, et al. “Abnormal regulation of the sympathetic nervous system in alpha2A-adrenergic receptor knockout mice”. *Molecular pharmacology* 56.1 (1999), 154–61.
- [369] M. Eichler. “Causal inference in time series analysis”. In: *Causality - Statistical Perspectives and Applications*. Ed. by C. Berzuini, P. Dawid, and L. Bernardinelli. Wiley Online Library Chichester, 2012, pp. 327–352.
- [370] H. Lütkepohl. “Stable vector autoregressive processes”. In: *New Introduction to Multiple Time Series Analysis*. Springer Science and Business Media, 2005, pp. 13–68.
- [371] I. Goodfellow, Y. Bengio, and A. Courville. *Deep learning*. MIT press Cambridge, 2016.
- [372] J. Peters, D. Janzing, and B. Schölkopf. “Time Series”. In: *Elements of Causal Inference*. Ed. by J. Peters, D. Janzing, and B. Schölkopf. Cambridge: MIT press, 2017, pp. 197–211.
- [373] A. Tank, I. Cover, N. J. Foti, A. Shojaie, and E. B. Fox. “An interpretable and sparse neural network model for nonlinear granger causality discovery”. *arXiv preprint arXiv:1711.08160* (2017).
- [374] H. Zou and T. Hastie. “Regularization and variable selection via the elastic net”. *Journal of the Royal Statistical Society: Series B (Statistical Methodology)* 67.2 (2005), 301–320.

# Appendices





## Abbreviations

ACE	angiotensin-converting enzyme
ADP	adenosine diphosphate
AHI	apnea-hypopnea index
AMPK	adenosine monophosphate dependent protein kinase
ARB	angiotensin-receptor blocker
ASAT	aspartate-aminotransferase
ATP	adenosine triphosphate
AUC	area under the curve
AUROC	area under the receiver operating characteristic curve
BCAA	branched-chain amino acids
BMAL1	aryl hydrocarbon receptor nuclear translocator-like protein 1
BMI	body mass index
CCGs	clock controlled genes
CI	confidence interval
CK1	Casein Kinase 1
CLOCK	circadian locomotor output cycles kaput protein
cMLP	componentwise multilayer perceptron
CPAP	continuous positive airway pressure
Cry	Cryochrome
CSF	cerebrospinal fluid
CV	cross validation
DD	dark-dark
DMH	dorsomedial nucleus of the hypothalamus
DRP1	dynamain-related protein 1
EBC	exhaled breath condensate
ECG	electrocardiography
EEG	electroencephalography
EMG	electromyography

EOG	electrooculography
ESI	electrospray ionization
ESS	Epworth Sleepiness Scale
FCS	fetal calf serum
FEV1	forced expiratory volume in one second
FNR	false negative rate
FPR	false positive rate
FVC	expiratory forced vital capacity
GABA	gamma-aminobutyric
GC	gas chromatography
GC-MLP	Granger causal multilayer perceptron
GHRH	growth hormone releasing hormone
GLP-1	glucagon-like peptide 1
GWAS	genome-wide association study
HbA1c	glycated hemoglobin
HDL	high-density lipoprotein
HPLC	high-performance liquid chromatography
(HR)MS	(high-resolution) mass spectrometry
ID	identification
IL	interleukin
IQR	inter-quartile range
IRS-1	insulin receptor substrate 1
KS-test	Kolmogorow-Smirnow
LC	liquid chromatography
LD	light-dark
LDL	low-density lipoprotein
LL	light-light
m/z	mass-to-charge ratio
MAP	mitogen-activated protein
MCP	microchannel plate
MCTQ	Munich chronotype questionnaire
MLP	multilayer perceptron
MOI	multiplicity of infection
MS/MS	tandem mass spectrometry
MSn	multistage mass spectrometry
mTOR	mechanistic target of rapamycin
mTORC1	mechanistic target of rapamycin complex 1
NA	non applicable
NAD+	oxidated form of nicotinamide adenine dinucleotide
NADH	reduced form of nicotinamide adenine dinucleotide
NMR	nuclear magnetic resonance
NN	neural networks
NONO	non-POU domain-containing octamerbinding
NREM	protein



---

ODI	oxygen desaturation index
OSA	obstructive sleep apnea
PBS	phosphate buffered saline
PCA	principal component analysis
Per	Period gene
PSG	polysomnography
PTR-MS	proton transfer reaction mass spectrometry
QC	quality control
REM	rapid eye movement
RNA	ribonucleic acid
ROC	receiver operating characteristic
ROR	retinoic acid receptor-related orphan receptor
RP	reversed phase or respiratory polygraphy in OSA chapter
SCFA	short-chain fatty acid
SCN	suprachiasmatic nucleus
SD	standard deviation
SESI	secondary electrospray ionization
SIFT-MS	selected ion flow tube mass spectrometry
SIRT1	Sirtuin-1
SLD	sublaterodorsal
SNP	single nucleotide polymorphism
SUR1	sulfonylurea receptor 1
SVM	support vector machine
SWS	slow-wave sleep
T2D	type 2 diabetes
TCA cycle	tricarboxylic acid cycle
TMN	tuberomammillary nucleus
TNF	tumor necrosis factor
TNR	true negative rate
TOF	time of flight
TPR	true positive rate
tR	retention time
TSH	thyroid stimulating hormone
UPLC	ultra-high performance liquid chromatography
VAR	vector autoregression
vIPAG	ventrolateral part of the periaqueductal grey matter
VLPO	ventrolateral preoptic nucleus
VOC	volatile organic compound
WK	wakefulness



B

Supplementary information

## B.1. Rapid and reversible control of human metabolism by individual sleep states

### B.1.1. Inferring nonlinear Granger causality with neural networks

The Granger causality approach that we adopt has seen few applications in the analysis of time course MS data. This method has several advantages over conventional approaches, such as correlation analysis and analysis of variance (ANOVA):

- It can represent non-additive nonlinear dependencies between sleep stage labels and multiple mass spectrometric features;
- It deals with time series in a principled way and can account for time-delayed (auto)regressive relationships;
- Granger causality is a directed relationship, whereas (cross-)correlation does not focus on precedence in time;
- It does not merely examine marginal relationships, it performs multiple regression.

More formally, when inferring Granger causality, we consider the following setting. We assume that we are given  $N$  replicates of MS and sleep stage time series retrieved from  $N$  different subjects. These time series include:

- A categorically-valued sleep stage time series  $\{Y_t\}_{t=1}^T$ ,  $Y_t \in \{W, N_1, N_2, N_3, R\}$ , for each  $t$ ;
- $M$  continuously-valued time series  $\{X_t^j\}_{t=1}^T$ , where  $j = 1, \dots, p-1$ , and  $X_t^j$  corresponds to the relative intensity of ion  $j$  in the mass spectrum of exhaled breath at time step  $t$ .

Our goal is then to identify metabolites that are causally related to sleep stages, i.e. metabolites that drive the sleep stage, denoted by  $X^j \rightarrow Y$ , and metabolites that are driven by the stage,  $Y \rightarrow X^j$ .

#### B.1.1.1. Granger causality

Granger causality, introduced by C. W. J. Granger<sup>258</sup> is one of the most popular approaches to practical causal time series analysis. Intuitively, if time series  $X$  is a cause of  $Y$ , then the past of  $X$  should be useful for predicting the future of  $Y$ .<sup>369</sup> Formally, Granger causality from stationary time series  $\{X_t\}_{t \in \mathbb{Z}}$  to  $\{Y_t\}_{t \in \mathbb{Z}}$  can be defined as follows.<sup>369</sup> Let  $\mathcal{I}^*(t-1)$  be an information set containing all information available in the universe up to time  $t-1$ , and let  $\mathcal{I}_{-X}^*(t-1)$  be the same set as  $\mathcal{I}^*(t-1)$ , but with values of time series  $X$  removed (up to time  $t-1$ ). We say that  $X$  Granger-causes  $Y$  if and only if  $Y_t$  and  $\mathcal{I}^*(t-1)$  are not conditionally independent given  $\mathcal{I}_{-X}^*(t-1)$ , for all  $t \in \mathbb{Z}$ . This definition for the bivariate case can be easily extended to multivariate time series. In practice, Granger causality is often inferred by assuming some time series model, for, instance, vector autoregression (VAR). It can be shown

that in VAR Granger causality can be determined from zero constraints on the coefficients.<sup>370</sup> Although simple and interpretable, such representation does not allow for nonlinearities and complex interactions between variables. Therefore, we leverage highly expressive neural networks (NN)<sup>371</sup> to infer Granger causality.

### B.1.1.2. Limitations of Granger causality

While the concept of Granger causality is practically compelling, it has some shortcomings and can be misleading in certain cases. Granger causality analysis can yield spurious conclusions if the set of considered variables is not *causally sufficient*.<sup>372</sup> For example, if there exist “superior” mechanisms that regulate both metabolism and sleep, statements of causality between ion intensities and sleep phases could be meaningless. (Such superior mechanisms would be biologically logical to imagine.) Issues can also arise if time series are not sampled frequently enough to recover relationships (unlikely in our case) or if there exist instantaneous interactions between variables, which are imaginable in biochemical pathways.<sup>372</sup>

### B.1.1.3. Model

Inspired by componentwise multilayer perceptron (cMLP),<sup>373</sup> we introduce our own feedforward NN architecture for *unsupervised* Granger causal discovery. For the sake of convenience, we refer to it as Granger causal multilayer perceptron (GC-MLP). Supplementary figure B.5 depicts the schematic of a GC-MLP. This network is trained in a *supervised* manner to forecast target time series  $Y$  based on past  $K$  values of predictors  $X^1, X^2, \dots, X^{p-1}$  and  $Y$  itself. Note that the network consists of  $p$  disjoint encoders which produce “hidden” representations for each variable. These representations are then multiplied with *importance weights*  $c_1, c_2, \dots, c_p$  and concatenated into one vector.

Consequently, this vector is fed into a multilayer perceptron (MLP) to compute forecast  $\hat{y}_t$  of  $Y_t$ . Granger causality from  $X^j$  to  $Y$  can then be identified by inspecting importance weight  $c_j$ . Ideally, we expect that  $|c_j| \approx 0$  when  $X^j \not\rightarrow Y$ , and  $|c_j| > 0$  when  $X^j \rightarrow Y$ . The loss function of GC-MLP is crucial for estimating Granger causality. It encourages importance weights to be sparse by using an elastic-net-style<sup>374</sup> term that penalizes  $\ell_1$  and  $\ell_2$  norms of  $c = [c_1 \dots c_p]$ :

$$- \sum_{t=K+1}^T \sum_{j=1}^C \gamma_j \{ (y_t)_j \ln((\hat{y}_t)_j) + (1 - (y_t)_j) \ln(1 - (\hat{y}_t)_j) \} + \lambda (\alpha \|c\|_1 + (1 - \alpha) \|c\|_2^2),$$

where  $K$  is the maximum lag of autoregressive relationships;  $C$  is the number of classes;  $\gamma_j$  is the weight for class  $j$ ;  $\hat{y}_t$  refers to the forecast for the value of  $y_t$ ;  $(v)_j$  stands for the  $j$ -th component of vector  $v$ ;  $\lambda > 0$  is the regularization parameter; and  $\alpha \in [0, 1]$  controls the tradeoff between  $\ell_1$  and  $\ell_2$  penalties. Note that herein  $y_t$  is assumed to be categorical and encoded with the one-hot encoding scheme.

**B.1.1.4. Bootstrapping**

In order to quantify our uncertainty about Granger causal relationships (i.e. to infer a conventional p-value), we leverage bootstrapping.<sup>253</sup> Many GC-MLPs are trained on resampled time series replicates to construct a confidence interval for each  $c_j$  that can be used to decide whether relationship  $X_j \rightarrow Y$  is significant. The full procedure is summarized in Algorithm 1.

---

**Algorithm 1:** Bootstrapping procedure for discovering metabolites with Granger causal associations with sleep stages

---

**Input:**  $N$  replicates of target  $\{Y_t\}_{t=1}^T$  and predictors  $\{X^j\}_{t=1}^T$ , for  $j = 1, \dots, p - 1$ ; maximum lag  $K \in \mathbb{N}$ ; regularization parameter  $\lambda > 0$ ; parameter  $\alpha \in [0, 1]$ ; threshold  $c_{th} > 0$ ; confidence level  $\gamma \in (0, 1)$ ; number of re-samples  $B \in \mathbb{N}$ .

**Output:** Set  $\hat{S}$  of predictors that Granger-cause  $Y$ .

$\hat{S} \leftarrow Y$

**for**  $b = 1$  to  $B$  **do**

Sample  $N$  replicates  $I^b = \{i_1^b, \dots, i_N^b\}$  with replacement from  $I = \{1, \dots, N\}$ .

Train the neural network on replicates in  $I^b$  with parameters  $K$ ,  $\lambda$  and  $\alpha$  using mini-batch gradient descent.

Retrieve absolute values of importance weights  $c_1^{*b}, c_1^{*b}, \dots, c_{p-1}^{*b}$  from the trained model.

**end**

**for**  $j = 1$  to  $p - 1$  **do**

Compute the empirical  $(1 - \gamma)$ -quantile of bootstrapped weights for the  $j$ -th variable

$q_j = q_{c_j^*}(1 - \gamma)$ .

**if**  $q_j \geq c_{th}$  **then**

$\hat{S} \leftarrow \hat{S} \cup \{j\}$

**end**

**return**  $\hat{S}$

---

### B.1.1.5. Time reversal

Algorithm 1 identifies a set of Granger causes of response variable  $Y$ . We might be interested in solving the inverse problem: finding a set of predictors Granger-caused by the response. The naive solution would be to train a GC-MLP for each predictor variable  $X^j$  as the response and identify if  $Y$  Granger-causes  $X^j$ . In high-dimensional mass spectrometric time series, this approach is prohibitively costly. We can leverage time-reversed Granger causality<sup>252</sup> by performing inference on time-reversed sequences. Intuitively, we expect that, if  $Y \rightarrow X^j$ , then the future values of  $X^j$  should be useful for predicting the past values of  $Y$ . Thus, instead of naively training  $p - 1$  models, with time reversal we only need one GC-MLP.

### B.1.1.6. Hyperparameters and network specification

We implemented the model in Python programming language (version 3.7.1) using PyTorch machine learning library (version 1.0.1) We considered (auto-)regressive relationships up to lag  $K = 30$  ( $\approx 300s$ ). We choose the model order sufficiently large, to avoid potential misspecification. Each GC-MLP had 100 hidden units in each encoder and 200 shared hidden units. We set the regularization parameter  $\lambda$  to 0.001 and  $\alpha = 0.8$ . The choice of  $\lambda$  is motivated by simulation experiment results discussed below. In the cross-entropy loss, the weight of 0.9 is assigned to the less prevalent sleep stage, whereas the weight of 0.1 is assigned to the more prevalent one. The training is performed for one epoch by gradient descent using Adam optimizer with mini-batches of 100 data points. For the bootstrapping procedure, we trained  $B = 1000$  models and used parameter values  $c_{th} = 0.0025$  and  $\gamma = 0.95$ .

### B.1.1.7. Cross-validation

To investigate whether it is possible to predict sleep stages solely based on mass spectrometric profiles, we performed cross-validation. Granger causal discoveries discussed before would be meaningless, if trained neural networks possessed no predictive power. During validation we did not include sleep stage time series as a predictor. We used the leave-one-subject-out cross-validation (CV) procedure to see how well GC-MLPs generalize across different subjects. Namely, for each iteration, we left out one subject and trained a neural network on the rest. To evaluate performance, we employed the balanced accuracy score. This metric is more appropriate than the normal accuracy because of imbalances in frequencies of classes. Average balanced accuracy CV scores are shown in supplementary table B.1. For all responses, mean scores are significantly greater-than 0.5 ( $\alpha = 0.05$ ). Thus, on average, in all prediction tasks GC-MLPs perform better than the random classifier. To sum up, the results of cross-validation suggest that there might be some structure in the data driven by differences between stages of sleep.

### B.1.1.8. Simulation experiments

We performed experiments on perturbed mass spectrometry data to verify that our neural network technique for discovering Granger causality behaves as expected. We explored the

number of false discoveries made in different scenarios and investigated the relationship between the number of false discoveries and regularization parameter  $\lambda$ . Note that in these experiments we did not reverse the time series.

First, we examine inference results under permuted ion intensity time series. We considered five features that had been originally discovered as Granger-causing REM sleep stage transitions with mass-to charge ratios 69.070, 118.065, 152.128, 229.252 and 271.299. We generated 10 synthetic datasets wherein we randomly permuted all metabolic time series except for the sequences of these five variables (10 random seeds used). Subsequently, we applied the bootstrapping procedure on these datasets with  $B = 100$  resamples. We expect that none of the variables the time series of which were permuted are identified as causal, whereas the five features that remain fixed should be. In all simulations, every of the invariant variables is discovered as causal. Moreover, none of the permuted time series are falsely claimed to drive the response.

Another experiment we performed was with randomly permuting REM sleep stage labels while keeping metabolic time series untouched. In this setting, we expect our inference technique to identify no variables that are causally related with the permuted target. We ran the bootstrapping procedure on 10 different simulated datasets with  $B = 100$  resamples. In all datasets, no spurious relationships were found from predictors to the target.

Finally, we replaced the original REM signal with a synthetic target time series that behaves like a sleep stage sequence. Similarly, to the setting above, we expect no causal links to be inferred. We performed bootstrapping on 10 simulated datasets with  $B = 100$  resamples. We ran the inference for  $\lambda = 0.10^{-4}, 10^{-3}, 10^{-2}$ . Supplementary table B.3 contains numbers of false discoveries made by the inference technique under different values of  $\lambda$ . Observe that for the largest value almost no false discoveries are made. A decrease in the value of the regularization parameter seems to lead to more spurious causal relationships being inferred. For  $\lambda = 10^{-2}$ , the value we used in the causal analysis of MS and sleep stage time series, on average, 14.4 false discoveries are made. Although this result is not ideal, larger values of the regularization parameter could be, in practice, too conservative and, thus, may lead to inferring a causal graph that is much sparser than the true structure, i.e. the loss of power.

In general, the results of the simulation experiments are promising. The inference technique we proposed behaves as expected on perturbed MS data; and we can adequately control the number of false discoveries with parameter  $\lambda$ .



## B.1.2. Supplementary figures

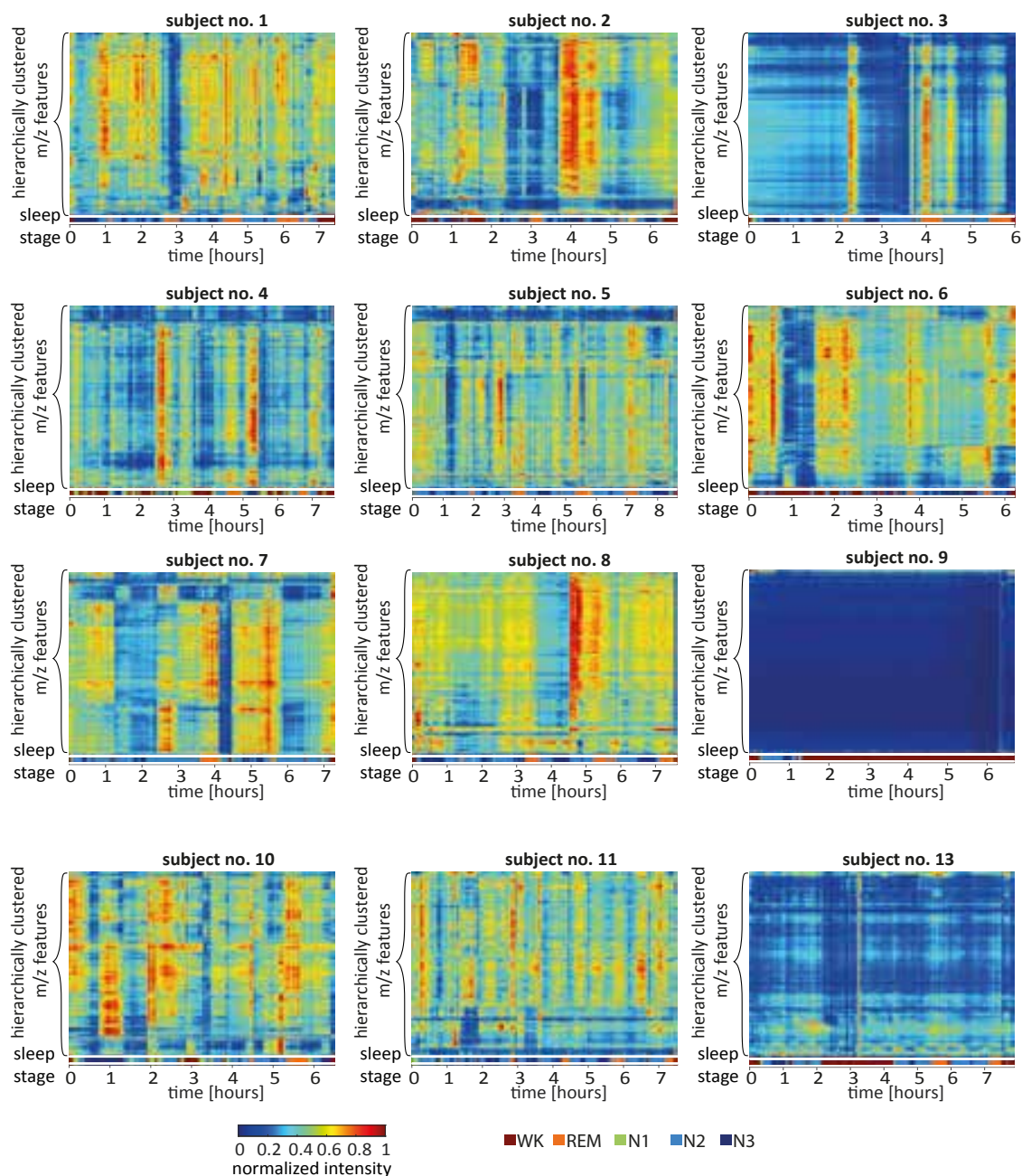


**Figure B.1.:** Heatmap of 1271 m/z features detected in positive ionization mode in all individuals. Subject no. 12 is shown in figure 4.2. Subject no. 9 was awake during almost the whole night and accordingly, nearly no instantaneous metabolic changes were observed in breath. Note that gradual changes across the night are not visible here since the data has been detrended.

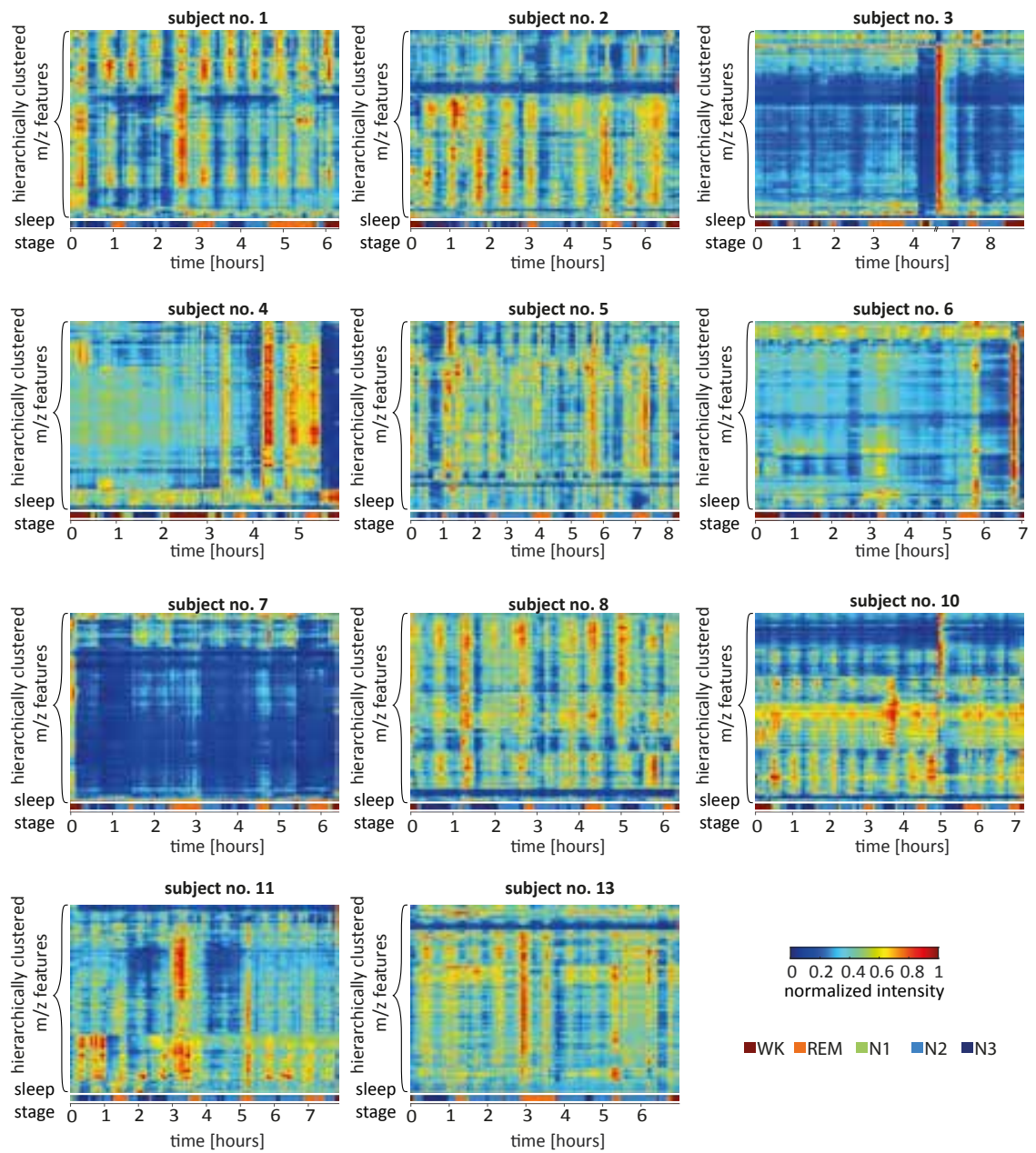


**Figure B.2.:** Heatmap of 725 m/z features detected in negative ionization mode in all individuals. Subject no. 12 is shown in figure 4.2.

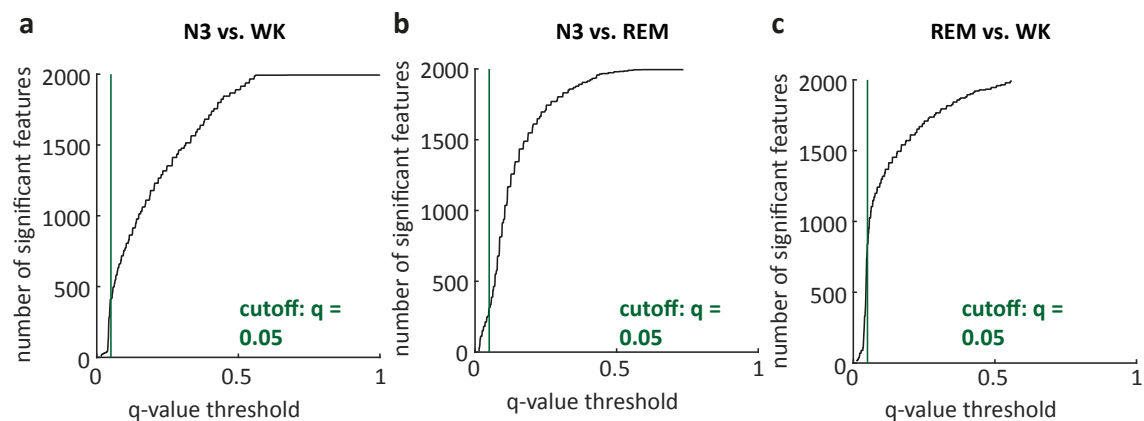


**Figure B.3:** Evolution of numbers of significant m/z features with different significance thresholds of q-values in pairwise comparisons between N3 and WK (a), N3 and REM (b) and REM and WK (c).

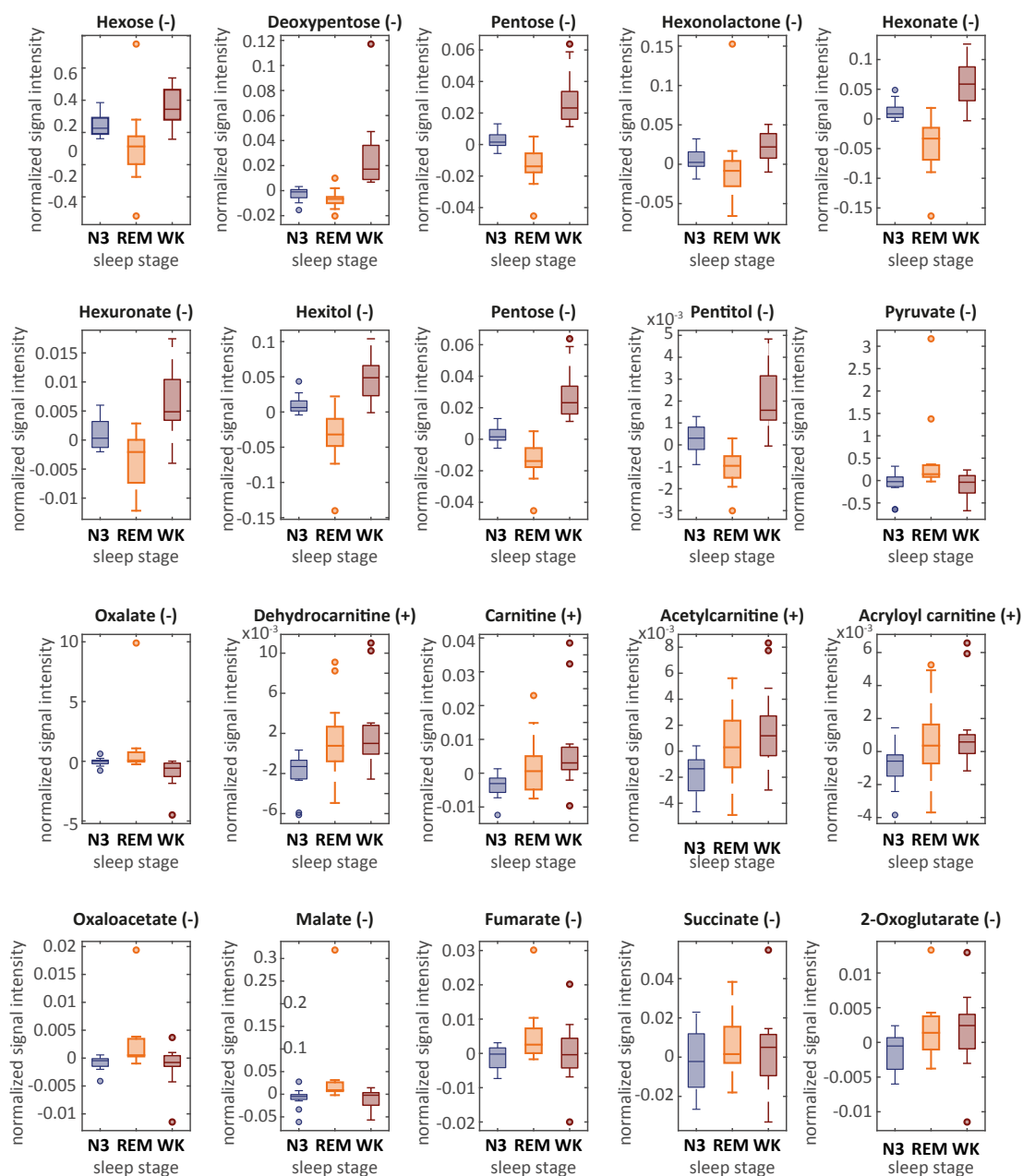
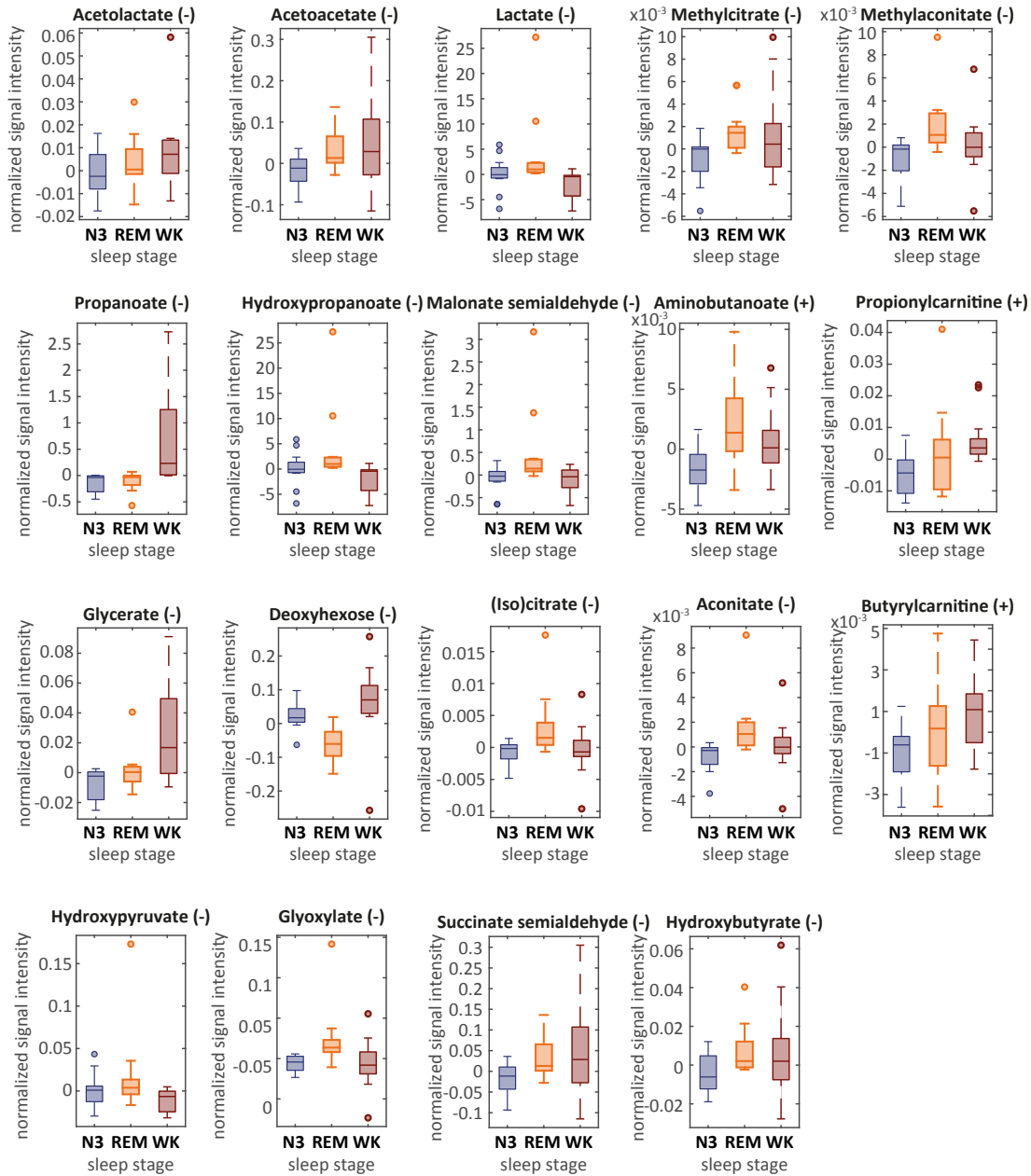


**Figure B.4:** Boxplots of top candidate metabolites for N3 sleep, REM sleep and wakefulness. Boxplots (center line: median, box limits: 25<sup>th</sup> and 75<sup>th</sup> percent quantile, whisker length: 1.5 interquartile range) correspond to metabolites mapped on pathways in figure 4.8.

## B.1. Rapid and reversible control of human metabolism by individual sleep states



The central mark in each box represents the median and the edges of the box correspond to the 25<sup>th</sup> and 75<sup>th</sup> percentiles, respectively. Extreme data points are represented by the whiskers, and outliers are indicated with circles.

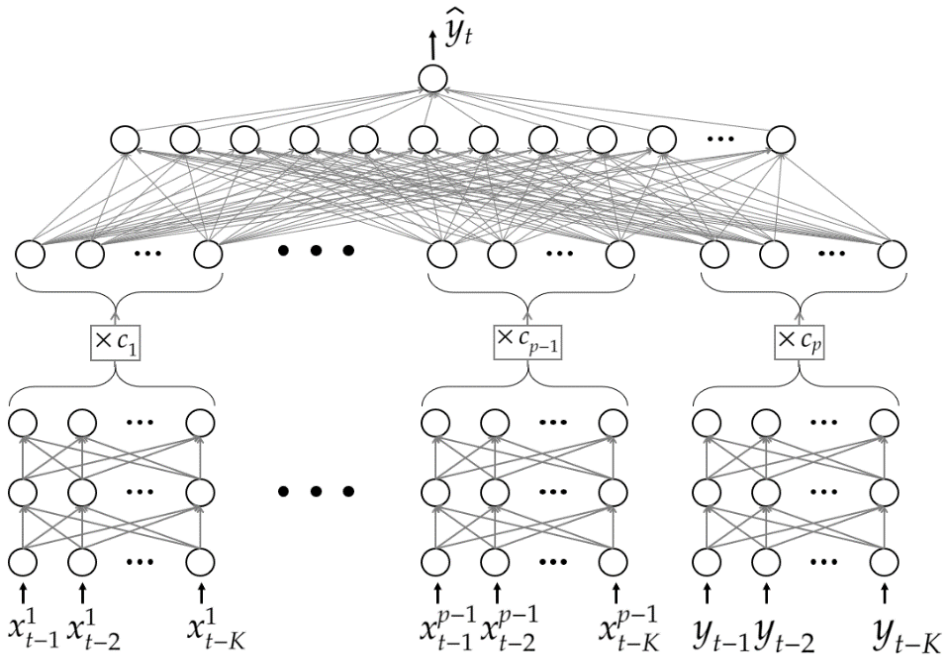


**Figure B.5.:** The schematic of a feedforward neural network for identifying Granger causes of time series  $Y_t$  among predictors  $X_t^1, X_t^2, \dots, X_t^{p-1}$ .

### B.1.3. Supplementary tables

**Table B.1.:** Balanced accuracy scores for predicting past sleep stages based on the future values of metabolic features from the positive mode with neural networks. We used the leave-one-subject-out cross-validation procedure to evaluate classifiers. 95 % confidence intervals for the mean accuracy were constructed with the  $t$ -distribution.

Sleep stage	Average balanced accuracy	95 % t CI for the mean balanced accuracy	ion mode
Wake	0.771	[0.727, 0.815]	positive
N3	0.676	[0.622, 0.729]	positive
REM	0.691	[0.577, 0.806]	positive
Wake	0.763	[0.678, 0.847]	negative
N3	0.67	[0.640, 0.700]	negative
REM	0.747	[0.692, 0.802]	negative

**Table B.2.:** Summary of all features with differential regulation across different stages of vigilance. This table is available online in a curated data archive at ETH Zurich (<https://www.research-collection.ethz.ch>) under the DOI 10.3929/ethz-b-000453100.

**Table B.3.:** Numbers of features falsely identified as Granger-causing the synthetic target time series for different values of the regularization parameter  $\lambda$ .

$\lambda$	Numbers of False Discoveries	Average Number of False Discoveries
0	7, 27, 32, 118, 38, 26, 28, 34, 9, 48	36.7
$10^{-4}$	43, 21, 73, 29, 70, 14, 12, 60, 17, 14	35.3
$10^{-3}$	13, 1, 7, 18, 32, 5, 23, 33, 8, 4	14.4
$10^{-2}$	1, 0, 0, 0, 1, 0, 1, 0, 0, 0	0.3



## B.2. Validation of breath biomarkers for obstructive sleep apnea

### B.2.1. Supplementary results

The classification performance that we estimated with this stratification in the cross-validation based on the training data is considerably lower than the one reported in the pilot study (reported  $AUC_{\text{cross-validation}} = 0.87$ ). Previously, only the ODI was used for stratification. To evaluate whether the metabolic pattern of exhaled breath predicts groups defined only by ODI better, we repeated the classification procedure again with the following grouping criteria: ODI > 30/h (OSA), ODI < 10/h (control) (figure B.12). For the training set we reduced the control group to ODI < 2/h in order to get balanced group sizes (figure B.12). With these stratification criteria we achieved similar predictive performance in the training set as in the pilot study ( $AUC_{\text{cross-validation}} = 0.79$ , figure B.12b and c). Nevertheless, the prediction of the validation set declined to  $AUC = 0.62$  (figure B.12e and f).

Since technical improvements have been made between the pilot study and this validation study and both studies were time-wise separated, we assessed the comparability of both data sets in a principal component analysis (figure B.13a). Even though only a slight shift between the two sets is noticeable, we corrected it successfully by applying a batch correction algorithm based on an Empirical Bayes method (figure B.13b). We subsequently repeated the classification procedure with the adjusted data. The results are presented in figure B.13. However, the AUC improved only by 0.01 to 0.67. The results from all classification procedures are summarized in table B.6.

### B.2.2. Supplementary discussion

We further investigated the samples that were false negatives in all three classification procedures as indicated in supplementary figure B.15. One of them was wearing lipstick, which we observed often to be confounding due to ion suppression caused by prominent plasticizers or other ingredients with a good ionization efficiency. Even though visual inspection of the spectra of this study participant did not capture our attention, it is possible that a contamination from the lipstick compromised the results. The three remaining false negatives have in common that the respiratory polygraphy was not carried out on the same day as the SESI-HRMS breath measurement. It could thus be that the MS-based diagnosis does not match the clinical diagnosis due to night-to-night variability of OSA, which is well-known. To overcome this problem, multiple measurements would be required.



B.2.3. Supplementary figures

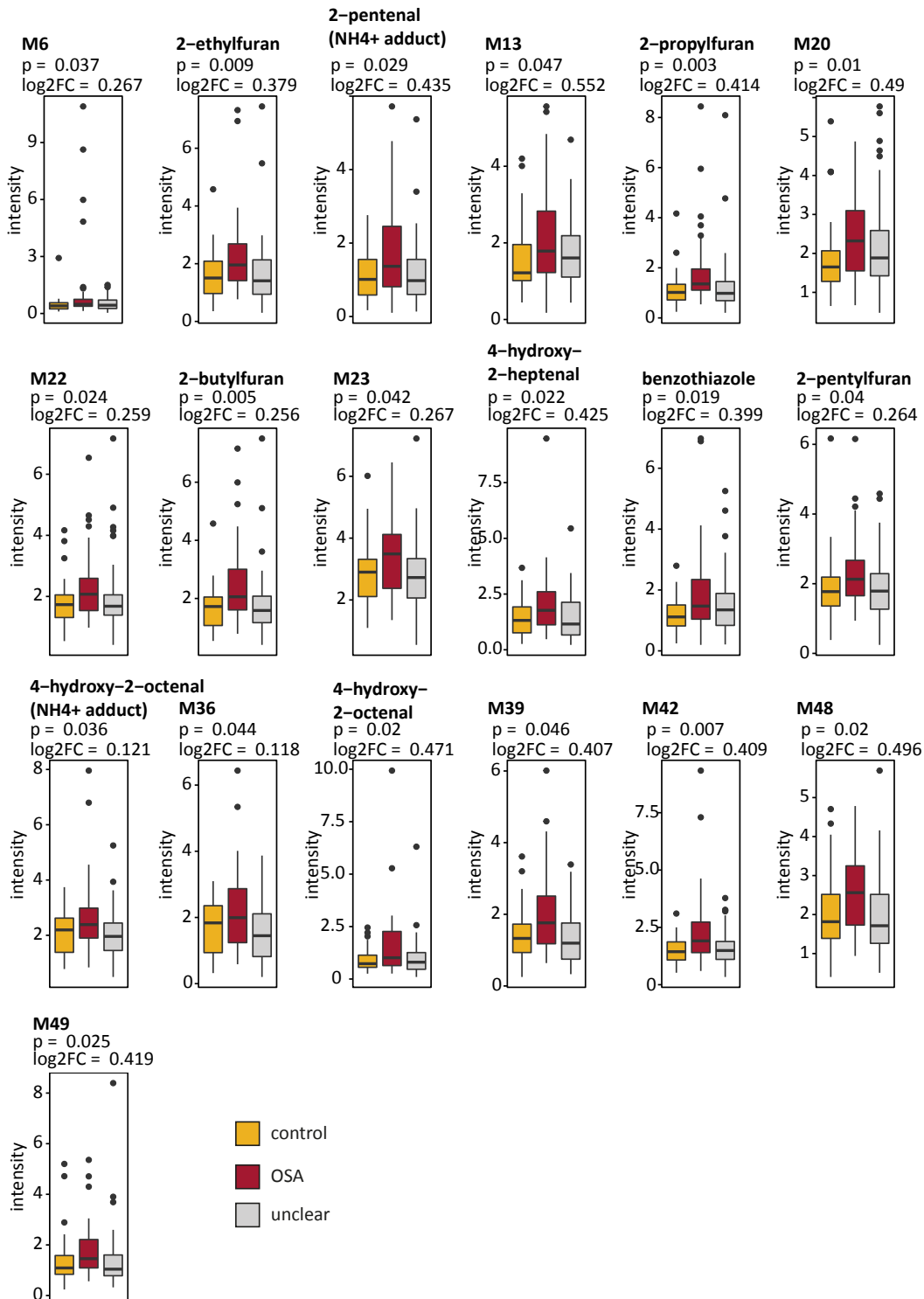
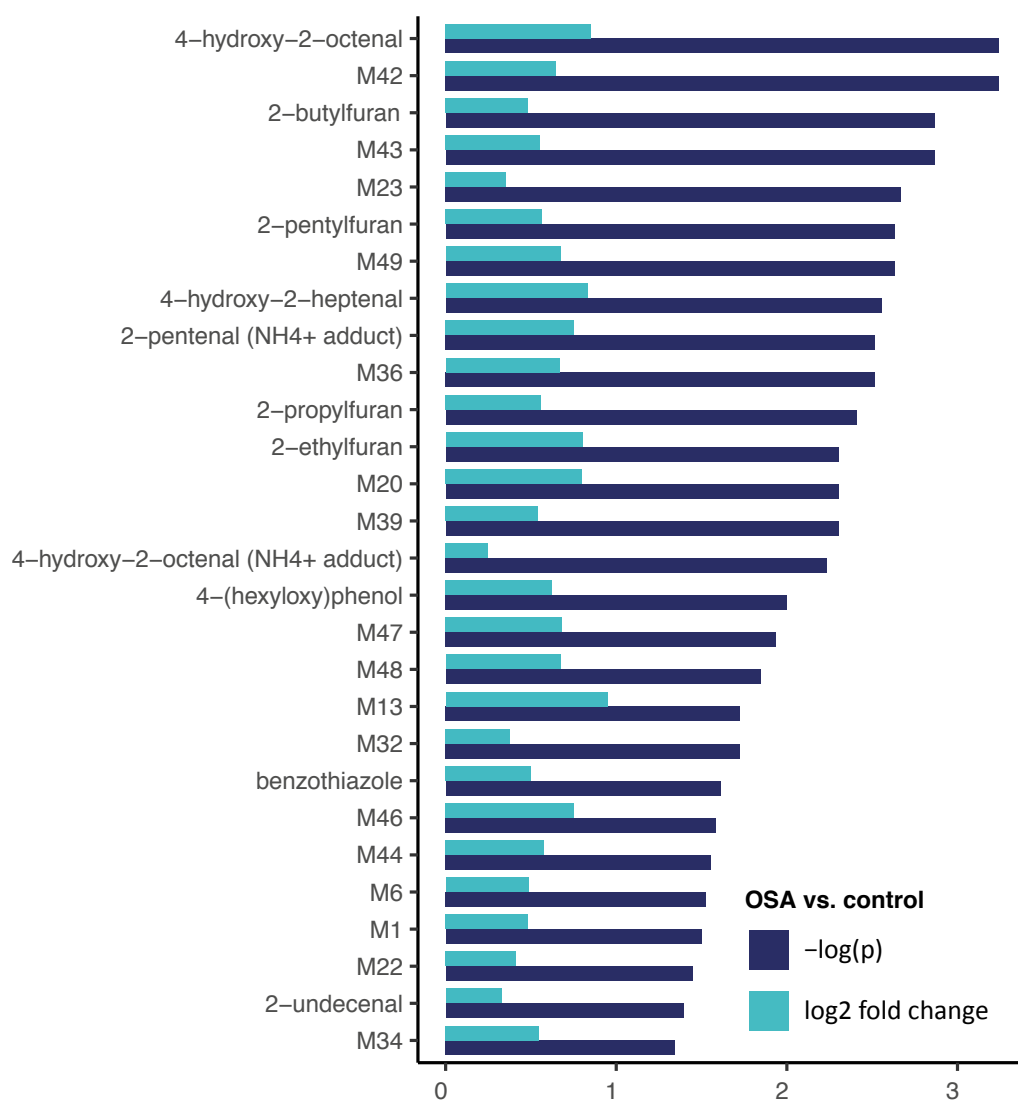
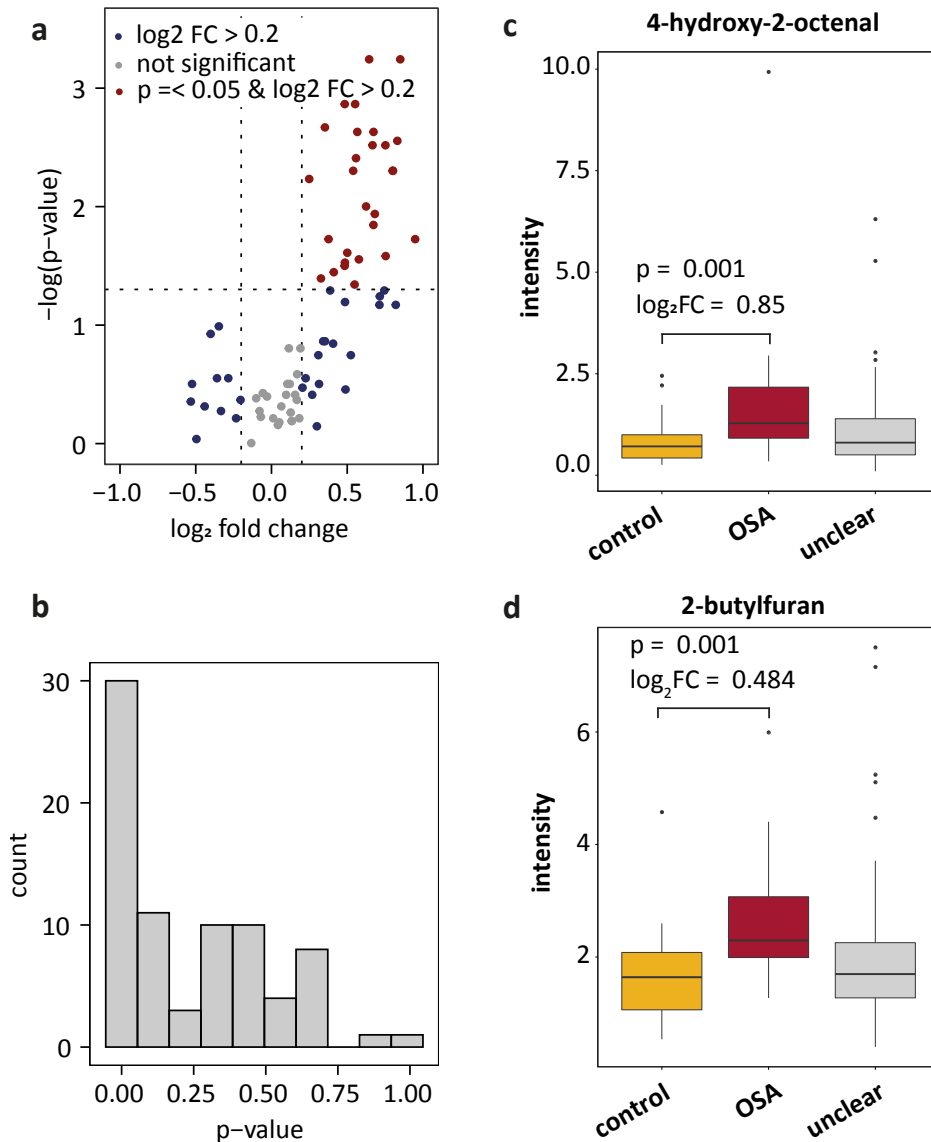


Figure B.6.: Boxplots (center line: median, box limits: 25th and 75th percent quantile, whisker length: 1.5 interquartile range) for all features with significant differences between OSA patients and subjects without OSA. (OSA: ODI > 30/h or ODI > 10/h & ESS > 10 points; control: ODI < 5/h or ODI < 10/h & ESS < 11 points; unclear: in between; stratification 1). log2FC: log2 fold change, p: p-value.



**Figure B.7.:** Significant differences in metabolic breath patterns between OSA patients and individuals without OSA (control: ODI < 10/h & ESS < 11 points; OSA: ODI < 30/h & ESS > 10 points; unclear: in between; stratification 2). P-values and fold changes of significant features sorted by significance. Boxplots for all significant features are provided in figure B.9, numeric results for significant features are summarized in table 5.2 and 5.3 and numeric results of all 78 features are given in supplementary table B.4 and B.5.



**Figure B.8:** Significant differences in metabolic breath patterns between OSA patients and individuals without OSA (control: ODI < 10/h & ESS < 11 points; OSA: ODI < 30/h & ESS > 10 points; unclear: in between; stratification 2). **a** volcano plot for all 78 metabolites. **b** p-value distribution for between-group differences from Mann-Whitney-U test. **c, d** Exemplary boxplots (center line: median, box limits: 25th and 75th percent quantile, whisker length: 1.5 interquartile range) of 4-hydroxy-2-octenal and 2-butylfuran. Boxplots for all significant features are provided in figure B.9, numeric results for significant features are summarized in table 5.2 and 5.3 and numeric results of all 78 features are given in supplementary table B.4 and B.5.

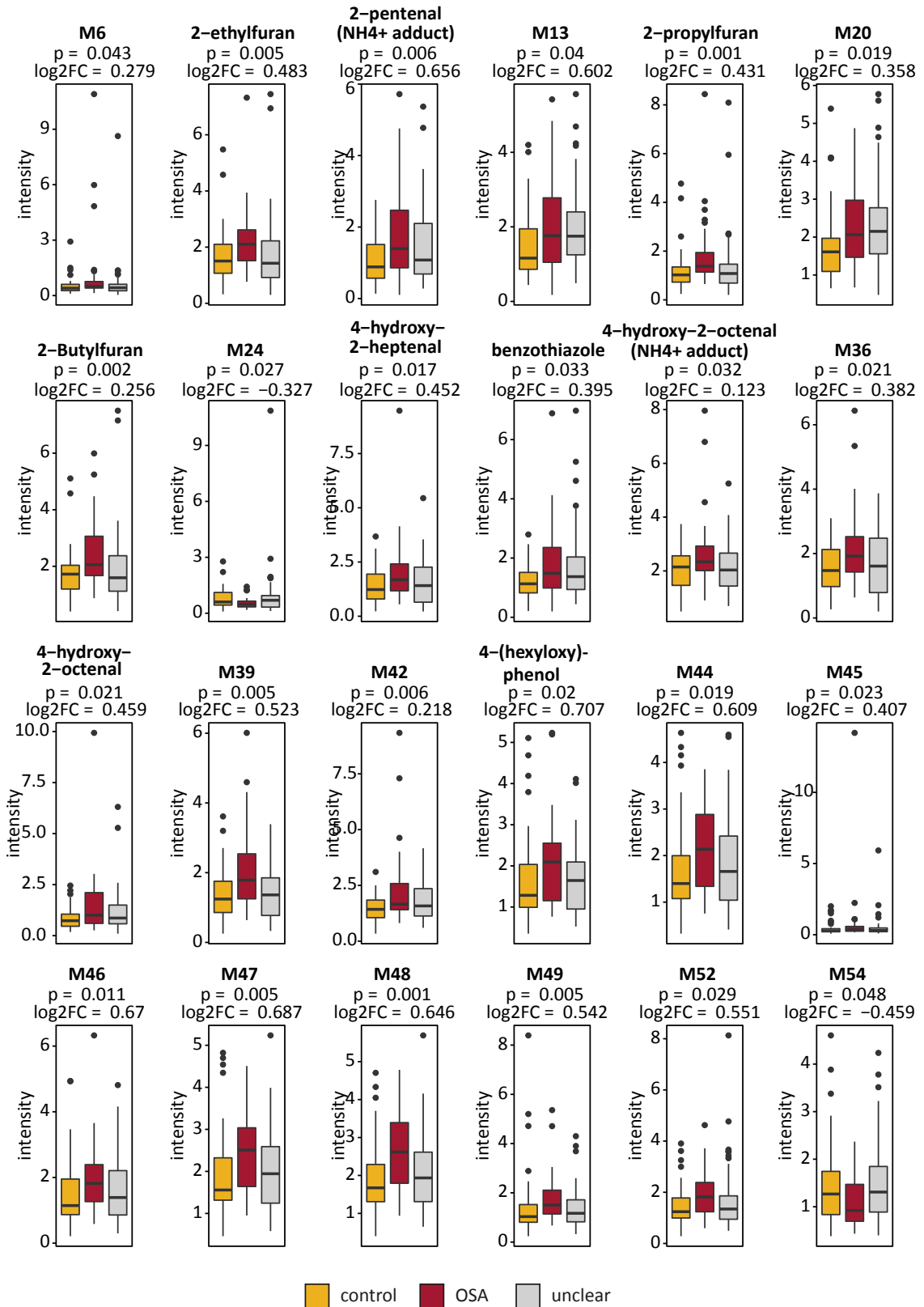


**Figure B.9.:** Boxplots (center line: median, box limits: 25th and 75th percent quantile, whisker length: 1.5 interquartile range) for all features with significant differences between OSA patients and individuals without OSA (control: ODI < 10/h & ESS < 11 points; OSA: ODI < 30/h & ESS > 10 points; unclear: in between; stratification 2).

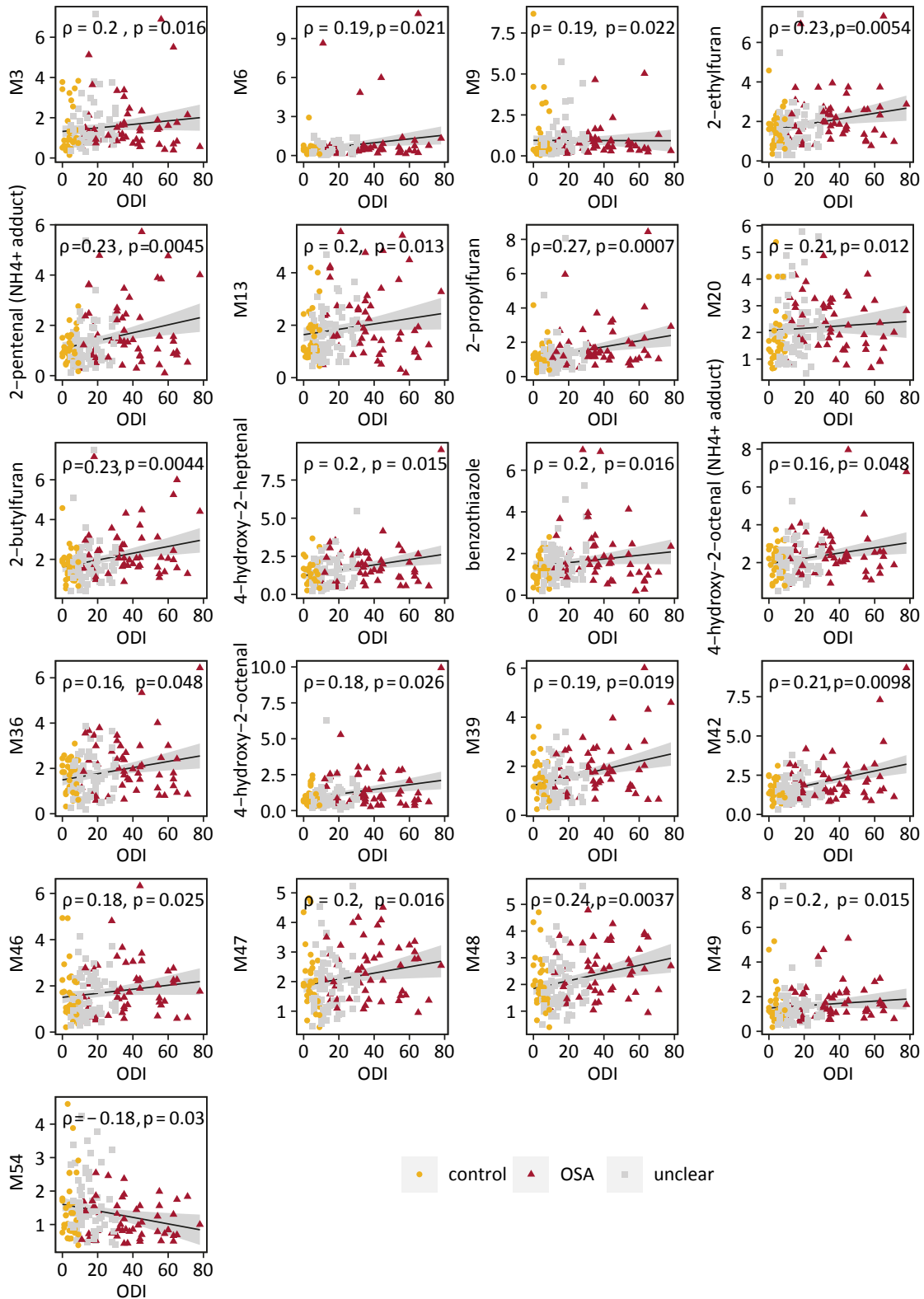


**Figure B.10.:** Linear regression for all features that correlate significantly ( $p < 0.05$ ) with ODI (OSA: ODI > 30/h or ODI > 10/h & ESS > 10 points; control: ODI < 5/h or ODI < 10/h & ESS < 11 points; unclear: in between; stratification 1).

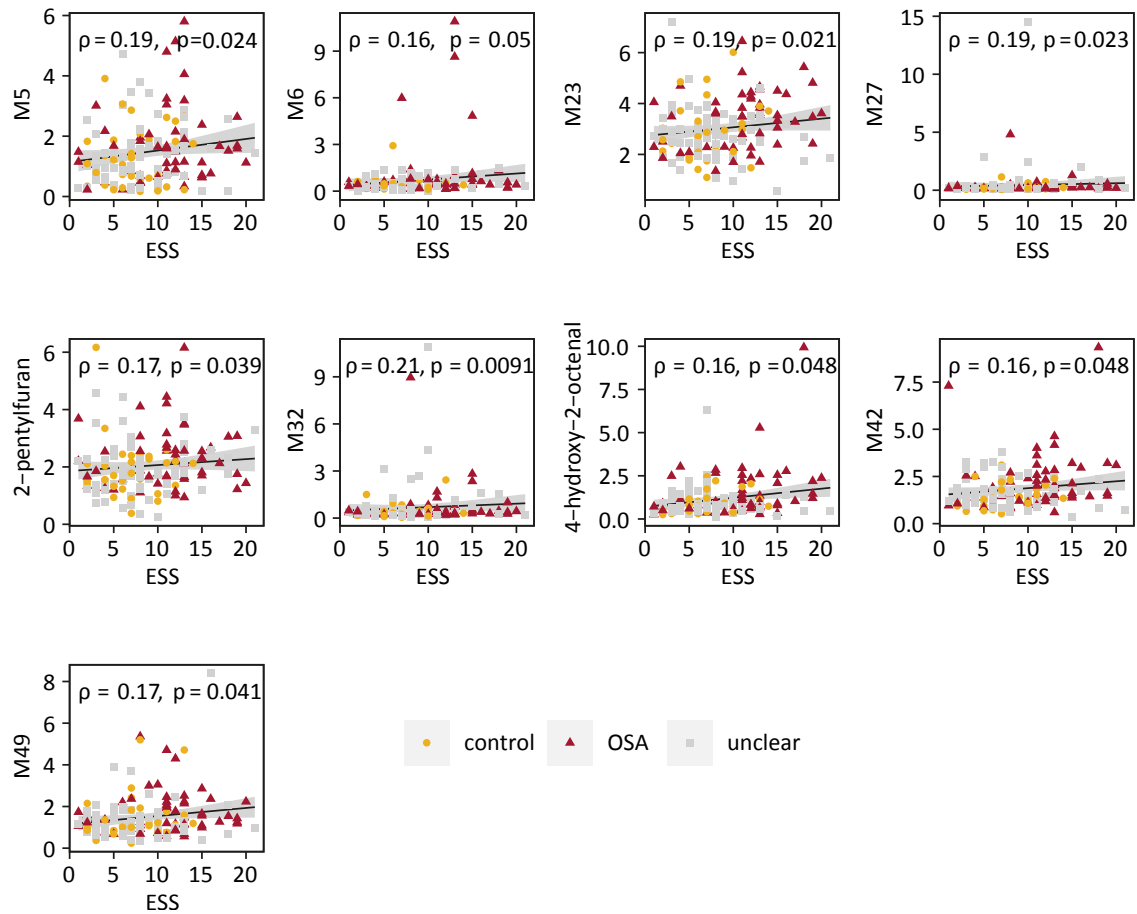


**Figure B.11.:** Linear regression for all features that correlate significantly ( $p < 0.05$ ) with ESS (OSA: ODI > 30/h or ODI > 10/h & ESS > 10 points; control: ODI < 5/h or ODI < 10/h & ESS < 11 points; unclear: in between; stratification 1).

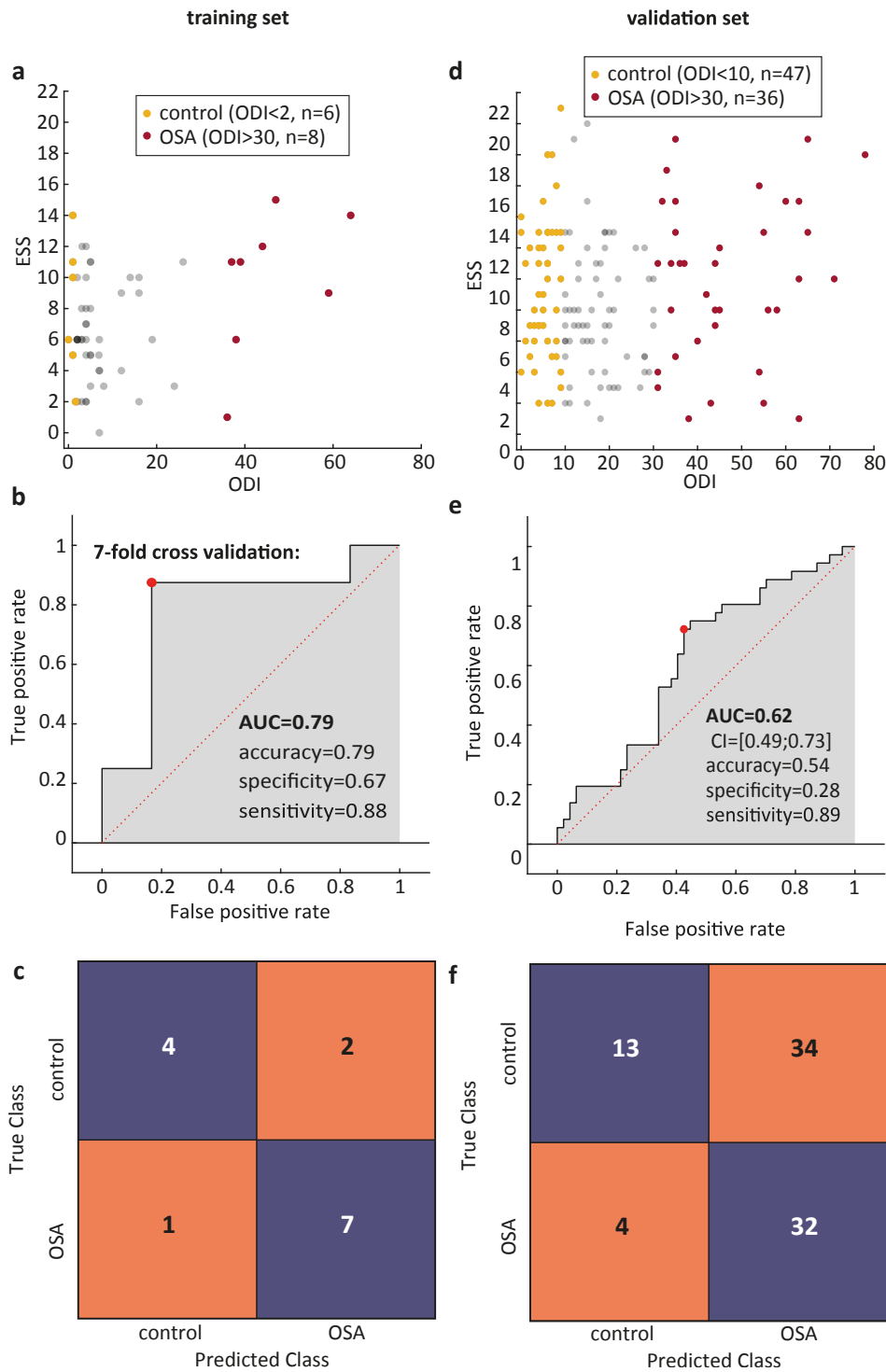


**Figure B.12.:** Classification results with stratification similar to pilot study (classification 2). **a** ESS and ODI of samples in the training set. **b** ROC curve from 7-fold cross validation of the classification model with the training set and **c** corresponding confusion matrix. **d** ESS and ODI of the samples in the validation cohort. **e** ROC curve from predictions of the validation cohort and **f** corresponding confusion matrix.

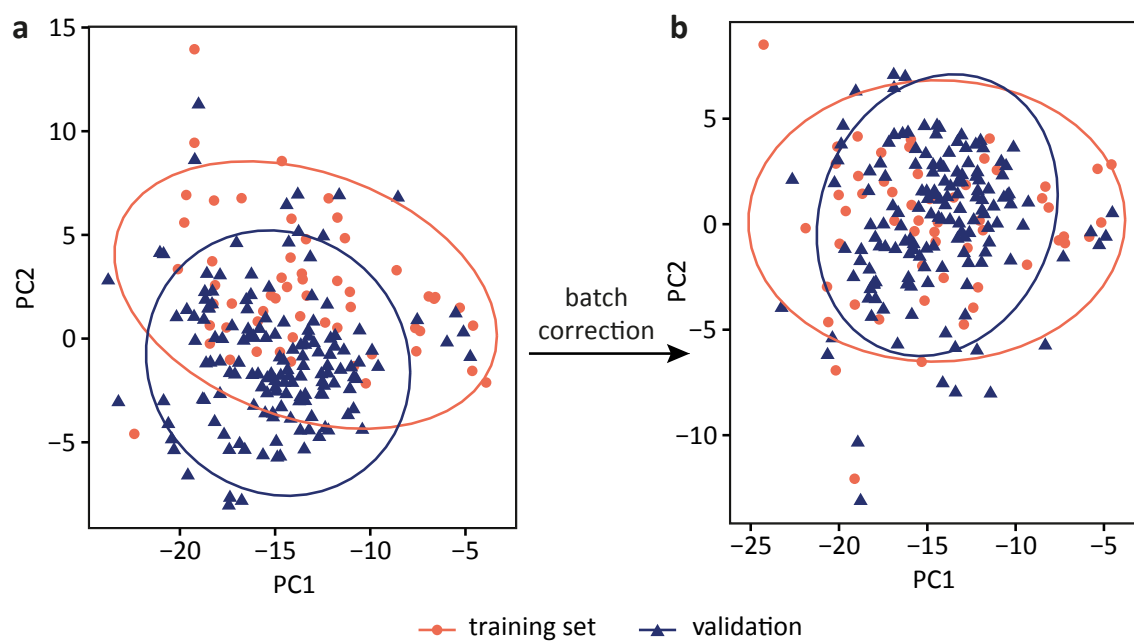


**Figure B.13.:** PCA plot before (a) and after (b) batch correction.



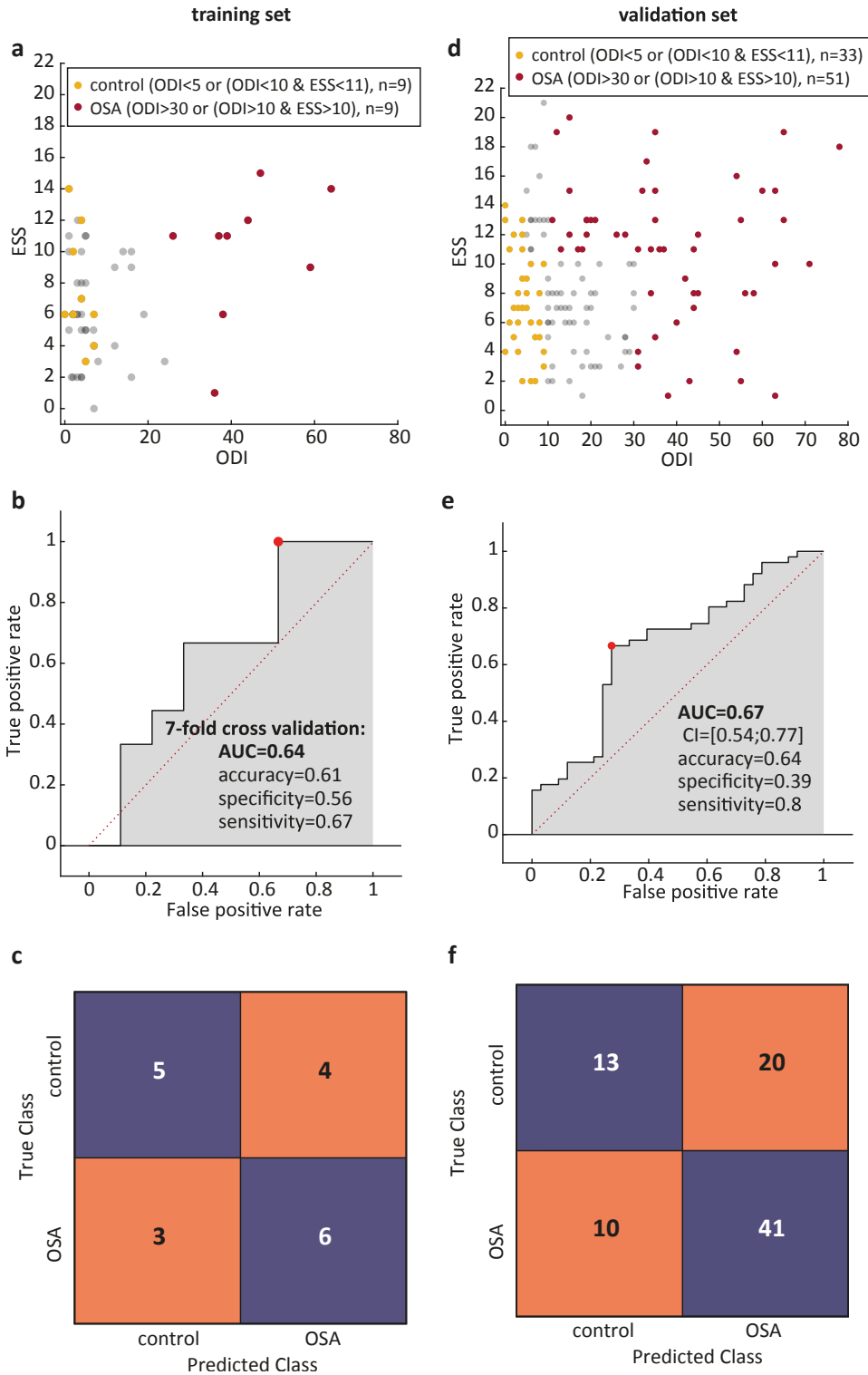


**Figure B.14.** Classification results after batch correction (classification 3). **a** ESS and ODI of samples in the training set. **b** ROC curve from 7-fold cross validation of the classification model with the training set and **c** corresponding confusion matrix. **d** ESS and ODI of the samples in the validation cohort. **e** ROC curve from predictions of the validation cohort and **f** corresponding confusion matrix.

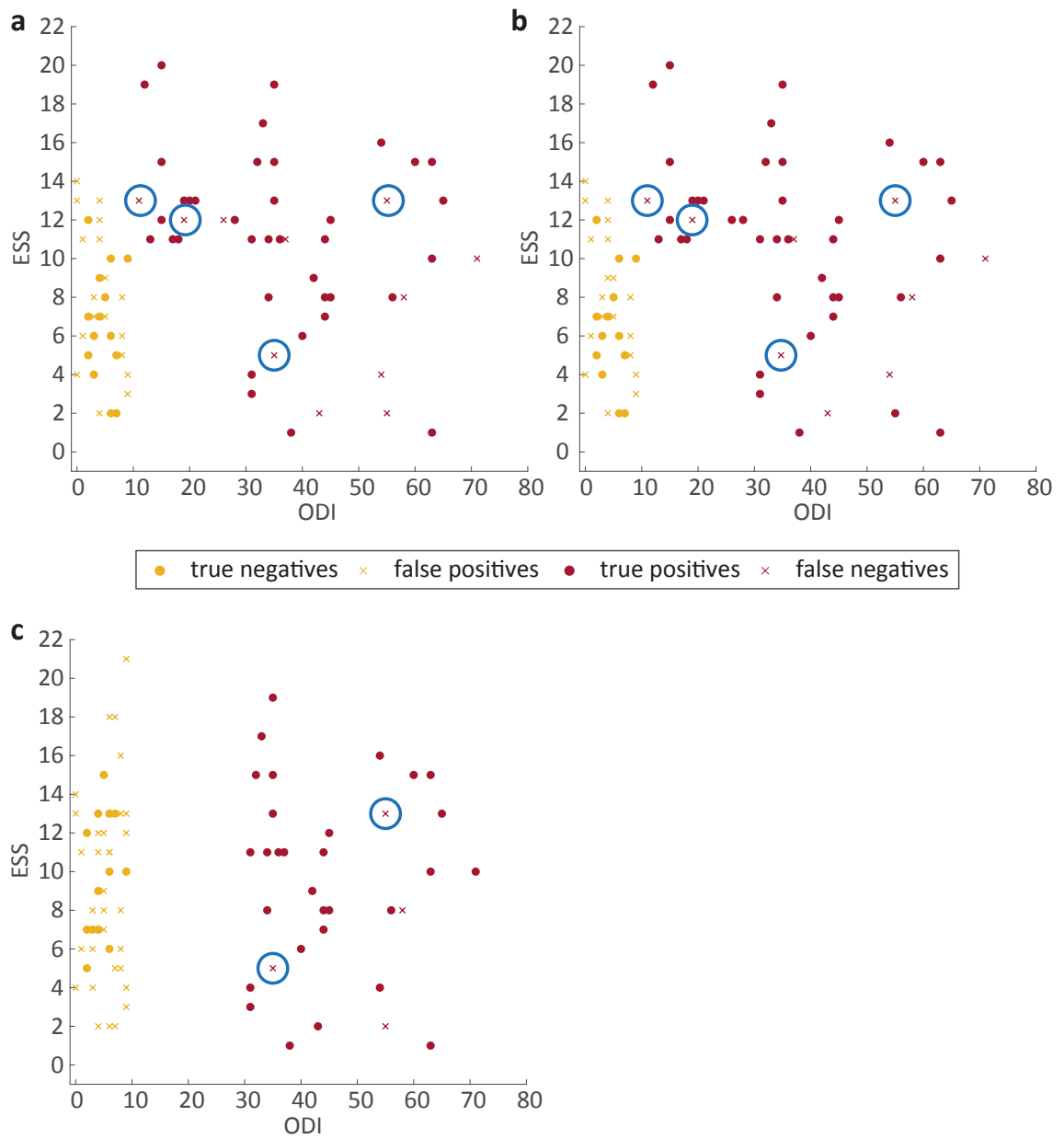


**Figure B.15.:** Accuracy of diagnosis based on metabolic pattern of exhaled breath. Correctly and wrongly predicted samples of validation data set in classification 1 (a), in classification 2 (b), and in classification 3 (c). Samples that are false negatives in all three classification procedures are highlighted with blue circles.

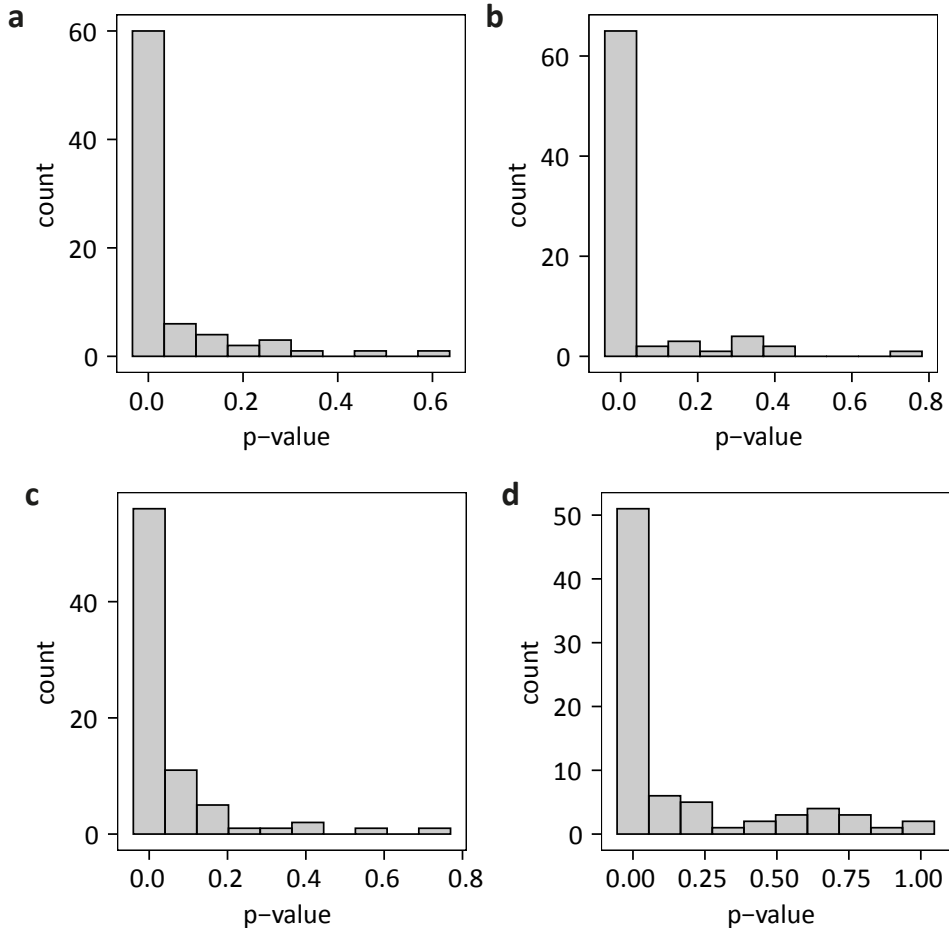


**Figure B.16.:** P-value distributions from Shapiro-Wilk's test for normality. **a** Control group from stratification 1 (OSA: ODI > 30/h or ODI > 10/h & ESS > 10 points, control: ODI < 5/h or ODI < 10/h & ESS < 11 points). **b** OSA group from stratification 1. **c** Control group from stratification 2 (control: ODI < 10/h & ESS < 11 points, OSA: ODI < 30/h & ESS > 10 points). **d** OSA group from stratification 2.

## B.2.4. Supplementary tables

**Table B.4.:** Results from statistical analysis of validation data for all 78 features that have been reported previously as potential biomarkers of OSA.

metabolite name	metabolite class	m/z	significant difference between groups	correlation with delta ODI	Pearson correlation coefficient	selected as predictor for classification
M1	unknown	53.0391	no	no		yes
isoprene	terpenes	69.0693	yes	no		yes
M2	unknown	71.0487	no	no		yes
M3	unknown	79.0409	no	no		yes
M4	unknown	81.0328	no	no		yes
M5	unknown	81.0525	yes	no		no
M6	unknown	83.0854	no	no		yes
4-hydroxy-2-butenal	unsaturated aldehydes	87.0439	no	no		yes
M7	unknown	88.0472	no	no		yes
M8	unknown	91.0413	yes	no		no
M9	unknown	93.0574	no	no		yes
M10	unknown	95.0494	no	no		yes
M11	unknown	97.0285	yes	no		no
2-ethylfuran	furanes	97.0647	yes	no		yes
M12	unknown	101.0598	no	no		yes
2-pentenal (NH <sub>4</sub> <sup>+</sup> adduct)	unsaturated aldehydes	102.0913	yes	no		yes
M13	unknown	103.0943	no	no		yes
M14	unknown	104.0495	yes	no		no
M15	unknown	105.0551	yes	no		no
M16	unknown	109.0281	yes	no		yes
M17	unknown	109.0648	yes	no		no
M18	unknown	110.0678	no	no		yes
2-propylfuran	furanes	111.0803	yes	yes	0.4	yes
M19	unknown	112.0211	no	no		yes
M20	unknown	122.0835	yes	no		no
M21	unknown	123.1165	no	no		yes
M22	unknown	124.0835	yes	no		no
2-Butylfuran	furanes	125.0958	yes	yes	0.44	no
M23	unknown	128.0701	no	no		yes
M24	unknown	129.0183	no	no		yes
4-hydroxy-2-heptenal	unsaturated aldehydes	129.0908	yes	yes	0.48	no
M25	unknown	131.0601	yes	no		yes
M26	unknown	135.0438	yes	no		no
benzothiazole	thiazoles	136.0216	yes	no		no
M27	unknown	136.0471	yes	no		yes
M28	unknown	137.0593	yes	yes	0.44	no

Continued from previous page.

metabolite name	metabolite class	m/z	significant difference between groups	correlation with delta ODI	Pearson correlation coefficient	selected as predictor for classification
M29	unknown	138.0171	yes	no		yes
M30	unknown	138.0571	yes	no		no
2-pentylfuran	furanes	139.1116	yes	yes	0.38	yes
4-hydroxy-2-octenal (NH <sub>4</sub> <sup>+</sup> adduct)	unsaturated aldehydes	143.1063	no	yes	0.42	no
M31	unknown	147.0551	yes	no		yes
M32	unknown	149.0971	yes	no		no
M33	unknown	151.1116	no	no		yes
M34	unknown	152.0699	yes	yes	0.42	no
M35	unknown	154.0651	yes	no		no
M36	unknown	158.1241	yes	no		no
M37	unknown	160.0611	no	no		yes
4-hydroxy-2-octenal	unsaturated aldehydes	160.1329	yes	yes	0.42	no
M38	unknown	164.0704	no	yes	0.41	no
M39	unknown	165.1272	no	no		yes
M40	unknown	167.1064	yes	no		no
M41	unknown	169.0867	yes	no		no
2-undecenal	unsaturated aldehydes	169.1584	no	yes	0.38	no
M42	unknown	175.1117	yes	no		yes
2-(methylthio)benzothiazole	thiazoles	182.0092	yes	no		yes
M43	unknown	182.0897	no	yes	0.38	no
4-(hexyloxy)phenol	benzenoids	195.1379	no	yes	0.38	no
M44	unknown	207.1378	no	yes	0.38	no
M45	unknown	208.1776	no	no		yes
M46	unknown	209.1168	no	yes	0.4	no
M47	unknown	209.1536	yes	no		no
M48	unknown	210.1568	no	no		yes
M49	unknown	211.1325	no	yes	0.38	no
M50	unknown	221.1532	no	yes	0.38	no
M51	unknown	221.19	yes	no		no
M52	unknown	223.1327	no	yes	0.44	no
M53	unknown	227.1269	no	yes	0.43	no
M54	unknown	228.0686	no	no		yes
M55	unknown	231.1741	no	no		yes
M56	unknown	233.1536	no	yes	0.41	no
M57	unknown	237.1123	no	yes	0.4	no
M58	unknown	243.1215	no	yes	0.38	no
M59	unknown	247.1697	no	yes	0.46	no
M60	unknown	249.1476	no	yes	0.38	no
M61	unknown	249.1846	no	yes	0.45	no
2-ethylhexyl-4-hydroxybenzoate	benzenoids	251.1641	no	yes	0.43	no
M62	unknown	263.1632	no	yes	0.38	no
M63	unknown	313.1127	no	yes	0.4	no

**Table B.5.:** Results from statistical analysis of validation data for all 78 features that have been reported previously as potential biomarkers of OSA.

metabolite name	m/z	Spearman correlation coefficient ODI	p correlation ODI	q correlation ODI	Spearman correlation coefficient ESS	p correlation ESS	q correlation ESS	p between groups (stratification 1)	q between groups (stratification 1)	log <sub>2</sub> fold change between groups (stratification 1)	p between groups (stratification 2)	q between groups (stratification 2)	log <sub>2</sub> fold change between groups (stratification 2)
M1	53.0374	0.1	0.237	0.079	0.08	0.37	0.34	0.314	0.223	0.19	0.032	0.015	0.48
isoprene	69.0698	0.06	0.454	0.119	-0.01	0.88	0.41	0.714	0.37	-0.01	0.314	0.075	0.1
M2	71.0493	0	0.989	0.2	-0.02	0.85	0.41	0.942	0.446	0.07	0.547	0.099	0.13
M3	79.0392	0.2	0.016	0.02	-0.06	0.49	0.34	0.094	0.143	0.51	0.067	0.024	0.71
M4	81.0338	0.1	0.225	0.077	-0.06	0.44	0.34	0.546	0.331	0	0.157	0.047	0.11
M5	81.0525	0.06	0.466	0.12	0.19	0.02	0.19	0.153	0.152	0.46	0.051	0.021	0.74
M6	83.0853	0.19	0.021	0.022	0.16	0.05	0.19	0.037	0.088	0.27	0.03	0.015	0.48
4-hydroxy-2-butenal	87.0442	0.05	0.575	0.129	-0.03	0.69	0.37	0.634	0.342	0.24	0.387	0.083	0.27
M7	88.0502	-0.11	0.163	0.072	-0.05	0.53	0.34	0.365	0.246	-0.19	0.281	0.073	-0.36
M8	91.0393	0.02	0.77	0.162	0.06	0.44	0.34	0.993	0.455	0.03	0.26	0.072	0.17
M9	93.0548	0.19	0.022	0.022	-0.1	0.24	0.34	0.213	0.184	0.43	0.179	0.051	0.52
M10	95.0491	0.08	0.314	0.097	-0.05	0.58	0.34	0.447	0.286	0.09	0.314	0.075	0.12
M11	97.0294	0.05	0.569	0.129	-0.02	0.83	0.41	0.288	0.221	0.04	0.611	0.105	0.01
2-ethylfuran	97.0646	0.23	0.005	0.017	0.1	0.25	0.34	0.009	0.068	0.38	0.005	0.004	0.8
M12	101.0597	0.11	0.183	0.072	0.06	0.47	0.34	0.169	0.16	0.44	0.064	0.024	0.49
2-pentenal (NH <sub>4</sub> <sup>+</sup> adduct)	102.0912	0.23	0.005	0.017	0.07	0.43	0.34	0.029	0.087	0.43	0.003	0.004	0.75
M13	103.0952	0.2	0.013	0.02	0.05	0.55	0.34	0.047	0.088	0.55	0.019	0.011	0.95
M14	104.0455	-0.07	0.42	0.114	0	0.96	0.43	0.819	0.407	-0.29	0.442	0.087	-0.53
M15	105.0545	0.12	0.161	0.072	0.09	0.3	0.34	0.128	0.144	0.63	0.067	0.024	0.82
M16	109.0285	-0.05	0.545	0.127	-0.1	0.25	0.34	0.296	0.221	-0.25	0.531	0.098	-0.33
M17	109.0648	0.11	0.194	0.074	0.12	0.15	0.3	0.113	0.143	0.34	0.143	0.045	0.41
M18	110.0713	0.08	0.362	0.107	0.06	0.46	0.34	0.099	0.143	0.12	0.414	0.085	-0.1
2-propylfuran	111.0803	0.27	0.001	0.011	0.1	0.21	0.34	0.003	0.068	0.41	0.004	0.004	0.56
M19	112.016	0.01	0.882	0.183	0.05	0.58	0.34	0.68	0.358	0.08	0.314	0.075	0.31
M20	122.0806	0.21	0.012	0.02	0.03	0.68	0.37	0.01	0.068	0.49	0.005	0.004	0.8
M21	123.1166	0.1	0.205	0.075	-0.03	0.7	0.37	0.148	0.151	0.16	0.375	0.083	-0.06
M22	124.0838	0.14	0.09	0.053	0.15	0.06	0.22	0.024	0.081	0.26	0.036	0.017	0.41
2-Butylfuran	125.0961	0.23	0.004	0.017	0.13	0.13	0.28	0.005	0.068	0.26	0.001	0.004	0.48
M23	128.0703	0.13	0.114	0.058	0.19	0.02	0.19	0.042	0.088	0.27	0.002	0.004	0.35
M24	129.0178	-0.15	0.066	0.043	-0.05	0.52	0.34	0.094	0.143	-0.19	0.281	0.073	-0.28
4-hydroxy-2-heptenal	129.0908	0.2	0.015	0.02	0.13	0.11	0.26	0.022	0.081	0.42	0.003	0.004	0.83
M25	131.0568	-0.07	0.365	0.107	0	0.98	0.44	0.949	0.446	-0.64	0.915	0.145	-0.5
M26	135.0438	0.05	0.532	0.127	0.06	0.45	0.34	0.521	0.322	0.3	0.137	0.044	0.34
benzothiazole	136.0213	0.2	0.016	0.02	-0.04	0.62	0.35	0.019	0.081	0.4	0.025	0.014	0.5
M27	136.0511	-0.06	0.485	0.123	0.19	0.02	0.19	0.96	0.446	-0.18	0.401	0.084	-0.03
M28	137.0594	-0.05	0.513	0.126	0.06	0.48	0.34	0.608	0.342	-0.16	0.697	0.113	0.04

B.2. Validation of breath biomarkers for obstructive sleep apnea

Continued from previous page.

metabolite name	m/z	Spearman correlation coefficient ODI	p correlation ODI	q correlation ODI	Spearman correlation coefficient ESS	p correlation ESS	q correlation ESS	p between groups (stratification 1)	q between groups (stratification 1)	log <sub>2</sub> fold change between groups (stratification 1)	p between groups (stratification 2)	q between groups (stratification 2)	log <sub>2</sub> fold change between groups (stratification 2)
M29	138.0174	0.11	0.18	0.072	-0.07	0.43	0.34	0.107	0.143	0.15	0.387	0.083	0.1
M30	138.0549	-0.09	0.252	0.083	0.05	0.56	0.34	0.883	0.427	-0.16	0.991	0.155	-0.13
2-pentylfuran	139.1116	0.11	0.197	0.074	0.17	0.04	0.19	0.04	0.088	0.26	0.002	0.004	0.57
4-hydroxy-2-octenal (NH <sub>4</sub> <sup>+</sup> adduct)	143.1064	0.16	0.048	0.036	0.13	0.11	0.26	0.036	0.088	0.12	0.006	0.005	0.25
M31	147.0507	-0.05	0.549	0.127	-0.08	0.33	0.34	0.64	0.342	0.01	0.314	0.075	-0.52
M32	149.0959	0.11	0.176	0.072	0.21	0.01	0.19	0.126	0.144	0.3	0.019	0.011	0.38
M33	151.1117	0.05	0.521	0.126	0.06	0.47	0.34	0.256	0.208	0.16	0.531	0.098	-0.08
M34	152.0705	0.13	0.104	0.055	0.02	0.82	0.41	0.178	0.164	0.23	0.045	0.02	0.55
M35	154.0695	-0.13	0.104	0.055	-0.05	0.53	0.34	0.216	0.184	-0.32	0.428	0.085	-0.2
M36	158.125	0.16	0.048	0.036	0.14	0.09	0.25	0.044	0.088	0.12	0.003	0.004	0.67
M37	160.0603	-0.06	0.504	0.126	0.14	0.09	0.25	0.798	0.402	0.25	0.714	0.115	0.3
4-hydroxy-2-octenal	160.1331	0.18	0.026	0.023	0.16	0.05	0.19	0.02	0.081	0.47	0.001	0.003	0.85
M38	164.0693	-0.01	0.912	0.187	-0.05	0.54	0.34	0.735	0.376	0.18	0.645	0.108	0.13
M39	165.1273	0.19	0.019	0.022	0.1	0.24	0.34	0.046	0.088	0.41	0.005	0.004	0.54
M40	167.1066	0.06	0.439	0.117	0.05	0.52	0.34	0.145	0.151	0.15	0.157	0.047	0.19
M41	169.0859	0.1	0.209	0.075	0.11	0.2	0.34	0.318	0.223	0.25	0.051	0.021	0.39
2-undecenal	169.1586	0.11	0.17	0.072	0.09	0.3	0.34	0.36	0.246	0.16	0.04	0.018	0.33
M42	175.1134	0.21	0.01	0.02	0.16	0.05	0.19	0.007	0.068	0.41	0.001	0.003	0.64
2-(methylthio)benzothiazole	182.0089	0.08	0.36	0.107	-0.1	0.23	0.34	0.64	0.342	0.2	0.595	0.105	-0.07
M43	182.0809	0.12	0.146	0.071	0.14	0.09	0.25	0.064	0.11	0.18	0.001	0.004	0.55
4-(hexyloxy)phenol	195.1379	0.15	0.076	0.048	0.06	0.45	0.34	0.111	0.143	0.34	0.01	0.008	0.62
M44	207.1381	0.15	0.065	0.043	0.02	0.82	0.41	0.245	0.204	0.35	0.028	0.015	0.58
M45	208.1773	0.15	0.06	0.043	0.06	0.49	0.34	0.117	0.143	0.19	0.387	0.083	0.16
M46	209.1173	0.18	0.025	0.023	-0.03	0.69	0.37	0.111	0.143	0.54	0.026	0.014	0.75
M47	209.1536	0.2	0.016	0.02	0.03	0.72	0.37	0.057	0.102	0.37	0.012	0.008	0.68
M48	210.1568	0.24	0.004	0.017	0.02	0.83	0.41	0.02	0.081	0.5	0.014	0.01	0.67
M49	211.1328	0.2	0.015	0.02	0.17	0.04	0.19	0.025	0.081	0.42	0.002	0.004	0.67
M50	221.1542	-0.07	0.414	0.114	-0.08	0.34	0.34	0.42	0.273	-0.2	0.102	0.036	-0.35
M51	221.19	-0.05	0.583	0.129	0.01	0.86	0.41	0.621	0.342	-0.06	0.611	0.105	-0.23
M52	223.1329	0.14	0.098	0.055	-0.05	0.55	0.34	0.169	0.16	0.44	0.349	0.08	0.49
M53	227.1277	0.14	0.09	0.053	0.06	0.46	0.34	0.305	0.223	0.36	0.057	0.022	0.72
M54	228.0642	-0.18	0.03	0.025	-0.05	0.58	0.34	0.119	0.143	-0.37	0.119	0.04	-0.4
M55	231.1749	0.11	0.169	0.072	0.1	0.24	0.34	0.19	0.17	0.06	0.281	0.073	0.23
M56	233.1534	0.04	0.614	0.134	0.01	0.86	0.41	0.399	0.265	0.23	0.179	0.051	0.31
M57	237.1131	0.07	0.42	0.114	-0.01	0.93	0.43	0.602	0.342	0.11	0.428	0.085	0.17
M58	243.1223	0.1	0.222	0.077	0.09	0.26	0.34	0.481	0.302	0.09	0.137	0.044	0.35
M59	247.1695	0.03	0.757	0.161	0.04	0.61	0.35	0.589	0.342	0.1	0.645	0.108	0.13
M60	249.1487	0.12	0.149	0.071	0.05	0.56	0.34	0.143	0.151	0.2	0.337	0.079	0.2
M61	249.1847	-0.08	0.308	0.097	0.07	0.37	0.34	0.264	0.21	-0.06	0.485	0.092	0.07
2-ethylhexyl-4-hydroxybenzoate	251.1642	0.03	0.732	0.158	0.06	0.46	0.34	0.57	0.34	-0.07	0.662	0.109	0.05
M62	263.1646	0.09	0.281	0.09	0.04	0.61	0.35	0.292	0.221	0.27	0.611	0.105	0.18
M63	313.1136	-0.07	0.413	0.114	0.06	0.48	0.34	0.84	0.412	-0.16	0.485	0.092	-0.44

**Table B.6.:** Diagnostic performance of exhaled breath analysis for OSA. (C1: Classification 1; C2: Classification 2 (stratification similar to pilot study); C3: Classification 3 (after batch correction); AUC: area under receiver operating characteristic curve; CV: cross validation; TPR: true positive rate, FPR: false positive rate, TNR: true negative rate, FNR: false negative rate, CI: confidence interval)

		Training Set								
	stratification	ncontrol	nOSA	AUC (CV)	TPR	FPR	TNR	FNR		
<b>C1</b>	OSA: ODI>30 or (ODI>10 & ESS>10) control: ODI<5 or (ODI<10 & ESS<=10)	9	9	0.59	67%	33%	67%	33%		
<b>C2</b>	OSA: ODI>30 control: ODI<2	6	8	0.79	88%	33%	67%	13%		
<b>C3</b>	OSA: ODI>30 or (ODI>10 & ESS>10) control: ODI<5 or (ODI<10 & ESS<=10)	9	9	0.64	67%	44%	56%	33%		
		Validation Set								
	stratification	ncontrol	nOSA	AUC	CI1	CI2	TPR	FPR	TNR	FNR
<b>C1</b>	OSA: ODI>30 or (ODI>10 & ESS>10) control: ODI<5 or (ODI<10 & ESS<11)	33	51	0.66	0.55	0.79	76%	58%	42%	24%
<b>C2</b>	OSA: ODI>30 control: ODI<10	47	36	0.62	0.49	0.73	89%	72%	28%	11%
<b>C3</b>	OSA: ODI>30 or (ODI>10 & ESS>10) control: ODI<5 or (ODI<10 & ESS<11)	33	51	0.67	0.54	0.77	80%	61%	39%	20%



## B.3. Multi-omics correlates of insulin signaling and circadian function

### B.3.1. Supplementary figures

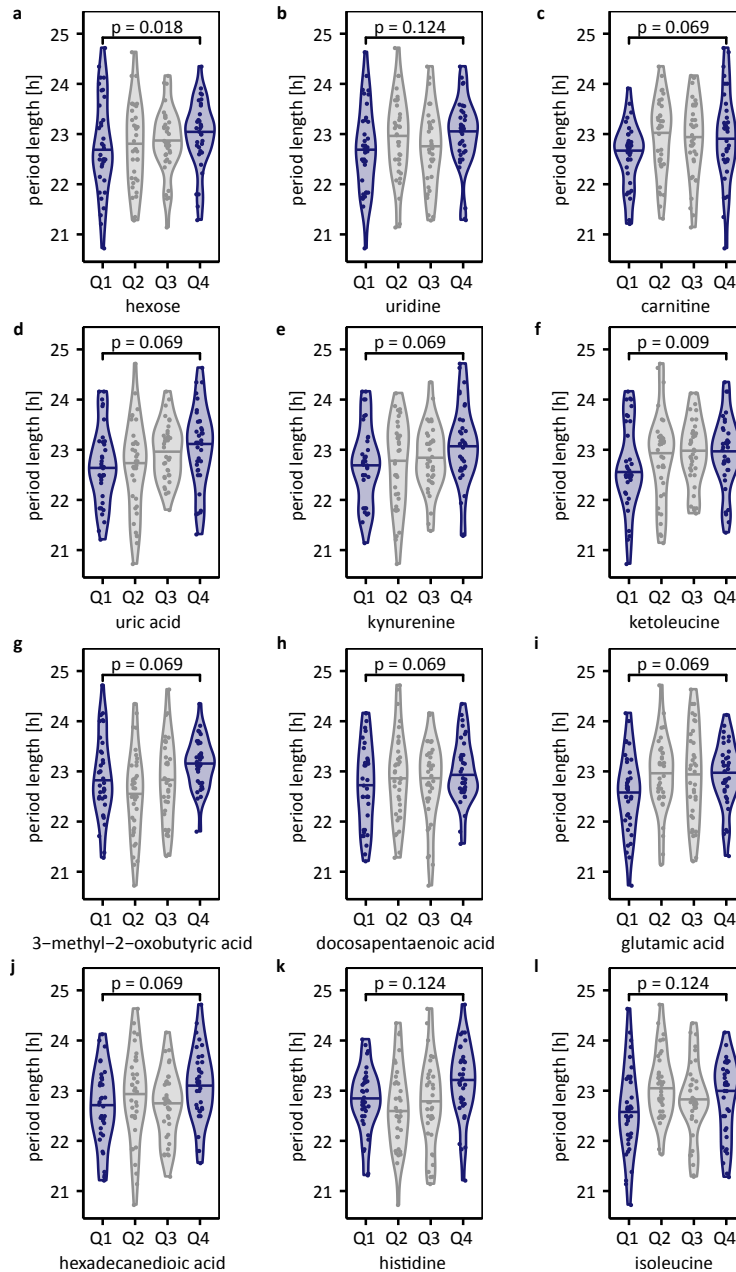


**Figure B.17.:** Violin plots of identified metabolites, for which we discovered an elongating influence on the circadian period length of U2OS cells. Data points are split in quartiles based on the metabolite levels and given p-values were obtained from two-sided Kolmogow-Smirnow test. Medians are indicated with horizontal lines.

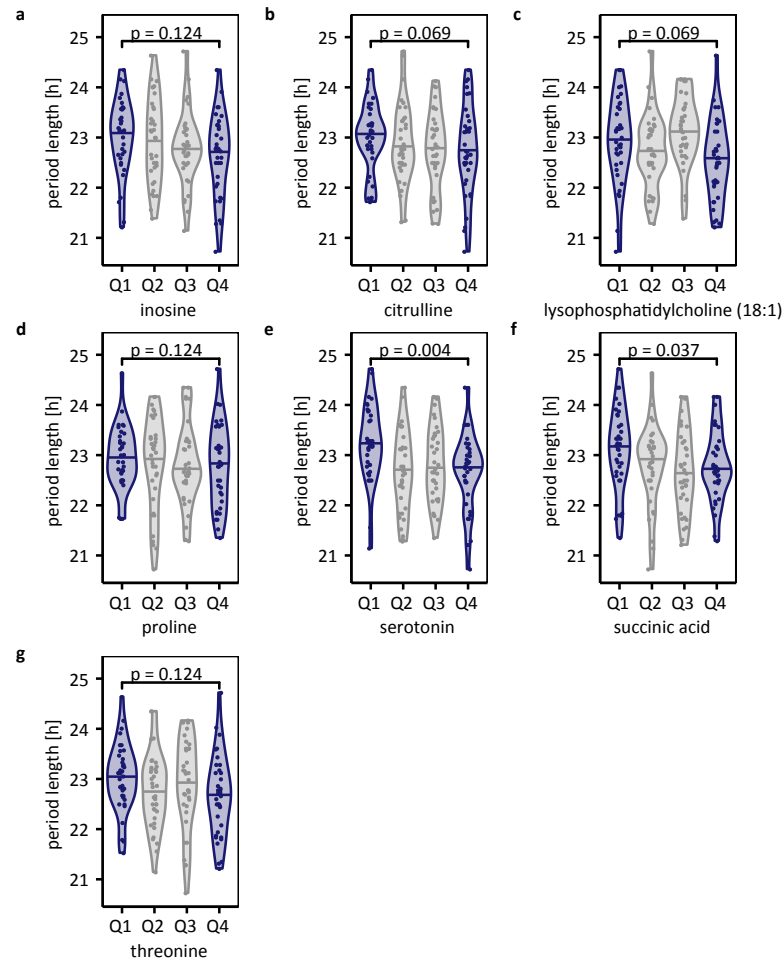


**Figure B.18.:** Violin plots of identified metabolites, for which we discovered an reducing effect on the circadian period length of U2OS cells. Data points are split in quartiles based on the metabolite levels and given p-values were obtained from two-sided Kolmogorov-Smirnow test. Medians are indicated with horizontal lines.

## B.3.2. Supplementary tables

Table B.7.: Participant inclusion and exclusion criteria.

Inclusion criteria						
Groups	Non T2D		T2D			
	Non obese	obese	Non obese	Obese		
Age (y)	40-75					
BMI (kg/m <sup>2</sup> )	18.5-29.9	≥ 30	18.5-29.9	≥ 30		
Antidiabetic treatment	-		-	+	-	+
HbA1c (%)	<6.0		≥ 6.5	all range	≥ 6.5	all range

Exclusion criteria
Age < 40y, > 75y
Type 1 diabetes or LADA diabetes
Steroid-induced diabetes or post-transplant diabetes
Active neoplasia
Not-recovered hepatitis
Immunosuppressive therapy
Corticosteroid therapy
Chronic sleeping treatment
Sleep apnea syndrome with machine therapy (≥ 2 hours/night)
Shift work

Table B.8.: Baseline characteristics of the participants divided into four groups (\* Values are means ±SD, # according to the supplemental table B.11, NA non applicable, IQR: Interquartile range)

Characteristics *	Non T2D Non obese (112)	Non T2D obese (94)	T2D non obese (52)	T2D obese (50)
Age (y)	57.93 ± 9.63	55.15 ± 8.86	59.72 ± 14.56	61.48 ± 9.87
Female sex – no. (%)	65 (58.04)	47 (50.0)	16 (30.77)	20 (40)
Body-mass index (kg/m <sup>2</sup> )	24.07 ± 3.5	34.16 ± 4.39	25.82 ± 2.96	34.95 ± 3.81
Median duration of type 2 diabetes – year (IQR)	NA	NA	10 (5-15.25)	4.5 (1-9.75)
Systolic blood pressure – mm Hg	121.86 ± 18.64	127.64 ± 14.84	129.67 ± 16.43	140.24 ± 48.19
Heart rate	66.75 ± 9.98	71.44 ± 11.73	74.37 ± 11.71	74.6 ± 14.67
Epworth somnolence score	5.87 ± 3.58	7.05 ± 3.91	5.56 ± 3.26	6.84 ± 4.58
Physical activity score #	3.75 ± 2.06	2.3 ± 1.35	2.75 ± 1.79	2.59 ± 1.66
History of coronary, stroke, peripheral arterial disease – no. (%)	0 (0)	3 (3.19)	6 (11.54)	3 (6)
History of cancer – no. (%)	0 (0)	2 (2.13)	6 (11.54)	3 (6)
Psychiatric disease – no. (%)	5 (4.46)	7 (7.45)	4 (5.77)	6 (12)
Inflammatory diseases – no. (%)	7 (6.25)	7 (7.45)	4 (5.77)	7 (14)
Sleep disorders – no. (%)	9 (8.04)	14 (14.89)	6 (11.54)	7 (14)

**Table B.9.:** Medications of the participants divided into four groups. (ACE denotes angiotensin-converting enzyme, ARB angiotensin-receptor blocker, DPP-4 dipeptidyl peptidase 4 and GLP-1 glucagon-like peptide 1. NA Non Applicable)

Medications	Non T2D non obese (112)	Non T2D obese (94)	T2D non obese (52)	T2D obese (50)
Glucose-lowering therapies – no. (%)	NA	NA	50 (96.15)	48 (96)
<b>Insulin</b>	NA	NA	13 (25)	14 (28)
<b>Metformin</b>	NA	NA	43 (82.69)	38 (76)
<b>Sulfonylurea</b>	NA	NA	13 (25)	11 (22)
<b>Gliptine (DPP4 inhibitors)</b>	NA	NA	26 (50)	18 (38)
<b>Gliflozine (SGLT2 inhibitors)</b>	NA	NA	14 (26.92)	14 (28)
<b>GLP-1 receptor agonist</b>	NA	NA	1 (1.92)	5 (10)
Cardiovascular therapies – no. (%)	13 (11.61)	26 (27.66)	42 (80.77)	39 (78)
<b>Beta-blocker</b>	3 (2.68)	1 (1.06)	7 (13.46)	3 (6)
<b>Statin</b>	3 (2.68)	7 (7.45)	29 (55.77)	19 (38)
<b>Antiplatelet agents</b>	3 (2.68)	8 (8.51)	23 (44.23)	14 (28)
<b>ACE inhibitor or ARB</b>	7 (6.25)	15 (15.96)	24 (46.15)	26 (52)
<b>Diuretics</b>	0 (0)	2 (2.13)	9 (17.31)	8 (16)
<b>Calcium channel blocker</b>	0 (0)	5 (5.32)	8 (15.38)	9 (18)
Antipsychotics – no. (%)	0 (0)	1 (1.06)	2 (3.85)	3 (6)
Antidepressant – no. (%)	3 (2.68)	9 (9.57)	1 (1.92)	4 (8)
Benzodiazepine – no. (%)	2 (1.79)	0 (0)	0 (0)	1 (2)
Estrogens – no. (%)	12 (10.71)	3 (3.19)	2 (3.85)	0 (0)
Sleeping therapies – no. (%)	4 (3.57)	0 (0)	1 (1.92)	0 (0)

**Table B.10.** Blood parameters of the Participants divided into four groups. (2-way ANOVA tests, Red: comparison to the Non T2D Non obese group, Blue: comparison to the Non T2D obese group, Green: comparison to the T2D non obese group, Adjusted p-value \* p<0.05, \*\*p<0.005, \*\*\*p<0.001, \*\*\*\*p<0.0001)

Characteristics	Non T2D Non obese (112)	Non T2D obese (94)	T2D Non obese (52)	T2D obese (50)
HbA1c (%)	5.28 ± 0.25	5.41 ± 0.28	7.57 ± 1.35	7.67 ± 1.4
Glycemia (mmol/l)	5.18 ± 0.5	5.53 ± 0.59	8.56 ± 2.27	8.81 ± 2.23
Insulin (mU/l)	7.48 ± 3.75	17.28 ± 11.15*	11.58 ± 9.95	21.36 ± 12.8**
Cortisol (nmol/l)	402.79 ± 131.45	334.97 ± 116.02****/****	379.79 ± 120.69****/****	379.54 ± 116.1****/****
TSH (mU/l)	2.28 ± 1.08	2.54 ± 1.49	2.37 ± 1.36	2.41 ± 1.17
Total Cholesterol (mmol/l)	5.39 ± 0.96	5.35 ± 0.89	4.62 ± 1.12	5.11 ± 1.47
Triglycerides (mmol/l)	1.16 ± 0.63	1.73 ± 1.1	1.95 ± 1.51	2.72 ± 3.41
HDL (high density lipoprotein) (mmol/l)	1.81 ± 0.52	1.31 ± 0.34	1.27 ± 0.38	1.29 ± 0.67
LDL (low density lipoprotein) (mmol/l)	3.03 ± 0.89	3.07 ± 1.18	2.29 ± 1.15	2.42 ± 1.32
Urea (mmol/l)	4.89 ± 1.25	5.47 ± 1.35	6.18 ± 1.74	6.02 ± 1.97
Creatinine (umol/l)	75.51 ± 15.51	76.34 ± 14.23	82.46 ± 23.09	81.9 ± 29.38
ALT (alanine transaminase) (U/l)	24.02 ± 9.54	32.54 ± 15.76	30.92 ± 13.86****	44.24 ± 23.61*/*
AST (aspartate transaminase) (U/l)	25.04 ± 9.26	26.3 ± 11.38	24.63 ± 9.92	30.42 ± 13.93
Alkaline phosphatase (U/l)	65.5 ± 21.42	67.82 ± 19.34	66.15 ± 21.68	74.04 ± 19.63
GGT (gamma-glutamyltransferase) (U/l)	28.97 ± 25.92	46.51 ± 82.59****	40.96 ± 55.89*	70.9 ± 74.37****/****/****
Total bilirubin (umol/l)	11.98 ± 6.21	9.86 ± 5.37	11.29 ± 7.45	8.46 ± 4.18
Conjugated bilirubine (umol/l)	1.29 ± 5.77	0.19 ± 1.3	0.9 ± 2.59	0.18 ± 1.23
Speed of sedimentation (mm/hour)	13.45 ± 8.27	15.14 ± 11.33	16.31 ± 13.93	19.46 ± 15.92
Erythrocytes (T/l)	4.82 ± 0.4	4.96 ± 0.43	5.01 ± 0.42	5.09 ± 0.46
Hemoglobin (g/l)	145.77 ± 12.89	148.5 ± 11.34	149.52 ± 13.54	147.52 ± 19.94
Hematocrit (%)	42.63 ± 4.22	43.6 ± 2.99	44.14 ± 3.59	43.74 ± 4
MCV (mean corpuscular volume) (fl)	89.24 ± 4.18	88.06 ± 4.45	88.2 ± 4.74	86 ± 5.19
MCH (mean corpuscular hemoglobin) (pg)	30.31 ± 1.83	29.99 ± 1.59	29.87 ± 1.82	29.02 ± 2.32
MCHC (mean corpuscular hemoglobin concentration) (g/l)	339.56 ± 10.43	340.53 ± 9.66	337.63 ± 9.1	337.02 ± 11.98
Reticulocytes (o/oo Ery)	12.88 ± 3.89	16.04 ± 4.09	16 ± 3.87	17.75 ± 4.24
Reticulocytes/Nb.Abs. (G/l)	61.97 ± 19.1	79.41 ± 20.86****	79.62 ± 18.39****	90.52 ± 23.55****
HFR (High Fluorescence Reticulocytes) (%)	1.08 ± 1.09	2.15 ± 1.86	2.01 ± 2.01	3.21 ± 2.29
Ret-He (Reticulocyte Hemoglobin Content) (pg)	33.09 ± 2.15	33.04 ± 1.98	32.81 ± 1.95	31.97 ± 2.61
Leucocytes (G/l)	5.72 ± 1.40	6.5 ± 1.54	7.6 ± 2.36	7.26 ± 2.09
Segmented neutrophils (%)	58.49 ± 11.49	59.41 ± 10.22	57.17 ± 9.42	58.48 ± 10.09
Non segmented neutrophils (%)	0.21 ± 0.43	0.31 ± 0.69	0.4 ± 0.82	0.36 ± 0.69
Segmented neutrophils /Nb.Abs. (G/l)	3.37 ± 1.27	3.86 ± 1.36	4.83 ± 3.38	4.28 ± 1.53
Eosinophils (%)	2.12 ± 1.69	2.41 ± 2.28	2.53 ± 2.38	2.58 ± 1.8
Basophiles (%)	0.54 ± 0.77	0.71 ± 1	0.75 ± 0.81	0.66 ± 0.71
Monocytes (%)	6.09 ± 3.33	6.57 ± 3.22	6.32 ± 2.71	6.54 ± 3.39
Lymphocytes (%)	32.54 ± 10.03	30.55 ± 9.18	32.89 ± 8.57	31.3 ± 9.88
Lymphocytes/Nb.Abs. (G/l)	1.83 ± 0.63	1.96 ± 0.71	2.46 ± 0.94	2.27 ± 0.94
Thrombocytes (G/l)	243.88 ± 51.88	250.05 ± 53.78	245.96 ± 81.44	253 ± 53.94
MPV (mean platelet volume) (fl)	10.32 ± 0.87	10.19 ± 0.85	9.71 ± 2.32	10.46 ± 1.01

**Table B.11.:** Physical activity criteria score.

<b>Physical activity</b>	<b>score</b>
No or very little physical exercise	1
Between one to three times per week	2
Between three to five times per week	4
Between six to seven times per week	6.5
More than several consecutive hours of physical exercise every day	7

## B.4. Understanding metabolic effects of seasonal light schedules in arctic reindeer

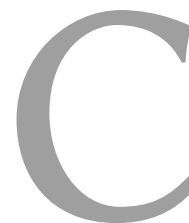
### B.4.1. Supplementary tables

**Table B.12.:** Summary of the results from rhythmicity analysis and prediction of rhythmic parameters for all m/z features. Metabolite names are given for annotated and identified features and the corresponding identification (ID) method is provided. This table is available online in a curated data archive at ETH Zurich (<https://www.research-collection.ethz.ch>) under the DOI 10.3929/ethz-b-000453100.

**Table B.13.:** Results from metabolic pathway enrichment analysis using the mummichog algorithm. Only pathways with at least two significant hits and with more significant hits than expected were considered. This table is available online in a curated data archive at ETH Zurich (<https://www.research-collection.ethz.ch>) under the DOI 10.3929/ethz-b-000453100.







## Scientific contributions

### Publications

**N. Nowak\***, A. Rawleigh\*, S.A. Brown, CIRCADIAN CLOCKS, SLEEP AND METABOLISM. In: Circadian clock in brain health and illness. Advances in Experimental Medicine and Biolog. Springer, Cham. *Manuscript submitted for publication.*

**N. Nowak**, T. Gaisl, D. Miladinovic, R. Marcinkevics, M. Osswald, S. Bauer, J. Buhmann, R. Zenobi, P. Sinues, S.A. Brown, M. Kohler, RAPID AND REVERSIBLE CONTROL OF HUMAN METABOLISM BY INDIVIDUAL SLEEP STATES. *Manuscript submitted for publication.*

**N. Nowak**, A. Engler, S. Thiel, A.S. Stöberl, P. Sinues, R. Zenobi, M. Kohler, VALIDATION OF BREATH BIOMARKERS FOR OBSTRUCTIVE SLEEP APNEA. *Manuscript submitted for publication.*

T. Bruderer, T. Gaisl, M.T. Gaugg, **N. Nowak**, B. Streckenbach, S. Müller, A. Moeller, M. Kohler, R. Zenobi, On-Line Analysis of Exhaled Breath, *Chemical Reviews*, **2019**, 119 (19), 10803-10828.

M. T. Gaugg, Y. Nussbaumer-Ochsner, L. Bregy, A. Engler, N. Stebler, T. Gaisl, T. Bruderer, **N. Nowak**, P. M.-L. Sinues, M. Kohler, Real-time breath analysis reveals specific metabolic signatures of COPD exacerbations. *Chest*, **2019**.

A. Tejero Rioseras, K. D. Singh, **N. Nowak**, M. T. Gaugg, T. Bruderer, R. Zenobi, P. M.-L. Sinues, Real-Time Monitoring of Tricarboxylic Acid Metabolites in Exhaled Breath. *Analytical chemistry*, **2018**, 90(11), 6453-6460.

M.T. Gaugg, T. Bruderer, **N. Nowak**, L. Eiffert, P. Martinez-Lozano-Sinues, M. Kohler, R. Zenobi. Mass Spectrometric Detection of Omega-Oxidation Products of Aliphatic Fatty Acids in Exhaled Breath, *Analytical Chemistry*, **2017**, 89(19), 10329-10334.

C. Hirtz, J. Vialaret, **N. Nowak**, A. Gabelle , D. Deville de Périère and S. Lehmann, Absolute quantification of 35 plasma biomarkers in human saliva using targeted mass spectrometry, *Bioanalysis*, **2016**, 8(1), 43-53.

C. Hirtz, J. Vialaret, A. Gabelle, **N. Nowak**, Y. Dauvilliers and S. Lehmann, From radioimmunoassay to mass spectrometry: a new method to quantify orexin-A (hypocretin-1) in cerebrospinal fluid, *Sci. Rep.* **2016**, 6, 25162.

## Conference contributions

### Scientific talks

Swiss Metabolomics Society Annual meeting **2019**

Title: REAL-TIME BREATH ANALYSIS PROVIDES NEW INSIGHTS INTO METABOLISM DURING SLEEP

European Biological Rhythms Society Congress **2019**

Title: REAL-TIME BREATH ANALYSIS PROVIDES NEW INSIGHTS INTO METABOLISM DURING SLEEP

Sleep & Health Symposium **2018**, Zurich (Switzerland)

Title: SLEEP-INDUCED METABOLISM MONITORED BY BREATH ANALYSIS

CHanalysis **2018**, Beatenberg (Switzerland)

Title: HOW CAN REAL-TIME BREATH ANALYSIS PROVIDE NEW INSIGHTS INTO METABOLISM DURING SLEEP?

Swiss Chemical Society fall meeting **2018**, Lausanne (Switzerland)

Title: A VALIDATION STUDY FOR REAL-TIME DIAGNOSIS OF OBSTRUCTIVE SLEEP APNOEA BY ANALYSIS OF EXHALED BREATH USING SESI-MS

### Scientific posters

Gordon Research Seminar and Conference on Chronobiology **2019** (Castelldefels, Spain)

Title: SLEEP-INDUCED METABOLIC CHANGES MONITORED BY BREATH ANALYSIS

Swiss Chemical Society fall meeting **2019**, Zürich (Switzerland)

Title: METABOLISM DURING SLEEP MONITORED BY REAL-TIME BREATH ANALYSIS

---

IABR breath summit **2018**, Maastricht (Netherlands)

Title: REAL-TIME DIAGNOSIS OF OBSTRUCTIVE SLEEP APNOEA BY ANALYZING EXHALED BREATH WITH SECONDARY ELECTROSPRAY IONIZATION MASS SPECTROMETRY - A VALIDATION STUDY

International Mass Spectrometry Conference **2018**, Florence (Italy)

Title: CAN OBSTRUCTIVE SLEEP APNOEA BE DIAGNOSED BY REAL-TIME ANALYSIS OF EXHALED BREATH USING SECONDARY ELECTROSPRAY IONIZATION MASS SPECTROMETRY - A VALIDATION STUDY

Anakon **2017**, Tübingen (Germany)

Title: STEPS TOWARDS QUANTIFYING BIOMARKERS IN EXHALED BREATH USING SECONDARY ELECTROSPRAY IONIZATION MASS SPECTROMETRY

American Society for Mass Spectrometry Conference **2017**, Indianapolis (USA)

Title: NOVEL BIOMARKERS FOR RESPIRATORY DISEASES DISCOVERED BY SECONDARY ELECTROSPRAY Ionization – High Resolution Mass Spectrometry

Swiss Chemical Society fall meeting **2017**, Bern (Switzerland)

Title: BREATH ANALYSIS USING SECONDARY ELECTROSPRAY IONIZATION MASS SPECTROMETRY – STEPS TOWARDS ABSOLUTE GAS-PHASE CONCENTRATIONS OF METABOLITES

